



**University of
Nottingham**
UK | CHINA | MALAYSIA

From the extracellular matrix to the
microprocessor:

Investigating the post-transcriptional
regulation of miRNA-155 by tenascin-C

Owen Dawson, BSc

*Thesis submitted to the University of Nottingham for the
degree of Doctor of Philosophy*

List of Contents

Abstract	8
Acknowledgements	10
Abbreviations	12
Introduction	22
1.1.0 - The Inflammatory Response	23
1.1.1 - Macrophages	23
1.1.3 - Toll-like Receptor 4 Signalling	25
1.1.2 - Mediators of Inflammation	29
1.2.0 – MicroRNA	30
1.2.1 – miRNA Biogenesis	31
1.2.2 – miRNA Strand Selection ⁸³	34
1.2.3 – The post-transcriptional regulation of miRNA biogenesis	35
1.2.4 – miRNA Function	46
1.2.5 – miRNAs and Inflammation	48
1.3.0 - miRNA-155	51
1.3.1 – Regulation of miRNA-155 Biogenesis	54
1.3.2 - miRNA-155 and Cancer	59
1.3.3 - miRNA-155 and Rheumatoid Arthritis	60
1.4.0 – Tenascin-C	61
1.4.1 – Tenascin-C in Inflammation	64
1.4.2 – Tenascin-C in Cancer	65
1.5.0 – Integrins	66
1.5.1 – Overview	66
1.5.2 – Integrins and TN-C	69
1.6.0 – The Actin Cytoskeleton	71
1.6.1 – General	71
1.6.2 – Actin Cytoskeleton and the macrophage	72
1.7.0 – Yes-Associated Protein (YAP)	74
1.7.1 – YAP and Inflammation	78
1.7.2 – YAP and miRNA regulation	80
1.7.3 – YAP and Tenascin-C	83

1.8.0 – The p38 α /MK2 Pathway	85
1.8.1 – p38 α	85
1.8.2 – MAPKAPK2 (MK2).....	88
1.8.3 – p38 α /MK2 pathway in macrophage inflammation	91
1.8.4 – p38 α /MK2 pathway and TN-C.....	94
1.8.5 – p38 α / MK2 pathway and miRNA Regulation	97
1.9.0 – Aims, hypothesis and objectives.....	100
1.9.1 - Aims.....	100
1.9.2 – Hypothesis	100
1.9.3 – Objectives.....	Error! Bookmark not defined.
Materials and Methods	102
2.1.0 – Reagents.....	103
2.1.1 – Cell culture reagents.....	103
2.1.2 – Molecular biology reagents.....	103
2.1.3 – Protein chemistry and blotting reagents and equipment	104
2.2.0 – Buffer recipes	104
2.3.0 – Primers	106
2.4.0 – Cell culture	107
2.4.1 – Preparation of bone marrow-derived macrophages.....	108
2.4.2 - RAW264.7 cells, Immortalised BMDMs, NIH-3T3 and EO771 cells	108
2.4.3 – Cell stimulation.....	109
2.4.4 – Plasmid nucleofection	110
2.4.5 – siRNA transfection	111
2.4.6 – MTT assay.....	113
2.4.7 – FACS analysis	113
2.5.0 – Molecular biology techniques	114
2.5.1 – RNA-immunoprecipitation	114
2.5.2 – Total RNA extraction and quantification	115
2.5.3 – Quantitative Real-Time PCR (SYBR Green)	116
2.5.4 – Quantitative Real-Time PCR (Taqman)	117
2.6.0 – Protein Extraction and Quantification	119
2.6.1 – Total protein extraction	119
2.6.2 – Protein extraction from Trizol organic fraction	120

2.6.3 – Nuclear / Cytoplasmic protein fractionation.....	121
2.6.4 – Bradford assay	121
2.7.0 – Immunoblotting	122
2.7.1 – SDS PAGE	122
2.7.2 – Western Blot.....	123
2.7.3 – Immunocytochemistry	125
2.8.0 – RNA Seq analysis	126
2.8.1 – RNA preparation and small RNA sequencing	126
2.8.2 – sRNA-seq data analysis by Novogene.....	127
2.8.3 – GO and KEGG analysis of miRNA targets.....	128
2.8.4 – pri-miRNA cis-regulatory element analysis	128
2.9.0 – Statistical Analysis.....	130
The potential role of YAP in the regulation of miR-155 expression.	132
3.1.0 – Introduction	133
3.2.0 – Analysis of miR-155 regulation by tenascin-C in RAW 246.7 macrophages.....	136
3.2.1 – TNC knockdown in RAW 246.7 macrophages.	136
3.2.2 – Examination of miR-155 post-transcriptional regulation at the microprocessor.	139
3.3.0 – The role of the actin cytoskeleton in tenascin-Cs regulation of miR- 155.	142
3.3.1 – The impact of TNC knockdown on the actin cytoskeleton of RAW 246.7 macrophages.	142
3.3.2 – Establishing potential links between actin cytoskeleton modulation and miR-155 expression.....	146
3.3.3 – Attempted rescue of miR-155 expression in TNC knockout macrophages via actin modulation	Error! Bookmark not defined.
3.4.0 – Examination of YAP and miR-155 in the RAW 246.7 macrophage.	151
3.4.1 – Detection of YAP in macrophages.	151
3.4.2 – Effect of low macrophage confluency on YAP expression.....	Error! Bookmark not defined.
3.5.0 – Establishing an alternative cell model for examination of the potential link between TN-C, YAP and miR-155.	321
3.5.1 – Investigating YAP, TNC and miR-155 expression in candidate cell lines.	321

3.4.2 – Examining potential links between YAP, TNC and miR-155 in NIH-3T3 cells.....	323
3.4.3 – Examining potential links between YAP, TNC and miR-155 in E0771 cells.....	157
3.6.0 – Using YAP overexpression to examine the YAP-miR-155 relationship in the RAW 246.7 macrophage.....	160
3.6.1 – The impact of overexpressing YAP on miR-155 expression in the RAW 246.7 macrophage.....	160
3.6.2 – Establishing whether NF-kB subunit p65 localisation is affected by YAP overexpression.	167
3.7.0 - Discussion	173
The role of the p38-MK2 pathway and integrin receptors in the regulation of miRNA-155 by TN-C	188
4.1.0 – Introduction	189
4.2.0 – Examination of known TN-C binding receptors with links to miR-155 expression regulation	191
4.2.1 – Identification of candidate receptors which may allow TN-Cs regulation of miR-155 expression.	Error! Bookmark not defined.
4.2.2 – Examination of α V integrin complexes as key candidates of TN-C signal transduction	192
4.3.0 – MK2: a kinase implicated in the regulation of miR-155 expression by TN-C?.....	198
4.3.1 – Identifying potential pri-miR-155 interacting RNA-binding proteins.	198
4.3.2 – MK2 expression in TNC knockdown and knockout macrophages	202
4.4.0 – TNC knockdown influences MK2 and p38 abundance in steady-state macrophages.....	205
4.4.1 – Optimisation and characterisation of MK2 protein detection in RAW 246.7 cells.	205
4.4.2 – Examining the impact of TNC knockdown on MK2 expression and phosphorylation in LPS stimulated RAW 246.7 cells.....	208
4.4.3 – Examining the impact of TNC knockdown on p38 expression and phosphorylation in LPS stimulated RAW 246.7 cells.....	211
4.5.0 – Examination of the potential regulation of p38 subcellular localisation and MK2 recovery by TN-C.....	215
4.5.1 – Investigating the effect of TNC knockdown on p38 subcellular localisation during the inflammatory response.	215

4.5.2 – Examining the effect of TNC knockdown on MK2 protein recovery following prolonged LPS stimulation of RAW 246.7 cells.....	217
4.6.0 – MK2 knockdown and macrophage miR-155 expression	221
4.7.0 – Discussion.....	224
The post-transcriptional regulation of miRNA and its links to tenascin-C in the macrophage early inflammatory response	233
5.1.0 – Introduction	234
5.2.0 - miRNA induction in the early inflammatory response to LPS is primarily driven by an increase in transcription factor activity.	237
5.2.1 - Characterising miRNA expression in early inflammatory BMDMs	237
5.2.2 - Examining evidence for the post-transcriptional regulation of miRNAs in early inflammatory BMDMs.	244
5.2.3 - Analysis of miRNA isomerism in inflammatory BMDMs.....	248
5.3.0 - Tenascin-C knockout in BMDMs causes a global shift in inflammatory miRNA expression.....	252
5.3.1 - Characterising the effect of TNC knockout on miRNA expression in early inflammatory BMDMs.	252
5.3.2 – TNC knockout increases the abundance of miRNA 3p strands and decreases that of 5p strands only in LPS induced BMDMs.	257
5.3.3 – Analysis of miRNA isomerism in TNC knockout BMDMs during LPS stimulation	262
5.4.0 – Analysis of pri-miRNA cis-acting elements in TNC knockout macrophages.....	265
5.4.1 – Examining the association between regulation of miRNA by TN-C and the presence of cis-acting elements.	265
5.4.2 – Lower stem region stability is the only cis-regulatory element of pri-miRNA associated with miRNAs downregulated by TNC knockout. .	267
5.4.3 – The composition of the mGHG motif does not have a significant impact on miRNA regulation by TN-C.	274
5.4.4 – Neither apical loop size nor stem binding energy correlate with miRNA regulation by TNC knockout.	276
5.4.5 – Pri-miRNA processing score is significantly higher in miRNAs downregulated by TNC knockout.	278
5.4.0 - Discussion	284
Final Summary	295
6.0.0 - Overall Discussion	296

6.1.0 - Summary 296
6.2.0 - Concluding Remarks and Future Investigations 302

Abstract

A highly controlled type of short RNA sequences called microRNAs (miRNAs) regulates cellular processes via translational repression or degradation of target mRNAs. In particular, miRNA-155 plays a central role in the macrophage inflammatory response to infection, with dysregulation of miR-155 associated with pathological inflammation.

Previous work in the Piccinini lab has identified a post-transcriptional mechanism of miR-155 regulation, showing that the extracellular matrix (ECM) glycoprotein tenascin-C (TN-C) regulates processing of the miR-155 transcript (pri-miR155) in lipopolysaccharide (LPS)-stimulated bone marrow-derived macrophages (BMDMs). However, how this regulation occurs is yet to be elucidated.

This project aimed to identify by what mechanism TN-C regulates miR-155 processing in activated macrophages, involving examination of candidate TNC receptors, intracellular signalling pathways associated with both TN-C and miR-155 biogenesis machinery, as well as identification of pri-miRNA features associated with TN-Cs regulatory activity.

Utilising gain and loss-of-function approaches, examination of the candidate yes-associated protein (YAP) pathway, an increasingly relevant pathway in the study of cancer and inflammation, showed no association between this pathway and the post-transcriptional regulation of miR-155 by TN-C.

Remarkably, however, for the first time ectopic expression of YAP was found

to negatively regulate macrophage miR-155 transcription, this being linked to inhibition of the critical pro-inflammatory transcription factor NF- κ B.

Additionally, knockdown of TN-C expression in steady-state RAW 246.7 macrophages found TN-C to regulate p38 α and MK2, a master regulator of RNA-binding proteins, total protein abundance, but not their phosphorylation, this being attributed to an increase in p38 α mRNA levels as a result of TN-C knockdown, occurring via an unknown mechanism.

Furthermore, siRNA-based knockdown analysis of candidate TN-C receptors pointed to integrin α V as potential transducer of TN-C signalling the regulation of miR-155 expression.

Finally, interrogation of RNA-SEQ data from LPS treated TNC knockout and wild type BMDMs found no significant association between specific pri-miRNAs cis-regulatory elements, known to facilitate miRNA processing, and miRNAs modulated by TN-C in a similar manner as miR-155. Interestingly, TNC knockout was found to associate with a significant decline in 5p strand mature miRNA, with a concurrent induction in the levels of the 3p strand, potential evidence of TN-C orchestrating a miRNA arm-switching event.

Overall, whilst this project rules out YAP and MK2 as molecular players in the TN-C-miR-155 pathway, it unveils two new research directions: YAP as potential regulator of miR-155 transcription independent of TN-C and, excitingly, TN-C as a potential regulator of cell-wide miRNA strand selection.

Acknowledgements

People tend to fill this section of their thesis with some kind of grand philosophising, contemplating their PhD years as this chapter of their life, which involves far too much fiddling with references, comes to a close.

However, I'm just going to skip straight to the "acknowledging" bit.

First and foremost, I would never have gotten to this stage without my academic supervisor Dr Anna M. Piccinini. Her tireless dedication to scientific pursuits has been a constant inspiration and I will always be thankful that an academic with such a brilliant mind saw something worthwhile in my tuition.

I would also like to thank Dr Catherine Jopling and Dr Keith Spriggs for their invaluable assistance throughout my PhD.

Thank you to everyone in the AMP group throughout the years. Hannah and Nicole for their warm welcome, and Chai and Grace for helping me make the most of the last year in the lab.

Thank you to all the members of the GRRB lab over the past four years have each left their mark on my project, be it through their shared wisdom, heated lab debates, or laughter in the coffee room. I'd like to specifically thank Angie, Athena and Luc, for keeping me sane when days were difficult and making the good ones even better.

A huge thank you goes to my friends outside of the lab. Matt for always being there to have a pint and put the world to rights. Brandon for being there

whenever I wanted to share academic successes and woes. Anthony, Jojo, and Joseph, for all the games we played and procrastination you facilitated.

Thank you to my family. Tom for always taking an interest in my work when anyone else would be bored to tears. Dad and Lisa, Mum and Jan, for helping me when I needed to escape from it all and providing unlimited encouragement and love.

I would not have made it this far without my partner, Catherine, whose love, patience, and encouragement was the wind at my back to get me to this stage.

I would like to dedicate this thesis to my grandma, Dr Nancy Dawson, who sadly passed away in November 2023. It was her dedication and love for the scientific world, combined with that of my parents, which inspired me to undertake a PhD in biology. Thank you, Grandma.

Abbreviations

Abbreviation	Full name
ACHE	Acetylcholinesterase
ADAR	Adenosine deaminase acting on RNA
AGO	Argonaut
AIL	Asymmetric internal loop
AKT	Protein kinase B
AP-1	Activator protein 1
AMP	Adenosine monophosphate
APOBEC	Apolipoprotein B mRNA editing enzyme, catalytic polypeptide
Arp2/3	Actin-related protein 2/3 complex
BMDM	Bone marrow derived macrophage
BMP2	Bone morphogenetic protein 2
BRCA1	BRCA1 Cancer gene 1
BSA	Bovine serum albumine
CAF1	Chromatin assembly factor 1
CCR2	Chemokine receptor type 2
CCR4-NOT	Carbon catabolite repression-negative on TATA-less
CT	Cycle threshold
CD	Cluster of differentiation
C/EBPβ	CCAAT-enhancer-binding protein

CMP	Cytidine monophosphate
CMV	Cytomegalovirus immediate-early promoter
CREB	cAMP response element-binding protein
DAMP	Damage-associated molecular pattern
DC	Dendritic cell
DC-SIGN	Dendritic cell-specific intercellular adhesion molecule-3-grabbing non-integrin
DDX	DEAD-box RNA-helicase
DGCR8	DiGeorge syndrome chromosomal region 8
DKK	Dickkopf1
DMEM	Dulbecco's Modified Eagle Medium
DMSO	Dimethyl sulfoxide
dsRBD	Double-stranded RNA-binding domain
DSS	Dextran sodium sulphate
DUSPs	Dual specificity phosphatases
E-box	Enhancer box
ECL	Enhanced chemiluminescence
ECM	Extracellular matrix
EDTA	Ethylenediaminetetraacetic acid
EGFL	Epidermal growth factor-like repeats
EGFR	Epidermal growth factor receptor
EGTA	Ethylene glycol-bis(β -aminoethyl ether)- N,N,N',N'-tetraacetic acid

eIF	Eukaryotic initiation factor
EMT	Epithelial to mesenchymal transition
ERK	Extracellular signal-regulated kinase
EWS	EWS RNA binding protein
F-actin	Filamentous actin
FACS	Fluorescence-activated cell sorting
FBG	Fibrinogen globe
FBS	Foetal bovine serum
FUS	heterogeneous nuclear ribonucleoprotein P2
FNIII	Fibronectin-type III
G-actin	Globular actin
GDP	Guanosine diphosphate
GFP	Green fluorescence protein
GMP	Guanosine monophosphate
GLD	Germ line development 2
GO	Gene ontology
GPCR	G-protein coupled receptors
GTP	Guanosine triphosphate
HBSS	Hanks' Balanced Salt Solution
HDAC	Histone deacetylase
HEPES	4-(2-hydroxyethyl)-1-piperazineethanesulfonic acid
HMGB1	High mobility group box 1 protein

hnRNP	Heterogeneous nuclear ribonucleoprotein
HPRT	Hypoxanthine-guanine phosphoribosyltransferase
HuR	Human antigen R
IKK	Nuclear factor of kappa light polypeptide gene enhancer in B-cells inhibitor kinase
IL	Interleukin
iNOS	Nitric oxide synthase
IRAK	Interleukin-1 receptor-associated kinase
IRF	Interferon regulatory factor
ISRE	Interferon-sensitive response element
ITG	Integrin gene
Jasp	Jasplakinolide
JNK	c-Jun NH2-terminal kinase
KCNQ1OT1	Non coding RNA Potassium Voltage-Gated Channel Subfamily Q Member 1 overlapping transcript 1
kDa	Kilodalton
KEGG	Kyoto encyclopaedia of genes and genomes
KSRP	KH-type splicing regulatory protein
Lat B	Latrunculin B
LATS1/2	Large tumour suppressor 1/2
LBP	LPS-binding protein

LDL	Low density lipoprotein
LFA1	Lymphocyte function-associated antigen 1
lnRNA	Locked-nucleic acid
LPA	Lysophosphatidic acid
LPS	Lipopolysaccharide
M1 macrophage	Classically activated macrophage
M2 macrophage	Alternately activated macrophage
mAb	Monoclonal antibody
MAL1/2	Megakaryoblastic leukemia-1/2
MAPK	Mitogen-activated protein kinase
MAPK2K (MKK)	Mitogen-activated protein kinase kinase
MAPK3K (MKKK)	Mitogen-activated protein kinase kinase kinase
MATR	Matrin
MBNL1	Musclebind like splicing regulator 1
MCF-7	Human breast epithelial cell adenocarcinoma cell line
MD-2	Myeloid differentiation factor 2
MDM2	Mouse double minute 2
MEF	Murine embryonic fibroblast
MFI	Mean fluorescence intensity
mGHG	Mismatched GHG
MOB1A/B	Mob kinase activator 1 A/B
mRNA	Messenger RNA

miRNA	MicroRNA
MK2	Mitogen-activated protein kinase activated protein kinase 2
MKP	MAPK phosphatase
MSI2	Musashi-2
MST1/2	Mammalian ste-20-like kinase 1/2
MTPAP	Mitochondrial poly(A) polymerase
MTT	3-(4,5-dimethylthiazol-2-yl)-2,5-diphenyl-2H-tetrazolium bromide
MyD88	Myeloid differentiation primary response protein 88
NES	Nuclear export signal
NF	Nuclear factor
NF-κB	Nuclear factor kappa-light-chain-enhancer of activated B cells
NLS	Nuclear localisation signal
Nogo-B	Neurite outgrowth inhibitor B
NRP1	Neuropilin 1
OE	Overexpression
Opti-MEM	Optimised minimal essential medium
PABP	Poly(A)-binding protein
PACT	Protein kinase activator A
PAGE	Polyacrylamide gel electrophoresis

PAMP	Pathogen-associated molecular pattern
PAN	Poly(A)-specific ribonuclease
PAPD	P pilus subunit D
PAPOLG	Poly(A) polymerase gamma
PARN	Poly(A)-specific ribonuclease
PAZ	Piwi-argonaute and zwiille domain
PBS	Phosphate-buffered saline
PDCD4	Programmed cell death 4 protein
PEM	Peritoneal exudate macrophage
PEMs	Britton–Robinson buffer
PKA	Protein kinase A
PPARγ	Peroxisome proliferator-activated receptor gamma
Pri-miRNA	Primary-miRNA
Pre-miRNA	Precursor-miRNA
PRR	Pattern recognition receptor
qPCR	Quantitative polymerase chain reaction
RA	Rheumatoid arthritis
Ran	Ras-related nuclear protein
RANBP1	RAN binding protein 1
RAS	Rat sarcoma virus

RAW 264.7	<i>Mus musculus</i> monocyte/macrophage cell line derived from Abelson leukaemia virus-induced tumor.
RBD	RNA-binding domain
RBFOX	RNA-binding fox-1 homolog
RBP	RNA-binding protein
RGD	Arginylglycylaspartic acid
RIG-1	Retinoic acid-inducible gene I
RIP	RNA-immunoprecipitation
RISC	RNA-induced silencing complex
ROS	Reactive oxygen species
RPMI	Roswell Park Memorial Institute
SAV1	Salvadore homolog 1
SD	Standard deviation
SDS	Sodium dodecyl sulphate
SEM	Standard error of the mean
SF1	Splicing factor 1
SHIP1	SH-2 containing inositol 5'polyphosphatase 1
siRNA	Short-interfering RNA
SMAD4	Mothers against decapentaplegic homolog 4
SOCS1	Suppressor of cytokine signalling 1
SRF	Serum response factor
SRSF3	Serine and arginine rich splicing factor 3

TA	Tenascin assembly
TAB1	TAK1-binding protein 1
TAK1	Transforming growth factor β – activated kinase 1
TAZ	WW-domain-containing transcription regulator 1
TBK1	TANK-binding kinase 1
TBS	Tris-buffered saline
TBST	Tris-buffered saline with Tween
TDP-43	TAR DNA-binding protein 43
TEAD	Transcriptional enhancer factor domain
TEMED	N,N,N,N-tetramethylethylenediamine
TENT	Terminal nucleotidyl transferase
TGFβ	Tumour growth factor β
THP1	Tohoku Hospital Pediatrics-1 cell line
TIR	Toll/interleukin-1 receptor
TIRAP	Toll/interleukin-1 receptor domain containing adaptor protein
TLR	Toll-like receptor
<i>Tnc</i>	Tenascin-C gene
TN-C	Tenascin-C protein
TNF	Tumour necrosis factor
TNFR	TNF receptor

TRADD	Tumour necrosis factor receptor type 1-associated DEATH domain protein
TRAF6	TNF-receptor associated factor 6
TRAM	Translocating chain-associated membrane protein
TRBP	Transactivation response element RNA-binding protein
TRIP	TIR-domain-containing adapter-inducing interferon- β protein
TSS	Transcription start site
TTP	Tristetraprolin
TUT	Terminal uridyl transferase
UBS	Ubiquitin C promoter
UMP	Uridine monophosphate
UTR	Untranslated region
VASP	Vasodilator-stimulated phosphoprotein
XP5	Exportin 5
YAP	Yes-associated protein
YB-1	Y-box binding protein 1
ZAP70	Zeta chain of T cell receptor associated protein kinase 70kDa
ZNF	Zinc Finger Nuclease

Chapter 1

Introduction

1.1.0 - The Inflammatory Response

The inflammatory response is a coordinated cascade of processes which allows the body to remove detrimental stimuli as well as facilitating the repair of damaged tissue ¹. Primarily caused by tissue injury or microbial infection, acute inflammation is rapidly induced and terminated as part of the innate immune response, with prolonged inflammation being a hallmark of autoimmune and chronic inflammatory disorders such as rheumatoid arthritis and inflammatory bowel disease ^{2,3}.

The inflammatory response is initiated by pattern recognition receptors (PRRs) which are expressed by both immune and non-immune cells. Each PRR is activated by specific pathogen derived epitopes, known as pathogen-associated molecular patterns (PAMPs), or endogenous signifiers of tissue damage known as damage-associated molecular patterns (DAMPs). Activation of PRRs induces intracellular signalling cascades which elicit the activity of transcription factors responsible for the upregulation of genes encoding pro-inflammatory mediators, including cytokines. These pleiotropic polypeptides drive the inflammatory response, interacting with cytokine receptors on neighbouring cell surfaces to induce the further establishment of an inflammatory environment.

1.1.1 - Macrophages

Macrophages are innate immune cells found within every tissue of adult mammals, each playing an integral function within their specific tissue niche

as regulators of homeostasis, development and tissue repair in addition to their immune responsive functions ⁴.

During early development the majority of tissue niches are filled with macrophages derived from the embryonic yolk sac ⁵⁻⁷. These populations of tissue-resident macrophages persist throughout life and are thought to primarily contribute to tissue homeostasis through removal of excess tissue material, the preservation of vascular integrity or clearing of cellular debris ⁸. Alternately, macrophages may be differentiated from blood circulating monocytes upon their recruitment to tissues and exposure to inflammatory signals, with these monocytes themselves generated from the bone marrow ⁹.

Macrophages feature a number of cell surface and cytosolic PRRs as well as other environmental sensors. These facilitate the recognition, engulfment and breakdown of pathogens via a process called phagocytosis, as well as triggering the release of factors which regulate and maintain the local inflammatory microenvironment through modulating the behaviour of its constituent immune cells. These functions as well as the phenotype of the macrophage are in turn modified by microenvironmental cues, leading to an array of functional states which are often oversimplified with the duality of classically- (M1) and alternately-activated macrophages (M2) ¹⁰⁻¹⁵. M1 macrophages are responsive to pro-inflammatory cytokines as well as microbial products and act to promote an anti-pathogen, pro-inflammatory microenvironment ^{16,17}. Meanwhile, M2 macrophages are induced by anti-inflammatory cytokines, Tumour Growth Factor β (TGF β) and glucocorticoids,

this phenotype being associated with an anti-inflammatory microenvironment as well as functions such as tissue repair and wound healing ^{18–20}.

1.1.3 - Toll-like Receptor 4 Signalling

Toll-like receptors (TLRs) are a family of PRRs consisting of 10 members in humans and 12 in mice, deriving their name from their *D. melanogaster* homologue, Toll protein, the first receptor identified as a driver of inflammation ^{21,22}. Each TLR has a specific cellular localisation and PAMP recognition motifs, allowing for downstream inflammatory signalling tailored to the pathogenic threat ^{23–30}. Of interest is the cell-surface TLR4 which is activated by bacterial lipopolysaccharide (LPS), a glycolipid which serves as a major constituent of the gram-negative bacterial cell wall, as well as endogenous proteins such as HMGB1 and tenascin-C ^{23,31,32}. TLR4 can be primarily found on the surface of innate immune cells of the myeloid lineage such as monocytes, macrophages and dendritic cells, with variable levels of expression in all human tissues besides skeletal muscle and the skin, placing them at the fulcrum of pro-inflammatory signalling throughout the body ^{33–35}.

TLR4 is thought to bind lipopolysaccharide (LPS) with the aid of an LPS binding protein (LBP), facilitating a TLR4-dependent inflammatory response in the presence of only picomolar concentrations of LPS (Figure 1.1.1)³⁶. In macrophages CD14 extracts a single LPS molecule from the bacterial outer membrane, or LPS micelles which have been destabilised by the LBP, transferring this to the protein myeloid differentiation factor 2 (MD-2) which in turn interacts stably with the TLR4 ectodomain ^{36,37}. This interaction forms a

TLR4-MD-2 heterodimer, with crosslinking and dimerization of two adjacent heterodimers occurring as a result of an unbound LPS acyl chain (Figure 1.1.1) ^{38,39}. The dimerization of the TLR4 ectodomains causes the subsequent dimerization of the cytosolic Toll/interleukin-1 receptor (TIR) domains ⁴⁰, a process which occurs in tandem with the migration of the TLR4 dimer to lipid-raft structures on the plasma membrane ⁴¹.

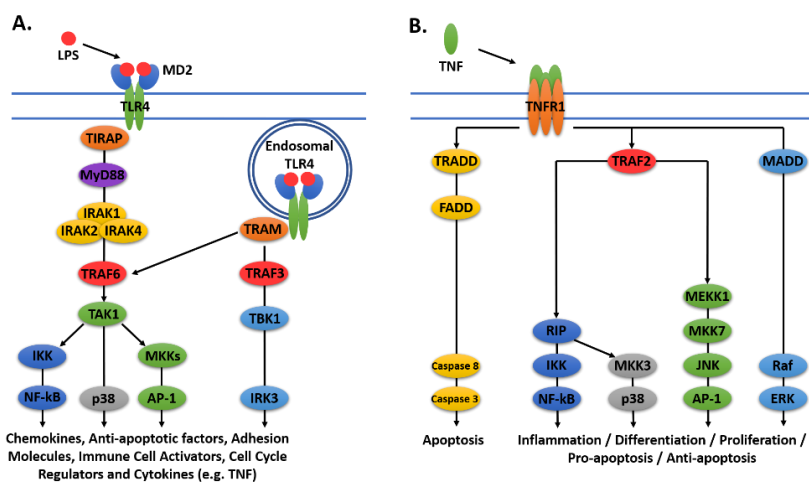


Figure 1.1.1. TLR4 and TNFR1 signalling. A) The TLR4 signalling pathway. LPS binding, facilitated by MD-2, leads to TLR4 dimerization and the recruitment of downstream adaptor molecules which cause the up regulation of pro-inflammatory transcription factors. B) The TNFR1 signalling pathway. TNF, produced as a result of TLR4 signalling, causes the upregulation of pro-inflammatory transcription factors via TRAF2 inducing the IKK and MAPK pathways. The protein MADD facilitates the upregulation of the pro-proliferation transcription factor ERK, while TRADD conducts pro-apoptosis signalling via a caspase cascade.

In all TLRs, except TLR3, recruitment of the lipid-raft associated Toll/interleukin-1 receptor domain containing adaptor protein (TIRAP) occurs, stimulating the assembly of a large cytosolic protein scaffold called a

myddosome (Figure 1.1.1) ^{42,43}. This facilitates the interaction of the dimerised TIR domains with myeloid differentiation primary response protein 88 (MyD88) which in turn recruits interleukin-1 receptor-associated kinases (IRAKs) and drives the recruitment of TNF-receptor associated factor 6 (TRAF6) an E3 ubiquitin ligase (Figure 1.1.1) ^{44,45}. Through activation of transforming growth factor- β (TGF- β)-activated kinase 1 (TAK1), the I κ B kinase (IKK) complex and mitogen-activated protein kinase (MAPK) pathways are stimulated, giving rise to the activation of the pro-inflammatory transcription factors, nuclear factor kappa-light-chain-enhancer of activated B cells (NF- κ B) and activator protein 1 (AP-1) (Figure 1.1.1) ⁴⁶.

Additionally, TLR4 can form a different structure on the endosomal surface, this event occurring after myddosome assembly as the macrophage internalises co-localised CD14 molecules (Figure 1.1.1) ⁴⁷. Dimerised endosomal TLR4 is detected by translocating chain-associated membrane protein (TRAM) in a similar manner to TIRAP, facilitating the formation of a triffosome, named for its constituent signalling adaptor TIR-domain-containing adapter-inducing interferon- β protein (TRIF). In this structure TRAF3-dependent activation of the kinase TBK1 occurs, driving the activity of pro-inflammatory interferon regulatory factor 3 (IRF3), NF- κ B and AP-1 in a MyD88-independent mechanism ⁴⁸.

As the regulation of the NF- κ B and MAPK pathways in the LPS stimulated macrophage are key points of examination within this project their mechanisms of activation have been further elaborated upon below.

The NF- κ B family proteins NF- κ B1 (p50), NF- κ B2 (p52), RelA (p65), RelB and c-Rel are localised to the cytoplasm of resting cells due to their inhibitory interactions with I κ B family proteins such as I κ B α as well as the NF- κ B1 and NF- κ B2 precursors p105 and p100 (Figure 1.1.2) ^{49–51}. Once activated by TRAF6 the IKK complex phosphorylates I κ B α at two N-terminal serine residues prompting its ubiquitin-dependent degradation, this leading to the rapid and transient nuclear translocation of NF- κ B family members, in particular p50/p65 and p50/c-Rel dimers, facilitating their action as pro-inflammatory transcription factors ^{52–54}.

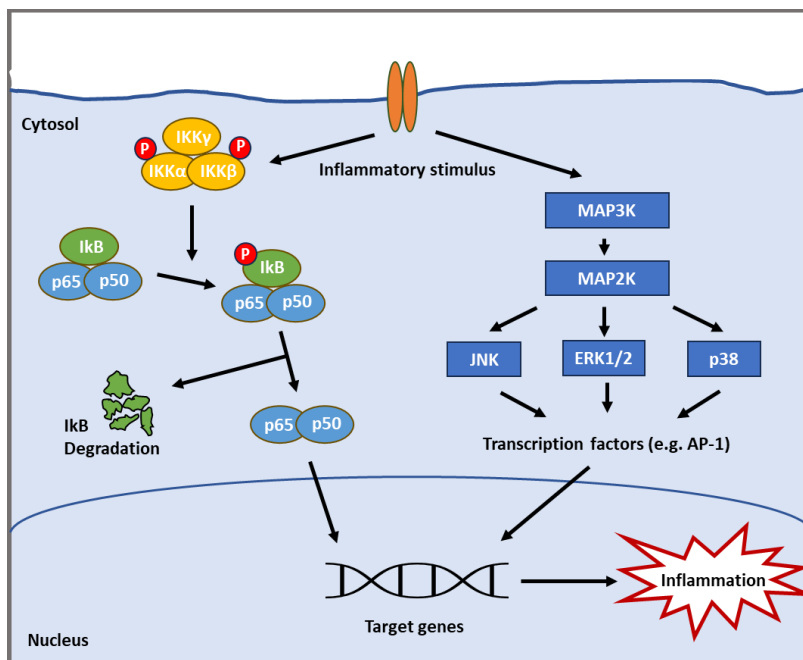


Figure 1.1.2. NF- κ B and MAPK signalling pathways in inflammation. Schematic representations of the NF- κ B and the MAPK signal pathways in inflammation. Adapted from Wu and Schauss. 2012⁵⁵.

TAK1 is also known as MAP3K7, denoting it as part of the MAP kinase kinase kinase (MAP3K) family of proteins⁵⁶. TAK1 stimulates a MAPK cascade upon its activation, phosphorylating MAPK2s including MKK3, MKK4, MKK6 and MKK7 (Figure 1.1.2)^{57,58}. These MKKs in turn stimulate the MK JNK and p38 pathways which lead to subsequent activation of the transcription factor AP1, formed from homodimers of Jun proteins (c-Jun, JunB and JunD) or heterodimers also containing a Fos protein (e.g. c-Fos, FosB and Fra1) (Figure 1.1.2)⁵⁹.

1.1.2 - Mediators of Inflammation

NF- κ B, AP-1 and IRF family members act as transcription factors to induce the expression of pro-inflammatory chemokines, anti-apoptotic factors, adhesion molecules, tissue degrading enzymes, immune cell activating factors, cell cycle regulators, microRNAs and cytokines⁶⁰⁻⁶³. NF- κ B is implicated in the polarisation of M1 macrophages, characterised by their high production of pro-inflammatory cytokines such as IL-1 β , IL-6, IL-12 and TNF⁶⁴. These cells are central drivers of a pro-inflammatory environment, with polarization into M2 macrophages signalling a switch to anti-inflammatory and tissue repair functionality via increased IL-10, IL-13 and TGF- β secretion⁶⁵.

Primarily produced by M1 macrophages, TNF is referred to as the “master mediator of inflammation” due to its myriad of pro-inflammatory functions and its fast-initial induction. The TNF receptor 1 (TNFR1) is expressed in all mammalian tissues, while the more regulated TNFR2 is typically expressed by

immune cells. TNF binds these receptors with a high affinity, with TNFR1 binding inducing an intracellular cascade that results in further AP-1 and NF- κ B activation. This leads to a positive feedback loop which drives inflammation and removes pathogenic stimuli via the creation of a hostile inflammatory environment and the activation of M1 macrophages (Figure 1.2.0).

Due to the potential damaging nature of the pro-inflammatory response, negative regulatory mechanisms exist to control TLR4-induced TNF signalling, with aberrant TNF production being associated with the pathogenesis of autoimmune diseases, including rheumatoid arthritis, Crohn's disease, and atherosclerosis⁶⁶⁻⁶⁸. TLR signalling components are regulated by a host of mechanisms, including phosphorylation, ubiquitination and proteasome-mediated degradation, physical interaction and conformational change⁶⁹. Of increasing interest is the role of microRNAs (miRNAs) in TLR4 and TNF regulation. These single stranded 20-25 nucleotide long RNA molecules mediate translational repression or degradation of mRNA by directing the targeting of the RNA-induced silencing complex (RISC)⁷⁰. Several miRNAs are implicated in negative feedback loops initiated by TLR4 signalling, with the fast induction of these miRNA making them prime mediators of inflammatory initiation⁷¹.

1.2.0 – MicroRNAs

Beginning with the miRNAs lin-4 and let-7 discovered in 1993 and 2000, respectively, these small non-coding RNAs have been implicated over the past several decades to be central to mammalian post-transcriptional regulation,

with ~2,588 miRNAs identified in humans and >60% of human protein coding mRNAs containing at least one miRNA binding site ⁷²⁻⁷⁵. miRNAs have been shown to participate in the regulation of core cellular processes including proliferation, development, differentiation, and the stress response, while also influencing the pathology of multiple human diseases such as rheumatoid arthritis, cardiac hypertrophy and Alzheimer's disease ⁷⁶⁻⁸². Due to this broad functionality, mammalian miRNA biogenesis is a tightly coordinated multi-step process, the dysregulation of which being a hallmark of disease and cancer ^{83,84}.

1.2.1 – miRNA Biogenesis

Included in this section are excerpts from Dawson and Piccinini 2022 where I have reviewed and discussed miRNA biogenesis ⁸⁴. miRNA genes can be located within the intronic or exonic regions of both protein coding and non-coding DNA loci. They are generally transcribed by RNA polymerase II, and thus regulated by transcription factors and epigenetic regulators common to this polymerase such as p53 ^{85,86}. Transcription of miRNA genes gives rise to a >1kb primary-miRNA transcript (pri-miRNA), featuring single-stranded RNA interspersed with double-stranded hairpin regions, consisting of stem regions wherein the miRNA sequence resides, and topped with terminal loops ⁸⁷. Due to the polycistronic nature of >50% of human pri-miRNAs multiple such hairpins can be found within a single pri-miRNA transcript, this allowing co-transcription of some miRNAs ⁸⁸.

Identification and cleavage of the pri-miRNA into a precursor-miRNA transcript (pre-miRNA) is performed within the nucleus by a protein complex comprised of the RNase III containing Drosha and the ds-RNA binding domain protein DiGeorge syndrome chromosomal region 8 (DGCR8) (Figure 1.2.1). This complex, known as the microprocessor, cleaves ~11nt from the hairpin's dsRNA-ssRNA junction, with binding of DGCR8 to the pri-miRNA guiding the cleavage via Drosha⁸⁹⁻⁹¹. This produces a resultant ~70nt double-stranded pre-miRNA with a 5' phosphate and a 2nt 3' overhang. The core microprocessor is assisted in its functionality by the DEAD-box RNA helicases DDX17 and DDX5 as well as various heterogenous nuclear ribonucleoproteins, which are thought to regulate processing efficiency^{90,92}.

Within the nucleus, exportin 5 (XP5) recognises the dsRNA stem and short 3' overhang of pre-miRNA forming a complex with it, alongside the XP5 associated and GTP bound Ras-related nuclear protein (Ran). XP5 facilitates the translocation of pre-miRNA through the nuclear pore, after which the hydrolysis of GTP to GDP causes the dissociation of the XP5/pre-miRNA complex (Figure 1.2.1)⁹³.

Once within the cytoplasm pre-miRNA is bound by Dicer (Figure 1.2.1)⁹⁴⁻⁹⁶. This protein consists primarily of a C-terminal RNase III domain, responsible for pre-miRNA cleavage, an N-terminal helicase domain, which interacts with the hairpins terminal loop, and a Piwi-Argonaute and Zwillie domain (PAZ) which binds the pre-miRNA termini⁹⁷⁻⁹⁹. The PAZ domain preferentially binds to the pre-miRNAs 3' overhang, with RNase III domain-mediated cleavage of

the pri-miRNA occurring 21-25nt upstream¹⁰⁰. However, if the 5' end is thermodynamically unstable with weak pairing this can instead be bound by PAZ, changing the cleavage site¹⁰¹. This process is aided by transactivation response element RNA-binding protein (TRBP) and protein kinase activator A (PACT), both proteins which modulate the processing efficiency of some pre-miRNAs¹⁰²⁻¹⁰⁴. Cleavage by Dicer results in the removal of the pre-miRNA terminal loop, creating a double-stranded mature miRNA transcript which is loaded onto the protein Argonaute (AGO) to generate the effector RISC complex.

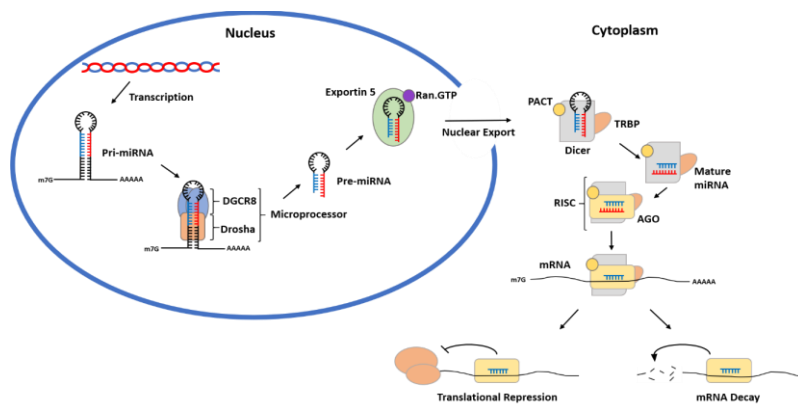


Figure 1.2.1. Classical miRNA biogenesis pathway. The primary miRNA transcript (pri-miRNA) is processed by the microprocessor, consisting of Drosha and DiGeorge syndrome chromosomal region 8 (DGCR8) proteins. This produces a preliminary miRNA transcript (pre-miRNA) which is exported from the nucleus via Exportin 5 in a Ran.GTP dependant mechanism. Within the cytoplasm the pre-miRNA is further processed by Dicer and associated proteins to produce a mature miRNA duplex, which is loaded onto the RNA induced silencing complex (RISC). Here strand selection occurs with the remaining strand targeting the RISC to complementary mRNA transcripts where it may perform its effector functions.

1.2.2 – miRNA Strand Selection⁸⁴

During AGO loading strand selection occurs, with one strand of the double-stranded miRNA being selected as the guide strand and utilised for effector targeting, while the other is removed and degraded as the passenger strand. Evidence suggests that this process occurs during the loading of the mature miRNA onto the Argonaute protein, an essential component of the RISC. Specifically, the 5' end of the retained miRNA strand interacts with a binding pocket in the Ago protein that is located at the interface between its MID (middle) and PIWI domains, while the 3' end fits into a hydrophobic cavity within the PAZ domain^{105–111}. The strand that binds to this pocket, either the 5' or 3' strand, denoted as 5p and 3p, respectively, is selected via two criteria. The first selection criterion is based on the thermodynamic features of each miRNA duplex end, with Ago showing a tendency to incorporate the strand with the lowest 5' end internal stability, probably due to increased access given to the MID/PAZ binding pocket, thought to be facilitated by regions such as the PAZ phosphate binding pocket^{112–114}. The second criterion involves the identity of the 5' terminal nucleotide of the miRNA strands, selected via a nucleotide specificity loop found within the MID domain of Ago¹¹⁴. In the case of human Ago2, this bias is expressed via a preference for 5' terminal uridine monophosphate (UMP) and adenosine monophosphate (AMP), with an affinity approximately 20 times greater than that for cytidine monophosphate (CMP) and guanosine monophosphate (GMP), which both sterically clash with the specificity loop in the MID domain^{107,109}. Together, these two criteria dictate a strand selection process that results in the asymmetrical functional

utilization of the miRNA 5' and 3' strands. However, these criteria do not account for all miRNA strand asymmetry, with the removal of key amino acids within *C. elegans* Ago-like protein not inhibiting all strand selection¹¹⁵. This was furthered by recent bioinformatic analysis of both miRNA strands, identifying that 17–25% of miRNAs examined did not follow either of these selection criteria¹¹⁶.

1.2.3 – The post-transcriptional regulation of miRNA biogenesis

miRNA Arm-Switching

miRNA arm-switching is a phenomenon whereby the strand ratio of miRNA-5p and -3p from the same mature miRNA can change between cell and tissue type, developmental stage and pathological state. Such regulation often involves the synthesis of isomiRs, mature miRNA strands whose RNA sequences are different to that of their genomic sequence^{117–120}. These are further grouped into template isomiRs, produced by altered cleavage of the miRNA by Drosha or Dicer, or non-template isomiRs, created as a result of remodelling factors acting on miRNA ends.

IsomiRs have been confirmed to functionally associate with the RISC and mRNA targets^{121,122}. For instance, an isomiR of miR-376 aids uric acid homeostasis through regulatory targeting not shared by the canonical form and, similarly, an isomiR of miR-140-3p regulates the cholesterol pathway by targeting unique to this isomiR^{123,124}. Generation of isomiRs has the potential to change the strand ratio as modifications to the 5' sequence and structure of the mature miRNA leads to changes in stability of both ends, thus

influencing strand selection by RISC. However, evidence suggests that miRNA arm switching events are not solely controlled by the mature strands thermodynamic properties, with expression of *Tribolium* and *Drosophila* miRNA-10 transcript within the same cell line finding each to lead to a different strand preference, even though both have an identical mature sequence ¹²⁵.

miRNA post-synthetic modification

Similarly to other double stranded RNA, pre-miRNA and mature miRNA are targeted by a number of nucleotide modifying proteins such as deaminases, uridylyltransferases and exonucleases, this leading to the formation of non-template isomiRs (Table 1.2.1) ^{126–128}. Such isomerism may modify RISC association by shifting Dicer cleavage sites or by directly modifying miRNA end architecture and the resultant strand selection criteria. Additionally, the addition or subtraction of 5' nucleotides may shift the miRNA seed sequence utilised by the RISC, this as well as direct seed sequence nucleotide modification influencing miRNA targeting and function ¹²².

RNA editing involves sequence modification following base-specific deamination of double-stranded RNA, ~90% of such events involving adenosine-to-inosine (A-to-I) transitions, with inosine interpreted as a functional substitute for guanine (Table 1.2.1) ¹²⁹. These changes are facilitated by the Adenosine Deaminase Acting on RNA (ADAR) family of proteins such as ADAR2, the knockout of which within adult mouse brain

tissue leading to significantly changes 5p/3p miRNA strand ratios, inferring that RNA editing has a direct impact on miRNA strand selection ¹³⁰.

In human hepatocellular carcinoma cells the exoribonuclease PARN has been shown to cause the deadenylation of the 3' end of miR-122 causing reducing its abundance through destabilisation, with similar activity seen within the *D.melanogaster* exoribonuclease Nibbler (Table 1.2.1) ^{131,132}. Thus, end nucleotide removal, as well as addition or substitution, may function in a wider context to regulate miRNA biogenesis.

Meanwhile, eight nucleotidyl transferases are known to add nucleotides to miRNA ends, these including GLD2, TUT3, TUT4, TUT7, PAPOLG, TENT1, TENT2 and TENT6 (Table 1.2.1) ^{120,132-134}. As an example, 3' terminal uridylyl transferases 4-7 (TUT4-7) have been shown to elicit 3' uridylation of miR-324 leading to a shift in the Dicer cleavage site, influencing end architecture and leading to consequential arm switching as miR-324-3p becomes the more abundant strand ¹³⁵.

Name	Type
Nibbler ^{120,131,136}	3'-5' exonuclease
PARN ¹³⁷	3'-exonucleases (poly (A) substrate preference)
TENT2, PAPD4, GLD2 ^{120,132,133}	Poly(A) RNA polymerase

TUT4 ^{120,134,138,139}	RNA uridylyltransferase
TUT3, PAPD5 ¹²⁰	Poly(A) RNA polymerase
MTPAP, TENT6 ¹²⁰	Mitochondrial poly(A) polymerase
PAPOLG ¹³²	Poly(A) DNA/RNA polymerase
TUT1, TENT1 ¹²⁰	Terminal uridylyltransferase and nuclear poly(A) polymerase
TUT7, ZCCHC6, PAD6 ^{120,138,139}	Terminal uridylyltransferase
ADAR enzymes ^{129,130,140,141}	RNA specific adenosine deaminase
APOBEC enzymes ¹⁴¹	RNA specific cytidine deaminase

Table 1.2.1. A summary of proteins which perform miRNA post-synthetic modifications.

Pri-miRNA cis-regulatory motifs

Publications from the past decade have highlighted the pivotal role of pri-miRNA cis-acting elements in determining both the propensity of pri-miRNA binding to the microprocessor as well as the efficiency of cleavage. These elements take several forms and are located throughout the pri-miRNA transcript, with it being possible for a pri-miRNA to contain singular, multiple or no such elements (Figure 1.2.2)¹⁴².

Of these elements the basal UG and a stable lower stem have been found to be the most essential determinants of efficient pri-miRNA cleavage (Figure 1.2.2)¹⁴². The basal UG motif is located on the 5p arm ~14nt upstream of the DRISHA cleavage site at a region called the “basal junction”. The basal

junction is recognised and bound by the coordinated action of the DROSHA PAZ domain and MB helices, with the U of the basal UG motif taking direct part in this binding ¹⁴³. Once the basal junction is bound by DROSHA the RIIIDs is aligned with the RNA lower stem, with optimal placement determined by interactions between the RIIIDs and the lower stem. These two events are thought to act to position the catalytic residues of DROSHA's RNA cleavage domain ~11nt downstream of the basal junction, leading to accurate cleavage of the pri-miRNA into the pre-miRNA ¹⁴³. Thus, poor dsRNA stability in the lower stem region, due to multiple bulges and mismatched residues, or a lack of a basal UG motif can both highly impact DROSHA binding and cleavage efficiency ¹⁴².

As well as DROSHA the microprocessor complex also consists of a DGCR8 dimer, its greater pri-miRNA affinity leading to it being the first component to bind to the RNA (Figure 1.2.2) ¹⁴³⁻¹⁴⁵. This binding occurs at the pri-miRNA "apical loop" and is facilitated by the apical UGU motif located at the apical junction. The UGU motif has been found to interact with the Rhed domain of dimerised DGCR8, localising DGCR8 to the apical loop and ensuring the proper orientation of the pri-miRNA for subsequent cleavage by DROSHA ¹⁴⁶. Apical loop size is thought to also be a determinant of DGCR8 binding, with loops <7nt found to have reduced enrichment, potential due to a small loop hindering DGCR8 association ¹⁴⁷.

Another feature of the pri-miRNA lower stem critical to microprocessor cleavage is the basal mismatch GHG (mGHG) motif. This feature is

characterised by a guanine preference -7nt downstream of the DROSHA cut site on the 3p strand as part of a Watson-Crick or wobble pair, a strong preference against guanine at position -6 and a preference for guanine at -5, however this not being part of a wobble pair ^{142,148}. The mGHG motif is thought to be recognised by the dsRBD domain of DROSHA, facilitating a fine tuning of cleavage site determination in addition to the more general direction provided by the UG, basal junction and UGUG motifs ¹⁴². mGHG motifs have also been found elsewhere in the pri-miRNA such as at the apical junction ¹⁴⁹. These apical mGHG motifs are associated with misplaced DROSHA binding, leading to off-target cleavage events and unproductive miRNA processing.

Multiple loops, mismatches, wobble pairs and bulges are conserved and enriched within specific pri-miRNA regions and are thought to control both accuracy and the efficiency of pri-miRNA processing by Drosha/DGCR8. The lower stem asymmetric internal loop (AIL) inhibits cleavage of the pri-miRNA 3p strand potentially through blocking interaction between RIIIDb of Drosha and the RNA duplex, leading to decreased miRNA expression ¹⁵⁰. Within the middle of the upper stem 7-9nt from the cleavage site the presence of bulges, mismatches or wobble-pairs (midBMW_7-9) enhances Drosha cleavage accuracy, in a manner that is cooperative with other cis-regulatory elements such as UG, UGU and mGHG motifs, targeting Drosha 8bp upstream ^{151,152}. Similarly, the midBMW_10-12 reduces the occurrence of unproductive cleavage events which give rise to no pre-miRNA, thus enhancing miRNA expression, potentially by preventing Drosha from associating with the upper

stem region. Meanwhile a similar feature within the seed sequence (seedBMW_4-8) instead elicits reduced productive cleavage, pushing the Drosha cleavage site further upstream^{147,151,152}. The action of these latter two BMW elements on pri-miRNA processing is strand-dependent, with their presence on the 3p strand associated with an enhanced effect on pri-miRNA processing compared to the 5p strand¹⁵². Intriguingly, the presence of the midBMW_10-12 on the 3p strand, although enhancing pri-miRNA processing, blocks Dicer association, thus reducing miRNA expression¹⁵².

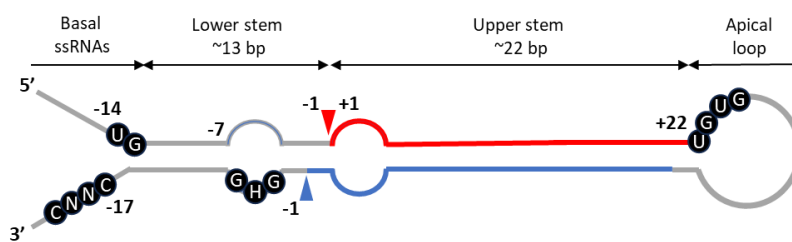


Figure 1.2.2. A schematic diagram of pri-miRNA cis-regulatory elements. Adapted from Kim et al., 2021¹⁵³.

RNA-Binding Proteins.

In addition to the traditional components of the microprocessor, Dicer and RISC complexes, the association of auxiliary protein cofactors have been found to influence miRNA biogenesis by modulating interactions between the biogenesis complexes and the RNA duplex (Table 1.2.2).

RNA-binding proteins (RBPs) dynamically interact with RNA structures via the proteins RNA-binding domains (RBDs), the binding of which being both RNA sequence and context dependent. By containing multiple such domains each RBP may have multiple, diverse RNA targets, facilitating the varied function of RBPs in roles such as RNA transport, processing, decay, localisation, folding, storage and post-transcriptional gene regulation ¹⁵⁴.

Multiple RBPs have been shown to bind to pri- and pre-miRNA structures, often regulating the association of microprocessor or Dicer components resulting in enhanced or aborted miRNA processing (Table 1.2.2). In particular, the pri- and pre-miRNA apical loops seems to serve as a key scaffold for RBP association, hosting proven functional binding sites for hnRNPA1, MATR3, YB-1 and Lin28 amongst others ^{155–160}. Alternately, the CNNC motif, located ~17-18nt downstream of the DROSHA cleavage site on the 3p strand, is responsible for the potential association of a range of RNA-binding proteins with the microprocessor complex, with processing implications dependent on the protein bound ¹⁴². For instance, SRSF3 and DDX17 have both been shown to bind the CNNC motif, resulting in enhanced pri-miRNA processing ¹⁴².

RNA-Binding Protein	Processing Step	Binding Motif	Pri/pre-miRNA Binding Location	Mechanism	Impact on pri/pre-miRNA processing
SRSF3 ¹⁶¹	Drosha	CNNC	3' Tail	Unknown	Enhances processing

DDX17 ⁹²	Drosha	VCAUCH	3' Tail	Unknown	Enhances processing
hnRNPA2/B1 162,163	Drosha	m6A	5' Tail	Aid Drosha targeting to pri-miRNA	Enhances processing
ADAR2 ¹⁶⁴	Drosha	-	Stem	Blocks Drosha binding to the stem independent of catalytic activity.	Inhibits processing
hnRNPA1 ^{155,1} 56	Drosha / Dicer	UAGGG	Apical loop	Promotes Drosha processing through pri-miRNA structural changes. Inhibits processing by outcompeting KSRP.	Inhibits or enhances processing
KSRP ¹⁶⁵	Drosha / Dicer	-	Apical loop	Unknown	Enhances processing

MATR3 ¹⁵⁷	Drosha / Dicer	AUCUU	Apical loop	Unknown	Inhibits processing
YB-1 ^{158,159}	Drosha / Dicer	UCAUC	Apical loop	Blocks the recruitment of Drosha and Dicer	Inhibits processing
Lin28A/B ¹⁶⁰	Drosha / Dicer	-	Apical loop	Blocks Drosha and Dicer processing	Inhibits processing
TDP-43 ¹⁶⁶	Drosha/ Dicer	-	Apical loop	Unknown	Enhances processing
RBFOX2 ¹⁶⁷	Drosha	GCAUG	Apical loop	Blocks Drosha binding to the apical loop through structural changes.	Enhances processing
EWS ¹⁶⁸	Drosha	-	Apical loop / stem	Recruits Drosha co- transcription ally	Enhances processing
HuR/MSI2 ¹⁶⁹	Drosha	-	Apical loop	Recruits MSI2, stabilising the	Inhibits processing.

				stem and blocking receptor cleavage.	
MBNL1 ¹⁷⁰	Drosha	UGC	Apical loop	Out competes binding of the negative regulator LIN28	Enhances processing
hnRNPH1 ¹⁷¹	Drosha	-	-	Unknown	Enhances processing
hnRNPR ¹⁷¹	Drosha	-	-	Unknown	Inhibits processing
RBFOX3 ¹⁷²	Drosha	GCAUG	-	Binds to the apical loop and facilitates Drosha association. Binds to the stem and blocks Drosha association.	Inhibits or enhances processing.

FUS/TLS ¹⁷³	Drosha	-	-	Recruits Drosha co-transcriptionally	Enhances processing
NF45/90 ¹⁷⁴	Drosha	-	-	Binds endogenous pri-miRNA, potentially blocking Drosha association.	Inhibits processing
DDX3X ¹⁷⁵	Drosha	-	-	Unknown	Enhances processing

Table 1.2.2. A summary of RNA-binding proteins which mediate miRNA processing.

1.2.4 – miRNA Function

Once a passenger strand is selected, the RISC complex can begin its effector activity, facilitated by the AGO protein which features a N-terminal PAZ domain and C-terminal middle (MID) and P-element-induced wimpy testis (PIWI) domains. The latter two domains create the interface which holds the guide strand (Figure 1.2.1) ^{105,176,177} .

The guide strand binds via nucleotide base pairing to complementary mRNA sequences within the cytoplasm, with miRNA binding sites being most abundant in the mRNA 3'UTR but also occurring elsewhere in the transcript ¹⁷⁸ . This binding targets the effector functions of the RISC complex, which vary depending on which of the four human AGO proteins are present. For

example, AGO2s slicer activity allows it to directly cleave target mRNA, leading to their suppression^{179,180}. This function of AGO2 requires perfect miRNA-mRNA base pairing, thus limiting the possible targets of this degradation pathway¹⁸¹. Alternative methods of translational suppression and mRNA decay have been found to require only partial complementarity, with targeting being dependent on the binding of the miRNA seed sequence, consisting of nucleotides 2-7 in the guide strand¹⁸². Importantly, this allows for a single miRNA to regulate multiple mRNA transcripts, facilitating their central regulatory role in complex networks such as those within development and inflammation¹⁸³.

Gene silencing via mRNA decay and translational repression requires the recruitment of additional effector proteins to the RISC (Figure 1.2.1)¹⁸¹. This is in part facilitated by the cytoplasmic co-localisation of AGO proteins and their effector proteins upon RISC-mRNA binding into discrete membraneless compartments, these including processing bodies (P-bodies) and stress granules¹⁸⁴. This localisation is thought to be controlled through a process of liquid-liquid phase separation (LLPS) whereby networks of interactions between multivalent molecules, such as proteins containing multi-modular interaction domains as well as RNA and DNA molecules, acquire liquid-like properties¹⁸⁵. This increased local concentration of RISC components and their targets is thought to potentially improve the efficiency of gene silencing through improved reaction kinetics, although these compartments are also considered as potential storage sites for inactive multivalent molecules, such as transcript bound-mRNA decay factors^{186,187}.

mRNA decay is the most common human effector of RISC-mediated silencing. In this process, the association of GW182 proteins serves to further recruit poly(A)-binding proteins (PABPs) and the deadenylase complexes; carbon catabolite repression-negative on TATA-less (CCR4-NOT) and poly(A)-specific ribonuclease subunits 2 and 3 (PAN2-PAN3) ¹⁸⁸⁻¹⁹². Upon removal of the mRNAs 3' poly(A) tail, decapping factors can be recruited by the RISC, facilitating removal of the mRNA 5' methyl cap and allowing 5'-3' exonucleolytic decay of the mRNA through the action of exonucleases such as XRN1 ¹⁹³⁻¹⁹⁷. One manner in which translational repression is thought to occur is via the interaction of the RISC associated protein GW182 with PABPs on the mRNA poly(A) tail. This is thought to inhibit the interactions between eukaryotic initiation factor 4F (eIF4F) and PABPs required for translational initiation, thus preventing association of the ribosome and resultant protein synthesis ^{198,199}.

1.2.5 – miRNAs and Inflammation

Many miRNAs form negative feedback loops with inflammatory signalling molecules, creating critical buffers which prevent run-away inflammatory activity as witnessed in chronic inflammatory disorders (Table 1.2.3) ²⁰⁰. An example of this is the prevention of inflammatory mediator inhibition via miRNAs such as miR-146, whose inhibition of IRAK1 and TRAF6 decreases the induction of NF- κ B, reducing production of pro-inflammatory mediators as well as miR-146 itself ²⁰¹. miRNAs are often induced by the same transcription factors that are activated by TLR signalling, granting them the same spatial

expression as the inflammatory mediators that they regulate⁸⁵. The fast inducibility of miRNAs, due to their lack of a requirement for protein synthesis, makes these some of the first effectors of TLR signalling, priming the transcriptome for inflammation before the initial cytokines are produced. This inducibility allows miRNAs to respond quickly to inflammatory signals, initiating the changes in pro- and anti-inflammatory mediator concentrations which mark the shift from inflammation to resolution of inflammation⁷¹.

miR-155-5p is one of the first effectors of TLR4 signalling, being induced ~2 hours after LPS treatment, and thought to promote the activity of the key pro-inflammatory cytokine TNF and to inhibit the anti-inflammatory regulator SH-2 containing inositol 5'polyphosphatase 1 (SHIP1) and suppressor of cytokine signalling 1 (SOCS1)²⁰²⁻²⁰⁷. This aids the induction of inflammation, alongside the downregulation of the anti-inflammatory miRNA let-7i and miR-125b, both of which are inhibitors of TNF synthesis^{208,209}. As the immune response progresses, anti-inflammatory miRNAs begin to be produced such as the miR-146 and miR-9, the latter directly targeting NFkB mRNA^{201,210}. This results in down-regulation of TLR4 signalling, giving rise to the resolution of inflammation as miR-21 induces IL10 production via the inhibition of the negative cytokine regulator, programmed cell death 4 protein (PDCD4)²¹¹. Upregulation of IL-10 induces a host of anti-inflammatory effects, including the down-regulation of miR-155-5p, leading to de-suppression of SHIP1 and increasing inhibition of TLR4 signalling, as well as inducing miR-187 which down regulates both TNF and IL-6^{204,212}.

miRNA	Cell Type	Inflammatory signals which regulate the miRNA	Inflammatory signals regulated by the miRNA	References
miR-155	BMDMs, THP1 cells, monocytes, macrophages, DCs, B cells, Treg cells	TLR2/3/4/9, MYD88, TRIF, JNK, AP1, NF-kB, KSRP, oxidised LDL, TNF, IFN β , IL-10, AKT	MYD88, TAB2, IKK ϵ , FOXP3, C/EBP β , TNF, SHIP1, SOCS1	201,202,204–206,213–223
miR-146	THP1 cells, macrophages, BMDMs, T cells	TLR2/3/4/5, MYD88, NF-kB, RIG-1, TNF, IL-1	IRAK1, IRAK2, TRAF6,	201,215,216,224,225
miR-132	THP1 cells, human monocytes and macrophages, BMDMs, splenocytes	TLR4/9	p300, ACHE	201,210,223,226,227
miR-21	Inflamed lung tissue, RAW264.7 cells, alveolar macrophages	TLR4, MYD88, TRIF, NF-kB	IL-12p35, PDCD4	211,215,228,229
miR-223	Inflamed lung tissue, DCs	TLR4	TLR4, TLR3, IKK α	221,229–231

miR-147	BMDMs, RAW264.7 cells, THP1 cells, alveolar macrophages	TLR2/3/4, MYD88, TRIF, NF-kB, IRF3	ND*	232
miR-9	Human monocytes and granulocytes	TLR2/4/7/8, MYD88, NF-kB	NF-kB1	210
miR-125b	H69 cholangiocytes, rheumatoid arthritis synovial fibroblasts, LPS-tolerized THP1 cells Splenocytes, BMDMs, DCs	TLR4, NF-kB NF-kB, AKT1	TNF	208,221,222,233,234
let-7e	Peritoneal macrophages	TLR4, AKT1	TLR4	222
miR-27b	Human macrophages	TLR4, NF-kB	PPAR γ	235
let-7i	H69 cholangiocytes	TLR4, NF-kB, C/EBP β	TLR4	209
miR-98	H69 cholangiocytes	TLR4	MAP4K4	236,237

Table 1.2.3. Verified miRNA interactions with immune signalling components. *ND = Not determined ⁷¹.

1.3.0 - miRNA-155

First identified in 1997 as a non-coding element within the host gene cluster *bic*, involved in chicken leukosis development, miR-155 has since been

established as a conserved component of regulatory networks in both mice and humans^{238–240}. *Bic* (miR-155 host gene) comprises a 13kb region of chromosome 21 and chromosome 16 in humans and mice, respectively (Figure 1.3.1). The human and mouse miR-155 host gene contain three exons, the last of which containing miR-155 and corresponding to the highest region of conservation within this gene across species.

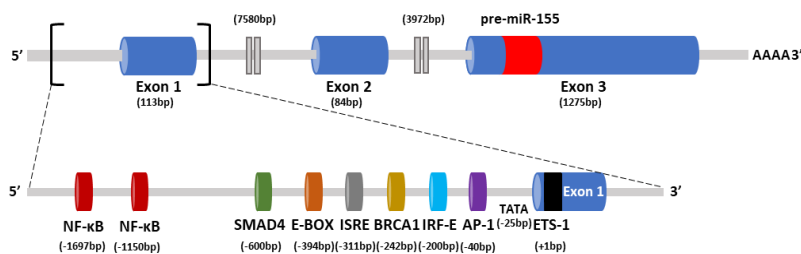


Figure 1.3.1. miR155 host gene schematic. Pictured is NC_000021.9:25562145-25575168, Homo sapiens, chromosome 21, GRCh38.p12. Transcription factor binding sites are labelled. Adapted from Elton et al., 2013²⁴¹.

The miR-155 host gene transcribes a mono-cistronic pri-miRNA which, after pri-mRNA splicing, is processed to produce a 65nt pre-miRNA which in turn is cleaved to a 24nt miR-155-5p or 22nt miR-155-3p mature miRNA transcript, the 5p strand being of greater abundance in the majority of cells which mediate inflammation (Figure 1.3.2)⁸⁴. The mature miR-155 sequence is highly conserved between humans and mice, differing in one nucleotide in the non-seed regions of both 5p and 3p strands and with the 3p strand featuring one nucleotide difference within the seed region. This having potential ramifications when comparing 3p's targeting between species. Recently, the functionality of miR-155-3p has begun to be characterised, with the

expression of this miRNA strand and its roles in inflammation, cancer and disease having been reviewed previously by Owen Dawson and Anna Piccinini⁸⁴. Due to its abundant induction upon stimulation of the TLR4 pathway by LPS in macrophage cells and its key roles in inflammation, miR-155-5p will be focused upon and referred to as miR-155 here onwards unless specific distinction must be made between strands.

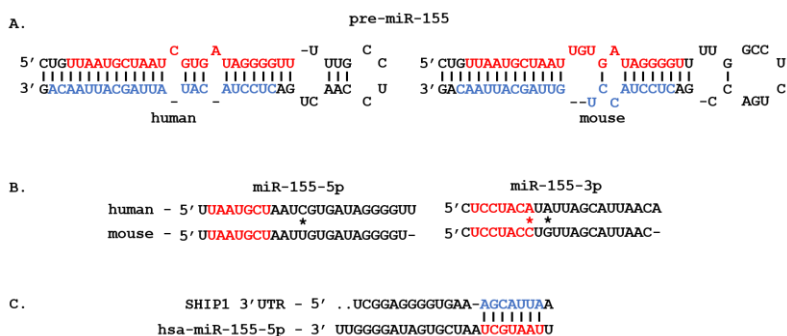


Figure 1.3.2. miR-155 sequence conservation and targeting. A) preliminary miR-155 (pre-miR-155) sequences in human and mouse. miR-155-5p strand (red), miR-155-3p strand (blue). **B) Conservation of miR-155 sequences.** Seed region (red) and sequence differences (*). Noticeably miR-155-3p features seed sequence variation between mice and humans, possibly leading to different functionality. **C) Human miR-155-5p and SHIP1 interaction.** Binding region, miR-155-5p (red), SHIP1 (blue). Adapted from ⁷¹.

miR-155 has been identified as functionally relevant in a host of cellular processes and pathologies, being primarily expressed in the thymus and spleen, with elevated miR-155 expression being associated with the development of pathological states in other tissues^{240,242}. Increased miR-155

expression has been linked to poor prognosis in multiple disorders such as rheumatoid arthritis, multiple sclerosis, infection, and cancers ^{243–246}.

The functional activities of miR-155 can be divided into three mechanisms.

Firstly, miR-155 can cause direct negative regulation of a target mRNA transcript via complementarity guided RISC association, such as when miR-155 inhibits IL-13R α mRNA, resulting in reduction of IL-13 activity and resultant M2 macrophage polarisation ²⁴⁷. Secondly, miR-155 can function by indirect negative regulation, such as by inhibiting the transcription factor PU.1 and thus causing inhibition of its target gene, dendritic cell-specific intercellular adhesion molecule-3-grabbing non-integrin (DC-SIGN) ²⁴⁸. This leads to a reduction in the pathogen binding ability of DCs, affecting their influence on T cell polarisation and resistance to viral infection ²⁴⁸. Finally, miR-155 has been shown to function by both direct and indirect positive regulation of mRNA, a key example of which is miR-155s apparent multi-level regulation of TNF. By inhibiting the negative regulator of TNF, SHIP-1, miR-155 can cause the cytokines functional upregulation ²⁰⁶. Similarly, by inhibiting the STAT pathway inhibitor, suppressor of cytokine signalling-1 (SOCS-1), miR-155 upregulates pro-inflammatory cytokine release ²¹⁷.

1.3.1 – Regulation of miRNA-155 Biogenesis

Transcriptional control

A number of transcription factors and enhancers have been associated with the induction of miR-155 expression with their binding sites mapped to the miR-155 host gene transcription start site (TSS) and promoter regions.

During TLR signalling both NF- κ B and AP-1 have been shown to activate transcription of miR-155 (Figure 1.3.1)^{201,204,249}. Three NF- κ B binding sites have been identified within the miR-155 host gene, two of which within the miR-155 promoter region far upstream of the TSS and one more proximal to the TSS^{250,251}. NF- κ B has been confirmed to bind to these sites via electrophoresis mobility shift assay and chromatin immunoprecipitation experiments, with such binding inducing miR-155 expression. Additionally, an AP-1 consensus sequence can also be found upstream of the TSS, the functionality of which has been found to be a requirement for LPS treatment to induce miR-155 expression in RAW 264.7 cells^{204,252–254}.

Intriguingly, the anti-inflammatory cytokine IL-10 has been implicated in the downregulation of the transcription factor-based induction of miR-155. IL-10 treatment was found to suppress the LPS-mediated induction of miR-155 via a STAT3-dependent mechanism which utilises the Ets1 binding site within the miR-155 host gene²⁰⁴.

Outside of the inflammatory context, key transcriptional regulators of miR-155 include Mothers against decapentaplegic homolog 4 (smad4), breast cancer gene 1 (BRCA1), interferon regulatory factor (IRF), interferon-sensitive response element (ISRE), enhancer-box elements (E-box), and forkhead box P3 (FOXP3) which also feature bindings sites within the miR-155 host gene (Figure 1.3.1)^{241,255–257}.

Beyond the transcriptional control of miRNAs, multiple regulatory proteins may facilitate the regulation of specific miRNA subsets through modulation of

the biogenesis process. In particular, by regulating processes such as the incorporation and cleavage of pri-miRNA at the microprocessor and pre-miRNA by Dicer, the export of miRNAs from the nucleus and their stability once mature, miRNA maturation can be closely regulated in response to specific cellular cues. In the case of miR-155 its pro-inflammatory function makes its post-transcriptional regulation imperative, so that the misregulation of such mechanisms do not give rise to the aberrant expression found within detrimental contexts such as cancers and chronic inflammatory disorders.

Regulation of pri-miR-155

The presence or absence of cis-regulatory motifs (section 1.2.3) have been found to be critical in facilitating pri-miRNA incorporation and efficient cleavage by the microprocessor.

Human pri-miR-155 does not feature an apical UGU motif, known to facilitate DGCR8 binding, while its mGHG motifs, associated with accurate Drosha-mediated cleavage, have been predicted by Chul Kwon *et al.* to have no significant effect on cleavage site determination¹⁴². Thus, its basal UG motif is the only key site of cleavage determination present. Its location 2 nt upstream of the predicted basal junction leads to the possibility of alternate cleavage events, with the Drosha known to cleave both 13 bp upstream of the basal junction and 14 bp upstream of the UG motif, depending on the contribution of other motifs¹⁴². In addition, the lack of a CNNC motif 17–18 nt downstream of the cleavage site makes regulation of pri-miR-155 processing by the Microprocessor co-factors DDX17 and SRF3 unlikely^{147,258}. Overall, these

factors, coupled with the predicted structural features of pri-miR-155 such as its small apical loop of 4 nt, present a pri-miRNA structure indicative of reduced accuracy and efficiency of processing as a result of sparse microprocessor interactivity¹⁴⁷. It could be speculated that this is advantageous, acting as a buffer against mis-regulated miR-155 transcription, the detrimental consequences of which being apparent in the known oncogenic and chronic inflammatory functions of miR-155-5p^{243,246}. For example, a hereditary breast cancer associated mutation within the pri-miR-155 sequence leads to increased expression levels, speculated to be due to enhanced microprocessor activity as a result of a more open pri-miRNA structure²⁵⁹.

KHSRP has been identified as an enhancer of pri- and pre-miR-155 cleavage efficiency within macrophage cell lines, conforming to a wider function of the protein as it interacts with the Microprocessor and Dicer through binding to the pri- and pre-miRNA apical loop, promoting cleavage in a subset of miRNAs^{165,223,260}. In addition, activation of KHSRP by type 1 interferon within TLR7 stimulated dendritic cells was associated with enhanced miR-155-5p but reduced miR-155-3p expression, implying that KHSRP may reinforce miR-155 strand selection²⁶¹.

Recently, it was found in a dextran sodium sulphate (DSS) induced murine model of ulcerative colitis that neurite outgrowth inhibitor B (Nogo-B) knockdown induces pri-miR-155 but reduces pre- and mature miR-155 expression in macrophage cells²⁶². Nogo-B was found via co-

immunoprecipitation experiments to associate with the RBP p68 (DDX5), with p68 knockdown preventing miR-155 induction as a result of Nogo-B overexpression. Elsewhere p68 has been identified as a regulator of microprocessor activity, showing association with both Drosha and DGCR8 in co-immunoprecipitation experiments^{90,263}. However, whether p68 regulates miR-155 outside of the context of DSS treatment remains to be seen.

Immobilised miRNA hairpins were used by Treiber *et al.*, to examine novel RBPs which act to regulate miRNA biogenesis. Lysates from 13 different human cancer cell lines showed pre-miR-155 to bind to multiple RBPs including zinc finger 346 (ZNF346), zinc finger 385A (ZNF385A) splicing factor 1 (SF1) and ADARB1²⁶⁴. Although associated with RNA binding, processing, and stabilisation none of these have been shown to regulate miRNAs, with further experimentation necessary to confirm this function.

Lastly, the timely control of miR-155 degradation is vital to facilitate the resolution of the inflammatory response once infection has been cleared. Notably, both miR-146a and miR-21 have long half-lives, with this prolonged stability leading to reduced miR-155 expression at later stages of inflammation as they enhance anti-inflammatory pathways^{249,265}. It has been demonstrated that a loss of miR-146-based control of miR-155 leads to more rapid and prolonged miR-155 induction. Beyond this, however, the mechanism by which miR-155 stability is controlled has yet to be identified.

1.3.2 - miRNA-155 and Cancer

miR-155 is one of the most studied oncogenic miRNAs, with its dysregulated expression identified in both solid and haematological cancers including lung, breast, pancreatic, gastric, colorectal and endometrial cancers as well as melanoma, glioblastoma and osteosarcoma^{266–274}. A core oncogenic feature of miR-155 is its association with cancer drug resistance, with the injection of miR-155 overexpression vectors into lung cancer cells eliciting elevated levels of resistance to the drug Cisplatin, while miR-155 inhibition resulted in impaired resistance development²⁷⁵. Additionally, administration of chemotherapeutics to osteosarcoma cells resulted in increased expression of miR-155 alongside an increase in autophagy and reduced drug effectiveness²⁷⁶. In lung cancer and leukaemia this drug-resistant function of miR-155 has been associated with miR-155's direct negative regulation of the tumour suppressor gene TP53, the gene that encodes p53, this gene itself forming a negative feedback loop with miR-155, although the precise mechanism whereby this contributes to cancer drug resistance is unknown²⁷⁵.

As well as playing a role in the cancerous tissue itself, miR-155 facilitates key processes which orchestrate the immune response to cancer and the development of the tumour microenvironment^{272,277}. These regulatory processes are immune cell dependent, with upregulation of miR-155 having pro- or anti-tumour effects in different immune cell types²⁷⁸. For example, through miR-155-mediated reduction in IL-13 signalling miR-155 expression promotes a decrease in the local population of pro-tumour M2 polarised

macrophages, while miR-15-mediated repression of SOCS1 and SHIP-1 in myeloid-derived suppressor cells promotes colony formation, proliferation and resultant tumour development ^{247,279}.

1.3.3 - miRNA-155 and Rheumatoid Arthritis

Rheumatoid arthritis (RA) is a chronic inflammatory disorder of the joints, whereby an autoimmune response gives rise to symptoms such as synovial hyperplasia, bone and cartilage degradation and autoantibody production ²⁸⁰.

miR-155 is implicated at the core of this disease, with blood and synovial monocytes of RA patients having significantly increased expression of the miRNA, and miR-155 deficient mice showing resistance to RA induction ²⁸¹.

miR-155 is thought to facilitate RA pathogenesis via a multi-level mechanism.

Synovial monocytic miR-155 promotes the release of inflammatory chemokines which recruit more monocytes to the synovium, while also supporting migration into inflamed tissue by upregulated lymphocyte function-associated antigen 1 (LFA-1) expression ^{282,283}. miR-155 also downregulates the chemokine receptor CCR2, reducing the migration of the monocytes already present in the synovium. Finally, miR-155 causes the upregulation of multiple pro-inflammatory cytokines, such as TNF, and inhibition of anti-inflammatory cytokines, such as IL-10, promoting M1 polarisation and the inflammatory phenotype ²⁸¹.

In order for miR-155 to perform its role in RA pathology a mechanism must exist for the miRNAs chronic induction. TLR4 has been shown to be highly expressed in synovial tissue of RA patients, with TLR4 deletion and inhibition

experiments showing a reduced RA phenotype^{284,285}. As previously outlined, miR-155 can be induced by the TLR4 pathway, which can be activated by not only exogenous LPS, but also endogenous ligands. Of these ligands tenascin-C (TN-C) has shown itself to be essential for the chronic inflammatory response within RA^{286–288}. This extracellular matrix glycoprotein is shown to be upregulated in the synovia, synovial fluid, and cartilage of RA patients, with its knockout eliciting a significantly reduced chronic inflammatory phenotype.

Importantly, TN-C has been found to directly signal downstream of LPS activated TLR4, causing upregulation of TNF translation via post-transcriptional induction of miR-155 expression in bone marrow-derived macrophages²⁸⁹. This induction appears to be miR-155 specific, not affecting other LPS-responsive miRNAs. Through this mechanism, TN-C plays a central role to the early inflammatory response, with its genetic ablation eliciting decreased TNF synthesis and a resultant reduction in pro-inflammatory mediators' synthesis *in vivo*, in a model of LPS-induced sepsis, and *in vitro*, in LPS-activated bone marrow-derived macrophages. This presents the central question of this thesis, in identifying by what mechanism TN-C induces post-transcriptional upregulation of miR-155.

1.4.0 – Tenascin-C

Tenascin-C (TN-C) is a glycoprotein component of the extracellular matrix (ECM), a dynamic cell surface lattice-work responsible for the maintenance of tissue morphology and architecture, as well as the regulation of cellular survival and behaviour in response to environmental stimuli. The ECM consists

of a diverse range of proteins, glycoproteins, proteoglycans and polysaccharides, the varying expression levels and interactions of which give rise to the structural, biochemical, and functional diversity of the ECM and the tissue it supports ^{290,291}.

The TN-C glycoprotein consists of six subunits arranged in a hexabrachion structure with the heptad repeats within each subunits N-terminal tenascin assembly (TA) domain interfacing to form the centre of the structure (Figure 1.4.1) ^{292,293}. Each subunit arm contains 14.5 epidermal growth factor-like (EGFL) repeats followed by up to 17 conserved and alternatively spliced fibronectin-type III (FNIII) domains and a C-terminal fibrinogen globe (Figure 1.4.1). This provides TN-C with a highly multivalent structure, with each subunit arm being able to interact with separate environmental, ECM and cellular factors or receptors, as well multiple subunits being able to reinforce interactions with the same target. Additionally, through alternative splicing of the FNIII domains, TN-C isoforms can be produced with varied functionalities ²⁹⁴. For example, the smallest TN-C isoform, lacking any optional FNIII domains, promotes cell attachment and focal adhesion formation via strong binding to fibronectin ²⁹⁵. Meanwhile, larger, less spliced, isoforms have been shown to drive cell migration and inhibit focal adhesion, possibly via a reduction in fibronectin binding affinity ²⁹⁶.

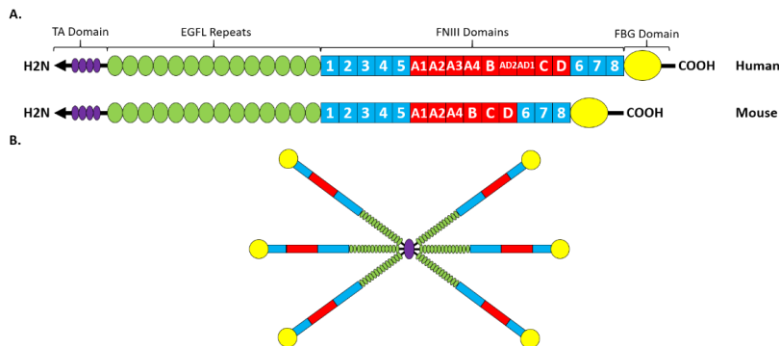


Figure 1.1.1.1. Protein Topology of Tenascin-C (TN-C). A) Subunit topology of mouse and human TN-C. Depicted are the N-terminal Tenascin Assembly (TA) domain, containing four heptad repeats, the epidermal growth factor-like (EGFL) repeats, the conserved (blue) and alternately-spliced (red) fibronectin-III (FNIII) domains and the C-terminal fibrinogen globe (FBG) domain. B) The TN-C hexabrachion complex topology. Adapted from ²⁹³.

TN-C is generally considered a modulator of cell adhesion, migration, spreading and proliferation, depending on environmental and intracellular cues ²⁹⁷. This is achieved via interactions with numerous ECM binding partners, including collagen, fibronectin and proteoglycans, as well as cell surface proteins such as syndecan-4, receptors such as TLR4, epidermal growth factor receptor (EGFR) and integrins, and signal molecules such as those of the TGF- β superfamily. Importantly, expression of TN-C is greatly restricted in adult tissue, being limited to areas of high tensile strain, such as tendons and ligament, and locations of obligatory cell turnover, plasticity, and remodelling such as stem cell niches, lymph nodes and the spleen ²⁹⁴. Outside of these locations TN-C induction is rapid and transient, acting as a hallmark of inflammatory or regenerative activity, while prolonged TN-C upregulation is indicative of cancerous or chronically inflamed tissue ^{298–300}.

1.4.1 – Tenascin-C in Inflammation

Cellular stress and tissue damage can give rise to a “sterile” immune response, so named due to the activation of PRRs in the absence of exogenous PAMPs, the purpose of which being to clear destroyed cell contents and to restore tissue integrity via immune cell localisation and regenerative mediator release³⁰¹. This requires the activation of PRRs via endogenous ligands such as TN-C whose expression is induced upon tissue injury and infection. TN-C can bind to three surface receptors to elicit a pro-inflammatory response, TLR4 and the integrins $\alpha9\beta1$ and $\alphaV\beta3$, all of which have been shown to act primarily via the NF- κ B activation pathway³⁰¹. This is of importance as TN-C is a transcriptional target of NF- κ B, leading to its upregulation in inflamed tissue and creating a positive feedback loop, with newly synthesised TN-C furthering the endogenous sterile response within the tissue³⁰¹.

Interestingly, activation of TLR4 by TN-C and LPS show distinct, though overlapping downstream effects. Both lead to the upregulation of NF- κ B and MAPK pathway activation, however while the LPS response yields an aggressive anti-infectious phenotype, TN-C based induction of TLR4 also leads to increased expression of ECM proteins, facilitating tissue repair and regeneration³⁰². TN-C has been shown to activate TLR4 in immune cells such as macrophages, neutrophils and dendritic cells as well as non-immune cell types such as chondrocytes and fibroblasts, illustrating the tissue wide need for this strong sterile immunity mediator^{32,303–305}.

As well as playing a role in sterile immunity, TN-C has also been shown to be intrinsic to the TLR4-mediated response to pathogenic infection²⁸⁹. LPS induction of murine macrophages shows rapid upregulation of cell surface TN-C, with TN-C itself being responsible for upregulation of the central pro-inflammatory cytokine TNF via post-transcriptional regulation of miR-155, as shown by TNC knockout models. Importantly, this effect of TN-C on TNF is not coupled to the action of TN-C as a TLR4 ligand, as its effects are translational as opposed to the TLR4 pathways transcriptional effects. This outlines a dual role for TN-C, as a driver of both sterile and pathogenic infection. The posttranscriptional response of TN-C to LPS leads to an immediate induction of pro-inflammatory mediators, faster than that of the TLR4 pathway, priming the inflammatory microenvironment against the pathogenic threat. Meanwhile, the sterile response to tissue injury promotes tissue repair and further induction of TN-C, the dysregulation of which can result in chronic inflammatory disorders such as RA and atherosclerosis.

1.4.2 – Tenascin-C in Cancer

TN-C is thought to aid in the formation of a pro-tumorigenic and metastatic microenvironment, promoting cancer cell dissemination, circulatory survival, proliferation and invasion in various tumours, including those of the lymph nodes, lung, and liver, leading to it being noted as a predictor of poor prognosis^{306–308}. One mechanism by which this is thought to occur is via TN-C acting to downregulate the Wnt suppressor Dickkopf1 (DKK1), stabilising beta-

catenin and promoting Wnt's pro-metastatic and pro-angiogenic target genes^{309,310}.

In 2017 it was discovered in an osteosarcoma cell line that TN-C promoted inhibition of yes-associated protein (YAP), an oncogenic factor associated with the suppression of apoptosis and the promotion of cell proliferation which lies at the centre of numerous cancers³¹¹. TN-C was shown to impair the formation of actin stress fibres, through activation of integrin $\alpha9\beta1$, a process which occurs in addition to TN-C acting as a competitive inhibitor for the stress fibre promoting interaction of fibronectin and syndecan-4/integrin $\alpha5\beta1$. Reduction in actin stress fibre formation leads to an increase in YAP phosphorylation and results in the transcriptional co-factors cytoplasmic localisation, away from its nuclear targets. This finding has far-reaching implications for TN-C, with a similar interaction in immune cells having the potential to bridge the mechanistic gap between TN-C and miR-155 post-transcriptional upregulation, opening potential new avenues for therapeutics.

1.5.0 – Integrins

1.5.1 – Overview

Since the identification of the integrin receptor family in 1987 by Hynes *et al.*, these receptors have been found to be key facilitators of cell-ECM and cell-cell interactivity and adhesion, in part due to their intracellular signalling capacity via the actin cytoskeleton³¹². Integrins play key roles in critical biological functions such as the immune response, development, leukocyte trafficking, haemostasis and cancer as well as multiple diseases^{313–317}.

There are 24 distinct integrins in humans, each forming a heterodimer containing one of eighteen α and one of eight β integrin subunits (Figure 1.5.1)³¹³. Each subunit is a type 1 transmembrane protein consisting of a short cytoplasmic tail, a single-pass transmembrane region and a large multidomain extracellular region. Each combination of subunits gives rise to an integrin receptor with unique ligand and signal specificity, leading to the grouping of integrin receptors into RGD, collagen, laminin and leukocyte-specific receptor subgroups based upon their primary ligands (Figure 1.5.1)

318.

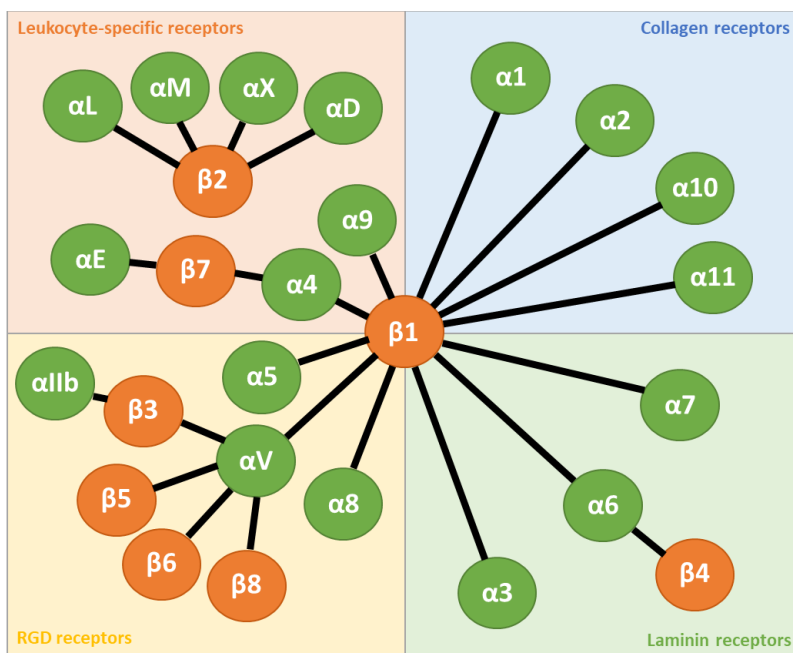


Figure 1.5.1. Summary of integrin subunits and their specificity of their complexes. Adapted from Steiger et al., 2021³¹⁹

The activation and downstream signalling of integrins is a multi-step bi-directional process with the receptor facilitating both intracellular and extracellular signals and outputs that are in turn regulated by cues from both environments (Figure 1.5.2) ³¹³. Often membrane integrins are expressed in an inactive state, with their activation controlled by intracellular cues (Figure 1.5.2.a). Through binding to the cytoplasmic tail region of integrins, intracellular adaptors such as talin and kindlin instigate conformational changes within the extracellular ligand binding domains, enhancing ligand binding affinity and activating inactive receptors (Figure 1.5.2.b) ^{311,320,321}. Binding to the extracellular ligand then leads to the integrins connecting to the actin cytoskeleton, the mechanical forces of which in turn promote integrin activation and clustering to form what is known as the focal adhesion complex (Figure 1.5.2.c) ^{322,323}. The formation of the focal adhesion complex promotes the association of additional intracellular binding partners and intracellular signal transduction ^{324,325}. Following signal completion, integrin receptors can be returned to an inactive state, this occurring through the destabilisation or inhibition of integrin-activating protein association ³²⁶. Additionally, active integrins may be removed from the plasma membrane via endocytosis, with these integrins being recycled back to the plasma membrane at a later time in response to regulatory cues.

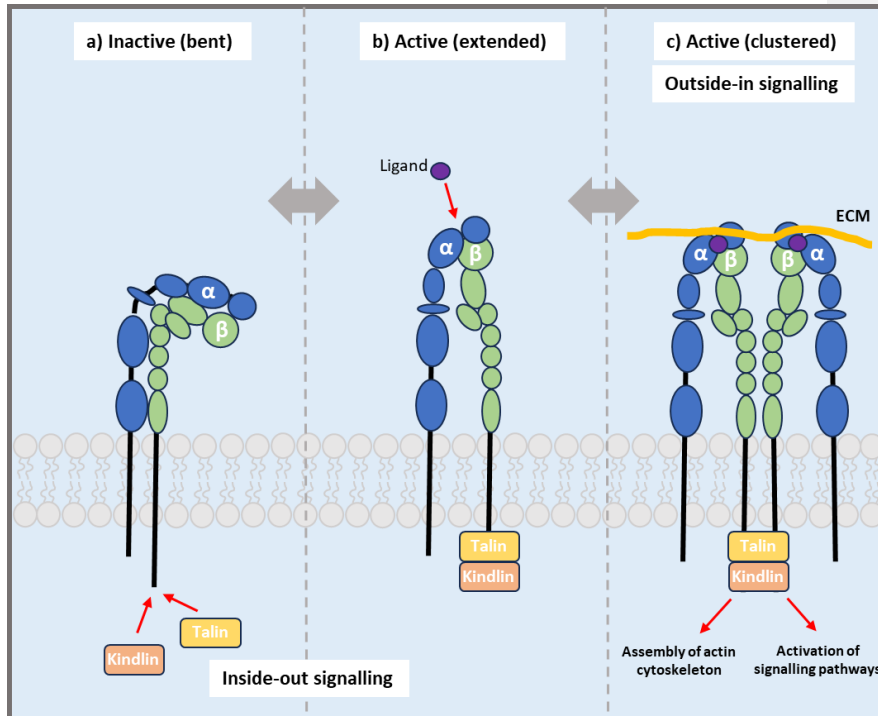


Figure 1.5.2. Summary of integrin membrane activation and clustering. Adapted from Chastney et al., 2021³²⁷.

1.5.2 – Integrins and TN-C

The large multi-domain hexameric structure of TN-C facilitates its interaction with a number of ECM components. This includes integrin receptors, with TN-C having the capacity to act as a direct integrin ligand or to modify other ligand-integrin interactions through binding to either participant.

TN-C acts as a direct ligand for the epithelial specific integrin $\alpha\beta6$ via predicted binding to the TN-C FNIII3 domain with binding associated with epithelial to mesenchymal (EMT) transition and potential poor cancer prognosis^{328–330}. A similar phenotype is seen as a result of TN-C binding to

$\alpha v\beta 1$, although the binding site is yet to be established³³¹. Exposure of MCF-7 cells to TN-C and TGF- β upregulates both mRNA and protein expression of $\alpha v\beta 6$, with only mRNA level rising with TGF- β treatment alone, thus marking TN-C as a potential stabiliser of the $\alpha v\beta 6$ protein³³¹. Integrin $\alpha 9\beta 1$ and TN-C have been found to co-localise within colorectal and gastric cancers with binding of TN-C facilitated via a non-RGD binding sequence within the glycoproteins FNIII3 repeat³³². Increased levels of both $\alpha v\beta 6$ and $\alpha 9\beta 1$ was also accompanied by increased TN-C staining within the epithelial cells of the oral mucosa undergoing wound repair³³³.

Integrin $\alpha v\beta 3$ binds to TN-C at two locations within the FNIII3 RGD sequence as well as at the C-terminal FBG^{334–336}. Plating of cells on TN-C-coated substrates shows enhanced proliferation and migration of smooth muscle cells, this being attributed to enhanced $\alpha v\beta 3$ and PDGF receptor- β crosstalk within focal adhesion complexes³³⁷. In human endothelial cells, both $\alpha v\beta 3$ and $\alpha 2\beta 1$ have been found to facilitate cell attachment and spreading on TN-C-coated plates, with both integrins identified as receptors via immunoprecipitation experiments³³⁸. However, no such binding is found to occur within a TN-C adhesion assay performed within osteosarcoma MG63 cells, while αv , $\beta 1$, and $\beta 6$, but not $\alpha 2$ subunits could be detected within a TN-C binding assay performed upon MCF-7 lysates³³¹. This illustrates the cell-type and condition specific nature of TN-C integrin binding.

Outside of direct action as an integrin ligand, TN-C has been found to modulate the co-receptor activity of syndecan-4, which itself facilitates

fibronectins activation of integrin $\alpha 5\beta 1$ signalling³³⁹. TN-C performs this function through either binding to the FNIII13 domain of fibronectin, blocking syndecan-4 association, or via direct binding to the syndecan-4 heparin sulphate side chains, thus preventing syndecan-4 by performing its co-receptor function^{339,340}. Through this modulation of integrin $\alpha 5\beta 1$ TN-C has been shown to impairing stress fibre formation within a murine xenograph model of osteosarcoma, this function also being facilitated via TN-Cs activation of integrin $\alpha 9\beta 1$ ³¹¹. This illustrates one of the primary intracellular effector functions of integrins in modulating the actin cytoskeleton.

1.6.0 – The Actin Cytoskeleton

1.6.1 – General

The actin cytoskeleton is comprised of polymeric actin filaments (F-actin) which dynamically assemble from cytoplasmic monomeric actin protein (G-actin) in a process regulated by a number of actin binding proteins^{341–343}. 10–30 actin filaments may form together into stress fibres, the F-actin being cross-linked together primarily via the action of the protein α -actinin and interspersed with non-muscle myosin and tropomyosin structures^{344–347}. Stress fibres play critical roles in maintaining cellular shape, substrate tension and cellular motility³⁴⁸.

In brief, F-actin constitutes a polar structure, with a barbed end (+) and a pointed end (-) (Figure 1.6.1)³⁴³. G-actin binds preferentially to the +-end due to the action of actin assembly factors such as profilin and the actin-related protein 2/3 complex (Arp2/3), while G-actin is actively removed from the –

end to be used in +-end elongation ³⁴⁹. Depending on the regulation of actin assembly factors, F-actin may form a number of differing structures, the most characterised of them being the linear unbranched actin filaments induced by formins or Ena/VASP proteins and the branched filament structure induced by Arp2/3 incurring the formation of 'daughter filaments' splitting off from the main F-actin structure ^{350,351}.

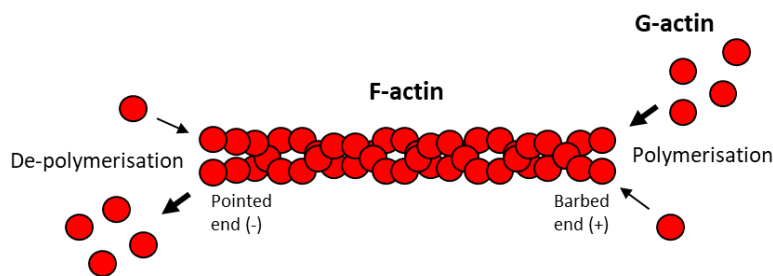


Figure 1.6.1. Schematic of the polar polymerisation of globular (G-) actin into filamentous (F-) actin. Elongation of the F-actin filament occurs at the barbed (+) end, while G-actin is actively removed from the pointed end (-), this facilitating the dynamic assembly and disassembly of the actin cytoskeleton.

The actin cytoskeletal structure aids in maintaining cell shape, driving cell movement and facilitating cellular mechanosensing ³⁴¹. Through the precise and coordinated control of actin filament assembly and disassembly, cellular contents may be manipulated through processes such as vesicle trafficking, endocytosis, exocytosis and organelle movement, while also facilitating wider processes such as cell-cell signalling and gene transcription ³⁵².

1.6.2 – Actin Cytoskeleton and the macrophage

As characteristically motile cells, a number of key macrophage functions are facilitated through the dynamic regulation of the actin cytoskeleton, including

chemotaxis, phagocytosis and antigen presentation^{353–355}. Moreover, the intrinsic links between the actin cytoskeleton and inflammatory induction and regulation continue to emerge.

Recently, Ronzier *et al.*, identified through a combination of gene knockout and microscopy experiments that the macrophage cytoskeleton undergoes distinct architectural changes in resting, acute and sustained inflammatory states³⁵⁶. BMDMs stimulated with LPS and IFN γ for 20 minutes were characterised by a tight association of myosin IIA and F-actin within the perinuclear space, leading to a contractile phenotype. Meanwhile, prolonged stimulation for 24h showed a loss of this association, with F-actin more uniformly distributed around the cell, creating a spreading phenotype. This temporal regulation of inflammatory macrophage morphology was found to be elicited by myosin-II induced contractility via tight stress fibre formation giving way to the Arp2/3 dependent spreading of actin filaments.

Furthermore, the actin cytoskeleton was found to directly regulate macrophage inflammatory activity. Inhibition of Myosin II was found to suppress the pro-inflammatory mediator iNOS, impeding inflammatory induction, while Arp2/3 disruption elevated iNOS levels leading to an opposed inflammatory impact³⁵⁶. As iNOS is an actin binding protein closely regulated by the proteasome, it is speculated that binding to myosin-II filaments may delay proteolytic turnover and thus leading to enhanced iNOS activity^{356–358}. Arp2/3 has also been found to negatively regulate NF- κ B and MAPK inflammatory activation within macrophages and fibroblasts^{356,359}. This

highlights the critical interplay between the actin cytoskeleton and macrophage inflammatory induction, with additional interplay being revealed as the role of the cytoskeleton-modulated protein YAP as an inflammatory regulator emerges.

1.7.0 – Yes-Associated Protein (YAP)

YAP1, and its genetic paralogue; WW-domain-containing transcription regulator 1 (WWP1/TAZ), are transcriptional co-factors, the primary function of which being to regulate activity of transcriptional enhancer factor domain (TEAD) family transcription factors³⁶⁰. The YAP1 gene is located at 9qA1 within the mouse genome, with this giving rise to the 488 amino acid primary isoform YAP1-201 (ensemble ID), with a theoretical molecular mass of 52.38 kDa (UniProtKB-P46938). In addition is YAP1-202, the most well validated isoform which lacks amino acids 313-328, potentially eliciting changes in interaction with targets³⁶¹. Due to the 46% amino acid homology of YAP1 and TAZ as well as their similar activity and the two being regulated by similar mechanisms, they are often functionally grouped (Figure 1.7.1)³⁶².

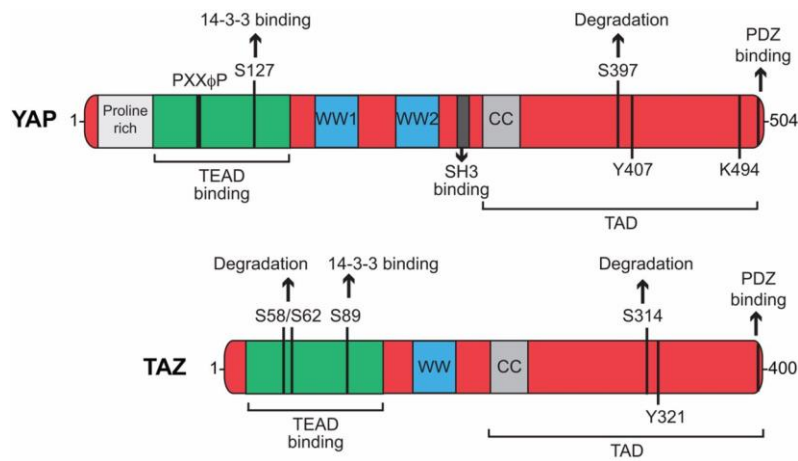


Figure 1.7.1. Schematic of YAP1/TAZ regulatory domains. Including; the coiled-coil (CC) domains, WW domain, the transcriptional enhancer factor domain (TEAD) binding domain, the transcriptional activator domain (TAD), the PDZ-binding motif and the YAP specific SH3-binding domain, second WW domain and proline rich region. Also indicated are the phosphorylation sites which induce degradation or 14-3-3 binding protein ³⁶³.

Both YAP and TAZ are the primary effectors of the Hippo pathway, a serine/threonine kinase signalling cascade, first identified in *Drosophila*, which is responsible for the regulation of organogenesis, cell proliferation, survival, differentiation, and tissue homeostasis through monitoring extracellular cues (Figure 1.7.2) ^{364,365}. The Hippo pathway begins with the activation of mammalian ste-20-like kinase 1/2 (MST1/2) with this kinase, alongside its scaffold proteins, protein salvadore homolog 1 (SAV1) and mob kinase activator 1 A/B (MOB1A/B), phosphorylating the hydrophobic residues of the large tumour suppressor 1/2 (LATS1/2) ^{366,367}. LATS1/2 then undergoes autophosphorylation, resulting in the proteins activation and phosphorylation of YAP/TAZ ³⁶⁸.

Importantly LATS1/2 phosphorylation has been found to be inhibited by actin cytoskeletal polymerisation (Figure 1.7.2)³⁶⁹. This has been shown in contexts of actin assembly as a result of G-protein coupled receptor (GPCR) or integrin receptor activity giving rise to actin polymerisation through activating Rho GTPases^{311,369}. Inhibition of actin cytoskeletal assembly through treatment with cytochalasin D or latrunculin B in turn induces phosphorylation of YAP, an effect that is reversed in cells featuring LATS1/2 knockout or a mutated YAP phosphorylation site^{370,371}. This may be attributed to the action of protein kinase As (PKAs) downstream of the actin cytoskeleton, which activate LATS1/2 via phosphorylation and elicit resultant YAP phosphorylation³⁷². Additionally, LATS1/2 has also been found to directly bind actin filaments and inhibit polymerisation in a N-terminal dependent manner, this binding perhaps also acting as a means for F-actin assembly to inhibit LATS1/2³⁷³. Thus LATS1/2 and F-actin may form a dynamic system, whereby F-actin assembly, based upon extracellular cues, inhibits LATS1/2 and subsequent downstream hippo pathway activity only when there is not a sufficient abundance of LATS1/2 to block filament assembly.

Phosphorylation of YAP at residues S127/S89 facilitates binding of 14-3-3 proteins to YAP/TAZ, resulting in YAPs cytoplasmic sequestration and inability to perform their effector functions (Figure 1.7.2)³⁷⁴⁻³⁷⁶. Alternately, phosphorylation by LATS1/2 at S381/S311 promotes further phosphorylation by casein kinase 1 δ/ϵ , allowing YAP/TAZ ubiquitination and degradation via Skp, Cullin, F-box containing (SCF) E3 ubiquitin ligase recruitment^{372,377}. Thus, suppression of the Hippo-pathway occurs during conditions such as tissue

injury, whereby YAP/TAZ nuclear localisation is unimpeded, and the resultant transcription factor activity gives rise to wound healing via increased cell proliferation and migration^{378,379}. However, YAP/TAZ have also been identified as hyper-activated in multiple human cancers, such as breast, prostate, ovarian and endometrial cancers as well as osteosarcoma, meningioma and acute myeloid leukaemia, leading to increased tumour cell survival, proliferation and epithelial to mesenchymal transition^{380–386}. This highlights the critical role of YAP/TAZ in our understanding of human malignancies, with more recent studies beginning to also uncover the proteins role in the innate immune response to infection³⁸⁷.

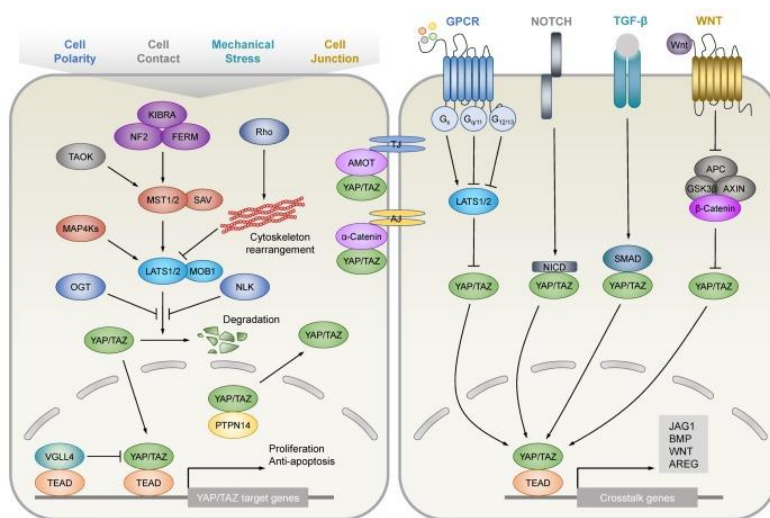


Figure 1.7.2. Schematic of the mammalian Hippo pathway and its cross-talk with other signalling pathways. The multiple stimuli which elicit suppression of YAP/TAZ via the MST1/2-LATS1/2 mediated signalling cascade and this pathways regulators (left). Additionally, the

other signalling pathways which have been found to crosstalk with the Hippo pathway (right)³⁸⁸.

1.7.1 – YAP and Inflammation

Due to a combination of the non-adherent and plastic structural nature of primary immune cells the role of YAP in the context of their mechano-regulation was little studied^{389,390}. Moreover, the role of YAP in the regulation of the innate immune response had been critically overlooked largely due to YAPs low abundance within monocyte lineage cells leading to an assumed non-functionality³⁹¹. However, in recent years a functionality of YAP within the primary inflammatory response has emerged, linking mechanical cues and inflammatory regulation.

Although low relative to endothelial and fibroblast cells, the expression of YAP1 by monocytes increases upon differentiation into adherent macrophages as well as during pro-inflammatory or wound healing responses. Examination of YAPs functionality within BMDMs shows YAP knockdown to inhibit differentiation of the macrophage cells into osteoclasts³⁹². Moreover, within BMDMs and peritoneal exudate macrophages (PEMs) YAP has been found to promote differentiation into M1 macrophages, while loss of YAP leads to differentiation in M2 cells³⁹³.

YAP1 has been identified as an inflammatory mediator, being implicated in the regulation of reactive oxygen species generation, the antiviral response and TLR4 driven bacterial inflammation^{394–398}. However, the exact role of

YAP1 within the macrophage is mixed, with seemingly contrasting pro and anti-inflammatory mechanisms being identified.

Through inhibition of YAP1 signalling the Hippo-pathway acts as a positive regulator of anti-bacterial inflammation in both drosophila and mammals ³⁸⁷.

Within endothelial cells YAP1 has been shown to downregulate the activation of the core inflammatory transcription factor NF- κ B via promoting the degradation of TRAF6, a signalling molecule of the LPS induced TLR4 response ³⁹⁶. Additionally, YAP1 overexpression in a murine osteoarthritis model attenuated NF- κ B signalling via disruption of TAK1, IKK α and IKK β interaction, leading to alleviation of osteoarthritic symptoms ³⁹⁷.

However, recent studies conflict with this evidence, showing that YAP1 may show a different functionality in the macrophage. Investigation into the effect of YAP1 on macrophage polarisation in inflammatory bowel disease (IBD) and myocardial infarction show that YAP1 knockdown instead enhances pro-inflammatory genes such as IL-6 in a non-NF- κ B-dependent manner ^{393,399}.

Additionally, YAP1 has been found in macrophages to bind the NF- κ B subunit p50 and aid NF- κ B nuclear translocation, with inhibition of this interaction via lactate treatment reducing pro-inflammatory cytokine production ⁴⁰⁰.

Consistent with these findings, knockdown of YAP in monocyte-derived macrophages has been shown to impair TNF- α secretion in response to LPS treatment, as well as suppressing LPS induced systemic inflammation in myeloid cells and proinflammatory cytokine production in LPS treated Kupffer cells ⁴⁰¹⁻⁴⁰³. Finally, contrary to discoveries in endothelial cells, macrophage

TRAF6 was found to bind to and increase YAP1 nuclear localisation, promoting the development of atherosclerosis ⁴⁰⁴.

A link between the role of YAP in mechano-transduction and the inflammatory response have also been identified. Culturing of cells on stiff substrates, such as the commonly used tissue culture plastic, leads to nuclear YAP localisation, with the inflammatory cytokines IL-1 β and LPS enhancing this effect ⁴⁰¹. Cell culture on stiff substrates is linked to increased production of pro-inflammatory mediators such as IL-1 β , IL-6, TNF- α and TLR4, with these factors in turn promoting YAP nuclear localisation which furthers pro-inflammatory signalling ^{401,405}.

Upstream MST1 and LATS1 also display a role in inflammation, as inflammatory cytokines such as TNF and IL-1 β have been shown to lead to their activation, potentially via MAP4K signalling, resulting in reduction of active YAP and attenuation of its anti-inflammatory role once pro-inflammatory cytokine expression is established ³⁹⁷.

1.7.2 – YAP and miRNA regulation

Increased cell confluency has been associated with enhanced miRNA expression in a diverse range of cell lines, including primary fibroblasts, HeLa, MCF7 and HEK293 cells among others, although not in lymphoma or leukaemia cell lines ⁴⁰⁶. This change in miRNA levels was attributed to the increased abundance of cell-cell contacts, with miRNA expression not found to correlate with enhanced cell proliferation or quiescence, these being two other outcomes of increased confluency. Hwang *et al.*, identified enhanced

Drosha processing as the primary cause of increased miRNA expression, with high confluency also shown to enhance the efficiency of RISC formation ⁴⁰⁶. Later Mori *et al.*, also found increased cell confluency to enhance miRNA expression, this time on a global basis but with examination limited to immortalised human keratinocytes (HaCaT). This change being also attributed to enhanced microprocessor activity ⁹². Regulation of the microprocessor by cell confluency was directly attributed to YAP, the nuclear localisation of which in low confluency cells lead to it binding and sequestering the microprocessor co-factor p72 (DDX17). The binding of p72 by YAP, confirmed by co-immunoprecipitation and gel-filtration, prevents p72's association with the microprocessor, leading to reduced pri-miRNA processing. Increased cell confluency or constitutively phosphorylated YAP, which both lead to YAPs cytoplasmic sequestration, as well as YAP knockdown or YAP-p72 binding site mutation, all lead to enhanced miRNA expression.

YAPs role as a transcriptional co-factor has been associated with reducing miRNA expression within colorectal cancer through promoting transcription of RAN binding protein 1 (RANBP1) ⁴⁰⁷. RANBP1 expression is associated with reduced nuclear export of miR-18a, miR-183 and miR-106b pre-miRNA via reduction of exportin-5 abundance. In addition, RANBP1 promotes the expression of YAP which itself promoted RANBP1 expression alongside TEAD, creating a positive feedback loop which hampers miRNA export.

However, the role of YAP as a negative regulator of global miRNA levels is disputed. Chaulk *et al.*, quantified miRNA levels in the human mammary

epithelial cell line MCF10A at low and high confluency, noting increased pre-miRNA but reduced mature miRNA levels in higher confluency cell ⁴⁰⁸. YAP knockdown in low confluency cells was found to mirror the high confluency pre/mature miRNA ratios. Notably, let-7a and let-7b did not conform to this regulatory effect, instead showing increased mature miRNA levels in high confluency and YAP knockdown cells. Overall, this effect of YAP was contributed to increase levels of the negative let-7 biogenesis regulator LIN28B as a result of a post-transcriptional mechanism reliant on the nuclear localisation of YAP ⁴⁰⁸. This coupled with the function of let-7a and let-7b as negative regulators of Dicer mRNA translation, leading to reduced pre-miRNA processing in high confluency cells where as a result of YAPs cytoplasmic localisation LIN28B levels are lowered and let-7a/b levels are enhanced ⁴⁰⁸.

Furthermore, YAP has also been found to directly upregulate miRNA transcription, promoting the expression of the gene MCM7 and its contained miRNA cluster of miR-25, miR-93 and miR-106b, all oncogenic miRNAs which inhibit p21 expression ⁴⁰⁹.

Interestingly, examination of miRNA expression in YAP1 depleted chondrosarcoma fibroblast-like (SW1353) cells identified a sizeable proportion of both up and downregulated miRNAs ⁴¹⁰. This illustrates the complexity of YAPs miRNA regulation functionality which is, similar as in its inflammatory function, likely heavily modified by the mechanical context of the cell such as cell confluency and the cells tissue origin.

1.7.3 – YAP and Tenascin-C

As outlined previously (section 1.6.0) TN-C is a key structural and functional element of the ECM which through moderating or directly binding to cell surface receptors may influence internal cellular properties such as the actin cytoskeletal structure. As such, TN-C and YAP are linked in a number of cellular systems as a sensor of and responder to extracellular cues.

The culturing of cells upon TN-C-coated plates or TN-C-supplemented cell-derived matrices has been associated within osteosarcoma, chondrogenic teratocarcinoma and endothelial cells with enhanced YAP phosphorylation, increased cytoplasmic localisation and reduced YAP transcriptional activity^{311,411,412}. This outcome has also been observed within prostate cancer epithelial cells treated with exogenous TN-C⁴¹³. This inactivation of YAP is attributed to TN-C mediated disruption of the actin cytoskeleton, being reversed via treatment with the stress fibre promoting factor lysophosphatidic acid (LPA)^{311,412}. Furthermore, Lee *et al.*, and Sun *et al.*, both directly attribute the regulation of the actin cytoskeleton by TN-C to integrin-based signalling, with Sun *et al.*, finding TN-C to trigger negative cytoskeletal regulation via integrin $\alpha 9\beta 1$ association, while Lee *et al.*, found blockage of integrin $\alpha 5\beta 1$ to alleviate the impact of exogenous TN-C treatment on YAP^{311,413}. Within these cases the regulation of YAP by TN-C is attributed to increased cell migration, metastatic progression and reduced patient survival, highlighting the clinical importance of YAPs regulation by TN-C^{311,411–413}.

However, evidence also exists indicating that TN-C may act to promote YAP activity. TNC knockout and TNC overexpressing Ewing sarcoma cells (A673) show decreased and enhanced YAP nuclear localisation, respectively ⁴¹⁴. Contrary to findings in prostate cancer cells made by *Lee et al.*, anti $\alpha 5$ antibody treated A673 cells show increased rather than decreased YAP inactivating phosphorylation ^{413,414}. Rather than negatively regulating YAP via disruption of the actin cytoskeletal, TN-C binding to integrin $\alpha 5\beta 1$ is proposed to promote YAP activity through activation of the Src pathway, with enhanced Src phosphorylation in TN-C overexpressing cells and the Src inhibitor saracatinib inhibiting YAP nuclear localisation ⁴¹⁴. Additionally, increased expression and subsequent secretion of TN-C by pancreatic cancer cells is associated with an increase in TN-C-mediated inhibition of the wnt signalling inhibitor dickkopf-1 (DKK1) through disruption of the actin cytoskeleton ^{310,415}. The inactivation of which is thought to enhance YAP activity via the wnt pathway triggering YAPs removal from the β -catenin destruction complex and subsequent nuclear localisation ^{415,416}.

Finally, in addition to TN-C regulating YAP activation, YAP itself is proven to function as a co-factor for TNC mRNA transcription. Within gastric cancer cells YAP was found to promote the expression of TN-C at both a protein and mRNA level, with YAP overexpression also found to activate the luciferase activity of a TNC promoter-luciferase construct ⁴¹⁷. Knockdown of YAP within a tenogenic cell line abolished the TN-C induction characteristic of tenogenic differentiation, this intriguingly not conforming to YAP knockdown experiments in superficial zone chondrocytes which show YAP knockdown to

not influence TNC expression^{418,419}. Meanwhile, YAP deficient embryonic kidney (HEK293) cells also show reduced TNC expression, with this attributed to binding of YAP/TAZ/TEAD4 to a TNC enhancer site shown via chromatin-immunoprecipitation followed by next-generation sequencing (ChIP-seq)⁴²⁰. Overall, this evidence indicates that TNC is transcriptionally controlled by YAP, thus creating opportunities for homeostatic feedback loops between these two proteins as the regulation of YAP by TN-C in turn leads modification of TNC expression.

1.8.0 – The p38 α /MK2 Pathway

1.8.1 – p38 α

With its discovery in 1993 p38 was placed into the mitogen-activated protein kinase (MAPK) family, with later findings separating the p38 group into its four protein constituents, these being p38 α (MAPK14), p38 β (MAPK11), p38 γ (MAPK12) and p38 δ (MAPK13)^{421–424}. The expression of these proteins is ubiquitous across the majority of mammalian tissues with the exception of p38 γ , with enhanced expression in skeletal muscles, and p38 δ upregulated in endocrinologically active organs as well as lung, kidneys and the gut⁴²⁵.

P38 proteins are unified in the presence of a conserved dual phosphorylation motif Thr-Gly-Tyr (TGY) within their kinase activation loop. Phosphorylation of both Thr and Tyr residues is necessary for full kinase activation of p38 proteins with the notable exception of p38 α , the mono-phosphorylation of which at Thr180 leading to a degree of kinase activity albeit with modified targeting

specificity^{426,427}. Overall, p38 α and p38 β share ~70% amino acid sequence homology, while p38 α and p38 γ/δ share ~60%.

P38 α activation is pivotal to the cellular response to a variety of stress stimuli including UV light, osmotic pressure, heat shock and glucose starvation as well as inflammatory signals such as LPS, cytokines and T cell receptor activation^{428–435}. P38 α knockout mice are embryonic lethal with a similar phenotype witnessed in knockout mice for MKK3 and MKK6, upstream mediators of P38 α ^{436,437}. On the other-hand, knockout of other p38 MAPKs are viable, leading to them being considered as secondary actors compared to p38 α and as a result being less intensely studied^{438,439}.

The MAP2Ks MKK3 and MKK6 are the key upstream kinases responsible for the phosphorylation and subsequent activation of p38 α with MKK4 also having the potential to phosphorylate p38 α to a reduced extent^{424,440}.

Upstream of the MAP2Ks are MAP3Ks such as TAK1 (MAP3K7), ASK1 (MAP3K5), DLK (MAP3K12) and MEKK4 (MAP3K4), which have been found to induce MKK6/MKK3 activation and subsequent phosphorylation of p38 α ^{441–443}. Intriguingly Rho family GTP-binding proteins may also mediate p38 α via binding to upstream activators of MAP3Ks such as MEK1 (MAP2K1) and MLK1, this providing a means whereby integrin binding and other mechanical cues may mediate p38 α activation^{444,445}.

p38 α may also be activated via pathways outside of the traditional MAP-kinase cascade. One example of which is through TAK1-binding protein 1 (TAB1) which directly binds to and promotes autophosphorylation of both

Thr180 and Tyr182 residues leading to full activation of p38 α ⁴⁴⁶. Alternately, ZAP70 can bind and phosphorylate p38 α at Tyr323, leading to autophosphorylation of p38 α at Thr180 and allowing partial activation to occur ⁴⁴⁷.

In turn, p38 α may be inactivated through de-phosphorylation of its key activation loop residues primarily via the action of MAPK phosphatases (MKPs) and dual specificity phosphatases (DUSPs) ⁴⁴⁸. MKP1/DUSP1, MKP5/DUSP10, MKP8/DUSP26, DUSP8 and DUSP12 are all known to act as inhibitory phosphatases of p38 α ⁴⁴⁹. Notably, p38 α activity leads to upregulation of MKP1, presenting as example of p38 α self-regulation via a negative feedback loop ⁴⁵⁰.

Upon activation, p38 α localised to the nucleus due to a conformational change which exposes a binding site for nuclear chaperones ⁴⁵¹. This facilitates its subsequent interaction and regulation of a number of downstream proteins in a cell type and stimulus dependent manner. These targets include transcription factors, MAPK pathway regulators, structural proteins, RNA binding proteins and downstream MAPKAPK proteins such as MK2, which themselves regulate a number of downstream targets ⁴⁵². Binding of p38 α may positively or negatively affect target activity depending on the phosphorylation site location. Through this web of pathways p38 α is involved in a diverse range of biological functions such as embryonic development, differentiation, cell cycle regulation and inflammation ^{453–456}.

1.8.2 – MAPKAPK2 (MK2)

As its name suggests, the MAPK activated protein kinase 2 (MAPKAPK2, simplified to MK2 hereafter) is a member of a conserved family of MAPKAPKs, downstream effectors of the various MAPK kinase pathways. This family consists of MK2/3, MK5 (PRAK), MAPK-interacting kinase (MNKs) 1/2, mitogen- and stress-activated kinase (MSKs) 1/2, and p90 ribosomal kinase (RSKs) subfamilies⁴⁵⁷. MK2 and MK3 are ubiquitously expressed throughout mammalian tissue, both being activated solely via phosphorylation by p38 α / β in response to stress and inflammatory stimuli outlined previously (section 1.8.1)⁴⁵⁷.

These MKs consist of a core catalytic domain as well as a c-terminal region harbouring both a nuclear localisation (NLS) and nuclear export signal (NES) (Figure 1.8.1a)⁴⁵⁸. Notably, two isoforms of MK2 are commonly detected with a ~10 kDa difference, 53 kDa and 60 kDa, respectively⁴⁵⁹. This is due to the presence of an in frame alternative translation initiation start site CUG within the prolonged 5' UTR of MK2 mRNA, leading to an extended N-terminus⁴⁶⁰. The shorter MK2 isoform shows greater functional activity, with the longer isoform failing to phosphorylate the small heatshock protein Hsp27.

Inactive MK2 resides within the nucleus, with nuclear imported p38 α binding to the MK2 linear motif, a c-terminal region containing a docking motif and a reverse docking motif which bind to the common docking site of p38 α (Figure 1.8.1b)⁴⁶¹. This binding has been shown to occur with both proteins in a non-phosphorylated state, with binding leading to rapid translocation of the p38 α -

MK2 complex into the cytoplasm as p38 α binding masks the NLS of MK2^{462,463}. Upon phosphorylation of p38 α the complex undergoes a conformational shift, moving the distant p38 α catalytic site and MK2 substrate residues into a close vicinity⁴⁶⁴. This in turn facilitates the phosphorylation of MK2 residues by p38 α including two kinase domain residue T222 and S272 and the hinge domain residue T334, all of which are required for maximal activity⁴⁶⁵. Phosphorylation of T334 elicits a conformational change within MK2, revealing the NES which, through Exportin-1-dependent shuttling further promotes nuclear export of the p38 α -MK2 complex^{463,466}.

Within the cytoplasm MK2 may bind and phosphorylate numerous protein substrates, regulating biological processes such as the cell cycle, inflammation, transcription and tumour formation⁴⁶⁷. Notable amongst MK2 targets are the immediate-early genes such as c-MYC, c-FOS and TTP, induced in response to cellular stress via the action of MK2 in promoting SRF/MRTF-A transcription factor activity^{468,469}. Additionally, MK2 is noted as a regulator of mRNA degradation with MK2 knockout mice showing enhanced stability of ARE-containing mRNA^{470,471}. This 3'-UTR element ARE-element, found within ~10-15% of mRNA, facilitates the binding of specific ARE-associated RBPs, its presence often correlating with the reduced mRNA half-life of critical short-lived signal proteins such as inflammatory cytokines^{472,473}. Through regulation of these RBPs, MK2 may increase or decrease the stability of specific mRNA, marking it as a key regulator of mRNA fate determination.

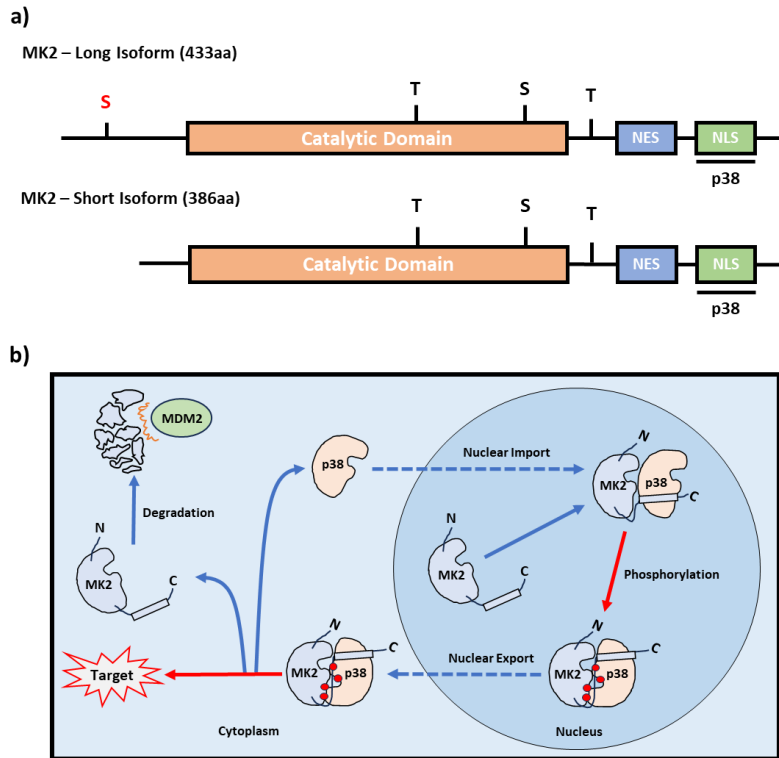


Figure 1.8.1. MK2 structure and p38-dependent activation / degradation. a) Schematic representation of the long and short isoforms of mouse MK2. Labelled are the catalytic domains, the nuclear export signal (NES), the nuclear localisation signal (NLS) and the serine (S) and threonine (T) phosphorylation sites. In the case of the long form an additional S site is present. b) Schematic representation of p38/MK2 pathway. Upon the nuclear import of p38 the protein associates with the C-terminus of MK2. Then upon phosphorylation of p38 via an upstream stimulus, a conformational shift occurs, facilitating activation of MK2 and release of the NES, leading to cytoplasmic localisation via an exportin-1-dependent mechanism. Within the cytoplasm MK2 phosphorylates its targets, leading to dissociation of p38 and degradation of MK2 via MDM2. Adapted from Ronkina and Gaestel., 2022⁴⁵⁷.

Beyond the modulation of the upstream kinase pathway few biological systems have been noted which directly regulate MK2 activity. Notably

however, upon MK2 activation and subsequent release from p38 α the cytoplasmic unbound MK2 becomes available for ubiquitination via the E3 ligase MDM2, leading to proteasomal degradation⁴³⁵. Therefore, consistent transcriptional expression of MK2 is required to replenish a functional population and to facilitate long-term stress-responsive signalling. Thus, long-term or excessive stress stimuli such as UV light, which elicits persistent p38 α activation, eventually lead to depletion of the p38 α -MK2 complex and cell death⁴³⁵.

1.8.3 – p38 α /MK2 pathway in macrophage inflammation

The p38 α /MK2 pathway is a critical component of the inflammatory cascade, responding to and stimulating paracrine and autocrine signals in parallel to other inflammatory pathways, together promoting a strong early induction of pro-inflammatory mediators. p38 α deficient macrophages are characterised by desensitisation to LPS treatment, showing resistance to septic shock and impaired production of key pro-inflammatory cytokines such as TNF, IL-12 and IL-18⁴⁵⁴. Similarly, MK2 deficient spleen cells show reduced production of TNF, IL-6, IL-10, IFN- γ and IL-1 β , with MK2 knockout macrophages also showing reduced IFN β and IL-10 levels^{474,475}. This regulation of the immune response occurs at multiple levels, the p38 α /MK2 pathways being implicated in the regulation of diverse macrophage processes such as protein localisation, protein degradation, mRNA stability, endocytosis, apoptosis, cell migration and cytoskeletal dynamics.

The p38 α /MK2 pathway is activated by a diverse range of inflammatory stimuli. These include infection associated TLR ligands, such as LPS and polyriboisoinic:polyribocytidylic acid (poly(I:C)) which signal via TLR4 and TLR3, respectively, as well as cytokines such as TNF- α , IL-1 β , IL-18 and IL-33. Activation of TLR4 and the interleukin receptors (IL1, IL1RL and IL33) signals via MyD88 and IRAK, leading to TRAF6 phosphorylation and subsequent activation of the classical MAPK-signalling cascade resulting in p38 α /MK2 pathway activation (section 1.2.2) ^{476,477}. TLR3 ligand binding also stimulates the MAPK-signalling cascade via TRAF6, however this is facilitated by MYD88 and TRIF rather than IRAK ⁴⁷⁸. Binding of TNF- α to tumour necrosis factor receptor 1 and 2 (TNFR1 and TNFR2) activates TNF receptor-associated factor 2 (TRAF2) which directly phosphorylates MKK3/6 thus activating the p38 α /MK2 pathway, this phosphorylation also occurring as a result of TNFR associated receptor-interacting protein-1 (RIP1) phosphorylating TAK1 which in turn targets MKK3/6 ^{479,480}.

p38 α deficient macrophages show the complete abolition of LPS induced CREB and C/EBP β transactivation, these transcription factors being responsible for enhanced expression of the pro-inflammatory cytokines TNF, IL-12 and IL-6 in response to inflammatory cues ⁴⁵⁴. Notably, p38 α deficient macrophages show reduced, AP-1 and NF- κ B activity. Findings in stress responsive murine embryonic fibroblasts (MEFs) show AP-1 family transcription factors Jun and Fos to be regulated in a p38 α -dependent manner ⁴⁸¹. Additionally, MK3 has been shown to negatively regulate NF- κ B signalling in the absence of MK2, which functions to inhibit MK3 activity, with dual

knockout of MK2 and MK3 leading to a degree of recovery in NF- κ B signalling⁴⁷⁵.

As well as via transcriptional control, the p38 α /MK2 pathway may also mediate inflammatory progression through regulation of mRNA decay. As outlined previously, MK2 is a known regulator of several AU-rich element binding RBPs, with these elements being commonly found within the short-lived mRNAs characteristic of inflammatory cytokines such as TNF, IL-10 and IL-8⁴⁸²⁻⁴⁸⁵. In particular, MK2 mediates the activity of the CCCH zinc finger protein tristetraprolin (TTP) by inhibiting the recruitment of the deadenylase CAF1 as well as by regulating the mRNA and protein levels of TTP⁴⁸⁴. This regulation results in downregulation of the TTP-mediated decay of TNF- α , with lack of TTP linked to stabilisation of TNF- α and a corresponding enhancement of the inflammatory response^{486,487}.

Additionally, the TTP/MK2 axis is implicated in the process of inflammatory resolution. MK2 has been shown to promote the stabilisation of SOCS3 mRNA, this protein acting as a major inhibitor of the IL-6 and IL-1 β mediated activation of STAT3, thus promoting a pro-inflammatory phenotype in the early-mid inflammatory response⁴⁸⁸. However, the TNF induced expression of the anti-inflammatory cytokine IL-10 is also dependent on MK2 activity, with MK2 acting to inhibit TTP-mediated decay of IL-10 mRNA⁴⁸³. Enhanced levels of IL-10 in turn lead to activation of STAT3 in a manner that is insensitive to SOCS proteins⁴⁸⁹. STAT3 promotes anti-inflammatory signals as well as positively regulating TTP expression, while IL-10 also enhances expression of

the p38 α inhibitor DUSP1⁴⁹⁰. Thus, during the late phase of macrophage inflammation, when IL-10 signalling is high, TTP mediated decay of pro-inflammatory cytokines is enhanced, aiding the anti-inflammatory molecular switch.

1.8.4 – p38 α /MK2 pathway and TN-C

TN-C has been found within multiple cellular and stimulatory contexts to elicit activation of p38 α (Figure 1.8.2). *In vivo*, TN-C administration via injection of recombinant TN-C lacking the fibronectin type III-like repeats and FBG domain had no impact on p38 α phosphorylation within the cerebral artery 24 hours after treatment, whereas full-length TN-C significantly increased p-p38 α abundance^{491,492}. Furthermore, this increase was abolished by treatment with a TLR4 antagonist, implicating the action of TN-C as an endogenous ligand of the TLR4 pathway, which is known to stimulate p38 α activation as outlined previously (section 1.2.2)⁴⁹³. A similar induction in p-p38 α abundance is seen in airway smooth muscle cells after 20 minutes of exposure to soluble TN-C, although intriguingly these cells lack TLR4 expression, with activation of p38 α instead attributed to TN-C binding to β 1 and β 5 integrin⁴⁹⁴.

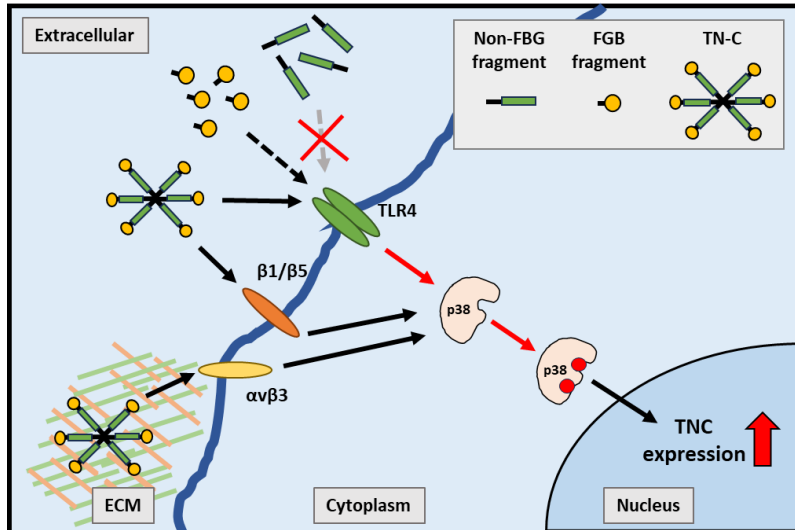


Figure 1.8.2. A schematic diagram of reported mechanisms of p38 stimulation by various forms of TN-C. Pathways represented were identified within mouse TNC knockout, cerebral artery, airway smooth muscle, MDA-MB-231 and M-CSF-MDM cells ^{302,491-496}. Red arrows represent phosphorylation events and red circles represent phosphorylation. Dotted lines represent lower potency activation. Extracellular matrix (ECM), fibrinogen globe (FBG), tenascin-C (TNC), toll-like receptor 4 (TLR4).

Notably, treatment of human M-CSF-MDMs with a recombinant FBG domain also stimulated p38 α phosphorylation, however this phosphorylation was more transient than that witnessed with LPS stimulation, falling after 30 minutes (Figure 1.8.2) ³⁰². Additionally, mass spectrometry analysis identified a phosphorylation event at the Ser127 residue of p38 α unique to the FBG stimulated protein. The FBG domain contains a known TLR4 binding site, this explaining the lack of p38 α activation elicited via treatment with recombinant TN-C lacking this domain ³⁰². The transiency of p38 α activation via FBG not seen in other TN-C treatment models may be due to the strict regulatory

mechanism within macrophages for controlling TLR4 induced signals, while it would be intriguing to see whether mass spectrometry of cells treated with full-length TN-C also shows the same unique phosphorylation event within p38 α .

In addition to the ability of soluble TN-C to induce p38 α activation, similar effects have been attributed to ECM-bound TN-C. For instance, TN-C knockout mice show reduced p38 α activation as a result of subarachnoid haemorrhage (Figure 1.8.2)⁴⁹⁷. Meanwhile, treatment of MDA-MB-231 breast cancer cells with TN-C or β 3 integrin blocking antibodies both lead to a reduction in p-p38 α abundance, with the authors hypothesising that this may be due to TN-C binding to integrin α V β 3 as integrin α V is known to induce p38 α activation^{495,496}. This provides further evidence for two potential routes for p38 α activation by TN-C, these being either TLR4 or integrin dependent.

In turn, the activation of p38 α by TN-C may itself instigate a positive feedback loop, with p38 α activation leading to increased TNC expression (Figure 1.8.2). Inhibition of p38 α has been found to significantly reduce TNC expression normally enhanced as a result of BMP2 treatment in pre-osteoblastic cells and TGF- β treatment in chick fibroblasts^{498,499}. Additionally, p38 knockdown was shown to lead to a reduction in TN-C detection via immunostaining within a nerve crush injury model of the murine sciatic nerve⁵⁰⁰. Although the mechanism by-which p38 α may induce TNC expression is unvalidated, a potential route is via p38 α s modulation of the TNC transcription factor AP-1,

its constituent subunits Jun and Fos both being notably activated by multiple stressors in a p38 α -dependent manner in mouse embryonic fibroblasts ⁴⁸¹.

Finally, TN-Cs activation of p38 α is also associated with its cellular function, marking p38 α as an effector of TN-C mediated signalling. Such functions include cell survival, vasoconstriction and asthma development, with the addition of a p38 α inhibitor reducing the TN-C-mediated induction of these events, often in a dose-dependent manner ^{491,494,501}.

1.8.5 – p38 α / MK2 pathway and miRNA Regulation

In addition to its role as a central pathway in the cellular stress response, the p38 α /MK2 axis also acts as a critical regulator of multiple miRNAs at both the transcriptional and post-transcriptional level. Through this regulatory activity the p38 α /MK2 pathway further mediates stress signalling within processes such as the inflammatory response and the cell cycle, as well as neurotoxic conditions, such as brain injury, Alzheimer's disease and Parkinsons disease, and also in multiple cancers.

The global regulation of miRNAs by the p38 α /MK2 pathway has been illustrated through four microarray analyses. Two such arrays examine p38 α inhibitor treated chemo resistant breast cancer cells (MCF-7TN-R) and promyeloblast macrophages (KG-1a), respectively, with the latter exposed to a chemotherapeutic ^{502,503}. These analyses found p38 α inhibition to promote miRNAs characteristic of an aggressive and chemoresistant cancer phenotype. An additional analysis within p38 α siRNA knockdown laryngeal cancer cells found p38 α knockdown to associate with the modulation of multiple miRNAs,

although their functionality was not examined⁵⁰⁴. Finally, Hong *et al.*, 2013 found ~25% of miRNAs to be downregulated >2-fold as a result of MK2 knockout, this being attributed to an intriguing regulation of miRNA biogenesis machinery performed by MK2⁵⁰⁵.

Hong *et al.*, 2013 identified p38 α as a regulator of miRNA processing at the microprocessor, with p38 α inhibition leading to reduced pre- and mature miRNA but not pri-miRNA levels, this occurrence also witnessed in MK2 knockout cells⁵⁰⁵. Expression of constitutively active MK2 led to increased miRNA expression, even alongside p38 α inhibition, directly implicating MK2 as the effector of this mechanism⁵⁰⁵. Finally, MK2 was identified via co-immunoprecipitation and yeast-two hybrid staining analysis as binding to and phosphorylating the microprocessor associated factor p68, with binding of p72 also identified but with phosphorylation unconfirmed⁵⁰⁵. These two proteins being associated with increased microprocessor activity and enhanced miRNA processing. Thus, MK2 activation was found to enhance the biogenesis of select miRNAs through promoting p68 association with the microprocessor⁵⁰⁵.

In addition to p68, a number of other miRNA biogenesis-associated proteins are known to be regulated by MK2-directed phosphorylation events. Multiple MK2-regulated RBPs have the capacity to associate with miRNA precursors, leading to modification of the biogenesis process. For instance, KSRP enhances miRNA processing via binding to the pri / pre-miRNA apical loop, with MK2 knockout MEFs showing reduced KSRP RNA association likely due to

phosphorylation events, this potentially impacting its ability to regulate miRNAs⁵⁰⁶. Intriguingly, p38 α -dependent phosphorylation of KSRP has also been identified within the differentiating muscle, leading to reduced KSRP binding to target mRNAs, this potentially illustrating an opposed function of p38 α and MK2⁵⁰⁷.

MK2 has been shown to phosphorylate and promote the localisation of Ago2 to sites of heightened miRNA density, called P-bodies, thus enhancing mature miRNA targeting with MK2 knockout shown to reduce miRNA target cleavage efficiency⁵⁰⁸. p38 α has also been associated with Ago2 localisation, with p38 α inhibition reducing Ago2 found within the midbody of dividing cancer cells⁵⁰⁹.

However, the most striking localisation induced by p38 α is that of Drosha, found within models of neuronal degeneration such as Parkinson's disease, Alzheimer's disease and traumatic brain injury in rats^{502,503,510}. Neuronal p38 α was found to be activated by cellular stressors such as oxidative stress, heat, acidity or neurotoxin administration^{502,503,510}. Such activation within neuronal models led to p38 α -dependent phosphorylation of the Drosha Arg-Ser rich N-terminal region, this instigating Drosha's nuclear export and degradation within the cytoplasm via the action of calpain and the ubiquitin proteasome⁵¹⁰. Degradation of Drosha within this context was associated with the increased neuronal death, potentially in part due to reduced miRNA biogenesis^{502,503,510}.

1.9.0 – Aims and hypothesis

1.9.1 - Aims

Work by Piccinini and Zordan has characterised the ECM glycoprotein tenascin-C as a key component of an effective macrophage inflammatory response through its regulation of miRNA-155 expression via a non-transcriptional mechanism.

This project aimed to identify by what non-transcriptional mechanism TN-C regulates murine macrophage miR-155 expression. Specifically, I intended to identify which molecules transduce the TN-C signal into the cell and facilitate changes to miR-155 biogenesis, including potential TN-C associated cell surface receptor(s) and TN-C-induced intracellular pathways. Additionally, using RNA-SEQ I sought to identify additional miRNAs regulated by TN-C, using sequence analysis to identify specific pri-miRNA elements which may facilitate TN-C mediated regulation of miRNAs.

1.9.2 – Hypothesis

Tenascin-C, through interactions with cell surface receptor(s), directly regulates YAP via depolymerisation of the actin cytoskeleton, this facilitating changes to the microprocessor complex which results in the heightened expression of miR-155.

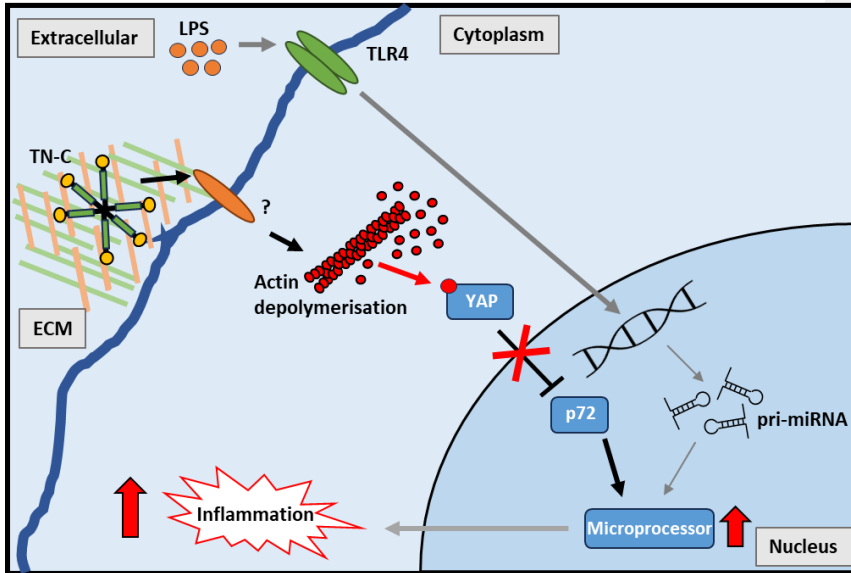


Figure 1.9.1. Schematic representation of research hypothesis and initial objectives. This schematic details the hypothesised pathway by which TN-C post-transcriptionally regulates miR-155 expression during the macrophage inflammatory response. Grey lines represents previously established pathways. Pointed arrows indicate stimulation while blunt headed arrows represent inhibition. Crosses represent a pathway that is inactivated by upstream interactions.

Chapter 2

Materials and Methods

2.1.0 – Reagents

2.1.1 – Cell culture reagents

DMEM with L-Glutamine and Na-Pyruvate, RPMI-1640 with L-glutamine, Optimem, trypsin (EDTA), HBSS without calcium and magnesium, and the SF Cell Line 4D-Nucleofector kit were from Lonza. Fetal Bovine Serum (FBS), β -Mercaptoethanol and cell dissociation buffer were from Gibco. Trypan blue, Penicillin-Streptomycin, HEPES and Lysophosphatidic acid were from Sigma-Aldrich. LPS (*E. coli*, serotype EH100 (Ra)) was from Enzo Life Sciences. Recombinant Mouse TNF- α (aa 80-235) and Recombinant Human TGF- β were from R&D Systems. Lipofectamine[®] RNAiMAX reagent was from Invitrogen. ONTARGETplus SMARTpool siRNAs were purchased from Dharmacon. Latrunculin B and Jasplakinolide were purchased from Abcam.

2.1.2 – Molecular biology reagents

Trizol[®] reagent was from Invitrogen. Quantitech Reverse Transcription Kit was from Qiagen. GoTaq[®] qPCR Master Mix was from Promega. SYBR green primers for qPCR purchased was from Sigma-Aldrich. TaqMan[™] MicroRNA Reverse Transcription Kit, MicroRNA Assays, Universal PCR Master Mix, no AmpErase[™] UNG were from Applied Biosystems. Quick-Load Purple 1kb and 100bp DNA Ladders as well as 6X purple loading dye were from NEB. YAP1-pcDNA3.1+C-(K)-DYK construct was purchased from GenScript. NE-PER[™] Nuclear and Cytoplasmic Extraction Reagents were supplied from Thermo Scientific.

2.1.3 – Protein chemistry and blotting reagents and equipment

PageRuler™ Plus Pre-stained protein ladder (10 to 250kDa) and the Dynabeads™ Protein G Immunoprecipitation Kit were from Thermo Scientific. SDS-PAGE apparatus, wet transfer apparatus and 0.45 µM nitrocellulose membranes, and Bradford reagent were all from Bio-Rad. Amersham ECL Western blotting Detection Reagents were from GE Healthcare Life Science. DTT solution was from VWR. Re-Blot Plus stripping solution was from Millipore. Protease inhibitor cocktail, phosphatase inhibitors, 30% bis-acrylamide, N,N,N,N-tetramethylethylenediamine (TEMED) and other buffer components were from Sigma-Aldrich.

2.2.0 – Buffer recipes

Buffers and Solutions	Recipe
4X Tris-Cl/SDS, pH 6.8	0.5 M Tris-Cl (pH 6.8) and 0.4% SDS
4X Tris-Cl/SDS, pH 8.8	1.5 M Tris-Cl (pH 8.8) and 0.4% SDS
Blocking Solution (Western Blot)	5% Bovine Serum Albumin (BSA) or 5% milk in 1X TBS
Blocking Solution (Immunofluorescence)	5% sheep serum, 3% BSA in PBS
Blocking Solution + PEMs (Immunofluorescence)	5% sheep serum, 3% BSA in PEM
Permeabilization buffer	0.1% Triton X-100 in 1x PBS
PBS 10X	70.1 g/L NaCl, 2 g/L KCl, 4.4 g/L Na ₂ HPO ₄ , 12.8 g Na ₂ HPO ₄ , 2H ₂ O

TBS 10X	24 g Tris base, 88 g NaCl, up to 1 L dH ₂ O (pH 7.6)
TBST	100 mL TBS (10X), 1 mL Tween, up to 1 L dH ₂ O
Transfer Buffer 10x	15 g Tris base, 72 g Glycine, up to 1 L dH ₂ O
Transfer Buffer 1x	100 mL Transfer Buffer (10X), 200 mL Methanol, up to 1 L in dH ₂ O
Running Buffer 10x	30 g Tris base, 144 g Glycine, 1% SDS (w/v), up to 1 L dH ₂ O
Laemmli Buffer 1x	63 mM Tris-Cl (pH 6.8), 2% SDS, 10% Glycerol, 0.1% B-mercaptoethanol, pinch of bromophenol blue, up to 10 mL dH ₂ O
Lysis Buffer	20 mM Tris-Cl (pH 7.5), 150 mM NaCl, 10 mM EDTA, 10 mM EGTA, 1% NP-40, protease inhibitor cocktail (1:1000; Roche), phosphatase inhibitor cocktail (1:100; Sigma).
Solubilisation Buffer 2x	100 mM Tris-Cl (pH6.8), 4% SDS, 200 mM DTT, up to 10 mL dH ₂ O.
Guanidine Hydrochloride	0.3 M guanidine hydrochloride, 95% Ethanol.
SDS PAGE Gel 10% (Separating Gel)	375 mM Tris-Cl (pH 8.8), 0.1% SDS, 10% acrylamide, up to 15 mL with dH ₂ O. 1:300 10% Ammonium persulfate (APS)

	and 1:1500 Tetramethylethylenediamine (TEMED).
SDS PAGE Gel 10% (Stacking Gel)	125 mM Tris-Cl (pH 6.8), 0.1% SDS, 3.9% acrylamide, up to 5 mL with dH2O. 1:200 10% Ammonium persulfate (APS) and 1:1000 Tetramethylethylenediamine (TEMED).
3-(4,5-Dimethylthiazol-2-yl)-2,5-diphenyltetrazolium bromide (MTT)	5 mg/ml in PBS, sterile filtered, 10 % (v/v) used in assay
MTT lysis buffer	10 % (w/v) SDS, 0.01 M HCl ₂ M
FACS Buffer	2% BSA, 2mM EDTA, 0.02% NaN ₃ , in 1x PBS
PEM Buffer	80 mM PIPES pH 6.8, 5 mM EGTA, 2 mM MgCl ₂
Hank's Balanced Salt Solution (HBSS)	NaHCO ₃ : 0.35 g/L, Phenol red: 0.011 g/L, Glucose: 1.0 g/L (Dextro).

Table 2.2.1. Buffer and solution recipes.

2.3.0 – Primers

The efficiency of all primers was validated via qPCR analysis of a 1:2, 1:3 or 1:10 sample concentration curve of 5 points or more, with optimal primer efficiency being noted by qPCR CT standard curve with an $R^2 > 0.9$ (Supplementary figure 7.1.0). Additionally, primer specificity was determined through the detection of a single narrow peak within the qPCR melting curve.

Gene	Orientation	Sequence (5'-3')
------	-------------	------------------

TNC	Forward	ACCATGCTGAGATAGATGTTCCAAA
	Reverse	CTTGACAGCAGAAACACCAATCC
Pri-miR-155	Forward	GCATTAACAGGACACAAGGCC
	Reverse	GACTTGTCATCCTCCCACGG
MBNL1	Forward	AGCTTAGCCACCAGTGCATC
	Reverse	GGTACTCTCGACACACCTCCA
HNRNPF	Forward	TTTTAAGGCGTCGGGTGGA
	Reverse	TCATGGACACTTGACAGGGC
MAPKAPK2	Forward	GGAAAGTCCCTAGGTTGCC
	Reverse	TCTAGAGCCAGTGAGGACCC
ITGAV	Forward	CGTTTCTATCCCACCGCAGG
	Reverse	ACCAGCGAGCAGTTGAGTTC
ITGB1	Forward	GGTCCCGACATCATCCCAAT
	Reverse	TAGGATTTTCACCCCGTGCCC
ITGB3	Forward	GTGAGTGCGATGACTTCTCTG
	Reverse	CAGGTGTCAGTGCGTGTAGTAC
HPRT1	Forward	CAGTCCCAGCGTGTGATTA
	Reverse	TGGCCTCCCATCTCCTTCAT
YAP1	Forward	TGAATTCTGCCTCAGGACCTC
	Reverse	AGTGATCCTCTGGTTCATGGC

Table 2.3.1. SYBR green primer sequences

2.4.0 – Cell culture

All cells were cultured using a humidified incubator at 37 °C, in 5% CO₂ atmosphere.

2.4.1 – Preparation of bone marrow-derived macrophages

Bone marrow-derived macrophages (BMDMs) were generated and cultured by Nicole Zordan⁵¹¹. To generate BMDMs, Hank's Balanced Salt Solution (HBSS) was used to flush bone marrow from the tibias and femurs of *tnc+/+* and *tnc-/-* mice acquired from Prof. Kim Midwood (Oxford). Erythrocytes were lysed by applying Red Blood Cell Lysis Buffer to pelleted cells at room temperature for 5 minutes, followed by three washes in DMEM and final resuspension in 1 mL culture medium. 5×10^6 cells were seeded in 10 cm petri dishes and cultured in DMEM supplemented with 20% (v/v) FBS, 1% (v/v) antibiotic-antimycotic solution, 50 μ M β -Mercaptoethanol and 100 ng/ml recombinant human M-CSF. After 7 days incubation, adherent cells were harvested using Non-Enzymatic Cell Dissociation Solution and were washed in 1x PBS before being used in experiments.

2.4.2 - RAW264.7 cells, Immortalised BMDMs, NIH-3T3 and EO771 cells

Immortalised Bone Marrow Derived Macrophages (iBMDM) were a kind gift from Prof Luisa Martinez-Pomares and Prof Uwe Vinkemeier (University of Nottingham) having been immortalised by Dr Graham Foster's lab via infection with J2 recombinant retrovirus⁵¹². iBMDMs and RAW246.7 cells were cultured using RPMI-L-glutamine and DMEM respectively, with 10% FBS and 1% penicillin / streptomycin.

EO771 cells were a kind gift from Prof Anna Grabowska (University of Nottingham) and NIH-3T3 cells were provided by Prof. David Heery (University of Nottingham). EO771 and NIH-3T3 cells were cultured using DMEM

supplemented with 10% FBS and 1% penicillin / streptomycin. EO771 cells were additionally supplemented with 20 mM HEPES.

RAW 246.7 cells were maintained between 4 and 20 passages, while iBMDMs, NIH-3T3 and EO771 cells, the original passage number of which was unknown, were permitted 10 passages after thawing. All cells were passaged at 70-80% confluency as determined via cell counting using trypan blue staining and a hemacytometer. A cell lifter was used to detach RAW 246.7 cells for passaging, while iBMDMs, NIH-3T3 and EO771 cells required 5-minute incubation with trypsin/EDTA at 37 °C.

2.4.3 – Cell stimulation

Treatment	Function	Source	Final concentration
LPS (<i>E. coli</i> Serotype EH100 (Ra))	TLR4 activation	Enzo Life Sciences	100 ng/mL
Latrunculin B	Actin cytoskeleton depolymerisation	Abcam (ab144291)	500 nM
Jasplakinolide	Actin cytoskeleton polymerisation and stabilisation	Abcam (ab141409)	500 nM
Lysophosphatidic acid	Actin stress fibre formation	Sigma (L7260-1MG)	10 µg
Recombinant TNF-α (<i>Mouse, aa 80-235</i>)	TNFR activation	Bio-technie (410-MT-010/CF)	5 ng/mL – 20 ng/mL

Recombinant TGF- β <i>(Human cell-expressed)</i>	TGFBR activation	Bio-technie (7754-BH-005/CF)	1 ng/mL – 10 ng/mL
---	------------------	------------------------------	--------------------

Table 2.4.1. Cell treatments

1 mg/mL LPS stock was vortexed for 1 minute before being used to create a 100 ng/mL solution in cell culture media (Table 2.4.1.). This dilution was performed immediately before use.

RAW 246.7 cells and BMDMs were treated with 100 ng/mL LPS for the durations indicated in the text, while EO771 and NIH-3T3 cells were treated with varying dosages of LPS, TNF- α or TGF- β for the durations indicated. All treatments were accompanied by replacement of culturing media (Table 2.4.1.).

Actin modulators were solubilised in DMSO. When conducting actin modulation experiments, media containing 500 nM Latrunculin B, 500 nM Jasplakinolide or 10 μ g Lyso-phosphatidic acid sodium salt (LPA) was administered to RAW 246.7 cells for 2 hours, before cell fixation, or media change and subsequent LPS treatment. (Table 2.4.1). Cells treated with an equal concentration of DMSO to that administered in the actin modulator solution were used as controls.

2.4.4 – Plasmid nucleofection

Nucleofection reactions were assembled and the 4D-Nucleofector unit programmed following the Lonza protocol for RAW 264.7 cells, with 2 μ g of YAP1-pcDNA3.1+C-(K)-DYK, pcDNA3.1 empty vector or GFP vector (Lonza)

being combined with a 100 μ L 4.5:1.0 ratio mixture of nucleofection solution and nucleofection supplement (Supplementary Figure 7.2.0). RAW 246.7 cells were pelleted via centrifugation at 90 xg for 10 minutes to preserve cellular integrity. Each plasmid solution was used to resuspend a separate pellet of 2×10^6 RAW 246.7 cells, before being transferred to a nucleocuvette and placed within the 4D-Nucleofector unit. Upon programme completion the cell suspension was allowed to incubate for 5 minutes before its dilution using pre-warmed cell culture media and subsequent plating.

Successful nucleofection was determined via GFP fluorescence after 48 hours.

24 hours post nucleofection cell culture media was changed.

2.4.5 – siRNA transfection

siRNA knockdown of mRNA expression was performed on cells at 60-65% confluency via transfection with Lipofectamine RNAiMAX reagent and siRNAs (Table 2.4.2).

Dharmacon siRNA – ON-TARGETplus SMARTpool	Species	Cat No
YAP1	Mouse	L-046247-01-0005
TNC	Mouse	L-046798-01-0005
MAPKAPK2	Mouse	L-040135-00-0005
ITGB1	Mouse	L-040783-01-0005
ITGB3	Mouse	L-040746-01-0005
ITGAV	Mouse	L-046779-01-0005

NRP1	Mouse	L-040787-00-0005
Non-targeting Pool	Mouse	D-001810-10-05

Table 2.4.2. siRNA reagents

Cells were seeded on 24-well (7.5×10^4 cells/well), 12-well (1.5×10^5 cells/well), or 10 cm plates (2.5×10^6) and incubated overnight, being treated with the following transfection reaction mixes when at the desired confluency the following day (Table 2.4.3. and 2.4.4.).

For a 12 well plate the transfection reaction was prepared as follows to create a final siRNA concentration of 10 nM.

Reagents	siRNA Mix (1x sample)
Opti-MEM	46uL
siRNA (10 μ M stock)	4uL

Table 2.4.3. siRNA mix for 12-well plate

Lipofectamine RNAiMAX mix (1x sample)	
Opti-MEM	52.0uL
RNAiMAX	3.0uL

Table 2.4.4. Lipofectamine solution

siRNA and lipofectamine solutions were thoroughly mixed and incubated for 20 minutes at room temperature. Cell media was replaced with 900 μ L media and 100 μ L transfection mixture was added in a dropwise manner followed by gentle swirling to evenly distribute. 24 h post-transfection media was

replaced. Functional experiments were conducted after 24 h post-transfection, being concluded by 48 h post-transfection.

2.4.6 – MTT assay

RAW 246.7 cells were seeded at 1.4×10^4 cells per well in a 96-well plate. After one day of growth, media was removed and cells were incubated with serial dilutions of actin modulators for 2 hours in 100 μ L of fresh media, as described in (Section 2.4.3). Following this, 10 μ L of sterile filtered 5 mg/mL of MTT solution was added to each well. Plates were incubated at 37 °C for 1 hour, or until formazan crystals were visible under a microscope. The MTT reaction was halted and formazan crystals solubilised via addition of 90 μ L MTT solvent to each well. MTT absorbance at 590 nm was measured using a BioTek Synergy HTX multimode microplate reader. Non-MTT wells were used as blank controls.

2.4.7 – FACS analysis

FACS analysis was performed by Xingyu Go. RAW 246.7 macrophages were dissociated via 30 minutes incubation with non-enzymatic cell dissociation solution on ice. 150,000 cells were washed and resuspended in FACS buffer before being incubated for 30 mins at room temperature with fluorescent-conjugated primary antibodies. Cells were then fixed using 4% PFA/PBS before being analysed on a ID7000 Spectral Flow Cytometer (Table 2.4.5). Data were analysed using FlowJo software, calculating the percentage of positive cells and mean fluorescence intensity (MFI).

Antibody	Fluorescent Protein	Concentration	Manufacturer
ITGB1	APC	0.5 µg	Invitrogen (#MA1-19458)
ITGA9	PE	0.5 µg	Invitrogen
ITGA5	FITC	1.0 µg	Invitrogen
ITGAV	PE	0.5 µg	Invitrogen
TGFBR2	PE	0.5 µg	Invitrogen

Table 2.4.5. Antibodies for FACS analysis

2.5.0 – Molecular biology techniques

2.5.1 – RNA-immunoprecipitation

RAW 246.7 cells were seeded onto 10 cm plates and underwent siRNA transfection of TNC or scramble control (siCTRL) siRNA, as described in Section 2.4.5. Once cells reached 70-80% confluency, 2-hour LPS stimulation was performed, as described in Section 2.4.3. Following stimulation, cells were washed in 10 mL ice-cold PBS, lifted into 500 µl PBS using a cell lifter, and transferred to a 1.5 mL tube. Cells were pelleted at 2000 xg for 3 minutes at 4 °C with the supernatant then removed. Pellets were then lysed via gentle rotation at 4 °C with 500 µL 1X lysis buffer for 30 minutes (Table 2.2.1). The lysate was then centrifuged at 14,000 xg for 15 minutes at 4 °C to remove cell debris.

The Dynabead Protein G Immunoprecipitation kit was used to immunoprecipitate protein-RNA complexes following manufacturer's

instructions with minor adjustments for RIP, as recommended by Galiardi and Matarazzo ⁵¹³.

Pre-clearing, a step which reduces aspecific bead-immunocomplex binding, was performed for each 500 μ L sample via rotation with 10 μ L of magnetic beads for 30 minutes at 4 °C. Concurrently, 50 μ L of beads per sample were incubated at room temperature with 4 μ g of anti-Drosha antibody or IgG isotype control diluted in 200 μ L of antibody binding and washing buffer sourced from the Dynabead Protein G Immunoprecipitation kit (Table 2.7.2).

50 μ L of pre-cleared samples were retained as an input control. 475 μ L of each pre-cleared lysate was combined with Drosha and IgG control antibody-bead complexes and incubated overnight at 4 °C under gentle rotation. The following day, supernatants were placed in new tubes, being retained as unbound controls. The bead-antibody-RNA immunocomplexes were washed three times in 200 μ L washing buffer, before resuspension in 100 μ L washing buffer and transfer to a fresh tube. Following complete removal of washing buffer, the bead-antibody-RNA immunocomplexes were resuspended in 500 μ L of Trizol, with RNA extraction performed as outlined below (Section 2.5.2).

2.5.2 – Total RNA extraction and quantification

Total RNA extraction from cell lysates was performed using Trizol following the manufacturer's instructions (Invitrogen). Samples were examined using a NanoDrop® (Thermo Scientific) with 260/280 nm and 260/230 nm absorbance ratios of ~2.0-2.2 indicating ideal RNA purity.

2.5.3 – Quantitative Real-Time PCR (SYBR Green)

SYBR Green based qPCR allows the relative quantification of mRNA expression by using a pair of primers and non-specific fluorescent dyes. Upon primer annealing intercalation of the dye occurs, producing a measurable fluorescent signal. Normalisation of readings was performed using the endogenous invariant control mRNA hypoxanthine phosphoribosyltransferase 1 (HPRT1) via the $\Delta\Delta CT$ method.

Prior to qRT-PCR, reverse transcription was performed using the Quantitech Reverse Transcription Kit (Qiagen) using 500 ng of total RNA per reaction. Samples were incubated with Genomic DNA elimination buffer at 42 °C for 2 minutes. Upon addition of the reverse transcription mix, samples were further incubated within a pre-warmed thermocycler under the conditions summarized in Table 2.5.1.

Temperature	Duration
42 °C	15 min
95 °C	3 min
4 °C	-

Table 2.5.1. Reverse transcription thermocycling conditions.

cDNA was diluted 1:3 with nuclease free water and the qPCR reaction mixes were created using GoTaq PCR Mastermix (Table 2.5.2). Thermocycling was performed under the following conditions in a Qiagen Rotor-Gene Q machine (Table 2.5.3).

Component	Volume
-----------	--------

GoTaq qPCR Master Mix (2X)	5.0 μ L
0.4 μ M Forward Primer	0.4 μ L
0.4 μ M Reverse Primer	0.4 μ L
cDNA	3.0 μ L
Nuclease-Free Water	1.2 μ L
Total	10.0 μ L

Table 2.5.2. SYBR-green qPCR reaction components.

Cycle	Temperature	Duration
1X	95 °C	10 min
40X	95 °C	5 sec
	62 °C	30 sec
	68 °C	15 sec

Table 2.5.3. SYBR-green qPCR thermocycling conditions.

2.5.4 – Quantitative Real-Time PCR (Taqman)

Taqman qPCR allows the relative quantification of miRNA expression within a sample. This utilises a forward and reverse primer with a sequence-specific probe. This probe contains a 5' fluorophore (FAM) and a 3' quencher (NFQ) and emits fluorescence when hybridised to a complementary sequence. Taq polymerase degrades the 3' quencher, increasing the strength of fluorescence as the amplicon extends. Normalisation was performed using the endogenous invariant control small nuclear Sno RNA U6 via the $\Delta\Delta$ CT method.

Taqman miRNA reverse transcription was performed following the manufacturer's instructions using 20 ng of trizol extracted total RNA per reaction (Table 2.5.4). Reactions were created using both miR-155 and U6

Taqman MicroRNA Reverse Transcription Kit and were placed in a pre-warmed thermocycler under the following conditions (Table 2.5.5).

Component	Initial Concentration	Volume
dNTPs (with dTTP)	100 mM	0.15 μ L
Multiscribe Reverse Transcriptase	50 U/ μ L	1.00 μ L
Reverse Transcription Buffer	10X	1.50 μ L
RNase Inhibitor	20 U/ μ L	0.19 μ L
TaqMan MicroRNA RT Primer	5X	2.0 μ L
Total RNA sample	20 ng/ μ L	1.0 μ L
Nuclease-free water		8.16 μ L
Total		15.0 μ L

Table 2.5.4. Taqman miRNA reverse transcription mix.

Temperature	Duration
16 °C	30 min
42 °C	30 min
85 °C	5 min
4 °C	∞

Table 2.5.5. Taqman miRNA reverse transcription thermocycling conditions.

qPCR reactions were compiled using the following components (Table 2.5.6).

These reactions were placed in a Qiagen Rotor-Gene Q machine under the following conditions (Table 2.5.7).

Component	Volume
TaqMan 2X Universal PCR Master Mix (No AmpErase UNG)	5.0 μ L
Nuclease-free Water	2.5 μ L
TaqMan MicroRNA Assay 20X	0.5 μ L
cDNA	2.0 μ L
Total	10.0 μ L

Table 2.5.6. Taqman qPCR reaction mixture.

Cycle	Temperature	Duration
1X	95 °C	10 min
40X	95 °C	15 sec
	60 °C	60 sec

Table 2.5.7. Taqman qPCR thermocycling conditions.

2.6.0 – Protein Extraction and Quantification

2.6.1 – Total protein extraction

Cell culture media was removed, and cells were washed twice with ice cold PBS with lysis buffer then applied evenly across the cells followed by 15-minute incubation on ice. Cells were thoroughly scraped using a cell lifter, checking under a microscope to ensure full detachment, then homogenizing via repeated pipetting. Samples were collected in 1.5 mL tubes and spun at

13,000 xg for 15 minutes at 4 °C with the supernatant placed into a fresh tube.

Samples were kept at 4 °C at all stages.

2.6.2 – Protein extraction from Trizol organic fraction

150 µL of 100% ethanol was added to the Trizol organic phase per 500 µL of Trizol used in phase separation. After mixing via 3-5 inversions, the samples were centrifuged at 3,000 xg for 5 mins at 4 °C. Following this, the supernatant was decanted into 1.5 mL Eppendorf tubes containing 750 µL of isopropanol per 500 µL of Trizol. The samples were then mixed thoroughly via inversion and incubated at room temperature for 30 minutes followed by centrifugation at 12,000 xg for 10 minutes at 4 °C. The supernatant was then discarded, and 1 mL of 0.3 M guanidine hydrochloride was added to wash, incubating at room temperature for 20 minutes before centrifugation at 12,000 xg for 5 minutes at 4 °C. This wash step was repeated twice, with a pipette tip used to break up the formed pellet after the initial wash to aid later resuspension. After washing, 1 mL of 100% ethanol was added to the pellet, with incubation at room temperature for 20 minutes followed by centrifugation at 12,000 xg for 5 minutes at 4 °C. After removal of the supernatant by decanting, the samples were left to air dry for 10 minutes or until all residual ethanol had evaporated. Following this, 125 µL of 2X solubilisation buffer or 60 µL of 1X Laemmli buffer (Table 2.2.1) was added to the pellets, with resuspension aided by incubation at 60 °C for 1 hour. In some cases, larger pellets did not resuspend, in which case the volume of buffer was increased, incubation time was extended and sonication was performed.

2.6.3 – Nuclear / Cytoplasmic protein fractionation

RAW 246.7 cells, having either undergone siRNA transfection or plasmid nucleofection two days prior to LPS stimulation, were resuspended in PBS following gently pelleting at 500xg for 5 minutes. Cells were counted and 2×10^6 cells from each condition were pelleted and their nuclear and cytoplasmic protein fractions obtained using the NE-PER™ Nuclear and Cytoplasmic Extraction Reagents following the manufacturer's protocol, using 100 μ L of CER1, 5.5 μ L of CER2, and 50 μ L NER1 buffers. All buffers were ice-cold, and all steps were performed at 4 °C.

2.6.4 – Bradford assay

A five-point standard-calibration curve was created using a 1:2 serial dilution of BSA, from 0.50 mg/mL to 0.032 mg/mL. Samples and standards were diluted to a final volume of 10 μ L using 1x PBS within a 96 well microplate. 200 μ L of diluted and sterile filtered dye reagent was added to each well. Each sample and standard was measured in triplicate at 595nm using a Biotek Synergy HTX plate reader. Standard curves of absorbance values against standard concentrations were plotted and fitted to a linear regression. The resultant equation (shown below) was used to estimate unknown protein concentrations of samples.

$$X = \frac{Y - B}{M}$$

X = protein concentration (mg/mL), Y = absorption (595mM), B = Y-intercept, M = slope of the line.

2.7.0 – Immunoblotting

2.7.1 – SDS PAGE

10 µg of protein samples was made-up to 40 µL in 1X PBS or TBS, before being combined with 10X Loading buffer and being boiled for 15 minutes at 100°C prior to loading. 40 µL samples were then loaded in their entirety into an SDS PAGE Gel, prepared as detailed in (Table 2.7.1), submerged in 1X Running Buffer alongside 5 µL of PAGE-Protein Plus Ladder. SDS PAGE gels were ran at 10 mA for 30 minutes then at 20 mA for 6 hours, using a BIO-RAD PowerPac Universal, or until the ladder had fully migrated down the gel.

In instances of low protein abundance, the entire protein sample was be loaded onto the gel. This required heating of the sample at 100 °C in a heat block placed under a fume hood with the tubes lid open to allow fluid evaporation, until 40 µL of sample remained which was then loaded onto the gel in its entirety.

Component	Separating gel			Stacking gel
	8%	10%	12%	3.9%
30% acrylamide / 0.8% bisacrylamide	2 mL	2.5 mL	3 mL	0.32 mL

4X Tris-Cl/SDS, pH 8.8	1.875 mL	1.875 mL	1.875 mL	-
4X Tris-Cl/SDS, pH 6.8	-	-	-	0.62 mL
H ₂ O	3.625 mL	3.125 mL	2.625 mL	1.525 mL
10% (w/v) ammonium persulfate (APS)	25 µL	25 µL	25 µL	12.5 µL
TEMED	5 µL	5 µL	5 µL	2.5 µL

Table 2.7.1. SDS-PAGE separating and stacking gel composition.

2.7.2 – Western Blot

A nitrocellulose membrane was hydrated with deionised water before incubation for 1 hour submerged in ice cold 1X transfer buffer with gentle shaking. The transfer sandwich was assembled ensuring no air bubbles were present before submerging in 1X transfer buffer within a PowerPac Universal from BIO RAD, at 350 mA for 60 minutes at 4 °C.

Blocking was performed via the addition of 20 mL blocking buffer and incubation for 1 hour at room temperature with rotation. Following this, the membrane was incubated with 5mL of primary antibody solution (in blocking buffer) overnight at 4 °C with rotation (Table 2.7.2). The membrane was then washed three times using 20 mL 1X TBST and 10 min rotation. 5 mL of fresh secondary antibody diluted in 5% milk was incubated with the membrane for 2 hours at room temperature with rotation before another wash was performed. The membrane was incubated for 2 mins with 800 µL of ECL with

chemiluminescence detected using the ImageQuant LAS 4000 system.

Densitometric quantification of band density was performed using ImageJ.

Membranes were either stored in 1X TBS or incubated for 5 minutes in 20 mL of Re-Blot plus stripping solution and then incubated twice in blocking solution for 5 min before being re-probed with a different primary antibody.

Primary antibodies	Dilution	Source
Drosha	1:1000 in 5% BSA / TBST (w/v)	Abcam (Ab12286, Rabbit)
Tenascin-C	1:1000 in 5% BSA / TBST (w/v)	Sigma (T3413, Rat)
α -tubulin	1:5000 in 5% milk / TBST (w/v)	Abcam (Ab52866, Rabbit)
YAP1	1:1000 in 5% BSA / TBST (w/v)	Cell Signalling (#14074, Rabbit)
p65	1:1000 in 5% BSA / TBST (w/v)	Cell Signalling (#4764, Rabbit)
Lamin-A/C	1:1000 in 5% milk / TBST (w/v)	NovusBio (NB100-56649SS, Rabbit)
MK2	1:1000 in 5% BSA / TBST (w/v)	Cell Signalling (#3042S, Rabbit)
pMK2	1:1000 in 5% BSA / TBST (w/v)	Cell Signalling (#3007S, Rabbit)
p38 α	1:1000 in 5% BSA / TBST (w/v)	Cell Signalling (#9218T, Rabbit)
p-p38 α	1:1000 in 5% BSA / TBST (w/v)	Cell Signalling (#9211S, Rabbit)
Anti-rat (secondary)	1:5000 in 5% milk / TBST (w/v)	Millipore (AP136P, Goat)
Anti-rabbit (secondary)	1:5000 in 5% milk / TBST (w/v)	Dako (P0217, Pig)

Table 2.7.2. Antibodies used in Western Blot and RNA-immunoprecipitation.

2.7.3 – Immunocytochemistry

RAW 246.7 cells cultured on Ibidi chambered coverslips were fixed via 15 minutes incubation at 4 °C with either 4% PFA/PBS solution, or 4% PFA/PEMS solution and stored at 4 °C in 1x PBS or 1x PEMS, respectively, supplemented with 0.2% sodium azide (Table 2.2.1).

Samples to be stained with phalloidin or p65 were permeabilised via 15 minutes incubation with 250 μ L permeabilization buffer at room temperature. 250 μ L blocking solution was administered to each coverslip chamber and incubated overnight at 4 °C. Samples were then incubated with primary antibody (Table 2.7.3) diluted 1:200 in blocking solution overnight at 4 °C. Samples were washed 4 times in 1x PBS or 1x PEMS followed by incubation for 1 hour at room temperature in darkness, with secondary antibody diluted 1:500 in blocking solution as well as DAPI stain, and phalloidin-488 in order to visualise the actin cytoskeleton. Following this, an additionally series of 4 washes was performed, the sample was then incubated for 20 minutes in the dark with 1 μ M DRAQ5 dye diluted in blocking solution. After an additional series of washes, if DRAQ5 was added, coverslips were filled with 1x PBS or 1x PEMS buffer and stored at 4°C in the dark (Table 2.2.1).

Images were captured using the Evos FL Cell Imaging System, Zeiss Exciter Wide Field Microscope, or the Zeiss LSM-510 Confocal System, as indicated in the text. Quantification of fluorescent intensity was performed using ImageJ.

Primary antibodies and probes	Dilution	Source	Secondary antibody (1:500; Invitrogen)
Anti-p65 (#4764, Rabbit)	1:200	Cell Signalling	Anti-rabbit, Alexa-fluor 546
Phalloidin Fluor™ - 488	1:200	ThermoFisher	-
DAPI staining	1:100	Invitrogen	-
DRAQ5 staining	1:5000	ThermoFisher	-

Table 2.7.3. Antibodies and stains used in immunofluorescence.

2.8.0 – RNA Seq analysis

2.8.1 – RNA preparation and small RNA sequencing

Total RNA was extracted from TNC +/+ and TNC -/- BMDMs treated or untreated with 10 ng/mL LPS for 4 hours, using a ReliaPrep™ miRNA Cell and Tissue Miniprep system following manufacturer's instructions. RNA integrity was determined at the University of Nottingham using the Agilent 2100 Bioanalyser system, with all samples showing an RNA integrity numbers (RIN) >9. Further assessment of RNA integrity was performed by Novogene, using agarose gel electrophoresis to detect contaminants and a nanophotometer to assess RNA purity.

3 µg of total RNA in RNase-free water, in triplicate for each condition, was supplied to Novogene for library preparation and sequencing. Libraries were prepared using NEB Next® Multiplex Small RNA Library Prep Set for Illumina® following the manufacturer's recommendations. The resultant 10-50 bp libraries were sequenced using an Illumina Novaseq 6000 platform.

2.8.2 – sRNA-seq data analysis by Novogene

The quality of raw reads was assessed using an in-house Novogene script, leading to the removal of low-quality reads, reads with retained adapter sequences, reads featuring poly(A/T/G/C) repeats, and reads containing >10% non-designated 'N' bases.

Clean reads were mapped to the mouse genome using Bowtie with alignments containing zero mismatches being carried forward to miRNA identification. miRDeep 2.0 was used to identify mature miRNA and pre-miRNA with alignment based upon the miRbase v20.0 database. Aligned miRNA with zero mismatches within the seed sequence and up to two mismatches outside of the seed sequence were counted. miRNA identification was further validated and quantified by miRDeep 2.0 through the mapping of identified mature miRNA sequences to known pre-miRNA reference species from miRbase v20.0, allowing for a single mismatch in the pre-miRNA and zero mismatches in mature miRNA alignments. Finally pre-miRNA and mature miRNA mapping data were intersected, a mature miRNA read representing a sequenced mature miRNA aligning with its pre-miRNA sequence with a -2 nt upstream and +5 nt downstream tolerance, to account for untemplated isomiRs. Transcripts per million (TPM) were estimated:

$$TPM = \frac{\text{Mapped Read Count}}{\text{Total Reads}} 10^6$$

Differential expression analysis was performed using the DESeq2 package (v1.8.3) with p-values adjusted using the Benjamini Hockberg method. For samples without biological replicates the read counts were adjusted using the

Trimmed Mean of M-values, followed by differential expression analysis using the EdgeR package (v3.24.3). The Benjamini Hockberg method was then applied. An adjusted p-value threshold of < 0.05 and a log₂ fold change of 1.0 were set as significance thresholds.

2.8.3 – GO and KEGG analysis of miRNA targets

Gene Ontology (GO) and Kyoto Encyclopedia of Genes and Genomes (KEGG) analysis was performed using the DIANA-miRPath v3.0 software⁵¹⁴. Gene union comparison of miRNA-targets was conducted by the software using a combination of the miRTarbase database of experimentally validated, and the microCD databases of predicted, miRNA-mRNA interaction. A significance threshold of p<0.05 was used with the Benjamin and Hockburg FDR correction applied.

2.8.4 – pri-miRNA cis-regulatory element analysis

In order to identify the presence or absence of specific cis-regulatory elements within pri-miRNA specific criteria were established based upon those previously used by Narry Kim¹⁵³.

First, the pri-miRNA sequence for each miRNA of interest was established through alignment of the pre-miRNA sequence, as catalogued on miRbase, with the NCBI murine genome. The FASTA sequence from -25nt downstream of the pre-miRNAs 5' end and +20nt upstream of the 3' end was extracted, this considered to represent the majority of documented pri-miRNA regulatory features¹⁵³.

Pri-miRNA secondary structure prediction was performed via the MXFold2 webtool, which uses deep learning integrated Turner's nearest neighbour free energy parameters to generate RNA secondary structures⁵¹⁵. The dot-bracket notation output was further visualised using the Pseudoviewer3 webtool, which also predicted potential pseudoknot formations within the pri-miRNA secondary structure (Supplementary figure 7.3.0 and 7.4.0)⁵¹⁶.

Cis-regulatory elements were identified within each pri-miRNAs predicted secondary structure using the following criteria, with the 5' end of the pre-miRNA sequence designated as position 0:

1) Basal UG

A UG at position -14 on the 5' strand.

2) Apical UGUG

A UGUG, UGU or GUG motif at position +21, +22 or +23 on the 5' strand.

3) Basal mGHG

An aligned sequence, without a bulge, between -7 to -5 on the 5' strand and +5 to +3 on the 3' strand. The "mGHG score" of the corresponding sequence was calculated using Kwon *et al.*, 2019's previous analysis of human mGHG motifs, the degree to which each mGHG motif impacted processing was assessed¹⁴². A functional mGHG motif was defined as having a score >38.

4) Apical mGHG

An aligned sequence, without a bulge, -7 to -5 from the start of the pri-miRNA apical loop. The “mGHG score” of the corresponding sequence was calculated as above¹⁴².

5) CNNC motif

A CNNC, DNNC or CNND motif +17 downstream on the 3' strand.

6) Lower stem stability

The lower stem of a pri-miRNA was determined to be stable if fewer than 4 mismatched nucleotides were present from position -1 to -13 on the 5' strand. Furthermore, detailed analysis of this regions thermodynamic stability was calculated using the RNA co-fold webtool.

2.9.0 – Statistical Analysis

GraphPad Prism version 10.0.2 (GraphPad Software, Inc.) was used to calculate mean values, standard deviation (SD), standard error of mean (SEM) and to perform statistical tests, as indicated in figure legends. A maximum of a single outlier was removed from qPCR technical replicates if $SD > 0.5$, with the outlier determined via the largest deviation from the sample mean.

2.9.1 – Statistical Test Workflow

First a Shapiro-Wilk test was performed to determine data normality, with a $p > 0.05$ indicating normal data.

If assessing the significance of the effect of a single nominal variable on a continuous variable within a normal dataset (e.g. The effect of siRNA treatment on miR-155 expression) an independent t-test was used.

When identifying the significance of the effect of two nominal variables on a continuous variable within a normal dataset (e.g. The effect of LPS timepoint + siRNA treatment on miR-155 expression) a two-way ANOVA with Sidak's multiple comparison, while a Kruskal-Wallis test with Dunns multiple comparison was used for non-normal data.

In order to identify whether a significant association exists between two categorical variables in a normal dataset (e.g. upregulated / downregulated miRNA groups and 5p/3p strand identity) a Fischers exact test was used, while a Mann-Whitney U test was used for non-normal data.

Chapter 3

The role of YAP in the regulation of miR-155 expression.

3.1.0 – Introduction, hypothesis and objectives

The acute inflammatory cascade is a complex multi-step process with each component undergoing strict regulation to ensure appropriate timing and magnitude of the response ¹. Mis-regulation of inflammation can lead to chronic inflammatory and autoimmune disorders such as rheumatoid arthritis and ulcerative colitis ^{2,3}. Central to this regulation is the appropriate function of macrophage cells which, in addition to their capacity for direct pathogen removal, act to fine-tune the local inflammatory microenvironment through the release of pro- and anti-inflammatory cytokines, chemokines and other secreted factors ⁵¹⁷.

miRNA-155 has been found to play a vital pro-inflammatory role within the macrophage inflammatory response to infection. Induced ~2 hours after stimulation of the TLR4 pathway via LPS treatment, this miRNA directly inhibits the anti-inflammatory regulators SHIP1, SOCS1 and Bcl6 as well as promoting the activity of the key pro-inflammatory cytokine TNF ^{202–207,518,519}.

The early induction of miR-155 alongside its association with multiple malignancies and disorders makes it a key subject of study regarding early macrophage inflammatory dynamics and potential therapeutics.

Piccinini and Zordan have identified and further validated the role of the extracellular matrix (ECM) glycoprotein tenascin-C (TN-C) in the regulation of miR-155 in murine macrophages ^{289,511}. More widely, TN-C is transiently induced upon tissue injury and infection, acting upon TLR4, $\alpha 9\beta 1$ and $\alpha v\beta 3$ integrins to activate the innate immune response ^{32,520,521}. As such, prolonged

TN-C expression is associated with chronic inflammatory disorders such as rheumatoid arthritis and ulcerative colitis ^{286,522}.

Reduction of TN-C expression in macrophages is shown to elicit a decrease in pre-miR-155 and mature miR-155 levels, without a change occurring to the pri-miR-155 transcript ^{289,511}. Additionally, only ECM-bound TN-C leads to this response and blockade of the TLR4 pathway fails to inhibit this activity.

Therefore this represents a biological mechanism involving TN-Cs mediation of miR-155 expression in a post-transcriptional manner.

Yes-associated protein (YAP) is a primary candidate for regulating miRNA biogenesis events as a result of TN-C signalling. TN-C has been shown to elicit YAP inactivating phosphorylation events within multiple cellular contexts including osteosarcoma and endothelial cells through TN-C induced destabilisation of the actin cytoskeleton ^{311,411,412}. YAP in turn has been shown to act as a regulator of miRNA biogenesis, localising to the nucleus and sequestering p38 when activated, leading to a reduction in global miRNA processing ⁹². This, coupled with the emerging role of YAP within the pro-inflammatory macrophage, presents a compelling post-transcriptional mechanism whereby TN-C may regulate miR-155 biogenesis.

In this project we aimed to validate the regulation of miR-155 by TN-C within RAW 246.7 macrophage cells. This cell line was then utilised in examining the potential role of (YAP) within the TN-C-miR-155 pathway.

3.1.1 – Hypothesis

Tenascin-C directly regulates YAP via depolymerisation of the actin cytoskeleton, this facilitating changes to the microprocessor complex which results in the heightened expression of miR-155 (Figure 1.9.1).

3.1.2 – Objectives

To assess the role of the candidate protein yes-associated protein (YAP) in the regulation of miR-155 expression by tenascin-C. This will be achieved by:

- a) Examining YAP expression within murine macrophage cell lines, as well as its relationship to TN-C, using quantitative PCR (qPCR) and western blot;
- b) Identifying additional murine cell lines which show TN-C to regulate miR-155, this facilitating YAP loss-of-function analysis through siRNA mediated knockdown;
- c) Establishing an ectopic model of YAP expression within RAW 246.7 cells, using nucleofection of a YAP overexpression plasmid, and examining the effect of this expression upon miR-155 biogenesis;
- d) Interrogating the role of the actin cytoskeleton in miR-155s regulation of TN-C by examining the effect of actin-modulating molecules and biological factors on miR-155 expression.

Results -

3.2.0 – Analysis of miR-155 regulation by tenascin-C in RAW 246.7 macrophages.

3.2.1 – TNC knockdown in RAW 246.7 macrophages.

Previous analysis by Zordan into the regulation of miR-155 by TN-C was primarily conducted using bone marrow derived macrophages (BMDMs) from *tnc +/+* and *tnc -/-* mice⁵¹¹. The utilisation of primary cells from a knockout mouse model allowed complete ablation of TNC expression as well as more close modelling of *in vivo* murine macrophages biology compared to immortalised cell lines. However, in order to facilitate future transfection-based experiments, which are lethal to BMDMs, the regulation of miR-155 by TN-C in the RAW 246.7 immortalised murine macrophage-like cell line was examined⁵²³.

Before future experimentation the knockdown of TNC by short-interfering RNA (siRNA) was optimised and validated (Figure 3.1.1a/b).

qPCR was used to examine TNC mRNA expression in RAW 246.7 macrophages incubated with 10nM TNC siRNA or a non-targeting control (Figure 3.1.1a).

Total RNA was extracted 48h after transfection, with cells stimulated with LPS for the last 24h. This was due to evidence from Zordan, showing that TN-C was undetectable by western blot in the supernatants of unstimulated RAW 246.7 macrophages, with 24h LPS substantially increasing detection⁵¹¹.

A single transfection and double transfection method were performed, with the latter utilising two transfections of 10nM siRNA 24h apart (Figure 3.1.1a). This showed no impact on TNC knockdown efficiency, with single and double transfections showing 83% and 71% knockdown, respectively. As a result, all future experiments utilise a single dose of 10nM TNC siRNA.

Successful reduction of TN-C protein expression via siTNC treatment was validated using western blot of cell lysates (Figure 3.1.1b). A reduction in TN-C is evident with 4h LPS treatment, however as suggested previously by Zordan non-stimulated macrophages show too low expression to be detected by western blot⁵¹¹. Attempts were made to detect TN-C protein within the cell supernatant, as TN-C must be secreted in order to incorporate into the ECM, form cell surface complexes or act in its capacity as a soluble signal molecule, however these attempts were unsuccessful.

In order to determine whether TNC knockdown in RAW 246.7 cells lead to a reduction in miR-155 expression similar to that seen in *tnc*^{-/-} BMDMs, knockdown of TNC in RAW 246.7 macrophages was conducted alongside stimulation with LPS for 0, 2, 4, 8 or 24h and analysed by qPCR (Figure 3.1.1c).

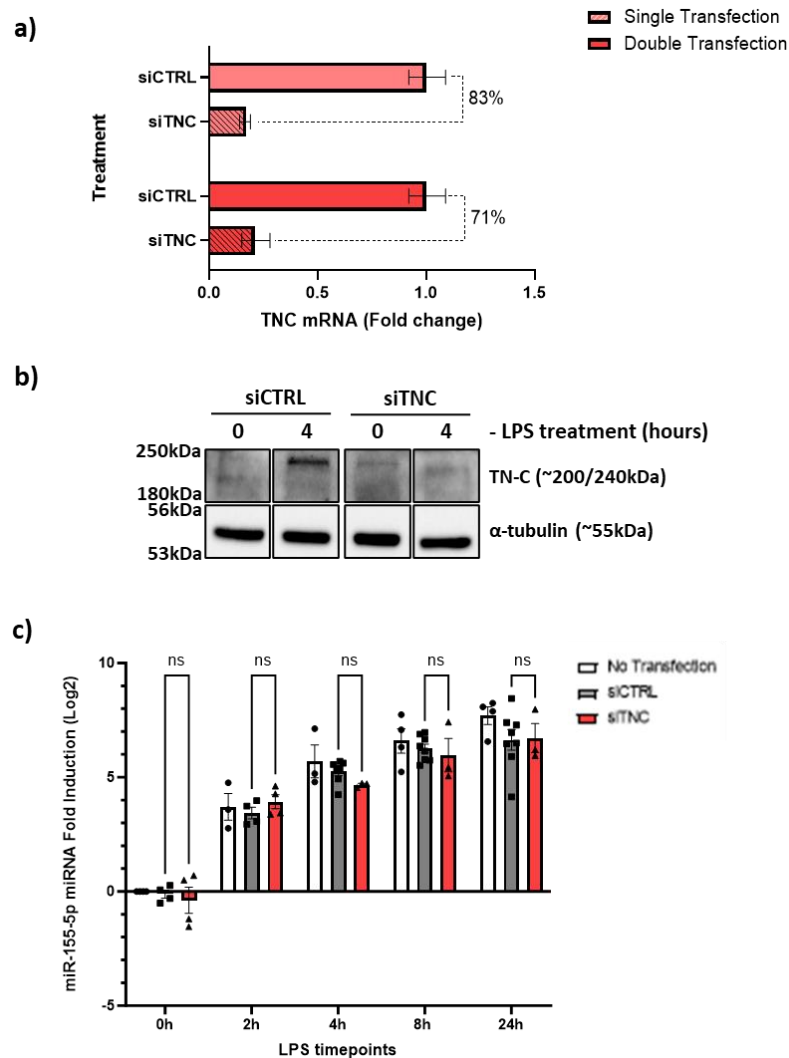


Figure 3.1.1: Tenascin-C knockdown in RAW246.7 macrophages does not significantly impact miR-155 expression following LPS treatment. RAW 246.7 macrophages were transfected with 10nM non-targeting siRNA control or TNC siRNA using lipofectamine RNAiMAX. **a)** Transfection was performed either 48h before RNA extraction (single transfection) or 48h and 24h before RNA extraction (double transfection). **b/c)** Transfection was performed 48h before treatment with 100ng/mL LPS for the durations indicated followed by protein or RNA extraction. **a)** Expression levels of TNC mRNA were quantified by qPCR using HPRT1 as an endogenous housekeeping gene. Relative expression of TNC mRNA was determined via the $\Delta\Delta C_t$ method with siCTRL as the calibrator. Data derived from a single

experiment, technical replicates = 3, mean fold change presented with error bars depicting \pm SD. Percentage reduction in fold change is stated. **b)** Western blot was used to measure TN-C abundance. α -tubulin was used as a loading control. These are not the same samples as used in c. **c)** Mature miR-155 was quantified by qPCR using U6 snRNA as an endogenous housekeeping gene. Relative expression of miR-155 was determined via the $\Delta\Delta$ Ct method with untreated non-transfected RAW 264.7 as the calibrator. \pm SEM; $n\geq 3$; two-way Anova with Tukey's multiple comparison test ($p>0.05$).

MiR-155 expression in cells incubated with siCTRL and siTNC was found to be equivalent in 0, 2, 4, 8 and 24h LPS stimulated samples with no significant difference occurring. Interestingly, previous investigation found a significant decline in miR-155 in *tnc*^{-/-} BMDMs 4h, 8h and 24h after LPS treatment^{289,511}.

3.2.2 – Examination of miR-155 post-transcriptional regulation at the microprocessor.

Previous work by Zordan identified, via northern blot and qPCR, that *tnc*^{-/-} BMDMs show a reduction in pre-miR-155 expression but no change to pri-miR-155 expression or splicing compared to wild-type⁵¹¹. Thus, it was hypothesized that TN-C may be regulating miR-155 processing at the microprocessor, the protein complex responsible for binding and cleaving pri-miRNA into pre-miRNA. Following this hypothesis, RNA-immunoprecipitation (RIP) of the core microprocessor component Drosha was conducted to determine whether TN-C knockdown influences the physical association of pri-miR-155 to the complex (Figure 3.1.2).

RAW 246.7 macrophages were transfected with TNC (siTNC) or scramble control siRNA followed by treatment for 2 hours with LPS before immunoprecipitation using Drosha antibody or IgG control. In parallel to the

RIP analysis, qPCR was also performed upon total RNA from each condition in order to validate TNC knockdown (Figure 3.1.2a). Notably, an exceedingly low average knockdown of TNC (-5.0%) was identified, with two out of four biological replicates showing no reduction in TNC expression, while the others showed only a marginal knockdown (~-35%).

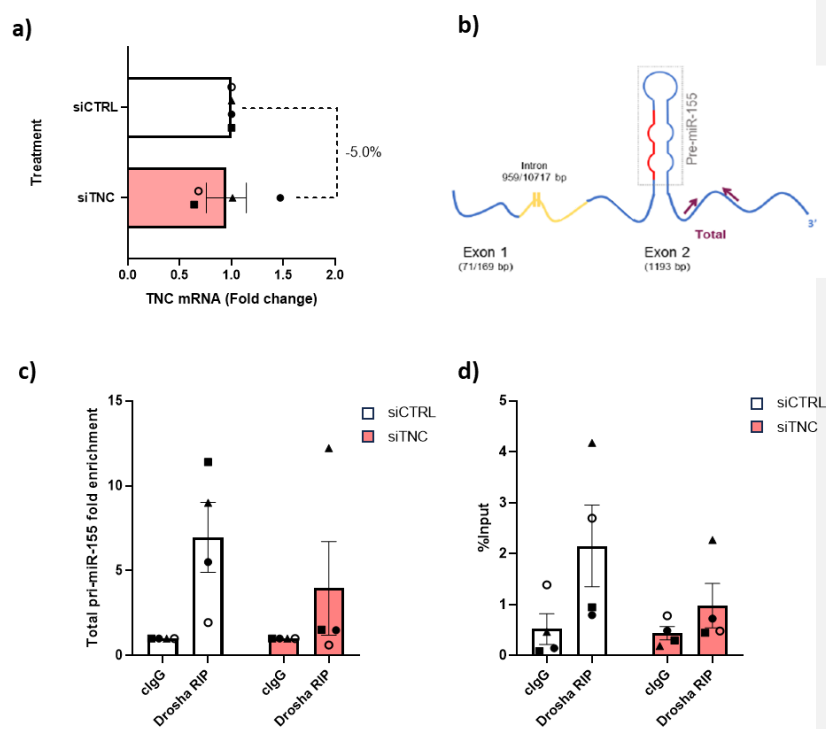


Figure 3.1.2: Tenascin-C knockdown potentially reduces the association of pri-miRNA-155 with Drosha in RAW246.7 macrophages. RAW 246.7 macrophages were transfected with 10nM non-targeting control or TNC siRNA using lipofectamine RNAiMAX and stimulated with 100ng/mL LPS for 2 hours, before immunoprecipitation with anti-Drosha antibody or IgG control. **a)** Expression levels of TNC mRNA were quantified by qPCR using HPRT1 as an endogenous housekeeping gene. Relative expression of TNC mRNA was determined via the $\Delta\Delta C_t$ method with siCTRL as the calibrator. \pm SEM; n=4. **b)** Diagram of pri-miR-155 primer

binding site. **c)** Total pri-miR-155 enrichment was analysed by qPCR and presented as mean fold enrichment relative to IgG control, \pm SEM; n=4. **d)** pri-miR-155 percentage in comparison to input was analysed by qPCR and presented as mean % of input using normalised RIP Δ Ct, \pm SEM; n=4. Two-way Anova with Sidak's post-hoc test. Shape of datapoints is used to differentiate between each biological replicate.

qPCR was used to analyse RNA purified from these immunocomplexes, with pri-miR-155 interaction with Drosha quantified as described by Gagliardi and Matarazzo⁵¹³. To account for variability between samples, IP values were normalised to the 10% input sample. Relative quantification was then utilised, with total pri-miR-155 reported as fold enrichment, with Drosha fractions normalised to the negative control, (Figure 3.1.2c) or percentage of input (Figure 3.1.2d).

Irrespective of the poor TNC knockdown, a clear trend is evident in the RIP data using both normalisation methods, showing reduced pri-miR-155 in the Drosha RIP fraction of macrophages incubated with siTNC compared to those incubated with siCTRL. Although non-significant, this could indicate that TN-C promotes a more stable interaction between pri-miR-155 and Drosha.

Comparison between TNC knockdown effectiveness and the degree of pri-miR-155-Drosha association within each biological repeat fails to identify any correlation (Figure 3.1.2). For instance, RIP 1 (black circle) and RIP 3 (black square) show opposite impacts of TNC siRNA treatment, the prior showing a 48% increase in TNC expression while the later shows a 46% decrease in expression. However, both samples show a similar negative impact of siTNC treatment on pri-miR-155-Drosha association with both analysis methods.

These results illustrate the variability of the RIP process, with more repeats being necessary to reveal the true impact of TNC KO on pri-miR-155 processing.

The potential regulation of pri-miR-155 at the microprocessor directs investigation towards RNA-binding proteins and potential upstream pathways whereby TN-C may influence the microprocessors binding capabilities.

A primary candidate in this regard is yes-associated protein (YAP), with active YAP within human keratinocytes being shown to bind and sequester the microprocessor accessory protein DDX17 leading to reduced pri-miRNA processing⁹². In turn YAP activity within endothelial and osteosarcoma cells has been shown to be regulated by TN-C via the integrin-mediated depolymerisation of the actin cytoskeleton which leads to YAP inactivation^{311,411,412}. As such the relationship between TN-C, the actin cytoskeleton and miR-155 within the macrophage was next examined, acting as a critical link between TN-C and its potential regulation of YAP.

3.3.0 – The role of the actin cytoskeleton in tenascin-Cs regulation of miR-155.

3.3.1 – The impact of TNC knockdown on the actin cytoskeleton of RAW 246.7 macrophages.

Sun *et al.*, 2018 identified in osteosarcoma KRIB cells that, via a joint action of activating integrin $\alpha 9\beta 1$ and inhibiting interactions between integrin $\alpha 5\beta 1$ and syndecan-4, TN-C causes a reduction in actin stress fibre formation³¹¹. This is

further linked to phosphorylation of YAP and the resultant inhibition of its nuclear localisation and primary effector functions, including potential regulation of the microprocessor complex via DDX17 sequestration ⁹². However, the effect of TN-C on the actin cytoskeleton has not been confirmed or characterised within the RAW 246.7 macrophage.

Thus, phalloidin staining and confocal microscopy was performed upon transfection of RAW 246.7 macrophages with siCTRL and siTNC in order to determine whether knockdown of TNC impacts actin formation. In addition, cells were unstimulated or stimulated with LPS for 1h in order to ascertain whether inflammatory induction modifies the effect of TNC on the actin cytoskeleton (Figure 3.2.1).

Within resting RAW 246.7 macrophages incubated with siCTRL F-actin filaments are heavily compacted within the cell cortex, a region along the internal surface of the plasma membrane, with filaments becoming more diffuse towards the cells centre (Figure 3.2.1a). The distribution of the cortical cytoskeleton is relatively even, with microspikes / filopodia visible anchoring the macrophage to the substratum, while adherens junctions connect neighbouring cells (Figure 3.2.1a). Comparably macrophages stimulated with LPS for 1h show a disrupted cortical cytoskeleton and less rounded cellular appearance, evidence of the beginnings of cell spreading which characterise later macrophage induction timepoints, as lamellopodia and more numerous microspikes / filopodia take shape (Figure 3.2.1.a) ³⁵⁶.

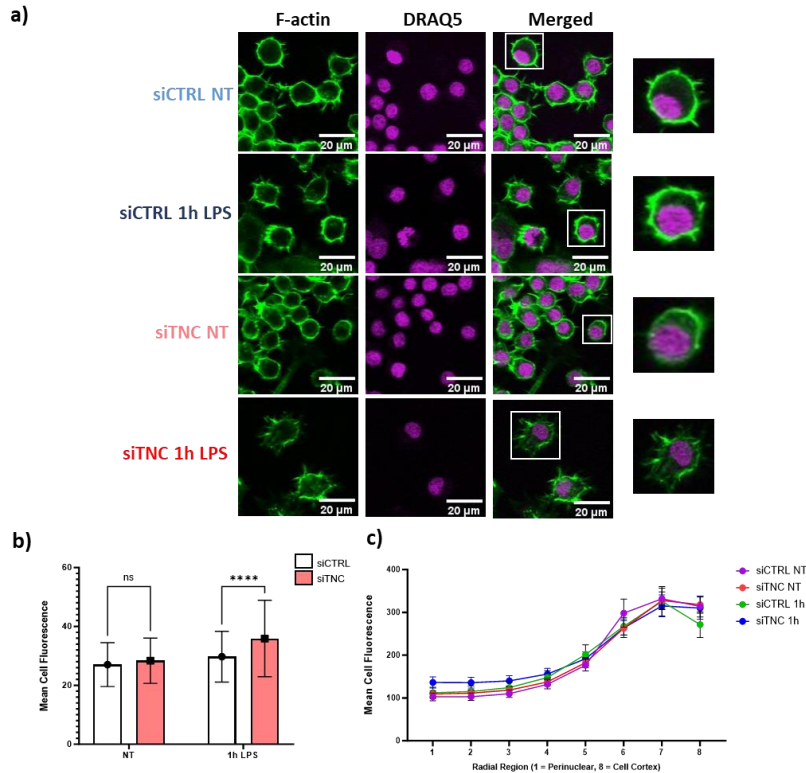


Figure 3.2.1: TN-C knockdown promotes actin polymerisation and increased cell size in LPS treated RAW246.7 macrophages. RAW 246.7 macrophages were transfected with 10nM non-targeting control or TNC siRNA using lipofectamine RNAiMAX and stimulated with 100ng/mL LPS for 1h before fixation. a) Immunofluorescence staining of samples using phalloidin-488 (green) and DRAQ5 (purple). Images visualised with Zeiss LSM-510 Confocal System, using an EX-Plan-Nuofluar 40X/1.30 Oil DIC objective. Scale bar, 20μm. b) Mean total cell actin intensity. c) Mean actin intensity distribution. All analysis performed using CellProfiler. All analysis performed using all available technical replicates from two biological replicates (siCTRL+NT n=180; siCTRL+1h LPS n=93; siTNC+NT n=272; siTNC+1h LPS n=156). Two-way Anova with Tukey's multiple comparison test, $p < 0.0001$ ****.

Compared to control, resting RAW 246.7 macrophages incubated with siTNC show a marked reduction in F-actin localised to the cell cortex, increased phalloidin staining within the cytoplasmic space, as well as a reduced occurrence of microspikes / filopodia formations (Figure 3.2.1a). 1h LPS stimulated macrophages incubated with siTNC maintain the reduced cortical cytoskeletal staining seen in resting TNC knockdown cells. However, they also feature abundant microspikes/filopodia at regions of high cortical cytoskeleton density alongside lamellopodia formed of organised cytoplasmic F-actin bundles, all indicative of an enhanced spreading phenotype (Figure 3.2.1a).

In order to better understand the changes to the actin cytoskeleton, fluorescence distribution analysis was performed using CellProfiler. Notably, this analysis was conducted upon all cells available within the two biological replicates.

Examination of mean total cell fluorescence shows a significant increase in total cellular actin intensity in LPS stimulated cells treated with siTNC compared to those treated with siCTRL (Figure 3.2.1b). However, no such increase is seen in non-LPS stimulated cells.

Fluorescence distribution analysis further identified the primary region of increased actin intensity in LPS stimulated cells treated with siTNC to be within the perinuclear space (Figure 3.2.1c). Additionally, cortical actin intensity is shown to be higher in LPS stimulated cells treated with siTNC than those treated with siCTRL.

Overall, increased whole cell phalloidin intensity is an indicator of enhanced actin polymerisation in LPS treated TNC knockdown cells, providing evidence in support of TN-C causing actin depolymerisation in RAW 246.7 macrophages. However, further biological replicates are necessary to prove a robust relationship between TNC and the actin cytoskeleton within these cells, with culturing upon 3D matrices providing a more biologically relevant environment to analyse the relationship between TNC and macrophage morphology.

3.3.2 – Establishing potential links between actin cytoskeleton modulation and miR-155 expression.

The establishment of the role of TN-C as an enhancer of actin polymerisation in the RAW 246.7 macrophage provides a potential route for TN-C to modulate intracellular activity from the ECM, including the potential changes to miRNA biogenesis occurring at the microprocessor. As such, the links between the actin cytoskeleton and regulation of miR-155 expression were next examined.

Latrunculin B (Lat B), Jasplakinolide (Jasp) and Lysophosphatidic acid (LPA) are three actin modulating compounds used to artificially promote different actin cytoskeletal formations (Figure 3.2.2) ^{524–526}. Lat B binds to actin monomers (G-actin), sequestering them and preventing formation of filamentous actin (F-actin). Meanwhile, Jasp binds G-actin trimers, promoting polymerisation into F-actin, in doing so depleting polymerisation competent G-actin required to maintain stress fibre formation. Finally, LPA is an extracellular signal

molecule which acts as a ligand for multiple G protein-coupled receptors (GPCRs), including LPA_{1/2/4/5/6} which activates G $\alpha_{12/13}$, promoting stress-fibre formation via stimulation of the Rho-Rock cascade ⁵²⁷.

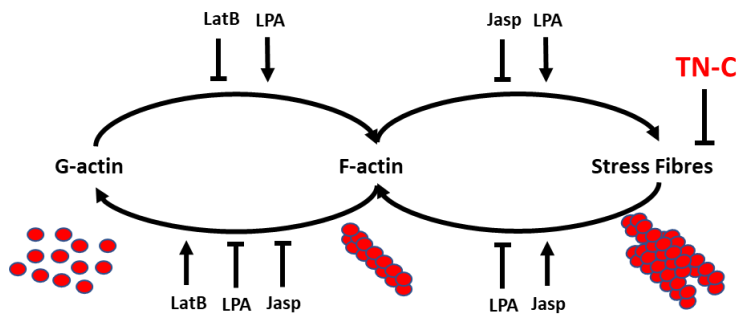


Figure 3.2.2: A schematic depiction of cytoskeletal regulation caused by actin modulators and tenascin-C. The impact of Latrunculin B (LatB), Lysophosphatidic acid (LPA) and Jasplakinolide (Jasp) on the actin cytoskeleton are depicted alongside that of TN-C. Actin monomers are depicted as red circles.

A 3-(4,5-dimethylthiazol-2-yl)-2,5-diphenyl-2H-tetrazolium bromide (MTT) assay was performed to gauge the correct dosage of actin modulators in order to not adversely affect RAW 246.7 macrophage viability (Figure 3.2.3). Cells were treated with modulators for 2h before the assay was performed.

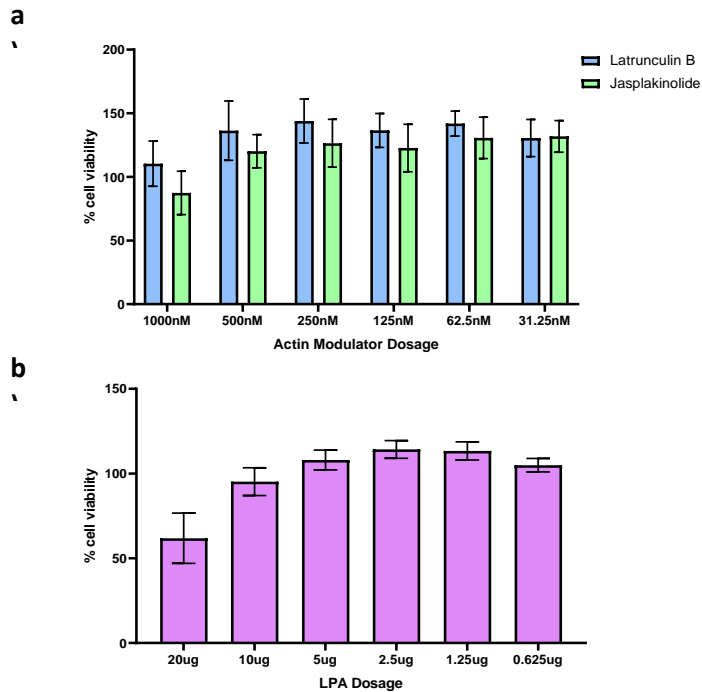


Figure 3.2.3: Actin modulator toxicity analysis. MTT assay of RAW246.7 macrophages after treatment with varying dosages of Latrunculin B (a), Jasplakinolide (a) or Lysophosphatidic acid (LPA) (b) for 2h. Depicted is % cell viability relative to DMSO control. \pm SEM; n=3.

This analysis showed 500nM of Lat B and Jasp and 10ug of LPA to have no negative impact on cell viability (Figure 3.2.3a/b).

To ensure that these modulators at these dosages elicit the expected changes to the actin cytoskeleton of RAW 246.7 macrophages, immunofluorescence analysis was performed (Figure 3.2.4). F-actin formation was assessed via phalloidin staining, this however being incompatible with Jasp treatment as both phalloidin and Jasp bind to the same actin epitope.

Lat B treatment completely blocked phalloidin staining, corresponding to its F-actin depolymerising activity. Interestingly, neither 10 μ g nor 20 μ g of LPA caused visibly enhanced phalloidin fluorescence. This potentially being due to already maximised stress-fibre formation in the non-treated RAW 246.7 macrophage.

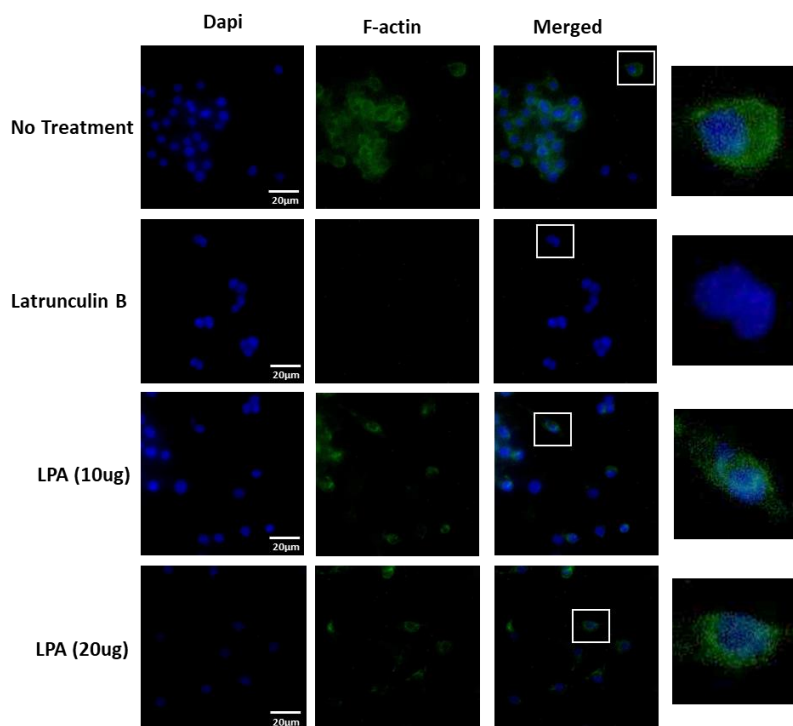


Figure 3.2.4: Validation of the effect of LPA and LatB on the actin cytoskeleton of RAW246.7 macrophages. Immunofluorescence staining of RAW246.7 macrophages treated with 10 μ g or 20 μ g LPA, or 500nM latrunculin B. Actin visualised using phalloidin-488 (green) and the nucleus with Dapi (blue). Images visualised with 20x objective. Representative image of one experiment.

We next aimed to assess whether the enhanced polymerisation of the actin cytoskeleton may lead to miR-155 downregulation. To do so, actin

polymerisation was inhibited or enhanced using Lat B or LPA treatment, respectively, alongside 24h LPS stimulation (Figure 3.2.5).

No significant change in miR-155 expression was apparent with Lat B, LPA or treatment with both modulators.

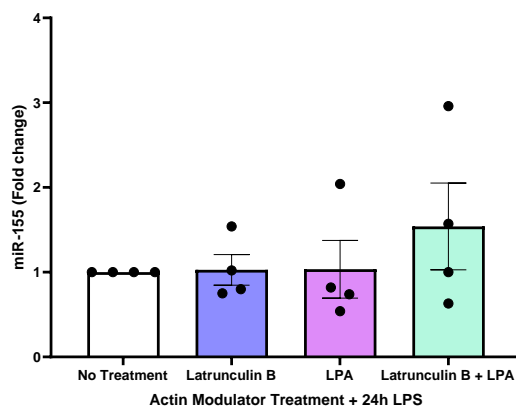


Figure 3.2.5: Modulation of actin polymerization by LatB and LPA has no impact on mature miR-155 expression. RAW 246.7 macrophages were treated with 500nM Latrunculin B and/or 10ug LPA for 2 hours before 24-hour LPS treatment and subsequent RNA extraction. Mature miR-155 was quantified by qPCR using U6 snRNA as an endogenous housekeeping gene. Relative expression of miR-155 was determined via the $\Delta\Delta C_t$ method with no treatment RAW 264.7 as the calibrator. \pm SEM; n=4; Kruskal-Wallis test with Dunn's Multiple Comparison.

This lack of change in miR-155 expression with actin modulation conforms to our previous result showing no significant change in miR-155 expression in RAW 246.1 macrophages incubated with siTNC (Fig 3.1.1). Additionally, each modulator has off target effects which could mask changes to miR-155 expression. For instance, LPA also stimulates the RAS-ERK1/2 pathway and MKP1, both linked to anti-inflammatory induction and masking the potential

effects caused by actin polymerisation⁵²⁸. Lat B treatment stimulates the release of reactive oxygen species (ROS) with these incurring both pro and anti-inflammatory effects⁵²⁹.

Overall, this further illustrates the difficulties in defining how the actin cytoskeleton may link TNC and miR-155 expression within the macrophage. The impacts of actin cytoskeletal rearrangement caused by the actin modulators affect numerous aspects of cell activity introducing many unknowns to our investigation. For example, we have shown that cytoskeletal modulation through Lat B and Jasp seems to reduce TNC expression, with no reduction in mature miR-155 expression as a result of this (Figure 3.2.6a). Most importantly these unknowns are further compounded by the lack of regulation of miR-155 shown by TNC knockdown. However, the modulation of the actin cytoskeleton by TNC demonstrated may provide valuable insight into future examination of the relationship between TNC, the actin cytoskeleton, and miR-155 in BMDM cells.

3.3.0 – Examination of YAP and miR-155 in the RAW 246.7 macrophage.

3.3.1 – Detection of YAP in macrophages.

With examination of the role of the actin cytoskeleton in the regulation of miR-155 by TN-C proving inconclusive, the hypothesised downstream effector of the actin cytoskeleton, YAP, was next examined.

The candidacy of YAP as a transducer of the TN-C signal to the microprocessor is based upon the following evidence. Firstly, Sun *et al.*, 2018 found in osteosarcoma cells that actin depolymerisation by TN-C leads to an increase in YAP phosphorylation and its resultant sequestration within the cytoplasm, away from its nuclear effector function³¹¹. Additionally, chondrocyte cells plated on TN-C coated dishes are reported to show increased YAP phosphorylation, with induced actin cytoskeleton polymerisation by LPA treatment reducing this effect⁴¹². However, He *et al.*, 2019 describes the dephosphorylation and subsequent activation of YAP through TN-C interacting with integrin $\alpha 5\beta 1$ and the stimulation of the Src pathway in Ewing sarcoma⁴¹⁴. This highlights the potential tissue specificity of the TN-C – YAP pathway which has yet to be explored in macrophages.

Aside from its function as a transcriptional co-factor, unphosphorylated YAP has been shown to regulate miRNA biogenesis through binding and sequestration of DDX17 within the nucleus⁹². DDX17 is a microprocessor co-factor which promotes accurate cleavage of specific pri-miRNAs, thus YAP nuclear localisation can lead to reduced pri-miRNA processing. Notably, miR-155 was not identified within the pool of regulated miRNAs within this study, however as experimentation were performed on immortalised keratinocytes it is expected that the inflammatory miR-155 would show low expression.

Based upon this evidence, gain and loss of function experimentation was imperative to ascertain whether there could be a functional link between TN-C, YAP and miRNA regulation in macrophages.

YAP mRNA abundance in multiple murine macrophage cell lines was measured by qPCR, alongside a range of LPS stimulation durations (Figure 3.3.1a). These cell lines included primary and immortalised BMDMs and RAW 246.7 macrophages with either 0.5 μ g or 2.0 μ g of RNA inputted into the reverse transcription reaction. All cell lines exhibited low YAP expression, with CT values $> \sim 30$, with a trend visible of increased LPS incubation further reducing expression.

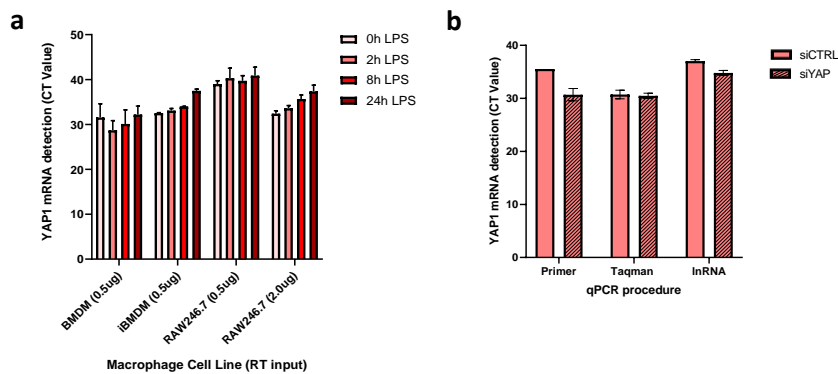


Figure 3.3.1: YAP expression in RAW246.7, BMDM and iBMDM macrophages. a) RAW246.7 macrophages and primary or immortalised bone-marrow derived macrophages were treated with 100ng/mL of LPS for the time indicated before RNA extraction. Expression levels of YAP1 mRNA were quantified by qPCR using cDNA synthesized from 2 μ g or 0.5 μ g total RNA. Data represents CT values of three technical replicates, \pm SD. **b)** RAW 246.7 macrophages were transfected with 10nM non-targeting control or YAP1 siRNA using lipofectamine RNAiMAX. Expression levels of YAP1 mRNA in were quantified by qPCR using three different qPCR methods. Data represents CT values of 2-3 technical replicates, \pm SD.

In an attempt to improve YAP detection via qPCR, three sample preparation and detection techniques were compared using RAW 246.7 RNA extracts

(Figure 3.3.1b). Taqman qPCR probes, locked-nucleic acid primers (LnRNA) and custom oligonucleotide primers all showed the same degree of YAP detection. Moreover, treatment with YAP siRNA did not show a decline in YAP expression utilising any of these methods.

Published research into YAP expression in monocyte/macrophage cell lines shows little evidence for YAP detection via qPCR, with the lack of reported CT values or qPCR data in general supporting our findings of low YAP mRNA detection^{393,399,404}. However, substantial literature evidence exists for YAP detection at the protein level by western blot within these cell lines, provoking our own analysis by this method (Figure 3.3.2).

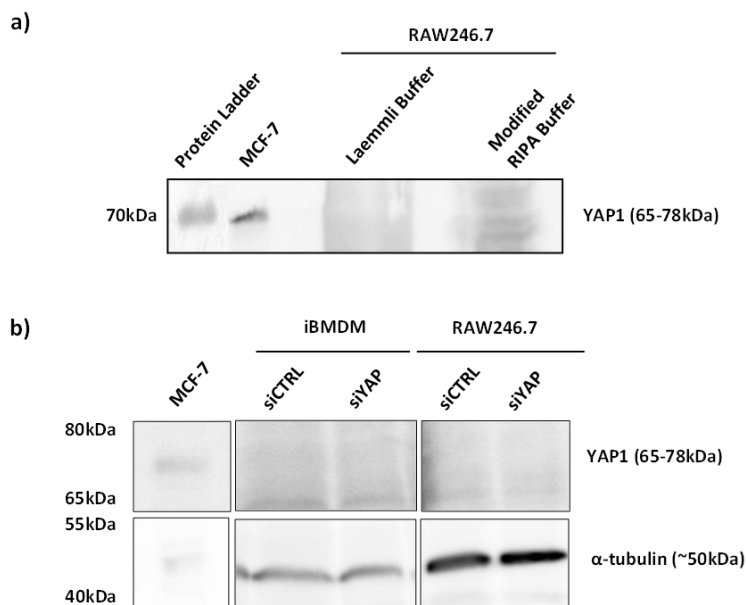


Figure 3.3.2: Attempted siYAP treatment of iBMDMs and RAW246.7 macrophages.

Expression levels of YAP1 were analysed by Western blot using MCF-7 lysate as a positive control. **a)** RAW 246.7 macrophages were lysed using 1x Laemmli Buffer or Modified RIPA

Buffer with their YAP1 banding compared. **b)** RAW 264.7 macrophages and immortalised BMDMs were transfected with 10nM non-targeting control or YAP1 siRNA using lipofectamine RNAiMAX before protein extraction using Modified RIPA Buffer. α -tubulin was used as a loading control. Representative images from a single experiment.

Western blotting was performed using RAW 246.7 macrophage cells lysed using Laemmli or modified RIPA buffer in order to identify whether the gentler lysis provided by the latter would improve YAP detection (Figure 3.3.2a). Distinct banding was not identified using either buffer at the corresponding molecular weight. However, a faint degree of banding using the modified RIPA buffer prompted follow-up analysis using YAP knockdown to determine these bands validity.

siRNA knockdown of YAP was conducted on RAW 246.7 macrophages and immortalised BMDMs which were lysed using modified RIPA buffer (Figure 3.3.2b). Neither cell line showed banding corresponding to YAP, with faint, most likely non-specific, bands being unaffected by the siYAP treatment.

With YAP proving largely undetectable in iBMDMs and RAW 246.7 cells, the expression of YAP in *tnc*^{-/-} and *tnc*^{+/+} BMDMs was investigated via qPCR, as BMDMs are frequently reported to express YAP in the literature and showed the highest expression in our previous analysis (Figure 3.3.3).

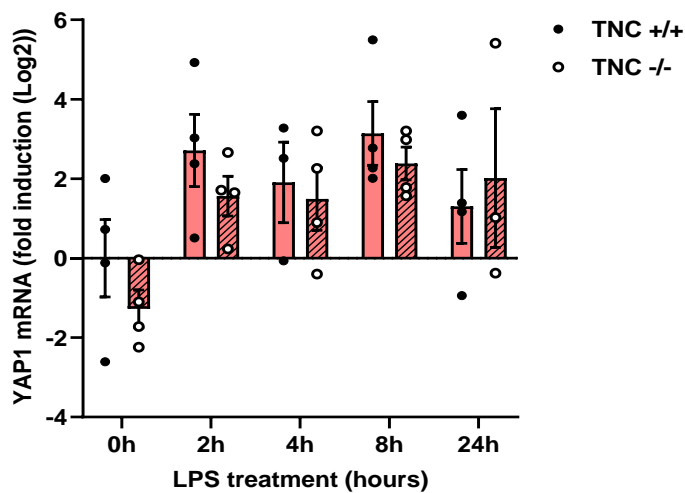


Figure 3.3.3: YAP expression in TNC KO BMDMs. WT and TNC KO BMDMs were treated with 10ng/mL of LPS for the durations indicated, before RNA extraction. Expression levels of YAP1 mRNA were quantified by qPCR using HPRT1 as an endogenous housekeeping gene. Relative expression of YAP1 mRNA was determined via the $\Delta\Delta C_t$ method with 0h LPS TNC^{-/-} as the calibrator. \pm SEM; $n \leq 4$; two-way anova with Sidak's multiple comparison.

Neither TNC knockout nor LPS induction was found to have a significant impact on YAP expression in the BMDM. YAP expression does appear to be potentially induced by LPS treatment, however the large variability in results confounds this effect, likely due to the expression level of YAP being close to or out of the detection range of the qPCR assay.

With the expression of YAP within RAW 246.7 cell found to be undetectable, methods of inducing YAP expression via modifying cellular confluency

(Supplementary Section 8.1.0) were explored. Additionally alternate cell lines showing functionality of a TNC-YAP-miR-155 axis were examined (Supplementary Section 8.2.0).

3.4.2 – Examining potential links between YAP, TNC and miR-155 in E0771 cells.

Following the failure of RAW 246.7 cells to model the potential connection between TNC, YAP and miR-155, this proposed mechanism was next examined in E0771 cells. These cells showing robust expression of both miR-155 and YAP (Supplementary Figure 8.2.3).

qPCR was utilised to examine the efficiency of YAP knockdown and the impact on miR-155 expression upon siYAP treatment (Figure 3.4.2).

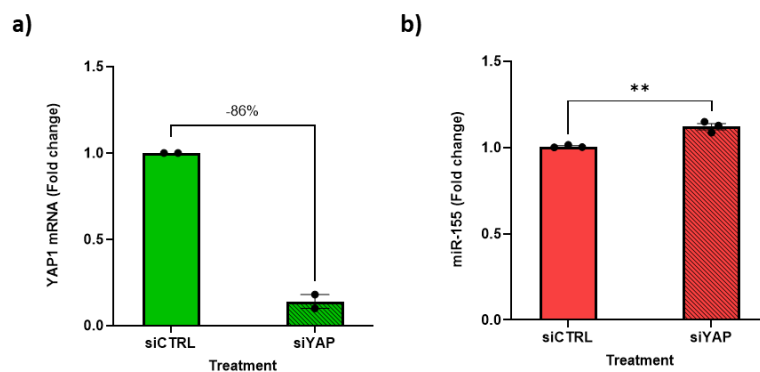


Figure 3.4.2: YAP knockdown in unstimulated E0771 cells leads to a significant upregulation in miR-155 expression. E0771 cells were transfected with 10nM non-targeting control or YAP1 siRNA using lipofectamine RNAiMAX, before RNA extraction. **a)** Expression of YAP1 mRNA in E0771 cells were quantified by qPCR using HPRT1 as an endogenous housekeeping gene. Relative expression of YAP1 mRNA was determined via the $\Delta\Delta C_t$ method with siCTRL as the calibrator. \pm SEM; n=2. Percentage reduction in fold change is stated. **b)** Mature miR-155

was quantified by qPCR using U6 snRNA as an endogenous housekeeping gene. Relative expression of miR-155 was determined via the $\Delta\Delta C_t$ method with siCTRL as the calibrator. \pm SEM; n=3; independent t-test ($p < 0.005^{**}$).

A ~86% decline in YAP mRNA expression due to incubation with siYAP led to a significant induction in miR-155 expression compared to samples of cells incubated with siCTRL (Figure 3.4.2a/b). However, although significant, it is unlikely whether the small 1.12 fold induction in miR-155 expression would cause a biological impact. Thus, induction of miR-155 expression in EO771 cells was attempted in order to determine whether YAP knockdown's upregulatory effect on miR-155 would be increased with heightened miR-155 expression.

siTNC and siYAP transfection was performed in EO771 cells alongside stimulation with 20ng/mL TNF for 24h. Knockdown efficiency and resultant miR-155 expression were determined by qPCR (Figure 3.5.4).

siTNC treatment and siTNC + siYAP dual knockdown incurred a ~60% reduction in TNC mRNA expression compared to control. However, siYAP and dual knockdown treatment showed a limited impact on YAP mRNA expression, ~40% and ~10%, respectively (Figure 3.5.8a).

siTNC and siYAP knockdown had no significant impact on miR-155 expression in TNF treated EO771 cells compared to control (Figure 3.5.8b). This potentially being due to poor YAP knockdown reducing the impact on miR-155 expression.

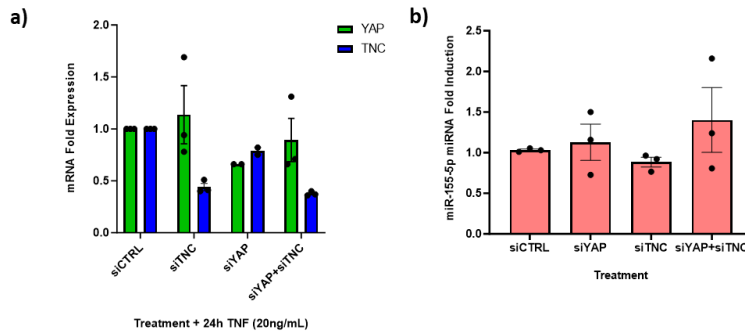


Figure 3.4.4: siTNC and siYAP treatment of TNF stimulated E0771 cells has no impact on miR-155 expression. E0771 cells were transfected with 10nM non-targeting control, YAP1 and/or TNC siRNA using lipofectamine RNAiMAX, before treatment with 20ng/mL TNF for 24 hours followed by RNA extraction. a) YAP1 and TNC mRNA in E0771 cells were quantified by qPCR using HPRT1 as an endogenous housekeeping gene. Relative expression of mRNA was determined via the $\Delta\Delta C_t$ method with siCTRL as the calibrator. \pm SEM; $n \geq 2$. b) Mature miR-155 was quantified by qPCR using U6 snRNA as an endogenous housekeeping gene. Relative expression of miR-155 was determined via the $\Delta\Delta C_t$ method with siCTRL as the calibrator. \pm SEM; $n=3$; two-way anova with Tukey's multiple comparison.

The lack of significant miR-155 modulation through knockdown of TNC in E0771, NIH-3T3 and RAW 246.7 cells highlights the specificity of the macrophage BMDM TNC-miR-155 axis, thus placing the potential downregulation of miR-155 by YAP in E0771 a different cellular context to the previously described TNC-miR-155 interaction in BMDMs.

In parallel to this analysis, the role of YAP within the macrophage TNC-miR-155 pathway was examined using a gain-of-function, RAW 246.7 macrophage YAP ectopic model.

3.4.0 – Using YAP overexpression to examine the YAP-miR-155 relationship in the RAW 246.7 macrophage.

3.4.1 – The impact of overexpressing YAP on miR-155 expression in the RAW 246.7 macrophage.

In order to examine the impact of YAP on miR-155 expression in macrophage cells, the only cell type where the regulation of miR-155 by TN-C is established, gain-of-function analysis was necessary. This is due to the characteristic low expression of YAP in RAW 246.7. Thus, through expressing YAP in RAW 246.7 macrophages to levels above those found natively we attempted to validate a relationship between YAP and miR-155.

Gain-of-function analysis was performed via nucleofection of a pcDNA3.1 plasmid vector containing a YAP1 insert (YAP OE) produced by Genscript (Figure 3.4.1). This is an electroporation-based technique which transfers the DNA directly into the RAW 246.7 cell nucleus and cytoplasm. Nucleofection of an empty pcDNA3.1 vector (Vector) was used as a control.

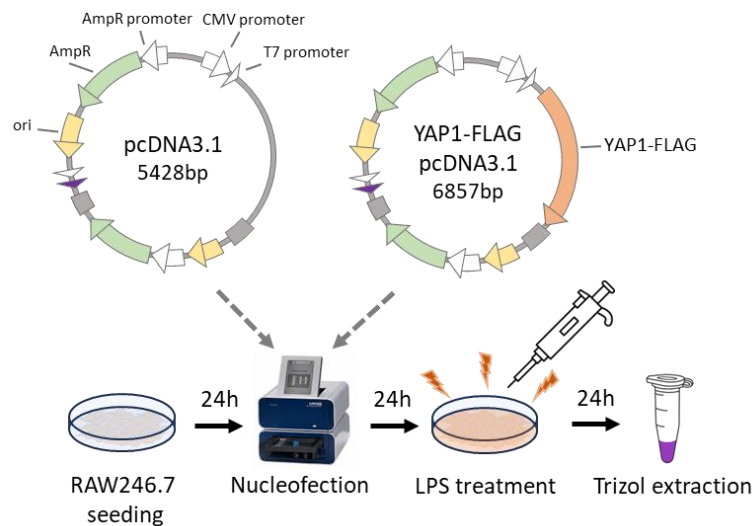


Figure 3.4.1: Schematic of YAP overexpression workflow. Depicted are the steps of the YAP overexpression workflow alongside the features of the empty vector and YAP overexpression plasmids important to YAP expression.

Nucleofection efficiency was assessed via transfection of a pmaxGFP plasmid into RAW 246.7 macrophages with GFP fluorescence detected 24h or 48h post-transfection (Figure 3.4.2a). ~41% and ~26% of cells were successfully transfected at 24h and 48h respectively.

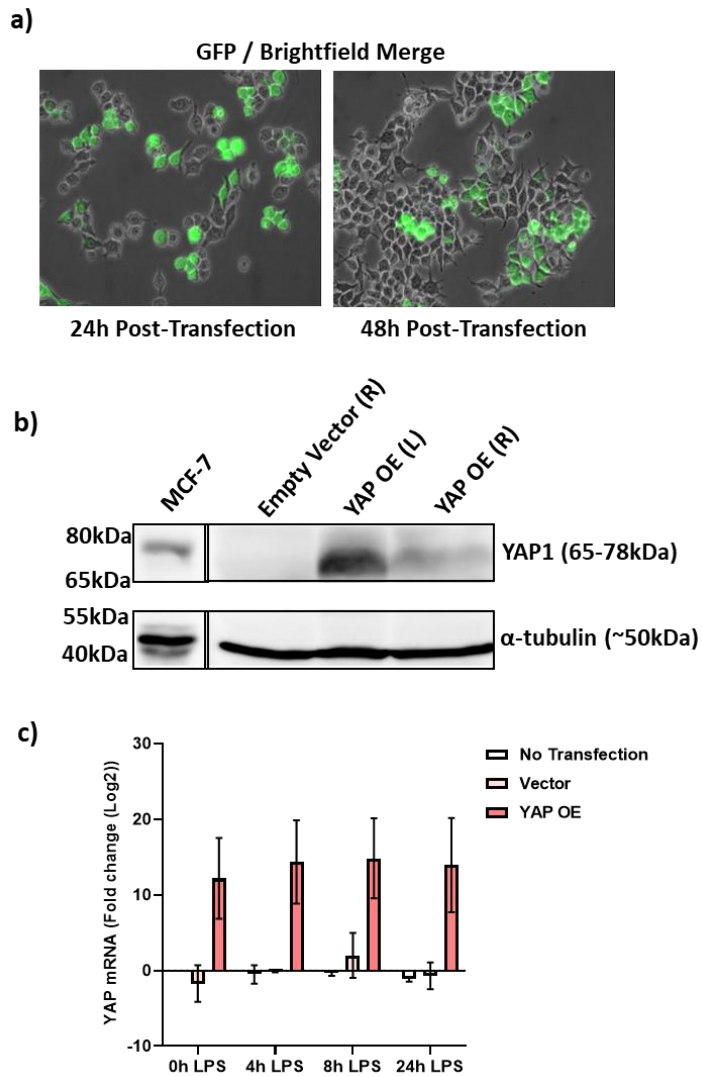


Figure 3.4.2: YAP overexpression validation. **a)** RAW 246.7 macrophages were transfected with 2 μ g pmxGFP plasmid control using the SF Cell Line 4D-Nucleofector X Kit and associated cell line specific protocol. The cultures were imaged 24 and 48 hours post-transfection using a fluorescence microscope. **b)** RAW 246.7 macrophages were transfected with 2 μ g pcDNA3.1 (empty vector) or pcDNA3.1+YAP1-FLAG (YAP OE) plasmids. Protein was extracted 48h post-transfection using either modified RIPA buffer (R) or 1x Laemmli buffer (L). YAP1 expression was analysed by western blot with MCF-7 as a positive control and α -tubulin

as a loading control. c) RAW 246.7 macrophages were transfected with 2 μ g of plasmids as in (b) alongside stimulation with 100ng/mL LPS for the duration depicted, before RNA extraction. YAP1 mRNA expression was quantified by qPCR using HPRT1 as an endogenous housekeeping gene. Relative expression of mRNA was determined via the $\Delta\Delta$ Ct method with 0h LPS non-transfected as the calibrator. \pm SEM; n=2.

Transfection of the YAP OE plasmid was validated via detection of YAP through western blot and qPCR analyses (Figure 3.4.2b/c). Both detection methods show significant upregulation in YAP expression in YAP OE transfected cells compared to those containing the empty vector. qPCR analysis shows no discernible difference in YAP expression in YAP OE transfected cells with 0, 4, 8 or 24h LPS treatment (Figure 3.4.2c).

With YAP overexpression successfully validated, the nucleofection procedure was further optimised. This involved identifying the appropriate plasmid dosage in order to maximise YAP overexpression while also minimising unwanted background inflammatory activation (Figure 3.4.2).

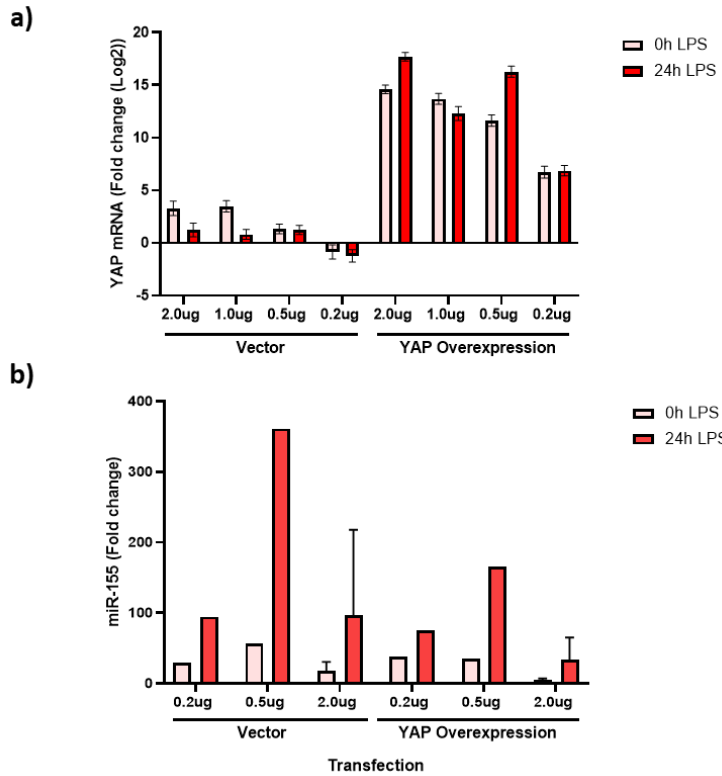


Figure 3.4.3: YAP overexpression optimisation. RAW 246.7 macrophages were transfected with 2.0, 1.0, 0.5 or 0.2 μ g pcDNA3.1 (empty vector) or pcDNA3.1+YAP1-FLAG (YAP OE) plasmids followed by no-treatment or 24h stimulation with 100ng/mL LPS. RNA was extracted 48h post-transfection. **a)** YAP1 mRNA expression was quantified by qPCR using HPRT1 as an endogenous housekeeping gene. Relative expression of mRNA was determined via the $\Delta\Delta$ Ct method with 0h LPS non-transfected as the calibrator. Data derived from three technical replicates, with error bars depicting upper/lower bounds. **b)** Mature miR-155 was quantified by qPCR using U6 snRNA as an endogenous housekeeping gene. Relative expression of miR-155 was determined via the $\Delta\Delta$ Ct method with 0h LPS non-transfected as the calibrator. \pm SEM; $n \leq 2$.

RAW 246.7 macrophages were transfected with 2.0, 1.0, 0.5 or 0.2 μ g of either empty vector or YAP OE plasmid followed by non-stimulation or 24h

LPS treatment (Figure 3.4.3). Assessment of YAP expression by qPCR identified that 2.0, 1.0, and 0.5 µg of YAP OE plasmid led to a similar degree of YAP mRNA upregulation, while 0.2 µg of plasmid showed a reduced YAP upregulation (Figure 3.4.3a). Interestingly, increased vector dosage also showed a small degree of increased YAP mRNA expression, this being potentially linked to morphological changes and reduced cell confluency visibly apparent as a result of nucleofection.

At all dosages, YAP OE transfection alongside 24h LPS treatment shows reduced miR-155 expression compared to the matched empty vector sample, this difference being minimal without LPS treatment (Figure 3.4.3b). Notably, all non-LPS stimulated samples show a baseline increase in miR-155 expression, this likely being the result of inflammatory induction caused by nucleofection of foreign DNA into the macrophage cells^{530,531}.

Based on this validation, 0.5 µg and 2 µg of plasmid were utilised in future analysis. This being due to these dosages showing maximised YAP expression and the same miR-155 expression pattern, while 0.5 µg elicits a greater miR-155 induction in both plasmid treatments (Figure 3.4.3a/b).

To evaluate the potential link between YAP and miR-155 in macrophages, RAW 246.7 cells were transfected with 0.5 or 2.0 µg of YAP OE plasmid or empty vector followed by no-treatment or 24h LPS stimulation. qPCR analysis was performed, examining mature miR-155 and pri-miR-155 expression.

No significant change in miR-155 or pri-miR-155 expression occurred in non-treated or LPS treated macrophages transfected with 0.5 µg of YAP OE

plasmid compared to empty vector controls (Figure 3.4.4a/b). However, transfection with 2.0 μ g YAP OE plasmid showed a significant decline (68-fold \pm 15) in miR-155 expression in non-LPS treated macrophages compared to the vector control (Figure 3.4.4c). A downregulation potentially mirrored in 24h LPS treated cells, however the results are not statistically significant.

The expression of pri-miR-155 in YAP OE macrophages was next assessed, as regulation of mature miR-155 not mirrored by pri-miR-155 would infer a post-transcriptional regulatory event, as seen in TNC knockdown cells. Assessment of pri-miR-155 expression finds the transcript to be downregulated in both non-treated and 24h LPS treated cells transfected with YAP OE plasmid compared to the empty vector controls.

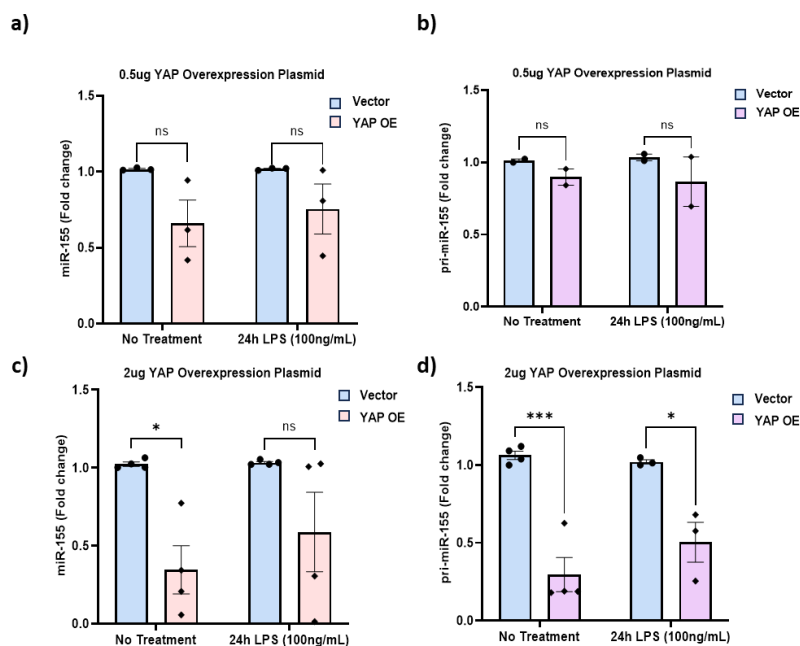


Figure 3.4.4: YAP overexpression causes a significant reduction in the expression of mature and miR-155 primary transcript. RAW 246.7 macrophages were transfected with 0.5 μ g (a/b) or 2.0 μ g (c/d) pcDNA3.1 (empty vector) or pcDNA3.1+YAP1-FLAG (YAP OE) plasmids. RNA

was extracted 48h post-transfection. **a/c)** Mature miR-155 was quantified by qPCR using U6 snRNA as an endogenous housekeeping gene. Relative expression of miR-155 was determined via the $\Delta\Delta\text{Ct}$ method with no treatment empty vector as the calibrator. \pm SEM; $n\geq 3$. **b/d)** pri-miR155 expression was quantified by qPCR using HPRT1 as an endogenous housekeeping gene. Relative expression was determined via the $\Delta\Delta\text{Ct}$ method with no treatment empty vector as the calibrator. \pm SEM; $n\geq 2$. two-way anova with Sidak's multiple comparison test ($p\leq 0.05^*$, $p\leq 0.005^{***}$).

Overall, through ectopic expression of YAP within RAW 246.7 macrophages the regulatory impact of YAP upon miR-155 expression has been identified for the first time. However, as both mature and pri-miR-155 are negatively regulated by ectopic YAP expression this does not conform to the TNC-dependent post-transcriptional regulation of miR-155 we aimed to investigate.

Nevertheless, further examination of this novel YAP-miR-155 axis may provide further insight into systems where these molecules share functional similarities such as oncogenesis in breast cancer and pro-inflammatory signalling within macrophages ^{267,404,518,532}.

3.4.2 – Establishing whether NF- κ B subunit p65 localisation is affected by YAP overexpression.

I have shown via gain-of-function analysis that overexpressing YAP in the RAW 246.7 macrophage elicits a marked downregulation in the expression of both mature miR-155 and pri-miR-155. This change in both the mature miRNA and its primary transcript indicates that YAP potentially regulates miR-155 at the transcriptional level. This conflicts with the hypothesised role of YAP in the

regulation of miR-155 by TN-C, regulating miR-155 in a post-transcriptional manner by targeting co-factors of the miRNA biogenesis pathway. However, by elucidating the potential role of YAP in miR-155 transcriptional regulation we may gain valuable insight into the role of YAP in macrophages during the early inflammatory response as well as specific cancers, such as breast and colon, in which YAP and miR-155 expression are both hallmarks^{206,532–534}.

YAP is a documented regulator of the NF- κ B pathway, with this pathway also serving as the primary means by which miR-155 is transcriptionally induced during the early inflammatory response in macrophages^{249–251}. However, the impact of YAP upon NF- κ B appears to vary depending on the cellular and tissue context. Lv *et al.*, 2018 shows YAP to reduce NF- κ B activation via the polyubiquitination and degradation of upstream TRAF6, while Deng *et al.*, 2018 finds YAP overexpression to disrupt interactions between TAK1 and IKK α /IKK β , thereby reducing NF- κ B activity^{396,397}. These findings have been demonstrated in murine endothelial cells and a model of experimental osteoarthritis, respectively.

Meanwhile, studies within immune cells reveal an inverse relationship between YAP and NF- κ B. Liu *et al.*, 2020 identifies a pro-inflammatory activity of YAP within macrophages, with its interactions with TRAF6 leading to YAP stabilisation and nuclear translocation where it promotes pro-inflammatory gene expression. This corresponds to another study which shows that YAP promotes pro-inflammatory macrophage polarisation^{399,404}. Similarly, p65 has also been found to co-localise with YAP in Jurkat cells, also stabilising and

promoting YAP nuclear translocation and promoting an inflammatory phenotype⁵³⁵.

In order to evaluate whether YAP overexpression is eliciting changes in inflammatory NF- κ B activity localisation, analysis of the NF- κ B subunit, p65, was performed in RAW247.6 macrophages.

RAW 246.7 macrophages underwent nucleofection of YAP OE or empty vector plasmids as previously, followed by no treatment or 60 minutes LPS stimulation. This early LPS timepoint was selected in order to capture the initial p65 influx into the nucleus typical of the early acute TLR4 inflammatory response. Nuclear cytoplasmic fractionation was performed upon protein lysates preceding western blot (Figure 3.4.5).

Lamin-AC (nuclear) and α -tubulin (cytoplasmic) loading controls show insignificant cross-contamination between the fractions (Figure 3.4.5a).

Nuclear localisation of p65 occurs in all treatments, with LPS stimulation leading to an increase in nuclear p65 in empty vector transfected samples but not for those overexpressing YAP. A large quantity of p65 is evident within the cytoplasm, however this is likely due to out loading of the entire cytoplasmic protein extract, which typically has a greater protein concentration than the nuclear extract.

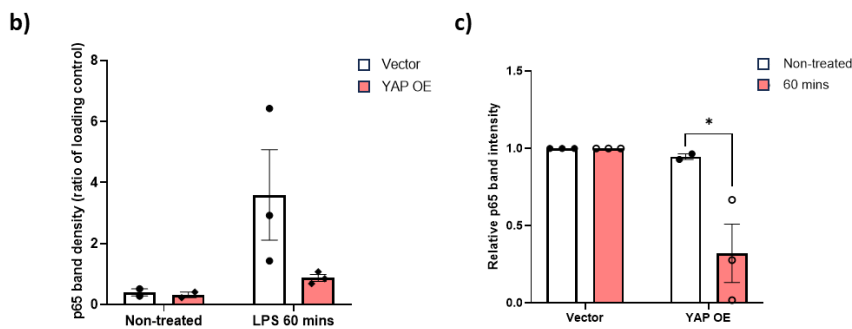
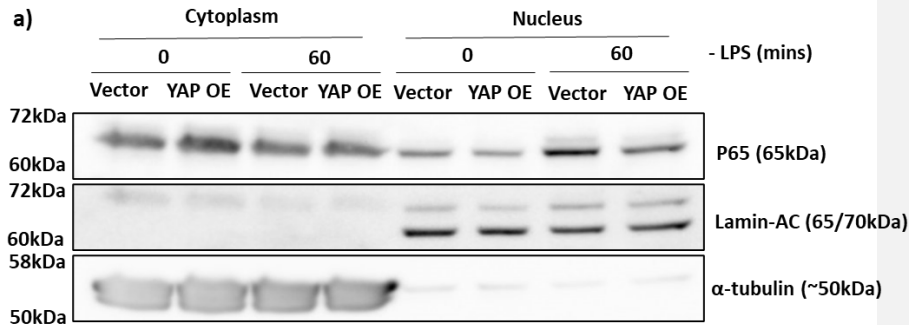


Figure 3.4.5: YAP overexpression leads to a potential reduction in nuclear localised p65.

RAW 246.7 macrophages were transfected with 2.0 μ g pcDNA3.1 (empty vector) or pcDNA3.1+YAP1-FLAG (YAP OE) plasmids. 48 hours post-transfection cells were left untreated or stimulated with 100ng/mL LPS for 1 hour before the protein contents of the nuclear and cytoplasmic compartments were fractionated. **a)** Western blotting was used to determine p65 expression in the cytoplasm and nuclear compartments. Lamin-AC and α -tubulin were used as nuclear and cytoplasmic loading controls respectively. **b/c)** Densitometric analysis of p65 detection within the nuclear fractions. P65 band density was normalised using that of lamin-AC (or α -tubulin in the first repeat where lamin-AC banding was not discernible). **b)** Depicts p65 density as a ratio of the loading control while **c)** shows this value relative to the p65 band density of the vector. \pm SEM; n=3. two-way anova with Sidak's multiple comparison test.

Densitometric analysis of three independent western blotting experiments shows a non-statistically significant decline in nuclear p65 in macrophages transfected with the YAP OE plasmid (Figure 3.4.5b). Normalisation of this

data to the empty vector control samples shows a significant decline in nuclear p65 in LPS stimulated samples compared to non-stimulated, showing that the potential reduction in nuclear p65 as a result of YAP overexpression is LPS dependent (Figure 3.4.5c).

Utilising the same experimental protocol, macrophages were instead fixed and p65 localisation examined using immunofluorescence (Figure 3.4.6).

In both plasmid transfected samples, 1h LPS treatment enhances the overall intensity of p65 staining, matching the well-documented inflammatory induction of NF- κ B (Figure 3.4.3a). Quantitative analysis of p65 pixel intensity within the nucleus and within the cytoplasm was performed on images from three independent experiments. Nuclear and cytoplasmic p65 pixel intensity showed a non-significant reduction compared to vector transfected samples in both non-stimulated and LPS stimulated cells (Figure 3.7.3b).

Through gain-of-function analysis we have identified YAP as a negative regulator of miR-155 transcription, with YAP overexpression downregulating both mature miR-155 and pri-miR-155 expression in RAW 246.7 macrophages. However, our attempts to link YAPs potential anti-inflammatory activity to its previous documented regulation of NF- κ B has shown mixed results. Western blot analysis depicts a non-significant, but consistent, decline in nuclear p65 with YAP OE transfection, this aligning with a reduction in pri-miR-155 expression. Meanwhile immunofluorescence analysis matches this finding, however the apparent decline in p65 fluorescence in the cytoplasm of YAP OE cells may be indicative of overexpression induced transcriptional inhibition.

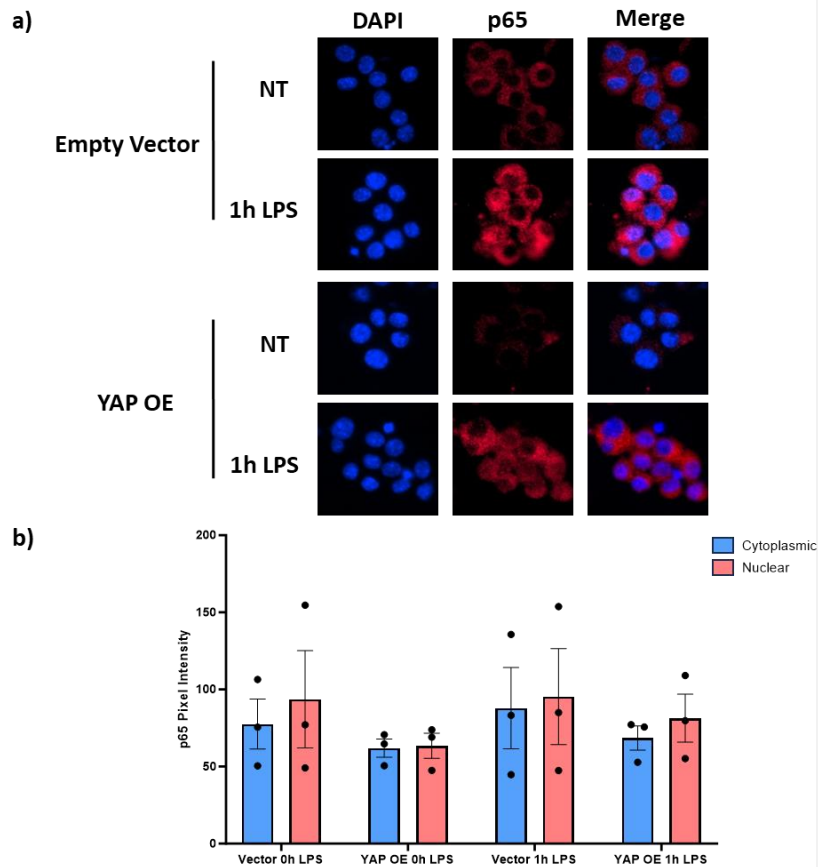


Figure 3.4.6: Analysis of YAP overexpression and p65 localisation by immunofluorescence.

RAW 246.7 macrophages were transfected with 2.0ug pcDNA3.1 (empty vector) or pcDNA3.1+YAP1-FLAG (YAP OE) plasmids. 48 hours post-transfection cells were left untreated or stimulated with 100ng/mL LPS for 1 hour before fixation. a) p65 localisation was observed by immunofluorescence using Dapi (blue) and p65 (red) antibodies. Images were visualised by the Zeiss Exciter Wide Field Microscope with 100x objective. b) Quantitative analysis of p65 staining intensity was performed using CellProfiler. Cells sampled (n), Vector 0h LPS, n=1768; Vector 1h LPS, n=1458; YAP OE 0h LPS, n=1241; YAP OE 1h LPS, n=791. \pm SEM; n=3. two-way anova with Sidak's multiple comparison test ($p < 0.005$).

3.5.0 - Discussion

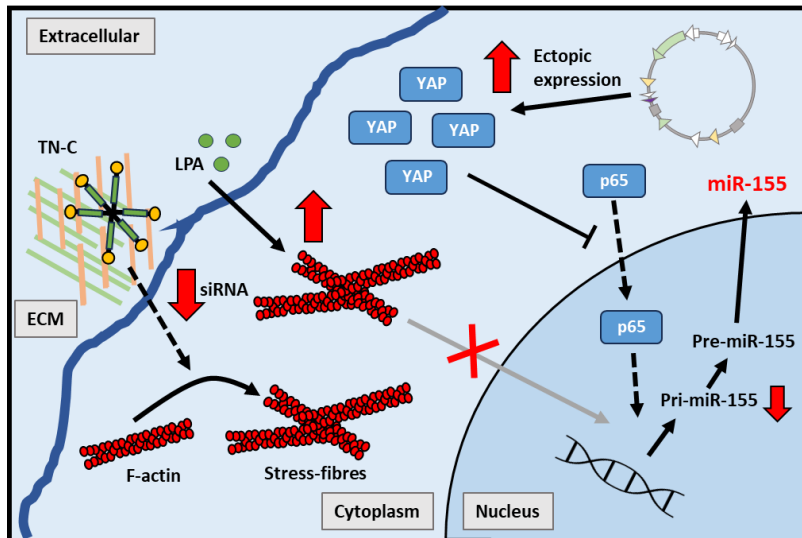


Figure 3.7.1. Results chapter 1 graphic summary. Red arrows indicate upregulation and downregulation respectively. Red crosses indicate pathways found to not be involved in the downstream regulation of miR-155. Inhibitory pathways are indicated by blunt ended arrows.

Previous work conducted by Zordan and Piccinini examining the regulation of miR-155 expression by TN-C was conducted primarily in bone marrow derived macrophages (BMDMs)^{289,511}. Therefore, the extent to which this interaction occurred within RAW 246.7 macrophage-like cells, and their ability to model potential *in vivo* mechanisms, required initial examination.

TN-C expression was shown to not be required for miR-155 induction in RAW 246.7 macrophages, this contrasting the findings of Zordan and Piccinini's BMDM analysis and previous RAW 246.7 validation. This lack of impact of TN-C knockdown on miR-155 expression was found at all timepoints, contrasting

the consistent impact on miR-155 confirmed in BMDMs via qPCR and northern blot ⁵¹¹.

RAW 246.7 cells represent an intermediate monocyte-macrophage stage of macrophage development thus exhibiting broadly similar characteristics to the fully differentiated BMDM cell ^{536–539}. Both BMDMs and RAW246.7 cells feature relatively equivalent cell surface phenotypes, showing similar expression of TLR4, CD11b and CD18 ⁵³⁷. However, RAW 246.7 cells show increased surface expression of CD40, CD11c, CD54 and CD14 compared to BMDMs, with the latter reported to contribute to RAW 246.7 cells exhibiting an enhanced degree of LPS-mediated cytokine induction ^{536,537,540–542}.

Therefore, it is potentially likely that the differences in *tnc* ^{-/-} BMDMs and RAW 246.7s regulation of miR-155 are derived from differences in the degree of TN-C reduction caused by TNC gene ablation (knockout) and transient TNC gene downregulation (siRNA) methods, respectively. miR-155 regulation has been shown by Zordan to be orchestrated by insoluble ECM-bound TN-C and not soluble TN-C secreted from cells ⁵¹¹. As such complete ablation of TN-C expression via gene knockout results in no promotion of miR-155 expression by TN-C at any timepoint, with the extent of miR-155 suppression becoming greater as wild-type expression increases with LPS treatment. Meanwhile the ~80% mRNA knockdown elicited from TNC siRNA treatment leaves a small population of ECM-bound TN-C to continue promoting miR-155 expression, potentially preventing any noticeable change in miR-155 expression.

Zordan previously outlined the potential post-transcriptional nature of TN-Cs regulation of miR-155, finding no change evident in the expression or splicing of the miR-155 primary transcript in *tnc* ^{-/-} BMDMs while pre-miR-155 showed reduced expression ⁵¹¹. This led to the hypothesised regulation of miR-155 at the microprocessor stage of miRNA biogenesis wherein pri-miRNAs are cleaved to form pre-miRNAs. Working alongside Zordan, I identified a consistent but non-significant downregulation in pri-miR-155 associated with the microprocessor component Drosha in TNC knockdown RAW 246.7 cells through RNA-immunoprecipitation. This reduced association could potentially explain reduced pre-miR-155 levels, as less pri-miR-155 is bound to the microprocessor to undergo processing. However, due to the experimental complexity and the challenges of maintaining native microprocessor-miRNA associations more repeats are necessary to reduce variability. In addition, alternative means of TNC knockdown validation, such as FACs analysis or immunoblotting of supernatants and lysates should be utilised, as mRNA measurement by qPCR fails to detect changes in TNC expression which evidently have an impact on the cell.

RNA-binding proteins (RBPs) acts as key accessory proteins to the activity of the microprocessor, their regulation providing a potential means by which TN-C could impact the association of pri-miR-155 to Drosha ²⁶⁴. Previous analysis by Zordan examined the key candidate RBPs tristetrapolin (TTP), KH-type splicing regulatory protein (KHSRP), zinc finger protein 385A (ZNF385A) and zinc finger protein 346 (ZNF-346), with no changes in nuclear localisation or microprocessor association being discernible and only TTP showing a change

in expression in *tnc*^{-/-} BMDMs⁵¹¹. TTP although having no known role in miRNA biogenesis is a prolific regulator of mRNA, leading to their destabilisation and resultant degradation⁵⁴³. Additionally TTP is a known regulator of miR-155, enhancing miR-1 expression which in turn targets pre-miR-155 and impedes its processing⁵⁴⁴. However, *tnc* knockout within BMDMs leads to a large reduction in LPS-dependent TTP expression, this regulation being opposite of that expected if TTP were directly regulating miR-155⁵¹¹.

As-such we focused upon a novel hypothesis, examining the potential role of YAP within the TNC-miR-155 mechanism.

Co-immunoprecipitation experiments within the literature show no direct interaction between YAP and the microprocessor components Drosha or DGCR8, however YAP has been shown to modulate pri-miRNA processing through RBP regulation⁹². Unphosphorylated YAP has been shown to localise to the nucleus and sequester DDX17, a known microprocessor accessory RBP, through its WW1 domain^{90,92,545}. DDX17 is known in this context to promote pri-miRNA processing through binding to a VCAUCH sequence +7 to +12nt downstream of the 3' strands pri-miRNA basal junction, with YAP nuclear localisation thus associated with reduced pri-miRNA processing⁹². However, it should be noted that the only study outlining this mechanism shows YAP inactivation to have no impact on pri-miR-155 processing⁹². This is likely due to the low expression of miR-155 within the immortalised keratinocytes examined placing miR-155 below the analysis cut-off. Notedly, pri-miR-155

does contain a potential DDX17 binding GCAUUC sequence within the +7 to +12nt window of its 3' flanking region conserved in both humans and mice. However, the 3' UC portion of this binding sequence is associated with reduced DDX17 regulation probability, potentially implying a reduced degree of pri-miR-155 regulation by DDX17. Although Mori *et al.*, 2014 show no effect of stem-loop deletion on the regulation of pri-miRNA by DDX17, a more recent study by Remenyi *et al.*, 2016 conflicts with this evidence, finding DDX17 to directly interact with closed stem-loop of pri-miR-132 and facilitate its enhanced processing^{92,545}. However, the stem-loop of pri-miR-155 does not resemble that of miR-132, reducing the likelihood of this mechanism of DDX17 action.

YAP has also been found to bind to histone deacetylase 3 (HDAC3) in macrophage cells, leading to direct binding and inhibition of the Arg1 promoter in a deacetylase independent manner³⁹⁹. HDAC1, HDAC2 and HDAC3 are known to associated with Drosha, with HDAC1 found to enhance miRNA processing through deacetylation of DGCR8⁵⁴⁶. Thus, YAP could potentially regulate miRNA processing through HDAC binding. This also furthers the possibility of YAP having as-of-yet undocumented associations with RBPs with the capacity to directly target miR-155.

TN-C has been shown to regulate YAP through depolymerisation of the actin cytoskeleton in osteosarcoma and chondrocyte cells, leading to YAP phosphorylation and subsequent cytoplasmic sequestration and degradation^{311,419}. This provides a means by which TN-C could facilitate changes to pri-

miR-155 processing at the microprocessor, eliciting YAP phosphorylation which reduces the quantity of nuclear YAP that negatively regulates miRNA processing through accessory RBP binding and sequestration. However, evidence from Ewing sarcoma cells shows TN-C to cause dephosphorylation of YAP, highlighting the tissue specificity of this pathway⁴¹⁴. As such I aimed to conduct novel examination of the TNC-YAP and YAP-miR-155 associations within macrophage cells.

The actin depolymerisation shown to be caused by TN-C was validated in RAW 246.7 macrophages, with knockdown of TNC expression via siRNA treatment leading to enhanced actin polymerisation. This corroborates evidence found in non-macrophage cell lines. Literature evidence describes TN-C modulating actin stress-fibre formation through activation of integrin $\alpha 9\beta 1$ as well as through inhibiting interaction between integrin $\alpha 5\beta 1$ and syndecan-4 which promote actin polymerisation⁹². In Chapter 2, the presence of these integrins on the RAW 246.7 macrophage cell surface will be tested, however literature evidence indicates that each of these integrins are present on the macrophage and thus potentially responsible for the effect of TN-C on actin polymerisation^{521,547,548}.

Further examination utilised actin modulating factors to identify whether changes to the actin cytoskeleton, such as those caused by TN-C, lead to a change in miR-155 expression. Neither actin polymerisation via LPA treatment nor actin depolymerisation via Latrunculin B treatment significantly affected miR-155 expression in the RAW 246.7 macrophage. Follow-up attempts were

made to determine whether actin polymerisation via Latrunculin B treatment would rescue the lowered miR-155 expression as a result of TNC knockdown. However, all actin modulator treatments resulted in a downregulation in TNC mRNA expression even when not accompanied by siRNA treatment. This attesting to a regulatory feedback loop, whereby the actin cytoskeletal state modulates TNC expression, matching evidence from superficial zone chondrocytes showing a similar downregulatory impact of latrunculin B treatment on TNC mRNA and protein expression ⁵⁴⁹. Within chondrocytes, fibroblasts, and epithelial cells TNC expression has been found to be promoted by myocardin-related transcription factor-A (MRTF-A), the function of which is inhibited during actin depolymerisation as it localises to the cytoplasm due to its binding to G-actin monomers ⁵⁴⁹⁻⁵⁵³. Functional expression of MRTF-A has been confirmed in BMDMs, indicating that this transcription factor likely plays a part in the regulation of TNC mRNA expression by the actin cytoskeleton that we observe ⁵⁵⁴.

Latrunculin B has been shown to increase and jasplakinolide has been shown to decrease NF-κB activation in epithelial cells, using equivalent dosages to our experiments, with long-term latrunculin B treatment also shown to increase NF-κB activation and transcription factor activity in intestinal cells ^{555,556}. Furthermore, latrunculin B and jasplakinolide have been shown in the macrophage to induce NF-κB mediated transcription as a result of increased reactive oxygen species (ROS) generation, this potentially explaining the increased mature miR-155 and pri-miR-155 expression we see as a result of Jasplakinolide treatment ⁵²⁹. In-fact miR-155 is an inhibitor of Foxo3a, itself a

ROS inhibitor, thus leading to ROS potentially creating a miR-155 positive feedback loop⁵⁵⁷. The ROS generated by actin modulation have also been shown to regulate enzymes involved in miRNA biogenesis, causing downregulation of Dicer-mediated processing and upregulation of the pro-Drosha processing transcription factor p53^{558,559}. LPA modulates the actin cytoskeleton by binding to cell surface LPA receptors which then signal through G-protein coupled receptor (GPCR) α 12/13 to activate the Rho-ROCK pathway and promote stress fibre formation⁵²⁷. However, through other GPCRs LPA treatment of macrophages has been shown to have an anti-inflammatory effect thought to be caused by the RAS-ERK1/2 pathways stimulation and activation of MKP1⁵²⁸.

This highlights how examination of miR-155 in macrophages exposed to exogenous actin modulators gives rise to numerous potentials off-target effects which may obscure the impact of native actin modulation, such as that performed by TN-C. These events couple with the general widespread impact of actin modulation on internal cellular dynamics to produce a large degree of variability between experimental repeats.

Recent investigations into YAP functionality within macrophage cells makes note of the reduced basal levels of YAP within these cell types^{393,400,404,560,561}. Our attempts to detect YAP have corroborated its low basal expression, with a lack of both protein and mRNA detection evident in multiple macrophage cell lines. Only in primary BMDM cells was suitable detection of YAP1 mRNA achieved, showing a non-significant upregulation in expression with LPS

treatment. This finding is supported by previous inflammatory stimulation experiments in BMDMs and peritoneal macrophages, having been performed with LPS and IFN γ , which show increased YAP protein expression with treatment ³⁹⁹.

Furthermore, we show that TNC knockout does not impact this inflammatory induction of YAP. TNC knockdown is reported to produce an impeded inflammatory phenotype and thus would be thought to have a negative effect on YAP inflammatory induction within the macrophage ²⁸⁹. However, experiments in Ewing Sarcoma cells support our findings showing TNC knockout to have no effect on YAP protein expression ⁴¹⁴.

The reduced basal expression of YAP in monocyte lineage cells is logical, due to the reduced necessity in non-tissue forming cells for proliferative signalling. The constraints on proliferation caused by space availability have been shown to be limited in the macrophage, with growth signals rather than the effect of mechano-transduction pathways, such as the Hippo-pathway, influencing proliferation ⁵⁶².

However, initial analysis showed a potential increase in YAP protein expression alongside reduced RAW 246.7 cell confluency. Follow-up attempts to validate the YAP protein banding by siRNA knockdown were unsuccessful, with only qPCR analysis confirming successful YAP mRNA knockdown. The small degree of YAP mRNA induction in the low-confluency workflow allowed us to examine the effects of YAP knockdown for the first time in the RAW 246.7 macrophage, finding YAP knockdown to not affect miR-155 expression.

However, likely due to the necessity of a cell dissociation step in the low-confluency siRNA workflow leading to altered expression patterns, TNC and YAP knockdowns were poor. Thus, further experimental refinement is necessary in order to see the true effect of natively expressed YAP on miR-155 in the RAW 246.7 macrophage.

Low YAP expression within monocytic cells led to the attempted adoption of an alternative cell model which would allow investigation into the role of YAP in the TN-C–miR-155 mechanism in a system where YAP expression is in abundance. NIH-3T3 and EO771 cells were selected for this purpose, both showing robust expression of YAP and miR-155. YAP was shown to negatively regulate miR-155 expression in unstimulated EO771 cells, with a significant induction in miR-155 expression occurring as a result of YAP siRNA knockdown. A similar but non-significant effect was seen with YAP knockdown in NIH-3T3 cells, however in both cell types the change in miR-155 expression was exceptionally small at an increase of ~ 1.1 fold, thus having dubious biological relevancy. Additionally, TNC knockdown did not elicit the reduction in miR-155 expression characterised in macrophage cells. With further investigation using TGF- β or TNF treatment attempting to determine whether miR-155 stimulation, as occurring in macrophages via LPS treatment, is necessary for its regulation by TN-C. No change in the stimulated expression of miR-155 was found to occur due to either TNC or YAP knockdown in either cell type, this lack of responsiveness rendering these cells unusable as a means of examining the hypothesised role of YAP in the TNC-miR-155 mechanism.

LPS treatment of macrophage cells induces upregulation in miR-155 expression primarily through the direct action of the TLR-4 pathway induced transcription factors NF- κ B and AP-1^{249–252}. Importantly, Zordan identified that the regulation of miR-155 by TN-C functioned independently of the TLR-4 pathway, with inhibition of TLR-4 signalling not hindering the reduction in miR-155 expression in *tnc*^{-/-} BMDMs⁵¹¹. Thus, it is striking that TN-C knockdown fails to elicit a change in miR-155 expression within EO771 and NIH-3T3 cells either with or without miR-155 stimulation, as these cells are abundant in TN-C, YAP and miR-155. This result indicates that either TNCs regulation of miR-155 requires an additional macrophage specific factor, potentially a cell surface component to interface with TN-C, or that the robust expression of miR-155 seen in resting EO771 and NIH-3T3 cells belies an upregulatory mechanism outside of or more substantial than the regulatory impact of TN-C. For instance, the IL-1B and TGF- β pathways have both been shown to induce miR-155 expression in fibroblasts and breast cancer cells, passive production of these pro-fibrotic factors potentially giving rise to the aforementioned robust expression of miR-155^{257,563}.

With low YAP expression in macrophage cells thwarting loss-of-function studies and the inability of alternative cell lines to model the TNC-miR-155 pathway, a YAP overexpression study was performed in RAW 246.7 macrophages. This experiment identified for the first time the downregulatory effect of YAP on miR-155 transcription, with transfection with a YAP expression plasmid resulting in a ~50% reduction in the expression of both mature miR-155 and the pri-miR-155 transcript. The reduction in mature miR-

miR-155 was only found to be significant without LPS stimulation, indicating that the TLR-4 mediated inflammatory cascade may overcome the negative modulation by YAP with sufficient miR-155 induction. This discovery that YAP negatively regulates miR-155 transcription further reduces the likelihood of our hypothesised role for YAP in the TNC-miR-155 mechanism, as the regulation of miR-155 by TN-C has been proven to elicit no change in pri-miR-155 expression and thus assumed to be post-transcriptional. However, the regulation of miR-155 by YAP in the macrophage lends further evidence to the growing role for YAP as an anti-inflammatory mediator.

In endothelial cells YAP has been shown to promote degradation of TRAF6, leading to subsequent downregulation of the NF- κ B pathway, an occurrence also reported to be caused by YAPs disruption of TAK1, IKK α and IKK β interaction in a model for osteoarthritis^{396,397}. NF- κ B is a key transcription factor responsible for the early induction of miR-155 expression²⁴⁹⁻²⁵¹. Thus, by overexpressing YAP we could be reducing the activity of this pro-inflammatory transcription factor causing the changes seen in both mature and primary transcripts. However, this functionality contradicts recent studies in macrophage cells, showing YAP to bind to the NF- κ B subunit p65 and aid NF- κ B nuclear translocation, promoting pro-inflammatory cytokine production⁵³⁵. Contrary to the discoveries in epithelial cells, macrophage TRAF6 was also found to bind YAP, but instead promoted YAP nuclear translocation⁴⁰⁴. Additionally, knockdown of macrophage YAP has previously been reported to enhance pro-inflammatory gene expression in a NF- κ B independent manner³⁹³. This cumulative evidence indicates a cell-type specific role for YAP in

inflammatory regulation, with macrophage YAP exhibiting a pro-inflammatory function. Intriguingly, the downregulation of miR-155 transcription due to YAP overexpression we witness within the macrophage would dispute this previous evidence, instead indicating an anti-inflammatory mechanism in the macrophage.

To further identify by what means YAP regulates miR-155 transcription within our YAP overexpression model, nuclear localisation of the NF- κ B subunit p65 was assessed. Immunoblotting identified a reduction in p65 localised to the nucleus in LPS treated macrophages overexpressing YAP, with no change evident in cytoplasmic abundance. However, immunofluorescence analysis of samples from the same experiments show high variability, with a reduction in total p65 evident in the un-stimulated YAP overexpressing cells, but no difference is seen in nuclear localisation of LPS stimulated samples to match that of the immunoblot. The disparity in these results is likely due to the basal inflammation elicited by the nucleofection procedure. This resulting in visible p65 nuclear localisation without LPS treatment as well as the miR-155 expression in non-stimulated cells seen previously. Immunofluorescence, as a more sensitive detection method is more liable to have results confounded by increased background p65 expression levels. Additionally, RAW 246.7 macrophages exposed to nucleofection often exhibit irregular cell morphologies, introducing difficulties in cell selection for immunofluorescence quantitative analysis which do not impede p65 detection by immunoblot. Thus, our immunoblot evidence serves to identify the regulation of p65 localisation as a likely means of miR-155 transcriptional regulation by YAP.

However, the mechanism by which this occurs remains unknown, with future experimentation examining the direct binding of overexpressed YAP to TRAF6 or p65 necessary to validate whether the previously described or a novel anti-inflammatory mechanism is at play.

It should be recognised that the YAP overexpression analysis serves as an imperfect model for the natively higher YAP expressing BMDMs, with loss-of-function analysis in these cells being necessary to fully validate the role of YAP in miR-155 regulation. Overexpression analysis includes several flaws. For instance, macrophages transfected with the empty plasmid vector and without LPS stimulation showed heightened miR-155 expression. This is likely a result of the transfection procedure inducing an inflammatory induction either due to the disturbance of the macrophages plasma membrane via electroporation, or in response to the insertion of foreign DNA^{530,531}. Indeed, plasmid DNA lipofection has been shown to stimulate NF- κ B transcription factor activity through DHX9 as well as induction of the MyD88 pathway via DHX36⁵⁶⁴⁻⁵⁶⁷. Such effects of the nucleofection procedure were corrected for through normalisation of results to the empty vector transfected samples, however they still represent a highly perturbed macrophage. Additionally, the >1000 fold upregulation in YAP mRNA expression in the transfected RAW 246.7 cells far exceeds the native expression of macrophages, which reportedly show a low YAP expression^{393,400,404,560,561}. It should also be noted that the introduction of ectopic promoters may also leads to the titration of transcription factors, resulting in the downregulation of generalised gene expression as we see with miR-155 and potentially p65.⁵⁶⁸

Thus, further use of this model would benefit from utilising the weaker ubiquitin C promoter (UBC) within the transfection vector in place of the strong cytomegalovirus immediate-early promoter (CMV) in order to limit YAP overexpression⁵⁶⁹.

Overall, our findings identify YAP as a potential negative regulator of miR-155 expression, with overexpression analysis within the RAW 246.7 macrophage and knockdown of YAP within EO771 cells supporting this claim. We additionally implicated the downregulation of p65 nuclear localisation by YAP as a contributor to this effect. However, the low endogenous YAP expression within macrophages, in particular RAW 246.7 cells, reduces the likelihood of this mechanism having an effect in our cell system of interest. The evidence for TN-C inducing actin cytoskeletal depolymerisation within the macrophage couples with the lack of miR-155 modulation elicited from changes to the actin cytoskeleton, showing the non-existence of the potential actin sensing role of YAP within the TNC-miR-155 mechanism. Finally, with the impact of YAP overexpression on miR-155 being transcriptional, not post-transcriptional as found in TN-Cs regulation of miR-155, we have disproved interconnectivity between TN-C-YAP and YAP-miR-155 within the RAW 246.7 macrophage.

With the role of the actin cytoskeleton and YAP within the TNC-miR-155 pathway disproved, I next aimed to identify by which cell surface elements TN-C regulates miR-155 and whether the RBP master regulator MK2 participates in the TN-C-miR-155 mechanism.

Chapter 4

The role of the p38-MK2
pathway and integrin
receptors in the
regulation of miRNA-155
by TN-C

4.1.0 – Introduction, Hypothesis and Objectives

In order for TN-C to influence pri-miR-155 association with the microprocessor a process of intracellular signalling must occur. Such a process would likely first involve the interaction of ECM bound TN-C with a cell surface receptor.

TN-C directly interacts with a number of cell surface receptors, including TLR4, EGFR and $\alpha\text{v}\beta\text{1}$, $\alpha\text{v}\beta\text{3}$, $\alpha\text{v}\beta\text{6}$, $\alpha\text{2}\beta\text{1}$, $\alpha\text{7}\beta\text{1}$, $\alpha\text{8}\beta\text{1}$ and $\alpha\text{9}\beta\text{1}$ integrins ^{32,570–572}.

These interactions facilitate direct communication into the cell, however TN-C may also influence cellular phenotype through binding to other ECM components, thus modulating their receptor interactions, as well as sequestering or acting as a reservoir for a variety of soluble factors ⁵⁷³.

Previous work by Zordan and Alessandro have found blockage of TLR4, EGFR and integrins $\alpha\text{9}\beta\text{1}$, $\alpha\text{v}\beta\text{3}$ and $\alpha\text{5}\beta\text{1}$ to not significantly influence miR-155 expression ⁵¹¹. Additionally, examination of the novel Mac1 receptor and NRP1 co-receptor found only the latter to influence miR-155, with knockdown of NRP1 in steady-state macrophages inducing miR-155 expression.

As both the primary candidate signal protein YAP and changes to the actin cytoskeleton have been shown to not elicit post-transcriptional regulation of miR-155 the examination of a new candidate signal pathway is required.

Monocyte-derived macrophage treatment with the TN-C FBG domain has been shown to stimulate phosphorylation of the kinase p38 α ³⁰². A downregulation in p38 α phosphorylation as a result of TNC knockdown could in turn leads to a reduction in activation of its downstream kinase, the master

regulator of RNA-binding proteins (RBPs) MAPKAPK2 (MK2) ⁴⁶⁷. MK2 is known to phosphorylate RBPs and modulate their RNA-binding capacity, potentially facilitating the post-transcriptional regulation of pri-miR-155 through modulation of the known pri-miRNA regulators such as HuR and p68 as well as the inflammatory regulator TTP ^{169,505,574–576}. In particular reduced MK2 activation is known to increase activity of TTP, this RBP being associated with the degradation of TNF- α mRNA, a similar phenotype to that seen in TN-C and MK2 deficient macrophages ^{289,474,574,577,578}.

In order to further specify which RBPs may be responsible for the regulation of pri-miR-155 at the microprocessor the presence of novel RBP binding sites within the miR-155 transcript were examined.

4.1.1 – Hypothesis

Tenascin-C, through interactions with cell surface receptor(s) directly regulates the p38/MK2 pathway, facilitating changes to pri-miR-155 associated RBPs (Figure 4.1.1).

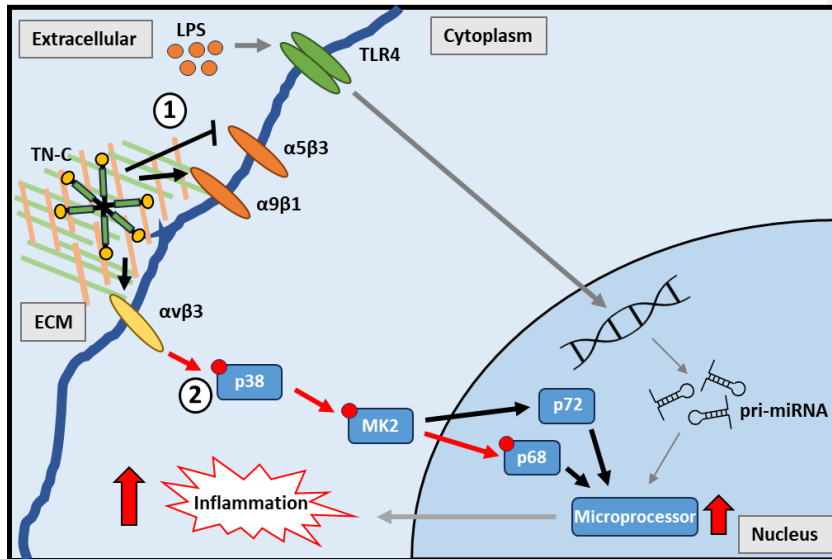


Figure 4.1.1. Schematic representation of research hypothesis and initial objectives. This schematic details the hypothesised pathway by which TN-C post-transcriptionally regulates miR-155 expression during the macrophage inflammatory response. Numbers indicate which objective aligns with that specific research objective. Grey lines represents previously established pathways. Red lines represent phosphorylation events. Pointed arrows indicate stimulation while blunt headed arrows represent inhibition. Crosses represent a pathway that is inactivated by upstream interactions.

4.1.2 – Objectives

1) To identify the cell surface receptor responsible for TN-C-mediated regulation of miR-155. This was achieved by:

- a) Interrogating literature sources to identify TN-C interacting candidate receptors;
- b) Identifying potential links between candidate receptors and miR-155 biogenesis through receptor siRNA knockdown and miR-155 expression quantification.

2) To determine the role of the candidate p38 α /MK2 pathway in the regulation of miR-155 expression by tenascin-C. This was achieved by:

- a) Validating potential regulation of the p38 α /MK2 pathway by TN-C via examination of p38 α and MK2 abundance and phosphorylation state in TNC siRNA knockout macrophages;
- b) Identifying potential ways by which TN-C may post-transcriptionally regulate the p38 α /MK2 pathway, utilising cellular fractionation methods combined with western blot analysis to examine protein localisation, and extended LPS treatment duration to examine protein recovery;
- c) Exploring the role of MK2 as a regulator of miR-155 expression through siRNA knockdown of MK2 and examination of resultant miR-155 biogenesis products.

4.2.0 – Examination of known TN-C binding receptors with links to miR-155 expression regulation

4.2.1 – Examination of α V integrin complexes as key candidates of TN-C signal transduction

Candidate TN-C interacting integrin complexes were identified via a literature search (Supplementary figure 8.4.1), with FACs analysis used to verify expression in RAW 246.7 cells (Supplementary figure 8.4.2).

The majority of these candidates contain either α v or β 1 subunits, this, combined with their validated cell surface expression, prompted their examination via siRNA knockdown.

Multiple attempts have been made previously to assess the function of β 1 integrin in miR-155 regulation through receptor blockage experiments⁵¹¹. These utilised anti β 1 and α 5 β 1 specific mAbs, thus providing a more specific indicator of the role of β 1 integrin complexes compared to the RGD peptide used to examine α v β 3. The RGD motif being present within multiple ECM components, including all α 5, α 8, and α v containing integrin complexes⁵⁷⁹. Thus, initial focus was placed on examining the role of α v subunit containing integrins in miR-155 regulation.

RAW 246.7 cells were transfected with non-targeting control or ITGAV siRNA before being stimulated with LPS for 6h (performed by Xingyu Guo). ITGAV, miR-155 and pri-miR-155 expression was quantified by qPCR.

Incubation with ITGAV siRNA led to significantly reduced miR-155 expression in 6h LPS treated cells, even with poor ITGAV mRNA knockdown efficiency (~11%) (Figure 4.2.2a/b). No matching change in pri-miR-155 expression is evident as a result of ITGAV knockdown alongside LPS treatment, potentially alluding to a post-transcriptional mode of miR-155 regulation (Figure 4.2.2c). Both pri- and mature miR-155 showed no significant change as a result of ITGAV knockdown in non-LPS stimulated cells, although cDNA-contamination led to the examination of pri-miR-155 levels in only two repeats of the no-treatment control samples.

As the α V integrin subunit is a component of multiple potential TN-C binding complexes it is not possible to identify which integrin receptor is responsible for the changes seen in miR-155 expression through ITGAV knockdown alone. Thus, further knockdown experiments were performed examining the candidate β 1 and β 3 integrins, both of which form complexes with α V.

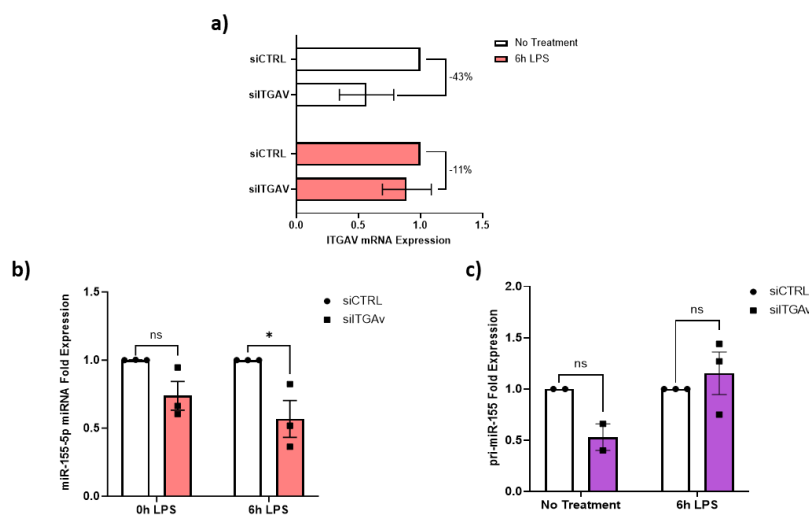


Figure 4.2.2: Knockdown of integrin α V leads to a decrease in miR-155 expression but not in that of pri-miR-155. RAW 246.7 macrophages were transfected with 10nM of non-targeting control or ITGAV siRNA using lipofectamine RNAiMAX then either non-stimulated or stimulated with 100ng/mL of LPS for 6 hours, before RNA extraction. a) ITGAV expression was quantified by qPCR using HPRT1 as an endogenous housekeeping gene. Relative expression was determined via the $\Delta\Delta$ Ct method with siCTRL as the calibrator. \pm SEM; n=3. b) Mature miR-155 was quantified by qPCR using U6 snRNA as an endogenous housekeeping gene. Relative expression of miR-155 was determined via the $\Delta\Delta$ Ct method with siCTRL as the calibrator. \pm SEM; n \geq 3; unpaired t-test (p \geq 0.05*). This experiment was performed by Xingyu Guo. c) pri-miR155 expression was quantified by qPCR using HPRT1 as an endogenous housekeeping gene. Relative expression was determined via the $\Delta\Delta$ Ct method with siCTRL as the calibrator. \pm SEM; n \geq 2; unpaired t-test.

siRNA treatment was performed as previously, with transfection of either ITGAV, ITGB1 or ITGB3 siRNA or dual-transfection with ITGAV+B1 or ITGAV+B3 siRNA. Cells were stimulated with LPS for 8h with ITGAV, ITGB3, ITGB1 miR-155 and pri-miR-155 expression quantified by qPCR.

Unlike the previous experiment performed by Xingyu, knockdown of ITGAV failed to elicit any change in miR-155 expression, even with comparable ITGAV mRNA reduction (Figure 4.2.3a/d). However, the effective knockdown of ITGB1 is joined by a significant increase in miR-155 expression, an increase that remains in cells incubated with ITGAV+B3, with a similar but non-significant change occurring with ITGB3 and ITGAV+B3 treatment (Figure 4.2.3 b/c/d).

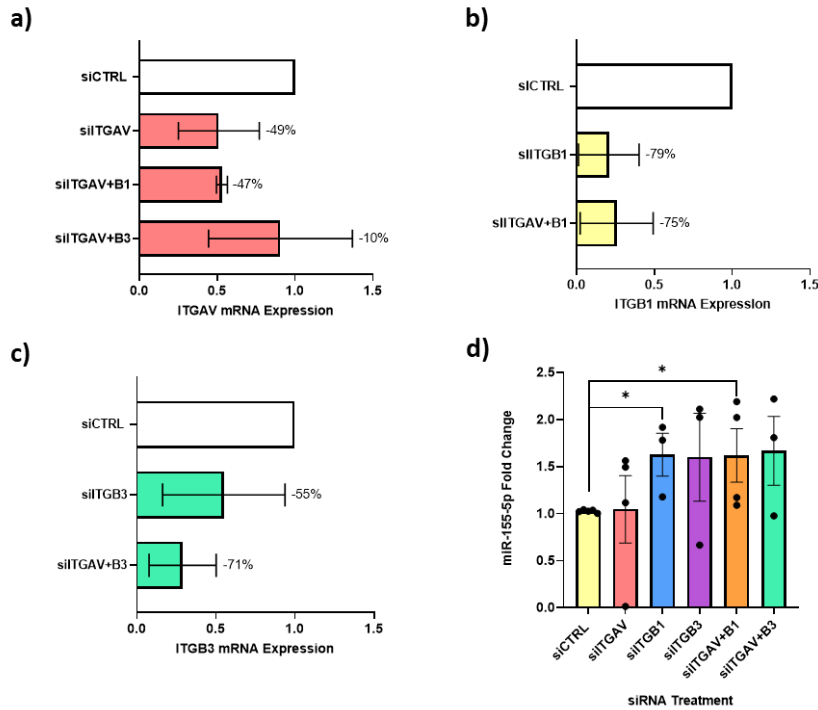


Figure 4.2.3: Dual knockdown of integrin α V complex partners identified integrin α V β 1 as a potential primary candidate. RAW 246.7 macrophages were transfected with 10nM of non-targeting control or a combination of ITGAV, ITGB1 and/or ITGB3 siRNA using lipofectamine RNAiMAX then either non-stimulated or stimulated with 100ng/mL of LPS for 8 hours, before RNA extraction. a) ITGAV, b) ITGB1 and c) ITGB3 mRNA expression were quantified by qPCR using HPRT1 as an endogenous housekeeping gene. Relative expression was determined via the $\Delta\Delta$ Ct method with siCTRL as the calibrator. \pm SEM; n=3. d) Mature miR-155 was quantified by qPCR using U6 snRNA as an endogenous housekeeping gene. Relative expression of miR-155 was determined via the $\Delta\Delta$ Ct method with siCTRL as the calibrator. \pm SEM; n \geq 3; unpaired t-test ($p\geq 0.05^*$).

The lack of miR-155 change with ITGAV knockdown is concerning, potentially occurring due to the low percentage of cells expressing α V, as seen in FACs analysis, accentuating variation between the LPS treatment timepoints (i.e. 6 hours in the first set of experiments and 8 hours in the following experiments)

and RAW 246.7 batches used in each experiment. On the other hand, the induction in miR-155 expression with ITGB1 knockdown conforms to previous β 1 blockade experiments conducted in BMDMs and RAW 246.7 macrophages. This illustrates that the resultant miR-155 induction is not due to endotoxin contamination, as assumed from β 1 blockade alone, instead representing a true effect of global β 1 integrin complex repression.

Although continued examination of integrin α V complexes as candidate TN-C receptors in the TNC-miR-155 axis showed promise, and will likely be explored in the future, further analysis of integrins was halted during this project. This is due the discrepancy in ITGAV knockdown results between separate knockdown experiments (Figure 4.2.2 and Figure 4.2.3) necessitating the design and optimisation of an alternative gain-of-function model, whereby TN-C coated cell culture plates would stimulate miR-155 expression. This, in combination with ITGAV knockdown, would facilitate direct examination of the potential TNC- α V-miR-155 connection. However, unfortunately the growth of RAW 246.7 cells upon TN-C supplemented plates has yet to be fully optimized.

4.3.0 – MK2: a kinase implicated in the regulation of miR-155 expression by TN-C?

4.3.1 – Identifying potential pri-miR-155 interacting RNA-binding proteins.

In tandem with the examination of cell-surface events which may mediate the regulation of miR-155 by TN-C, potential mediators of miR-155 post-transcriptional processing were also investigated.

Examination of miR-155 biogenesis products in TNC knockout macrophages identified the regulation of miR-155 by TN-C as a potential post-transcriptional mechanism, with pri-miR-155 expression remaining unchanged while pre- and mature miR-155 showed significant downregulation ^{289,511}.

Reduced pri-miR-155 association with Drosha was also found as a result of TN-C knockdown through RIP experiments, providing further evidence for a post-transcriptional mechanism of miR-155 regulation by TN-C.

Several RNA-binding proteins (RBPs) are known to function as modulators of pri-miRNA processing at the microprocessor, with the specificity of these RBPs determined by specific motifs or elements within the pri-miRNA which enable RBP binding ^{264,580,581}. Through modulation of these proteins cell surface signals have been shown to be transduced to the microprocessor, leading to modulation of pri-miRNA association as may be occurring as a result of extracellular TN-C function.

Previous attempts to identify potential RBPs which regulate miR-155 were performed by Zordan ⁵¹¹. Subcellular localisation of the key candidate RBPs KHSRP, TTP, ZNF-385A and ZNF-346 was unaffected by TNC knockdown, with only TTP showing a change in expression as a result of reduced TN-C. Additionally, co-IP analysis of these RBPs was found to be inconclusive.

With the lack of evidence for TN-C regulating these primary candidate RBPs, bioinformatic analysis of the pri-miR-155 sequence was conducted in order to identify novel RBP binding sites and thus additional potential pri-miR-155 regulatory candidate RBPs.

The oRNAment webtool utilises a database of RBP consensus target motifs acquired from *in vitro* binding assays of purified RBPs (or their RNA binding domains) and randomised RNA pools ⁵⁸². Input RNA sequences are scanned for these motifs, providing information of the motifs position on the input as well as its matrix score, a 0-1 value expressing the extent to which a motif matches the optimal RBP target motif.

oRNAment was used to examine the miR-155 host-gene (MIR155HG), finding 824 RBP binding motifs within the transcript (Figure 4.3.1a). The transcript was then paired down so that only an estimated pri-miR-155 sequence was examined, this being conducted by taking the known pre-miR-155 sequence and adding +25bp to the 3' end and +20bp to the 5' end. This region being chosen following estimations of pri-miRNA length defined by the Narry Kim lab ¹⁵³.

Four RBP binding sites were observed within the pri-miR-155 transcript (Figure 4.3.1b). Two binding sites for MBNL1 were located within the 5' tail region, with matrix scores of 1.000 and 0.672, one HNRNPF binding site was found within the 5' apical region, with a matrix score of 0.501, and a HNRNPL binding site with a matrix score of 0.767 was located within the 3' lower stem region.

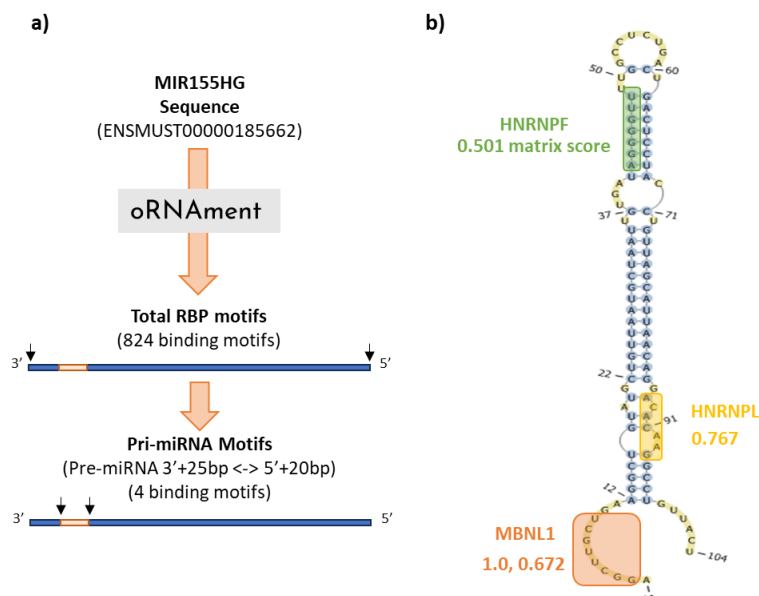


Figure 4.3.1: Identification of novel RBP binding sites in the miR-155 transcript. a) Workflow schematic of analysis using oRNAment webtool to identify RNA-Binding Protein (RBP) binding motifs in the mouse pri-miR-155 sequence. The pri-miRNA sequence was defined as the pre-miR155 sequence +25bp on the 3' end and +20bp on the 5' end. b) Schematic of murine pri-miR-155 and the four RBP binding motifs (two of which are for MBNL1) identified by oRNAment. Depicted are the names of each RBP and the degree to which the sequence matches its target motif (matrix score 0-1).

Of these prospective RBPs, HNRNPL was not further considered due to the low conservation of this motif between mice and humans. MBNL1 is a pre-mRNA splicing factor and is additionally shown to bind to the terminal loop of miR-1307, leading to impeded recruitment of Dicer⁵⁸³. Although HNRNPF has not been directly implicated in miRNA regulation, several other hnRNPs are known to associate with pri- and pre-miRNA. For example, hnRNPA1 binds to the stem and terminal loop of pri-miR-18a, enhancing microprocessor activity, as well as binding to the terminal loops of pri-miR-101-1 and pri-let-7a-1⁵⁸⁴. As such these two RBPs have the potential to influence pri-miR-155 association to Drosha and thus be responsible for TN-Cs potential regulation of this event.

Next the expression of these RBPs in RAW 246.7 cells was assessed alongside analysis of whether TNC knockdown has a transcriptional impact on their expression.

qPCR to detect MBNL1 and HNRNPF was performed upon RAW 246.7 cells incubated with TNC or scramble control siRNA and non-stimulated or stimulated with LPS for 2h.

MBNL1 showed no change in mRNA expression with either LPS treatment or TNC knockdown (Figure 4.3.2a). Meanwhile, HNRNPF mRNA expression was not significantly induced by 2h LPS treatment but only showed a non-significant decline due to TNC knockdown in non-LPS treated cells.

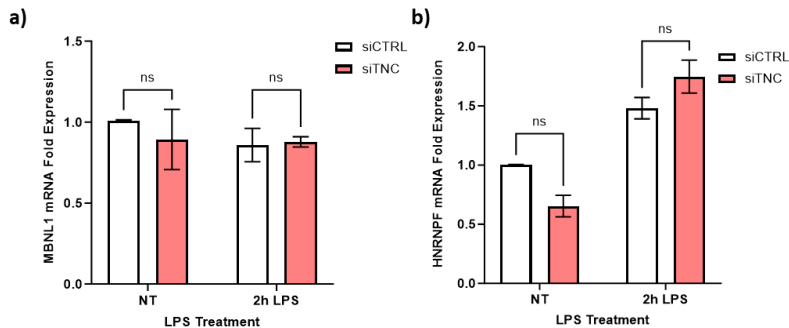


Figure 4.3.2: TNC knockdown elicits no significant change in the expression of candidate miR-155 binding RBPs. RAW 246.7 macrophages were transfected with 10nM of non-targeting control or TNC siRNA using lipofectamine RNAiMAX then either non-stimulated or stimulated with 100ng/mL of LPS for 2 hours, before RNA extraction. a) MBNL1 and b) HNRNPF mRNA expression were quantified by qPCR using HPRT1 as an endogenous housekeeping gene. Relative expression was determined via the $\Delta\Delta C_t$ method with non-stimulated siCTRL as the calibrator. \pm SEM; n=3; two-way anova with Sidak's multiple comparison test.

With no change evident in the expression of candidate RBPs in TNC knockdown cells a streamlined approach was necessary, as knockdown examination of additional candidates would be both costly and with diminishing chances of success, as besides MBNL1 and HNRNPF only HNRNPL contains a potential binding site in the pri-miR-155 sequence. Thus, RNA-seq data was analysed, with the aim of identifying RBPs or RBP mediators which may be regulated by TNC in LPS stimulated BMDM for further examination.

4.3.2 – MK2 expression in TNC knockdown and knockout macrophages

RNA-seq analysis had previously been performed using TNC KO and TNC wild-type BMDM cells (n=3) stimulated with LPS for 4 hours (See Chapter 5 for full details of this analysis).

Within this dataset gene expression was interrogated in order to identify potential TN-C regulated RBPs.

Within this dataset an alternative MK2 transcript (TCONS_1395) was found to be significantly upregulated within TNC knockout cells. MK2 is characterised as a master-regulator of RBPs, including ARE-binding proteins such as AUF1, HuR and TTP⁴⁶⁷. Thus, although TCONS transcripts are often dubious, further examination of canonical MK2 expression within BMDMs was conducted to gauge whether TN-C may transcriptionally regulate this protein.

RNA-seq read count data for the canonical and alternative MK2 transcripts expression in 4h LPS treated TNC WT and TNC knockout BMDMs was examined. Additionally, qPCR analysis was performed upon TNC +/+ or TNC -/- BMDMs alongside an LPS induction time-course to closer examine changes in canonical MK2 mRNA expression at varying stimulatory stages. No change in canonical MK2 expression as a result of TNC KO was evident in either the RNA-seq data or qPCR (Figure 4.3.3a/b). However, an upwards trend in MK2 expression is potentially present following LPS treatment.

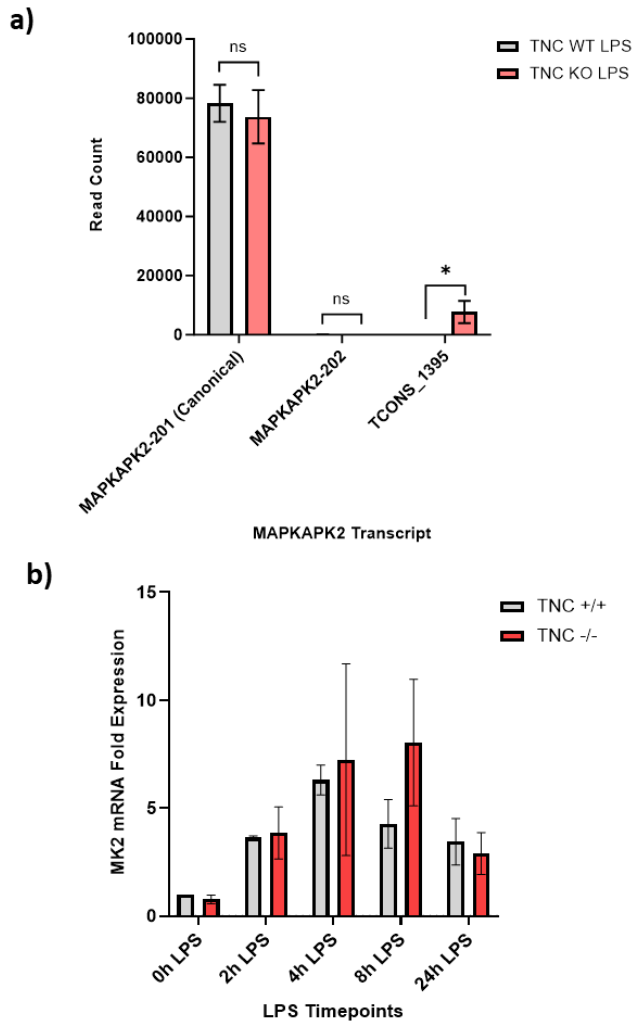


Figure 4.3.3: MK2 expression is induced by LPS treatment in BMDMs and is not affected by TNC knockout. a) Total RNA was extracted from wild-type BMDM cells, either untreated or stimulated with 100ng/mL of LPS for 4 hours (n=3). RNA-SEQ and subsequent read count analysis was performed by Novogene. The read count change of MK2 transcripts was analysed. b) TNC WT or KO BMDMs were stimulated with 10ng/mL of LPS for the durations depicted. Canonical MK2 mRNA expression was quantified by qPCR using HPRT1 as an endogenous housekeeping gene. Relative expression was determined via the $\Delta\Delta C_t$ method with TNC +/+ 0h LPS as the calibrator. \pm SEM; n=3; two-way anova with Sidak's multiple comparison test.

Although no transcriptional regulation of MK2 by TN-C was evident, MK2 still provides an intriguing candidate for further analysis, as the phosphorylation of MK2s upstream kinase p38 by the FBG domain of TN-C has been previously established within macrophage cells ³⁰². Therefore, through phosphorylation and activation of MK2, as a result of p38 activation, TN-C may in turn modulate multiple RBPs, facilitating regulation of miRNAs such as miR-155.

4.4.0 – TNC knockdown influences MK2 and p38

abundance in steady-state macrophages

4.4.1 – Optimisation and characterisation of MK2 protein detection in RAW 246.7 cells.

Prior to examination of the potential relationship between MK2 and TN-C in macrophages, the detection of MK2 via western blot was first validated utilising MK2 knockdown to confirm band specificity.

RAW 246.7 cells were transfected with non-targeting control or MK2 siRNA followed by LPS stimulation for 5 or 10 minutes. MK2 protein abundance in total protein extracts was examined by western blot using an anti-total MK2 antibody.

Two MK2 corresponding bands are visible via western blot (indicated by arrows in figure 4.4.1), these being known to correspond to two distinct MK2 isoforms, the expression of which is cell line-dependent (Figure 4.4.1) ⁴³⁵.

siMK2 treatment fully ablates the lower band in both 5 min and 15 min LPS treated cells while the upper band is reduced (Figure 4.4.1).

Based upon this validation, as well as evidence for its more ubiquitous expression across cells lines, future western blot assays utilise the lower band (indicated by the red arrow) for analysis (Figure 4.4.1) ⁴³⁵.

The response of MK2 to early LPS treatment was next characterised in order to establish appropriate timepoints for future experimentation.

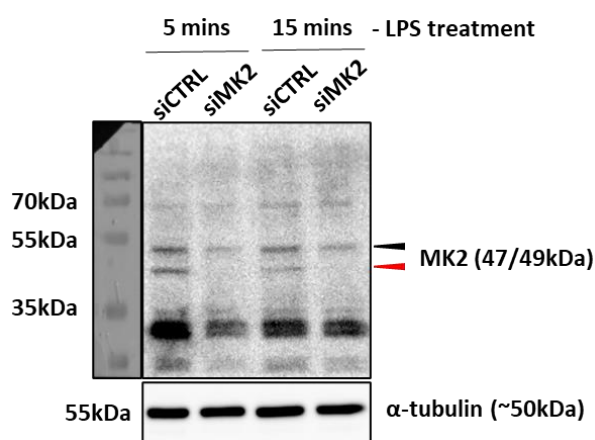


Figure 4.4.1: Total MK2 antibody detects two bands of distinct molecular weights.

The lower band is canonical and used for future analysis. RAW 246.7 macrophages were transfected with 10nM of non-targeting control or MK2 siRNA using lipofectamine RNAiMAX then stimulated with 100ng/mL of LPS for 5 or 15 minutes, before protein extraction. Western blot was used to semi-quantify total MK2 abundance. α -tubulin was used as loading control. n=1.

Western blot of total protein lysates was used to assess total MK2 and phospho-MK2 (Thr334) expression within RAW 246.7 macrophages treated with LPS for 0, 5, 10, 15, 30 and 60 minutes. The phospho-Thr334 MK2 antibody was used as this phosphorylation site is responsible for MK2 activation and nuclear export, with its location outside of the catalytic domain

or activity loop allowing potential association when MK2 is bound to another protein ⁴⁶⁵.

Total MK2 protein expression is shown to be highest in the steady-state macrophage, with LPS induction leading to a rapid depletion of total protein which does not recover within 60 minutes (Figure 4.4.2). Meanwhile, phospho-MK2 abundance increases rapidly at 10 mins before peaking at 15 mins and declining to basal levels by 60 mins post LPS treatment.

This induction of MK2 phosphorylation is characteristic of LPS treated macrophages, matching experiments performed in BMDMs ⁴³⁵. Based upon this data 0, 15, 30 and 60 mins of LPS induction were used in future experiments in order to best observe phospho-MK2 induction and decline.

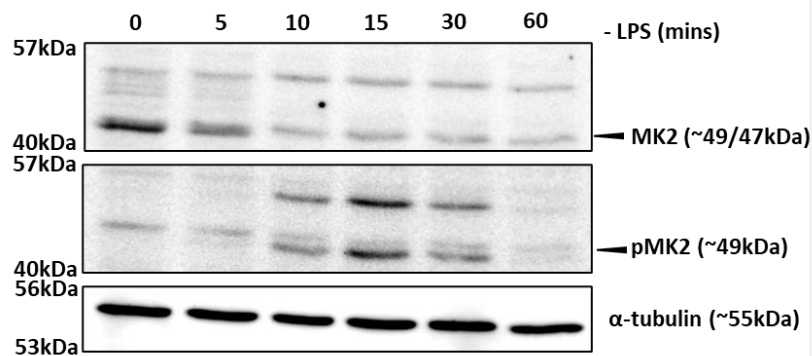


Figure 4.4.2. Characterisation of MK2 induction in the early macrophage response to inflammation. RAW 246.7 macrophages were either unstimulated or stimulated with 100ng/mL of LPS for 5, 10, 15, 30 or 60 minutes, before total protein extraction. Total MK2 and phospho-MK2 abundance was detected by western blot. α-tubulin was used as loading control. n=1.

4.4.2 – Examining the impact of TNC knockdown on MK2 expression and phosphorylation in LPS stimulated RAW 246.7 cells.

In order to examine whether TN-C regulates MK2 protein abundance or phosphorylation, and thus may impact RBP regulation, MK2 and phospho-MK2 were examined in TNC knockdown macrophages.

RAW 246.7 cells were transfected with non-targeting scramble control or TNC siRNA followed by LPS stimulation for 0, 15, 30 or 60 mins. Total protein lysates were prepared from these samples with MK2 and phospho-MK2 (Thr334) levels examined by western blot. Densitometric quantification of protein bands relative to loading controls was utilised to examine trends over multiple experiments.

siCTRL treatment did not alter MK2 or pMK2 expression across all timepoints (Figure 4.4.3a/b). However, TNC siRNA transfection led to a non-significant induction of MK2 in steady-state cells ($p=0.068$), total MK2 then proceeding to decline to levels below that of the siCTRL treatment following 30 ($p=0.8846$) and 60 mins ($p=0.703$) of LPS stimulation (Figure 4.3.3a/b). This disparity between treatments was not evident for phospho-MK2, with siCTRL and siTNC samples showing equivalent abundance at 0 ($p=0.999$), 15 ($p=0.998$) and 30 mins ($p=0.939$) with a potential reduced quantity of phospho-MK2 only 60 mins post LPS stimulation ($p=0.895$).

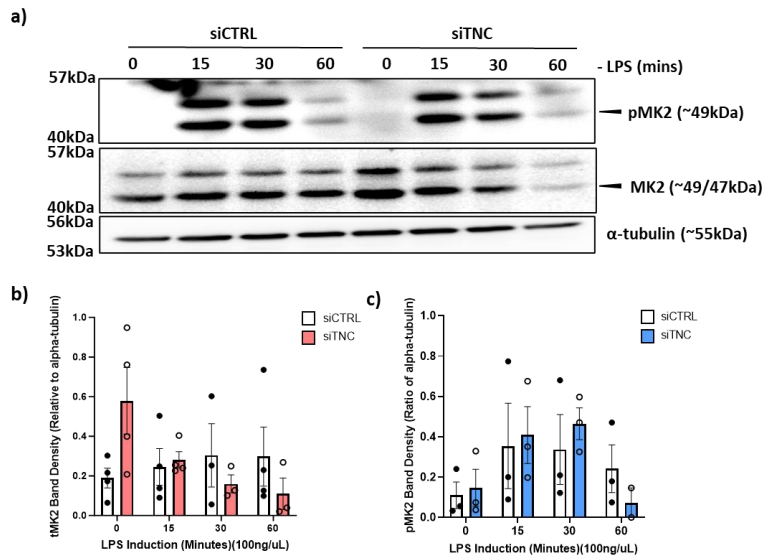


Figure 4.4.3: Tenascin-C knockdown leads to potentially increased steady-state MK2 abundance and decreased MK2 and pMK2 abundance 60 mins after LPS stimulation. RAW 246.7 macrophages were transfected with 10nM of non-targeting control or TNC siRNA using lipofectamine RNAiMAX then either unstimulated or stimulated with 100ng/mL of LPS for 5, 15, 30 or 60 minutes, before protein extraction. a) Western blot analysis was used to measure phospho-MK2 and total MK2 abundance. α -tubulin was used as a loading control. Densitometry was performed using Image J software with b) total MK2 and c) phospho-MK2 band densities calculated relative to that of α -tubulin. \pm SEM; $n \geq 3$; two-way Anova with Sidak's multiple comparison test.

The largest impact of TNC knockdown on MK2 was the increase in total MK2 seen in non-activated macrophages. Notably, MK2 banding in cells incubated with siTNC was more consistent with previous experiments examining the LPS induction of MK2 in wild-type macrophages than cells incubated with siCTRL (Figure 4.4.2 and 4.4.3). Therefore, siRNA incubation may be potentially influencing MK2 abundance.

As siTNC treatment leads to increased MK2 protein levels in steady-state RAW 246.7 cells the abundance of MK2 mRNA was next quantified to ascertain whether this upregulation was based upon changes in mRNA abundance.

siTNC treatment was conducted as previously with RAW 246.7 cells untreated or stimulated with LPS for 2h, this being followed by qPCR analysis of canonical MK2 transcript abundance.

No significant change in canonical MK2 expression was found to occur as a result of siTNC treatment, neither following treatment with siCTRL in the steady-state nor 2h after LPS stimulation (Figure 4.4.4).

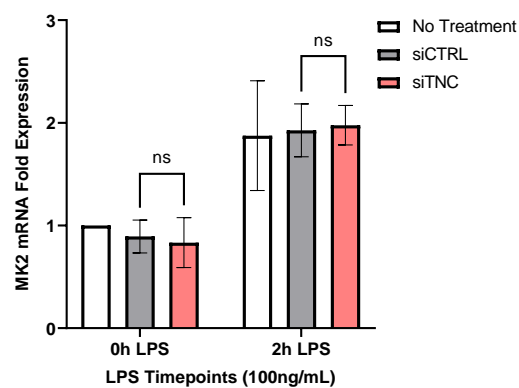


Figure 4.4.4: TNC knockdown does not impact MK2 expression in RAW246.7

macrophages. RAW 246.7 macrophages were transfected with 10nM of non-targeting control or TNC siRNA using lipofectamine RNAiMAX then either unstimulated or stimulated with 100ng/mL of LPS for 2 hours, before total protein extraction. MK2 mRNA expression was quantified by qPCR using HPRT1 as an endogenous housekeeping gene. Relative expression was determined via the $\Delta\Delta C_t$ method with no treatment 0h LPS as the calibrator. \pm SEM; n=3; two-way Anova with Sidak's multiple comparison test.

The lack of a transcriptional change in MK2 expression as a result of TNC knockdown infers that TNC may be regulating MK2 in steady-state macrophages via a post-transcriptional mechanism.

4.4.3 – Examining the impact of TNC knockdown on p38 expression and phosphorylation in LPS stimulated RAW 246.7 cells.

To further characterise how TN-C may be influencing MK2 abundance, the effect of TNC knockdown on the upstream signal protein p38 was next assessed.

P38 is a stress-responsive mitogen-activated protein kinase (MAPK) responsible for the phosphorylation and resultant activity of multiple targets, including MK2. In steady-state cells, p38 has been shown to form a stable complex with MK2, protecting MK2 from degradation until pathway activation, phosphorylation and MK2 subsequent degradation via the E3 ubiquitin ligase MDM2⁴³⁵. As such, it was hypothesised that p38 activation or expression may be being mediated by TN-C, resulting in an increase in steady-state MK2 levels as a result of repressed MK2 degradation.

Western blot analysis of multiple LPS timepoints was performed as with MK2, using p38 and phospho-p38 antibodies to semi-quantify protein expression and activation. The phospho-p38 antibody targets both the Thr180 and Tyr182 phosphorylation sites, either of which can lead to p38 kinase activity⁵⁸⁵.

siTNC treatment led to a potential, but non-significant, increase in total p38 abundance in steady-state cells, with levels of total p38 matching those of

cells incubated with siCTRL at all other timepoints (Figure 4.4.5 a/b).

Additionally, no difference in phospho-p38 is evident between the treatments at any LPS induction timepoints (Figure 4.4.5 a/c).

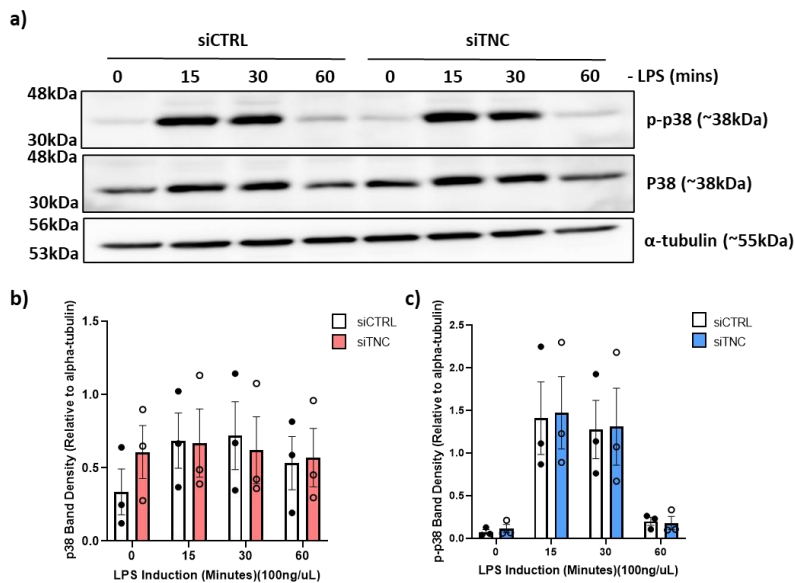


Figure 4.4.5: TNC knockdown does not impact p38 phosphorylation. RAW 246.7 macrophages were transfected with 10nM of non-targeting control or TNC siRNA using lipofectamine RNAiMAX then either unstimulated or stimulated with 100ng/mL of LPS for 5, 15, 30 or 60 minutes, before total protein extraction. a) Western blot analysis was used to measure phospho-p38 and total p38 abundance. α -tubulin was used as a loading control. Densitometry was performed using Image J software with b) total p38 and c) phospho-p38 band density calculated relative to that of α -tubulin. \pm SEM; $n \geq 3$; two-way Anova with Sidak's multiple comparison test.

The potential upregulation in total p38 observed in TNC knockdown steady-state macrophages matches the upregulation of MK2 within these cells seen previously (Figure 4.3.3 and 4.3.5). No change in phospho-p38 levels occurs due to siTNC treatment in steady-state cells, with this and the lack of

phospho-MK2 at steady-state inferring that the mechanism that leads to increased protein abundance is not reliant on p38 or MK2 activation.

With a potential increase in steady state p38 expression being caused by TNC knockdown the mRNA expression of p38 was next assessed. This being in order to determine whether TNC regulates p38 post-transcriptionally, as is the case for MK2.

RNA-SEQ data examining differentially expressed genes between steady-state wild-type and TNC knockout BMDMs was analysed. Differentially expressed genes were identified using DESeq2 (performed by Novogene)⁵⁸⁶. The differential expression of the p38 family members, p38 α / β / γ / δ , and their protein coding isoforms, as listed on the Ensemble database, were examined⁵⁸⁷.

The canonical p38 α transcript showed significantly upregulated expression in TNC knockout steady-state BMDMs (Figure 4.3.6). Although non-significant, this trend was mirrored in all p38 α isoforms, aside from p38 α -202 the expression of which being highly variable. All other p38 family members showed minimal expression and differential expression between the groups.

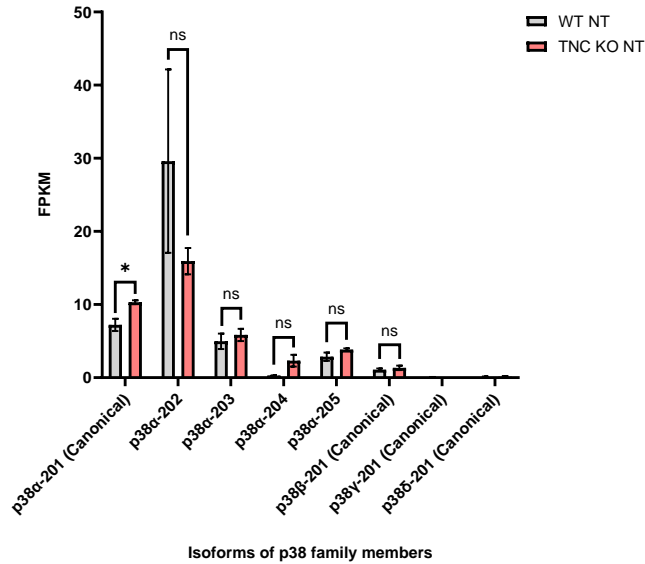


Figure 4.3.6: The canonical p38α isoform shows a significant, but modest, increase in expression when comparing wild-type and TNC knockout steady-state BMDMs by RNA-Seq. Total RNA was extracted from wild-type BMDM cells (n=3). RNA-SEQ and subsequent FPKM (Fragments Per Kilobase of transcript sequence per Millions) analysis was performed by Novogene (As outlined in the methods). Depicted statistical significance is based upon differential expression analysis using DESeq2 (p<0.05*).

These results depict TN-C as a regulator of p38α transcriptional expression, with TNC knockdown or knockout leading to heightened steady-state levels of the kinase. Increased levels of p38α may in turn act to stabilise and prevent MK2 degradation in steady-state macrophages.

4.5.0 – Examination of the potential regulation of p38 subcellular localisation and MK2 recovery by TN-C

4.5.1 – Investigating the effect of TNC knockdown on p38 subcellular localisation during the inflammatory response.

Following confirmation of the control of p38 α expression by TN-C in macrophages, potential changes to p38 α 's cellular localisation were examined as this mediates the kinases' ability to interact with target substrates such as MK2.

In steady-state cells the majority of p38 α is localised to the cytoplasm due to the action of multiple anchoring proteins⁵⁸⁸. Additionally, a portion of p38 α is thought to enter the nucleus, forming a stable complex with MK2⁴³⁵. p38 α activation leads nuclear import and phosphorylation of the MK2 Thr-334 site, leading to exposure of the nuclear export signal and shuttling into the cytoplasm where MK2 performs its effector functions⁵⁸⁸.

p38 α , phospho-p38 α , MK2 and phospho-MK2 cellular localisation was compared between RAW246.7 macrophages incubated with siCTRL and siTNC via nuclear/cytoplasmic fractionation of the total protein lysate.

Unfortunately, out of three biological repeats only one showed visible phospho- and total-MK2 protein bands as well as p38 α and phospho-p38 α within the nuclear fraction. Densitometric analysis was utilised semi-quantify p38 α banding.

p38 α showed a non-significant increase in cytoplasmic abundance in steady-state cells incubated with siTNC ($p=0.520$), this difference disappearing upon 15min LPS treatment ($p=0.998$) (Figure 4.5.1a/b). In both cells incubated with siCTRL and siTNC 15 mins LPS stimulation appears to elicit an increase in cytoplasmic phospho-p38 α (Figure 4.5.1a/c). No cytoplasmic MK2 or phospho-MK2 was detectable, with nuclear levels remaining equivalent between treatments (Figure 4.5.1a).

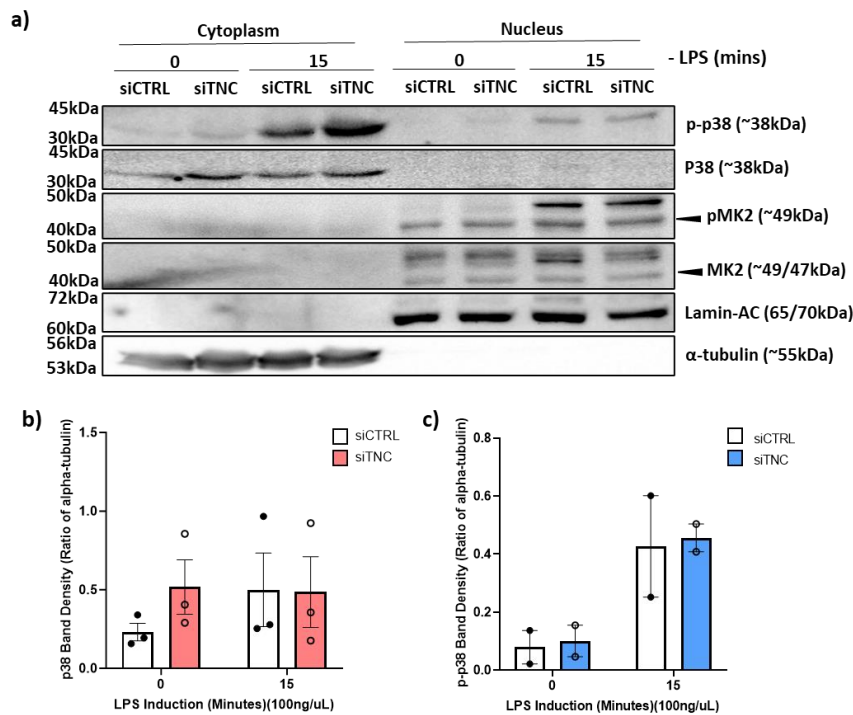


Figure 4.5.1: TNC knockout may increase the abundance of cytoplasmic p38 in resting cells. RAW 246.7 macrophages were transfected with 10nM of non-targeting control or TNC siRNA using lipofectamine RNAiMAX then either unstimulated or stimulated with 100ng/mL pf LPS for 15 minutes before the protein contents of the nuclear and cytoplasmic compartments were fractionated. a) Western blotting was used to determine phospho-p38, total p38, phospho-MK2 and total MK2 expression

in the cytoplasm and nuclear compartments. Lamin-A/C and α -tubulin were used as nuclear and cytoplasmic loading controls, respectively. Densitometry was performed using Image J software with b) total p38 and c) phospho-p38 band density within the cytoplasm calculated relative to that of α -tubulin. \pm SEM; $n \geq 2$; two-way Anova with Sidak's multiple comparison test.

The increase in cytoplasmic p38 α is in-line with previous evidence showing increased p38 α expression in steady-state cells. However, the lack of nuclear p38 α does not conform to studies showing p38 α and MK2 to associate within the cytoplasm and brings into question the hypothesised MK2 stabilising effect of increased p38 α in TNC knockdown cells⁵⁸⁸. Additionally, no upregulation in steady-state total MK2 is visible in the single experimental repeat where total MK2 is detected, raising the question of in which compartment the upregulated steady-state MK2 reside.

4.5.2 – Examining the effect of TNC knockdown on MK2 protein recovery following prolonged LPS stimulation of RAW 246.7 cells.

Stimuli which activate the p38-MK2 pathway can be loosely grouped into low and high stress based upon the longevity and recoverability of p38 and MK2 post-stimulation⁴³⁵. LPS treatment is categorised as a low stress stimulus, leading to transient p38 α activation and subsequent MK2 phosphorylation. Phospho-MK2 dissociates from p38 α and is degraded, with newly expressed MK2 re-forming stabilising complexes with the now de-phosphorylated p38 α , thus MK2 successfully recovers to basal levels. However, in response to stress stimuli such as UV exposure, which elicit a harsh or prolonged activation of

the p38 α pathway, p38 α is consistently phosphorylated, preventing newly expressed MK2 from being shielded from degradation through complex formation⁴³⁵. Thus, MK2 levels do not successfully recover.

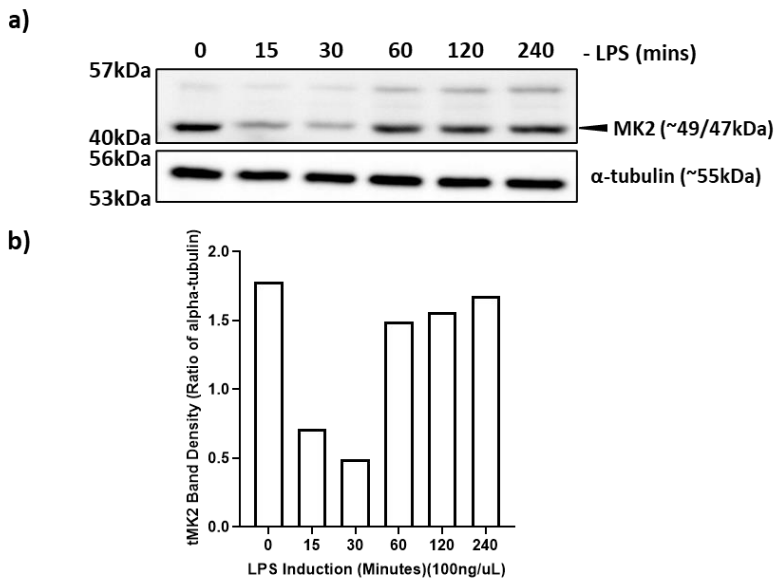


Figure 4.5.2: RAW246.7 macrophages show a characteristic MK2 recovery by 4 hours after lps stimulation. RAW 246.7 macrophages were either unstimulated or stimulated with 100ng/mL of LPS for 15, 30, 60, 120 or 240 minutes, before total protein extraction. a) Total MK2 was detected by western blotting. α -tubulin was used as a loading control. b) Densitometry was performed using Image J software with total MK2 band density calculated relative to that of α -tubulin. n=1.

As previous examination in TNC knockdown RAW246.7 cells shows reduced MK2 abundance after 60mins of LPS treatment, it is possible that TNC knockdown may be leading to a cellular stress response, eliciting increased MK2 depletion. This could have long term consequences on the cell,

potentially facilitating changes in miR-155 expression seen much later in the LPS response.

Prior to the examination of the effect of TN-C knockdown on MK2 recovery, the recovery of MK2 post-LPS stimulation in wild-type RAW 246.7 cells was assessed.

An LPS treatment time course was performed, assessing total MK2 expression at 120 and 240 minutes additional timepoints.

MK2 protein abundance was found to be high in steady-state cells, before being depleted with 15 and 30 mins of LPS treatment and recovering to a level equal to that of steady-state from 60 mins onwards (Figure 4.5.2a/b).

Based on this information, 0, 15, 60 and 240 mins of LPS treatment were used in a follow up experiment alongside siCTRL and siTNC transfection in order to assess whether TNC knockdown influences MK2 recovery.

Due to the usage of the 240 min timepoint, which grants sufficient TN-C expression to allow protein detection in the cell lysate, successful knockdown of TN-C via siTNC treatment was confirmed (Figure 4.5.3a/b). MK2 abundance at 60 ($p > 0.999$) and 240 mins ($p = 0.895$) post LPS treatment was not affected by TNC knockdown, with earlier timepoints showing potentially elevated MK2 levels in steady-state ($p = 0.924$) and 15-min ($p = 0.578$) LPS treated cells.

TNC knockdown does not influence MK2 recovery, this showing that even with TN-C knockdown LPS treatment remains a low stress p38-MK2 stimuli. It is notable however, that the results in this experiment for 0, 15 and 60 min

LPS treatments diverge from those seen previously for these timepoints

(Figure 4.4.5).

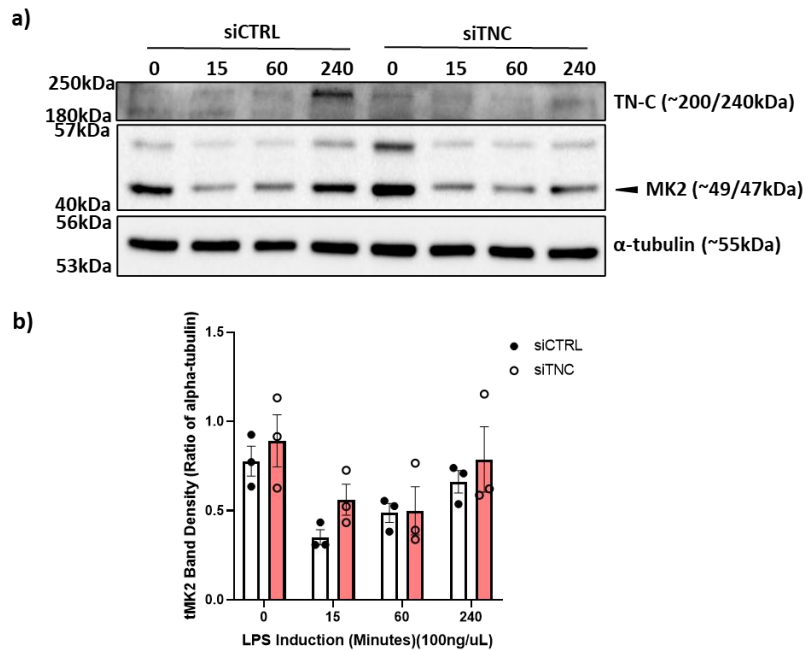


Figure 4.5.3: Tenascin-C knockdown does not impact MK2 recovery. RAW 246.7 macrophages were transfected with 10nM of non-targeting control or TNC siRNA using lipofectamine RNAiMAX then either unstimulated or stimulated with 100ng/mL of LPS for 15, 60 or 240 minutes, before total protein extraction. a) Western blot analysis was used to semi-quantify TN-C and total MK2 abundance in cell lysates. α -tubulin was used as a loading control. b) Densitometry was performed using Image J software with total MK2 band density calculated relative to that of α -tubulin. \pm SEM; n=3; two-way Anova with Sidak's multiple comparison test.

4.6.0 – MK2 knockdown and macrophage miR-155

expression

MK2 is known to regulate multiple RBPs, some of which, including HuR and TTP, being known to regulate pri-miRNA processing⁴⁶⁷. Thus, these represent a potential means whereby increased MK2 abundance within TN-C knockdown cells may lead to the regulation of miR-155 witnessed as a result of TN-C modulation.

With this in mind, the ability of MK2 to regulate miR-155 biogenesis was next assessed, utilising knockdown of MK2 to observe whether pri- or mature miR-155 would potentially be influenced by the increased MK2 abundance elicited by TNC knockdown.

RAW 246.7 cells were transfected with non-targeting scramble control or MK2 siRNA with the expression of MK2 mRNA and pri- and mature miR-155 measured by qPCR.

Successful knockdown of MK2 expression was confirmed with a 75% reduction in mRNA levels (Figure 4.6.1). However, no discernible change in pri- or mature miR-155 expression was seen to occur as a result of MK2 knockdown except for a small induction of mature miR-155 observed in the MK2 knockdown cells stimulated with LPS for 8h ($p=0.363$).

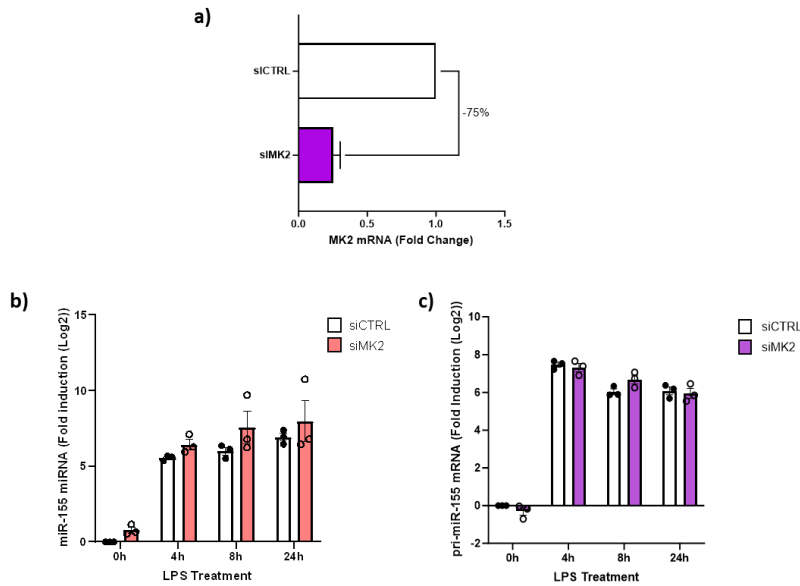
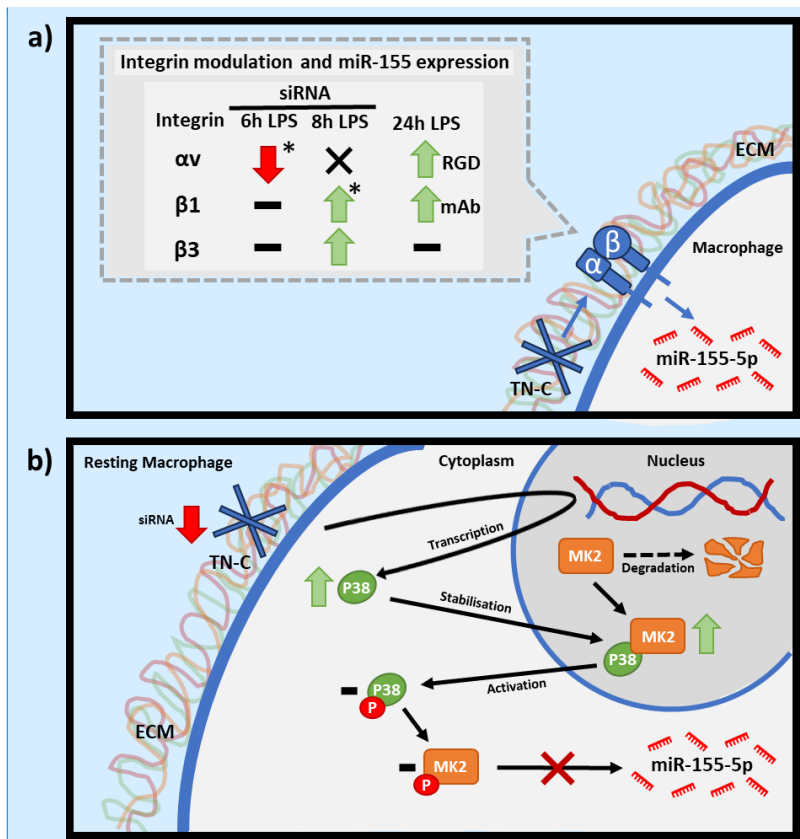


Figure 4.6.1: MK2 knockdown has no significant impact on mature or pri-miR155 expression. RAW 246.7 macrophages were transfected with 10nM non-targeting control or MK2 siRNA using lipofectamine RNAiMAX then either non-stimulated or stimulated with 100ng/mL LPS for 4, 8 or 24 hours, before RNA extraction. a) MK2 expression was quantified by qPCR using HPRT1 as an endogenous housekeeping gene. Relative expression was determined via the $\Delta\Delta C_t$ method with siCTRL as the calibrator. \pm SEM; n=3. b) Mature miR-155 was quantified by qPCR using U6 snRNA as an endogenous housekeeping gene. Relative expression of miR-155 was determined via the $\Delta\Delta C_t$ method with siCTRL as the calibrator. c) pri-miR155 expression was quantified by qPCR using HPRT1 as an endogenous housekeeping gene. Relative expression was determined via the $\Delta\Delta C_t$ method with siCTRL as the calibrator. \pm SEM; n=3; two-way anova with Sidak's multiple comparison.

The lack of miR-155 modulation following MK2 knockdown makes the hypothesis that TN-C regulates miR-155 via modulation of MK2 unlikely. This compounds with previous western blot analysis which shows no impact of TNC knockdown on MK2 phosphorylation, the means by-which MK2 would regulate RBPs.

Overall, this evidence suggest that TN-C could regulate p38 α mRNA expression in steady-state cells, leading to increased p38 α which in turn allows increased MK2 abundance through the potential formation of p38 α -MK2 complexes which protect against MK2 degradation. As knockdown experiments show that MK2 itself is unlikely to regulate miR-155 expression this could be instead orchestrated by p38 α which itself may stimulate a number of pathways irrespective of MK2 that facilitate changes at the microprocessor.

4.7.0 – Discussion



Commented [OD1]: Indicate in the second diagram which are non-significant MK2/p38 results

Figure 4.7.0: Graphical abstract of key findings. a) Combined findings from these and previous integrin modulation experiments conducted by Zordan⁵¹¹. * = significant results. green and red arrows indicate up- or down-regulation of miR-155, respectively. X = unchanged miR-155 expression, horizontal lines = unchanged. b) Schematic depiction of the regulation of the p38/MK2 pathway by TNC siRNA knockdown within steady-state RAW 264.7 cells. Arrows indicate up- or down-regulation of the labelled molecule. - = No change in abundance. X = an invalidated interaction.

Previous attempts to identify which receptor(s) facilitates the regulation of miR-155 by TN-C utilised function blocking antibodies against TLR4, EGFR, and the integrins $\alpha 9\beta 1$, $\alpha v\beta 3$ and $\alpha 5\beta 1$ ⁵¹¹. These confirmed the non-participation of TLR4 and EGFR receptors within this pathway, while treatment with RGD-peptide, $\alpha 5\beta 1$ mAB and $\beta 1$ mAB all elicited an unexpected non-significant induction in miR-155 expression alongside LPS stimulation. To further clarify the role of integrins as TN-C receptors potentially responsible for the regulation of miR-155, siRNA treatment was used to reduce expression of specific candidate subunits. siRNA knockdown of ITGAV, the gene encoding integrin αv , in RAW 246.7 cells elicited a significant downregulation of miR-155 expression upon 6h LPS induction. Notably, the expression of pri-miR-155 was unchanged, alluding to a post-transcriptional mechanism of miR-155 regulation similar to that witnessed with TNC knockdown in BMDMs.

Integrin complexes containing αv are known to regulate the induction of inflammation in multiple cell types, with potential existing for TN-C to modulate this activity via the αv binding RGD sequence within the FNIII3 repeat as well as within the C-terminal FBG⁵⁷². Seeding of monocyte derived macrophages onto anti- $\alpha v\beta 3$ mAbs elicits a rapid and transient activation of NF- κ B independent of LPS treatment, returning to initial levels after 4 hours and with a similar response shown via treatment with the $\alpha v\beta 3$ ligand vitronectin⁵⁸⁹. The transiency of this response may explain the lack of a significant change in pri-miR-155 expression within 6h LPS + siITGAV treated cells, as by this point $\alpha v\beta 3$ has ceased to contribute to pro-inflammatory transcriptional activity, with the effect of this upon the mature miR-155

population being delayed due to the miRNA biogenesis process. The pro-inflammatory role of $\alpha V\beta 3$ has been further illustrated in mouse macrophage-like cells P388D1, wherein TLR4 stimulation leads to the formation of a positive feedback loop, leading to phosphorylation of focal adhesion kinase (FAK) which in turn activates $\alpha V\beta 3$ which itself further phosphorylates FAK⁵⁹⁰. This loop perpetuating inflammation as pFAK stimulates NF- κ B activation.

Multiple integrin complexes containing αV are known to interact with TN-C as well as mediating inflammation and thus further validation was necessary to identify which may be responsible for the modulation of miR-155. siRNA knockdown of ITGB1 led to a significant increase in miR-155 expression, this being mirrored in a non-significant manner in ITGB3 knockdown. Intriguingly this upregulation is similar to that witnessed in previous $\beta 1$ mAb and RGD-peptide treatment experiments, assumed at the time to be due to endotoxin contamination leading to inflammatory induction.

Contrasting studies utilising other macrophage cell lines, Wang *et al.*, 2019 found that seeding RAW 246.7 cells onto a 3D biomimetic ECM supplemented with an $\alpha V\beta 3$ specific RGD peptide led to the promotion of an anti-inflammatory phenotype⁵⁹¹. This introduces the potential that by using RAW 246.7 cells alone the role of integrins in the pro-inflammatory cascade may be lost. It may also be the case that knocking down specific integrin subunits may have unforeseen effects on cell surface integrin populations, with changes in the presentation of non-targeted complexes also affecting macrophage inflammatory induction.

Attempts to replicate the ITGAV knockdown experiment using 8h rather than 6h LPS treatment proved unsuccessful, instead leading to no change in miR-155 expression even with a high degree of TN-C reduction. This may be due to LPS timepoint specificity, as miR-155 modulation and $\alpha V\beta 3$ regulation of the macrophage inflammatory response have both been shown to have a specific temporal element⁵⁸⁹. Additionally, these experiments were performed by different scientists using differing RAW 246.7 cell batches, the 6h LPS experiments being of a lower passage. Although both remained under 15 passages thus before the point at-which RAW 246.7 cells are known to genetically deviate, this may have led to variation in the cell surface expression of integrin αV ⁵⁹². Further validation using an LPS stimulation time course would ascertain the link between LPS timepoint and αV 's regulation of miR-155. Additionally, joint knockdown of αV alongside a TN-C gain-of-function approach such as plating of cells onto a TN-C supplemented ECM would give additional insight into whether αV 's potential modulation of miR-155 is TN-C dependent.

Overall, the majority of candidate receptors for TN-C's regulation of miR-155 have been exhausted, with the candidate-based examination of integrins proving problematic due to the multiple complexes each subunit may form and the high cost of integrin complex specific inhibitors. Therefore, future experimentation must focus upon non-candidate-based approaches that will further identify potential TN-C – receptor interactions within macrophage cells. Proximity tagging is a relatively new method, utilising a specifically engineered enzyme which interacts with a tag inserted into the protein of

interest⁵⁹³. This results in the creation of a short-lived reactive species leading to the covalent tagging of neighbouring molecules and facilitating their isolation via a tag-based pulldown. Utilising this methodology novel interaction partners of ECM bound-TN-C could be identified within the steady-state and early inflammatory macrophage, with proximity being influenced by the biological context, unlike traditional affinity purification approaches. The principal challenges of this approach would be the usage of a macrophage cell line, with enzyme treatment potentially modifying the cellular inflammatory response, and the large size of TN-C (~75nm per arm) placing greater importance on enzyme binding site placement as the labelling radius of the proximity tagging enzymes is only between 1-10nm⁵⁹⁴⁻⁵⁹⁶.

At the opposite end of the prospective TN-C – miR-155 pathway to TN-Cs receptor interactions are the events at the microprocessor which lead to the post-transcriptional downregulation of miR-155 expression seen in TNC knockout experiments. As of writing exploration of the post-transcriptional regulation of miR-155 is non-existent, except for a reported role of the RBP KHSRP1 which previous work by Zordan refutes^{223,511}. However, similar RBPs which bind and modulate pri-miRNA association to the microprocessor represent a principal means whereby pri-miR-155 processing may be modulated.

Novel bioinformatics analysis of prospective RBP binding domains within pri-miR-155 was carried out using the oRNAmnt webtool. This identified binding sites for MBNL1 within the 5' tail region and HNRNPF within the upper stem.

The expression of these RBPs was found to be not significantly affected by TNC knockdown in RAW 246.7 cells. However, the binding of RBPs to pri-miRNAs can be regulated by a number of post-transcriptional mechanisms, as such knockdown of MBNL1 and HNRNPF using siRNA would provide the best means of determining whether these RBPs facilitate miR-155 processing.

Additionally, two potential assays may be performed in order to identify by what means TN-C regulates the microprocessor. Firstly, mass spectrometry of Drosha pulldown samples within wild-type and TNC knockout macrophages would allow a more generalised view into how the components of the microprocessor change between these conditions. Following this, an *in vitro* processing assay, performed using TNC wild-type and TNC knockout macrophage lysates, would allow the validation of candidate RBP binding sequences within pri-miR-155 through site directed mutagenesis.

The potential role of the RBP mediator MK2 and its upstream kinase p38 α within the TN-C miR-155 pathway was examined utilising TNC knockout RAW246.7 macrophages at the earliest stages of the LPS inflammatory cascade.

Both MK2 and p38 α protein levels were found to be upregulated within TNC knockout steady-state cells, with upregulated p38 α being determined by fractionation to be cytoplasmic. Interestingly, no change in either kinases phosphorylation was found to occur. Previous evidence shows TN-C to induce p38 α phosphorylation within breast cancer, macrophage inflammation and multiple models of subarachnoid haemorrhage^{302,495,597}. This phosphorylation

is attributed to the action of TN-C as an endogenous ligand of TLR4 in all cases but breast cancer, where TN-C is hypothesised to signal via integrin $\beta 3$ ⁴⁹⁵. Therefore, the lack of a detectable change in p38 α phosphorylation within TNC knockdown macrophages is likely due to a combination of the low levels of p38 α phosphorylated within the non-stimulated steady-state cells confounding detection as well as LPS stimulation via the TLR4 pathway obscuring the activity of TN-C via the same pathway. Gain-of-function analysis of TN-Cs potential ability to signal phosphorylation of p38 α could be performed through seeding of macrophages on TN-C rich extracellular matrix, with the potential resultant increase in p38 α phosphorylation being easier to detected in steady-state cells.

Increased p38 α levels in steady-state cells can be attributed to an increase in mRNA expression, as determined by RNA-SEQ analysis of steady-state TNC WT and TNC KO BMDMs. The means by-which TN-C may modulate p38 α expression is unclear. Macrophages derived from TN-C knockout mice exhibit reduced proinflammatory cytokine release upon LPS stimulation ²⁸⁹. Meanwhile treatment with soluble TN-C acts to endogenously promote inflammation through binding to macrophage surface receptors such as TLR4 and $\alpha v\beta 3$ or $\alpha 9$ integrins, activating the NF- κ B, p38 and JNK pathways ^{32,302,521,598}. Thus, it is unexpected that TNC knockdown leads to an increase in the expression of p38 α , an inflammatory pathway component. Further clarification of p38 α expression in RAW 246.7 cells via qPCR alongside an LPS time-course is necessary to fully link the transcriptional and protein level increase in p38 α with TNC knockdown, as well as identifying whether this

function of TN-C is LPS-independent. Additionally, gain-of-function analysis of TN-C via seeding cells on ECM supplemented with TN-C would further verify the impact of TN-C on p38 α quantity.

While MK2 shows a non-significant increase in protein abundance in TNC knockout steady-state RAW 246.7 cells, analysis of mRNA expression in TNC knockout BMDMs and knockdown RAW 246.7 cells shows no modulation of MK2 expression by TN-C. Elevated MK2 levels may instead be due to the increased levels of p38 α acting to bind and protect MK2 from degradation⁴³⁵. The formation and function of this complex has been previously shown to occur in non-stimulated cancer-associated fibroblasts, the prevention of MK2 degradation facilitating an enhanced initiation of the p38 α -MK2 signalling pathway upon stimulation⁴³⁵. However, attempts to coimmunoprecipitate p38 α utilising an MK2 antibody were unsuccessful due to the Ab heavy chain masking MK2 binding and a lack of p38 α association to the capture antibody. Future incorporation of Ab-bead cross-linking aims to minimise the heavy chain binding and allow further optimisation of MK2 pulldown.

More repeats of TNC knockdown western blot experiments are necessary to completely identify whether changes to MK2 phosphorylation are occurring. This being due to the variable degrees of phosphorylation between independent experiments, potentially caused by minor changes in cell treatment or lysate preparation. However, the lack of p38 α phosphorylation change with TNC knockdown supports the consequential lack of a change in MK2 phosphorylation. This coupled with the lack of a significant impact of

MK2 knockdown on miR-155 or pri-miR-155 expression making it unlikely that TN-C is regulating miR-155 via MK2. A potential still exists for p38 α to modify miR-155 expression via an alternate, non-phosphorylation dependent mechanism or through modification of phosphorylation targets. Therefore, future p38 α inhibition using the small molecule inhibitor PH797804 or p38 α siRNA could be used to identify whether p38 α may regulate miR-155 and whether such a regulation is dependent on p38 α abundance (siRNA) or p38 α phosphorylation (PH797804).

Overall, the mechanism by which TN-C may regulate miR-155 remains unknown. Examination of TN-C receptor candidates has revealed integrin α V as potentially regulating miR-155 via a post-transcriptional mechanism, with this functionality shown to be highly LPS timepoint dependent. Notably, TN-C has been shown to regulate p38 α expression, leading to increased protein levels of p38 α and MK2. However, no evidence for MK2 facilitating a change in miR-155 expression or processing has been identified, leading to further investigation into the potential role of alternative downstream targets of p38 α being necessary to validate how modulation of this kinase by TN-C may influence inflammatory signalling.

Chapter 5

The post-transcriptional regulation of miRNA and its links to tenascin-C in the macrophage early inflammatory response

5.1.0 – Introduction

A number of biogenesis steps are required in order to synthesise functional mature miRNAs from their primary transcript (pri-miRNA). This introduces numerous opportunities for post-transcriptional regulation of the miRNA to occur, facilitating modulation of miRNA quantity as well as miRNA targeting through changes to seed sequence composition and strand selection as a result of 3' or 5' miRNA end modification ^{135,599–602}.

One such key processing event is the incorporation and cleavage of the pri-miRNA transcript by the microprocessor complex, comprised of the RNase III enzyme Drosha and a ds-RNA binding protein DiGeorge Syndrome Critical Region 8 (DGCR8) dimer ^{599–601}. The precision and efficiency of pri-miRNA processing by this complex is a key determinant of downstream miRNA activity, with reduced efficiency leading to lower mature miRNA levels, and off-target cleavage giving rise to aberrant downstream pre-miRNA which may be detrimental to future processing steps ^{142,149}.

Piccinini *et al.*, established in 2012 that tenascin-C (TNC) knockout bone-marrow derived macrophages (BMDMs) show reduced levels of mature miR-155, leading to a reduction in pro-inflammatory signalling ²⁸⁹. Subsequent work in the Piccinini lab found TNC knockout to elicit a reduction in levels of pre-miR-155 but not pri-miR-155 ⁵¹¹. This and the RNA-immunoprecipitation analysis of Drosha outlined previously in this thesis, which identified a potential reduction in pri-miR-155 association to Drosha in TNC -/-

macrophages, together implicating the microprocessor as a likely site of miR-155 regulation by TNC⁵¹¹.

In this chapter, RNA-sequencing was performed by Novogene on total RNA from wild-type and TNC knockout BMDMs either unstimulated or treated for 4 hours with lipopolysaccharide (LPS) to induce an early inflammatory response. This sequencing data was used to establish a) whether there are additional miRNAs post-transcriptionally regulated by TN-C in the inflammatory context; b) what determines whether a miRNA is subject to regulation by TN-C; and finally, if this regulation can be linked to known regulatory events at the microprocessor.

To accomplish this, bioinformatic analysis was utilised to isolate whether a specific miRNA's change in expression due to TNC knockout is likely caused by transcriptional or post-transcriptional regulation. Additionally, the occurrence of pri-miRNA cis-regulatory elements and their potential links to TN-C mediated regulation of miRNAs through the microprocessor were examined.

Surprisingly, TNC knockout in LPS induced macrophages was associated with a general reduction in mature 5p miRNAs and an upregulation of mature 3p miRNAs in a pattern indicative of miRNA arm-switching. Unfortunately, no specific cis-regulatory elements, microprocessor associated factors or miRNA isomerisms could be identified which would account for this apparent TN-C dependent modulation of miRNA strand selection.

5.1.1 – Hypothesis

TN-C regulates miR-155 abundance through changes to the association of pri-miRNA to the microprocessor, this mechanism relying on specific cis-acting elements within the pri-miRNA primary and secondary structures (Figure 5.1.1).

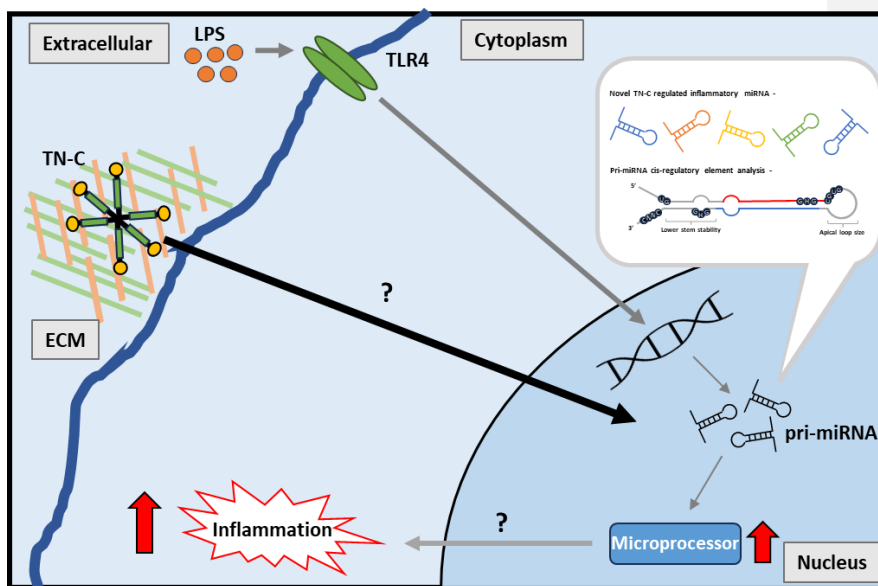


Figure 5.1.1. Schematic representation of research hypothesis and initial objectives.

This schematic details the hypothesised pathway by-which TN-C post-transcriptionally regulates miR-155 expression during the macrophage inflammatory response. Grey lines represents previously established pathways. Pointed arrows indicate stimulation while blunt headed arrows represent inhibition.

5.1.2 – Objectives

To assess the global regulation of macrophage miRNAs by TN-C and to identify specific miRNA structural and regulatory characteristics which are conducive to their regulation. This was achieved by:

- a) Identifying miRNAs with enhanced expression during the early macrophage response to LPS treatment using small RNA-Seq analysis, with specialized bioinformatic analyses utilised to identify potential post-transcriptional mechanism of regulation shared within these miRNAs;
- b) Examining miRNAs with a similar regulatory pattern to miR-155 in LPS treated TNC knockout macrophages, using bioinformatic analyses to identify common structural and regulatory characteristics within their pri-miRNA transcripts;
- c) Exploring potential post-transcriptional events which may facilitate the regulation of miR-155 by TN-C, examining miRNA processing efficiency, arm-switching events and RNA editing occurrence using bioinformatics tools.

5.2.0 - miRNA induction in the early inflammatory response to LPS is primarily driven by an increase in transcription factor activity.

5.2.1 - Characterising miRNA expression in early inflammatory BMDMs

TNC knockout BMDMs had previously been used to establish the role of TN-C in the regulation of miR-155, in addition to the role of TNC as an endogenous activator of TLR4 signalling^{289,511}.

BMDMs were differentiated from stem cells harvested from TNC WT and TNC KO mice. Subsequently macrophages were treated for 4h with LPS or left untreated before total RNA extracts were isolated. 4h LPS treatment was selected as a timepoint of interest due to it being late enough to allow mRNA expressional changes to be apparent and early enough to provide a novel insight into miRNA regulation in the early response to bacterial infection.

Multiplex small RNA libraries were synthesised using total RNA extracts from three independent wild-type (WT) / TNC knockout (TNC KO) and non-treated (NT) / LPS (LPS) stimulated BMDM samples (Figure 5.2.1). RNA integrity was determined at the University of Nottingham using the Agilent 2100 Bioanalyser system, with all samples showing an RNA integrity numbers (RIN) >9. While Novogene further confirmed RNA integrity via nanodrop and agarose gel-electrophoresis with a RIN cut-off of >8.

Non-random adapter sequences were utilised for library generation, with gel purification used to isolate 140-160bp fragments corresponding to small RNA + adapter sequences.

50bp single end reads were generated by Illumina sequencing followed by quality control (QC) and mapping of reads to the genome using the Bowtie mapping tool ⁶⁰³.

During QC of the three wild-type LPS treated BMDM samples two showed a low abundance of clean reads (48.78% and 52.88%) these being due to a high quantity of 3' adapter null or insert null samples (Sup Figure 7.5.0). The other

wild-type LPS samples and the three TNC KO LPS samples had ~90% clean reads.

Bowtie analysis showed consistent mapping of ~80% of sample reads to the mouse genome, this potentially indicating sample contamination or error during library construction (Sup Figure 7.6.0). It should be noted that at this stage two of the LPS WT data-sets consist of ~4 million mapped reads each, compared to the \geq ~7-8 million mapped reads of the other samples. This may introduce a bias, whereby only the higher expressed genes in the LPS WT samples are detectable due to a lack of read depth.

Mature and pre-miRNA annotation was performed by miRdeep2, requiring both the mapping of reads to the miRbase 20.0 database of known mature and pre-miRNA sequences as well as requiring mature miRNA to show alignment to detectable pre-miRNA reads for mapping to be confirmed⁶⁰⁴.

In order to identify miRNA significantly induced or repressed as a result of 4h LPS treatment, differential expression analysis was performed comparing WT NT and WT LPS small RNA-seq read count data (Figure 5.2.2).

Differential expression analysis was conducted using DESeq2, this programme providing more accurate quantifications of within group variance and LogFoldChanges via assumed similarity of variance across genes. DESeq2 utilises both a p-value of 0.05 and a padj, the latter representing the p-value adjusted for multiple testing using the Benjamini-Hochberg method.

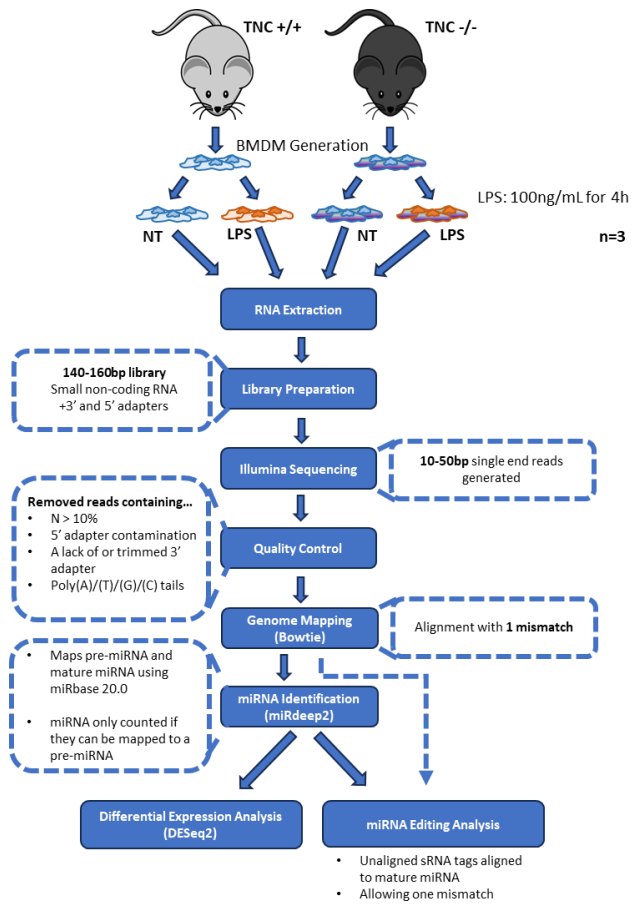


Figure 5.2.1. Schematic of RNA-Seq workflow and analysis pipeline. Total RNA was extracted from wild-type and TNC KO BMDM cells, either untreated or stimulated with 100ng/mL of LPS for 4 hours (n=3) by Dr Anna M. Piccinini. The described analysis pipeline was performed by Novogene.

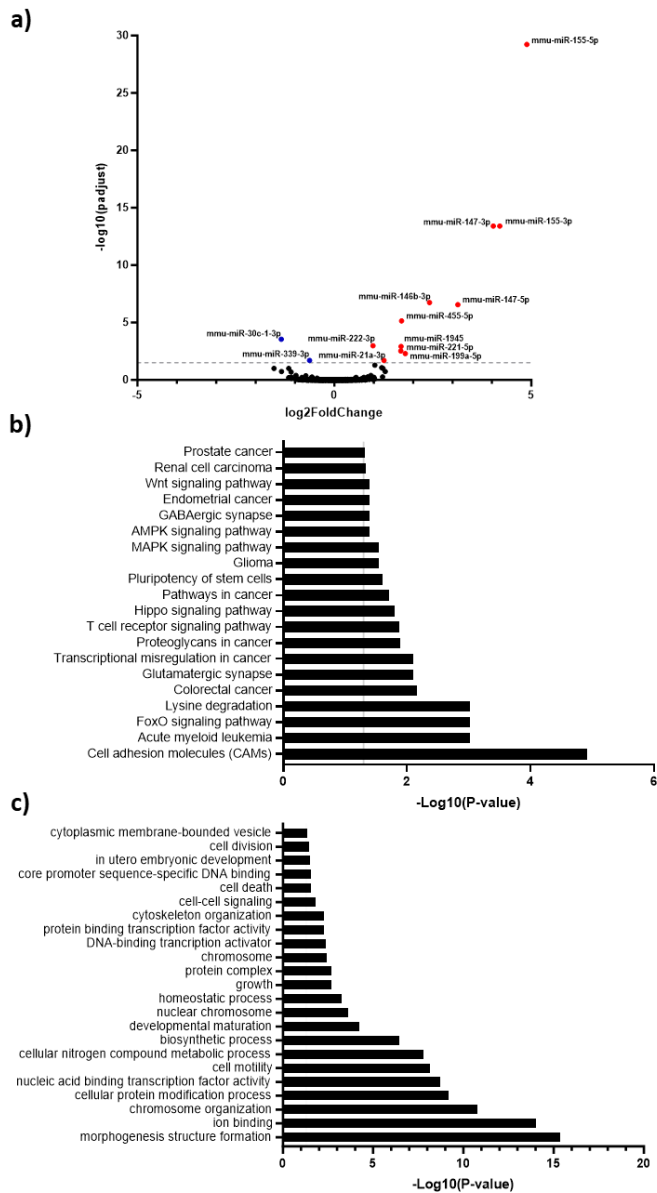


Figure 5.2.2. LPS treatment stimulates expression of multiple miRNAs which act to coordinate early inflammation through a range of pathways in BMDMs. Total RNA was extracted from wild-type BMDM cells, either untreated or stimulated with 100ng/mL LPS for 4 hours (n=3). Small RNA-SEQ and subsequent differential expression analysis was performed by Novogene. The differential expression of miRNA between untreated and 4h LPS treated BMDMs was depicted using a volcano plot (a) with miRNAs above an adjusted p-value threshold showing significant change (padj= 0.05). Significantly upregulated (red), downregulated (blue) or non-significant (black) miRNAs are shown. KEGG (c) and GO (d) analyses were performed on significantly upregulated miRNAs using mirPath v.3., taking predicted miRNA-mRNA interactions from microT-CDS. Results for gene union were determined with FDR correction and significance threshold applied ($p < 0.05$). The 20 most significant associations are depicted, with common parent terms removed.

Eleven mature miRNAs were found to be significantly upregulated (padj < 0.05) and two downregulated by 4h LPS treatment (Figure 5.2.2a). Of these miR-155-5p showed the greatest induction, followed by the miR-155 passenger strand miR-155-3p.

To further characterise the role of these miRNAs during early inflammation, pathway analysis using the Kyoto Encyclopedia of Genes and Genomes (KEGG) and gene ontology (GO) were performed (Figure 5.2.2b/c). The DIANA-mirPath v.3 webtool facilitated the analysis of miRNA associated networks using *in silico* miRNA target predictions from the DIANA-microT-CDS database with KEGG and GO analysis performed upon these predicted pathways by the webtool^{514,605}. Notedly, DIANA-Tarbase, a database of experimentally supported miRNA-mRNA interactions, was not used as this provided few or no results for the majority of the miRNA of interest⁶⁰⁶.

KEGG analysis using DIANA-mirPath v.3. functions by grouping predicted miRNA regulated mRNA into “pathways”, thus predicting “pathways” the miRNA dataset may regulate. Interestingly KEGG analysis of miRNA significantly upregulated by 4h LPS treatment did not find significant associations with any LPS linked inflammatory induction pathways, except for MAPK (Figure 5.2.2b). However, the highest associations was found with cell adhesion molecules, these being central to the effective migration of macrophage cells towards and within inflamed tissue. Additionally, the high association with pathways involved in acute myeloid leukemia illustrate the known role of macrophage inflammatory miRNA in this malignancy, where in particular miR-155 plays a core role⁶⁰⁷.

Unlike KEGG, GO analysis instead utilises the ontologies of predicted miRNA target mRNA, these categoric descriptors of gene function providing a broader view of potential miRNA impacts compared to “pathway” analysis. GO analysis found significant links to cell motility, anatomical structure formation and cytoskeletal organisation, possibly linking to the implied impact on cell adhesion molecules found using KEGG pathway analysis (Figure 5.2.2d). Additionally, multiple associations with transcription factor activity and cell-cell signalling were identified, these potentially having an indirect impact of these on inflammatory processes ⁶⁰⁸.

5.2.2 - Examining evidence for the post-transcriptional regulation of miRNAs in early inflammatory BMDMs.

With the identification of miRNAs significantly regulated by LPS treatment, literature and database analyses were conducted to assess the presence of transcriptional and functional characteristics common between these miRNAs (Table 5.2.1). A lack of common characteristics found in those similarly regulated by LPS stimulation serving to indicate a potential post-transcriptional element to a miRNAs regulation.

microRNA	Arm preference	Log2FoldChange	Gene location	Clustered miRNA	Previous implications in LPS stimulation of macrophages	TLR4 associated TF regulation		
						NF-KB	AP-1	CREB
miR-155-5p	5p	4.89	BIC (Exonic)	N/A	Upregulated by 1h, 2h, 4h and 8h LPS+IFN- γ ^{232,609}	+	+	-
miR-155-3p	5p	4.20	BIC (Exonic)	N/A	Upregulated by 1h, 2h, 4h and 8h LPS+IFN- γ ⁷	+	+	-
miR-147-3p	3p	4.04	AA467197 (Exonic)	N/A	Upregulated by 4h LPS ⁶ Upregulated by 1h, 2h, 4h and 8h LPS+IFN- γ ⁷	+ ²³²	-	-
miR-147-5p	3p	3.14	AA467197 (Exonic)	N/A	Upregulated by 2h, 4h and 8h LPS+IFN- γ ⁶⁰⁹	+ ²³²	-	-

miR-146b-3p	5p	2.42	Outside of gene	N/A	Upregulated by 1h, 2h and 8h LPS+IFN- γ ⁶⁰⁹	-	-	-
miR-199a-5p	5p	1.80	Dnm2 (Intronic)	N/A	Upregulated by 1h, 2h, 4h and 8h LPS+IFN- γ ⁶⁰⁹	-	+	+
miR-455-5p	3p	1.71	Col27a1 (Intronic)	N/A	Upregulated by 1h, 2h, 4h and 8h LPS+IFN- γ ⁶⁰⁹	-	-	-
miR-1945	N/A	1.69	Outside of gene	N/A		-	+	+
miR-221-5p	3p	1.69	Gm14636 (Intronic)	miR-222	Upregulated by 1h, 2h, 4h and 8h LPS+IFN- γ ⁶⁰⁹	-	-	-
miR-21a-3p	5p	1.26	Vmp1 (Exonic)	N/A	Upregulated by LPS treatment of Telocytes for 48h ⁶¹¹	-	+	+
miR-222-3p	3p	0.98	GM14636 (Intronic)	miR-221		-	-	-
miR-339-3p	N/A	-0.63	LOC118568760 (Intronic)	N/A		-	+	+
miR-30c-1-3p	5p	-1.35	Nfyc (Intronic)	miR-30f, miR-30e.		-	+	+

Table 5.2.1. The majority of differentially expressed miRNAs following 4h LPS stimulation of BMDMs can be linked to TLR4-associated transcription factor activity. Total RNA was

extracted from wild-type BMDM cells, either untreated or stimulated with 100ng/mL of LPS for 4 hours (n=3). Small RNA-SEQ and subsequent differential expression analysis was performed by Novogene. The characteristics of miRNA significantly upregulated (red) and downregulated (blue) are listed. miRNA arm preference and miRNA clustering are as described by miRbase 22.1. Chromosome (Chr) and gene location were identified using NCBI genome viewer (GRCm39). TLR4 associated transcription factor (TF) regulation of miRNA was determined based upon literature sources and the TransmiR v2.0 database. Symbols are used to represent presence (+) or absence (-) of TF association.

Each pre-miRNA may give rise to a functional mature miRNA from either the 3' (3p) or 5' (5p) strand. Often one strand will consistently show a greater abundance across tissues and treatments, with a post-transcriptional event such as 3' pre-miRNA end modification or off-target Dicer cleavage being necessary for the alternate strand to become dominant ¹¹⁶. As such the arm preference of each differentially expressed miRNA, as listed by the miRbase 22.1 database, was examined in order to identify instances where the non-dominant strand is significantly regulated with no such regulation seen in its partner strand (Table 5.2.1) ⁷⁴. miR-146b-3p, miR-455-5p, miR-221-5p, miR-21a-3p and miR-30c-1-3p were all found to be such non-dominant strands, thus implicating a degree of post-transcriptional regulation in their modulation by 4h LPS. Further analysis was conducted, comparing the expression of each differentially expressed miRNA and its partner strand in order to identify potential instances of LPS induced arm-switching, identified by both strands showing an opposed change in expression (Figure 5.2.3). Intriguingly, no such events were evident. The dominant strand of miR-1945 has yet to be determined and thus was not analysed.

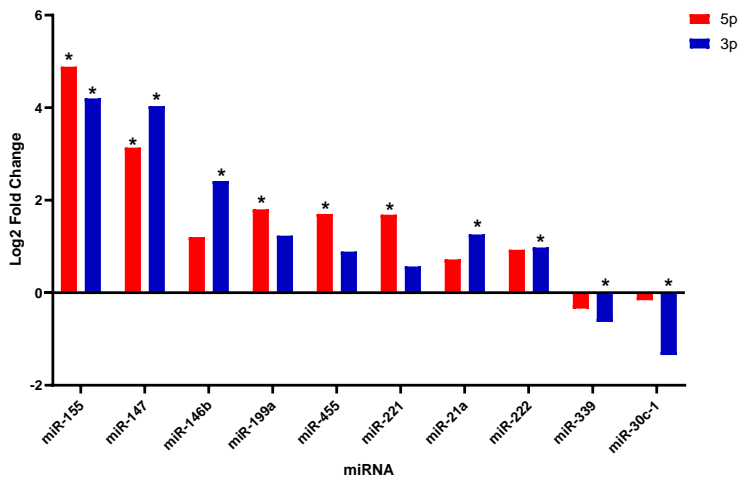


Figure 5.2.3. The partner strand of each miRNA significantly regulated in LPS treated

BMDMs shows similar expression characteristics to its dominant strand. Total RNA was extracted from wild-type BMDM cells, either untreated or stimulated with 100ng/mL LPS for 4 hours (n=3). Small RNA-SEQ and subsequent differential expression analysis was performed by Novogene. * = significant differential expression.

Notably, the four mature miRNAs with the highest upregulation following LPS treatment represent two pri-miRNA transcripts, pri-miR-155 and pri-miR-147, both of which are found within gene exons, BIC and AA467197 respectively. The induction of both strands of these miRNAs derived from the same transcripts suggests that transcription may be the primary driver of their induction.

To further examine the role of transcription in these LPS regulated miRNAs the TransmiR v2.0 database and a literature search were utilised to identify the presence of binding sites for the key TLR4 associated transcription factors, NF- κ B, AP-1 and CREB (Table 5.2.1) ⁶¹².

Pri-miR-155 and pri-miR-147 were the only two transcripts containing binding sites for NF- κ B, likely contributing to their high upregulation, with the addition of an AP-1 binding site in pri-miR-155 potentially leading to it having the highest induction. All other miRNA contained binding sites for AP-1 and CREB except for miR-222-3p, miR-221-5p, miR-146b-3p and miR-455-5p.

5.2.3 - Analysis of miRNA isomerism in inflammatory BMDMs

Within the miRNA biogenesis pathway post-transcriptional regulatory events may give rise to miRNA sequence isomerism, either directly through nucleotide modification such as in the case of TUT4 or through indirect consequence of changes in RNase cleavage accuracy^{142,613}. As such we next analysed the occurrence of RNA-sequence changes in miRNA differentially expressed by LPS treated BMDMs to gather insight into whether these events contribute to LPS-mediated miRNA regulation (Figure 5.2.4).

The occurrence of miRNA isomerism was determined through alignment of unannotated sRNA reads, gathered through the RNA-Seq pipeline, with mature miRNA sequences from miRbase 22.1⁶¹⁴. The proportion of sRNA reads lacking perfect alignment to mature miRNA, due to the presence of non-canonical nucleotides, was calculated as a percentage of the mature miRNA's total reads. Using this data the difference in the occurrence of mature miRNA modifications within miRNA significantly regulated by LPS was compared in non-treated and 4h LPS treated BMDMs datasets (Figure 5.2.4a). No significant difference in modification occurrence was identified between the groups within any of the miRNA examined.

Follow-up analysis was next performed to examine any possible correlation between change in miRNA modification occurrence and increased miRNA fold change between non-treated and 4h LPS treated BMDMs (Figure 5.2.4b). A significant, but weak, correlation was identified, linking increased miRNA expression to a decrease in mature miRNA isomerism occurrence ($R^2 = 0.3461$; $p < 0.05$). As this correlation is weak, this result is likely heavily influenced by the presence of an outlier with high variability.

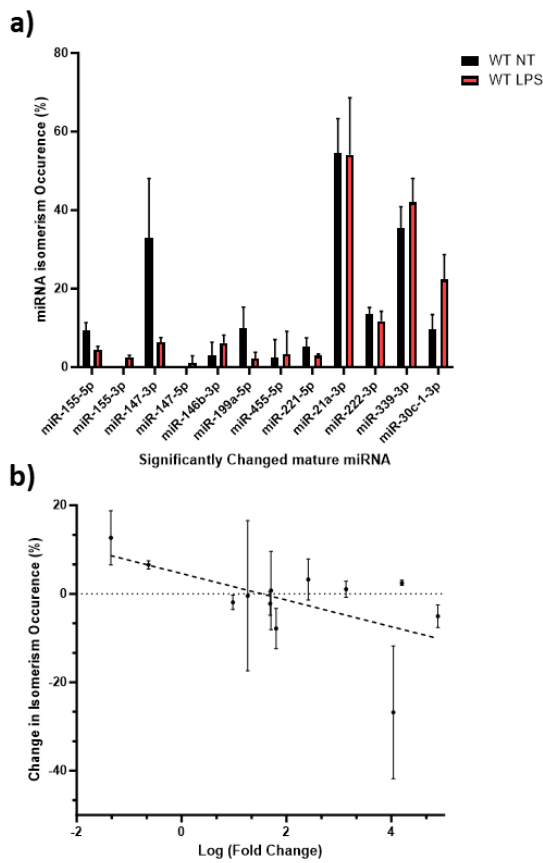


Figure 5.2.4. Changes in miRNA expression correlate with miRNA isomerism occurrence in 4h LPS induced BMDMs. Total RNA was extracted from wild-type BMDM cells, either

untreated or stimulated with 100ng/mL LPS for 4 hours (n=3). Small RNA-SEQ and subsequent differential expression analysis was performed by Novogene. miRNA isomerism events were determined through alignment of unannotated sRNA reads with mature miRNA from miRbase 22.1. Percentage occurrence of miRNA isomerism events are relative to the total miRNA reads in that sample. a) The miRNA isomerism occurrence of each differentially expressed mature miRNA, \pm SD, was compared between non-treated and 4h LPS treated samples. Single / multiple Mann Whitney U test; $p > 0.05$, ns. b) LPS induced significant changes in miRNA expression were plotted against each miRNAs change in isomerism occurrence, \pm SD, between non-treated and LPS treated samples. Simple linear regression; $R^2 = 0.3461$, $p = < 0.05^*$.

Finally, in order to potentially identify the activity of specific miRNA nucleotide modifiers the occurrence of miRNA isomerism within each nucleotide of the top three miRNA upregulated by 4h LPS treatment was examined (Figure 5.2.5). Known inducers of miRNA isomerism include uridylyltransferases, which lead to the 3' addition of uracil nucleotides, or cytidine / adenosine deaminases which change cytosine to uracil and adenosine to inosine, respectively ^{126–128}.

Of these miRNAs only miR-155-3p showed an overall significant change in miRNA isomerism with LPS treatment ($p < 0.05$), showing an upregulation in isomerism occurrence, in particular a C→U transition at the 3' terminus indicative of cytidine deaminase activity (Figure 5.2.5b). However, it should be noted that miR-155-3p's expression in non-treated cells is exceedingly low with no detectable miRNA isomerism and thus reducing the biological relevance of this percentage change in isomerism occurrence. Although highly variable, miR-147-3p does exhibit high isomerism occurrence, with ~10% of 3' terminal residues being edited in WT cells.

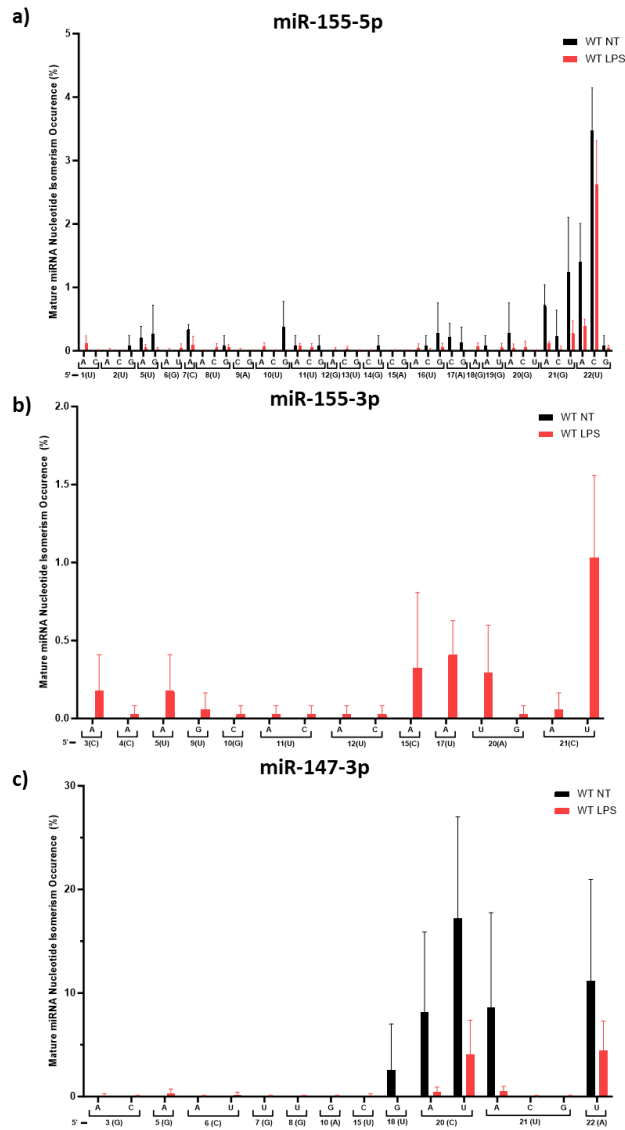


Figure 5.2.5. 4h LPS treatment of BMDMs causes a significant overall increase in miR-155-3p miRNA isomerism, but not for miR-155-5p or miR-147-3p. miRNA isomerism was determined through alignment of unannotated sRNA reads with mature miRNA from miRbase 22.1. Percentage occurrence of specific miRNA nucleotide isomerism was determined relative to the total canonical nucleotide reads in that sample. The location of each isomerism event relative to the 5' end of the mature miRNA were noted, with miRNA nucleotide isomerism

determined \pm SD. a) miRNA-155-5p, single/multiple Mann Whitney U; $p > 0.05$, ns. b) miR-155-3p, single Mann Whitney U; $p < 0.001$, ***. Multiple Mann Whitney U; $p > 0.05$, ns. c) miR-147-3p, single/multiple Mann Whitney U; $p > 0.05$, ns.

5.3.0 - Tenascin-C knockout in BMDMs causes a global shift in inflammatory miRNA expression.

5.3.1 - Characterising the effect of TNC knockout on miRNA expression in early inflammatory BMDMs.

With previous experimental evidence that TN-C regulates miR-155 post-transcriptionally during the early LPS response we next aimed to identify other miRNA which may be undergoing similar regulation in hopes of deriving a shared mechanism by-which TN-C influences miRNA biogenesis.

Differential expression analysis was performed by Novogene using DESeq2, as outline previously, using read count data from TNC wild-type and TNC knockout BMDMs stimulated with LPS for 4 hours (Figure 5.3.1a). This analysis identified miR-30a-5p, miR-30a-3p and miR-30c-2-3p as the only differentially expressed miRNA, with their expression reduced by TNC knockout.

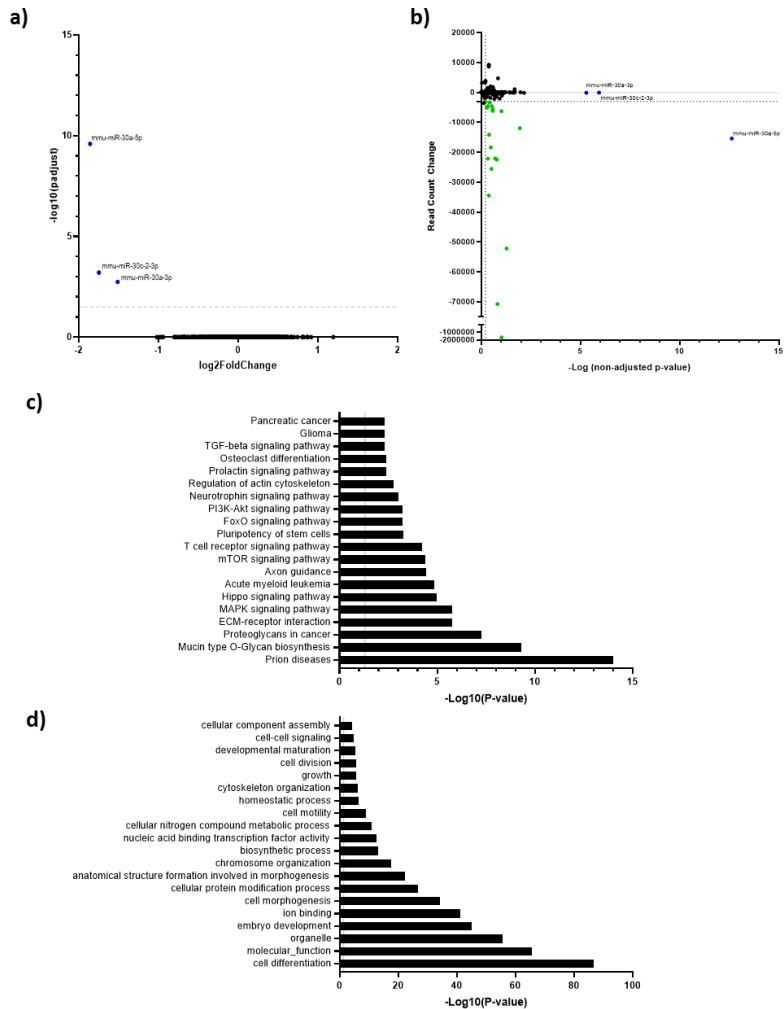


Figure 5.3.1. TNC knockout in 4h LPS stimulated BMDMs leads to few differentially expressed miRNA, leading to the establishment of a pool of regulated miRNA based upon experimentally validated miRNA-155-5p's differential expression characteristics. This group of miRNA share significant associations with multiple pathways previously implicated in regulation by TN-C. Total RNA was extracted from wild-type and TNC KO BMDM cells stimulated with 100ng/mL LPS for 4 hours (n=3). Small RNA-SEQ and subsequent differential expression analysis was performed by Novogene. a) The differential expression of miRNAs in TNC KO relative to TNC WT was depicted using a volcano plot with miRNAs above an adjusted

p-value threshold showing significant change ($p_{adj} = 1.301$). Significantly downregulated (blue) or non-significant (black) miRNAs are shown. b) The group of miRNA used for future analysis was created using the $-\log p$ -value of miR-155-5p, $-\log p = 0.20899$, and the read count change of miR-155-5p, ~ -3000 , as minimum thresholds. miRNAs above (green), below (black) and previously found to be differentially expressed (blue) are depicted. KEGG (c) and GO (d) analyses were performed on the miRNA-155-5p derived group using mirPath v.3., taking predicted miRNA-mRNA interactions from microT-CDS. Results for gene union were determined with FDR correction and significance threshold applied ($p < 0.05$). The 20 most significant associations are depicted, with common parent terms removed.

This analysis did not identify a significant decrease in expression of miR-155 with TNC knockout even though this has been demonstrated previously elsewhere in BMDMs^{289,511}. Previous qPCR analyses shows miR-155-5p to only have a significant reduction in TNC knockout BMDMs after 8 or 24 hours of LPS treatment^{289,511}. Thus, with only 4 hours of induction the abundance of miR-155-5p is likely not yet high enough to be significantly changed by TNC knockout. However, RNA-immunoprecipitation experiments on TNC knockdown BMDMs performed within 2 hours of LPS stimulation showed a potential reduction in pri-miR-155 association with the microprocessor, implying that even if not significantly changed miR-155 is still being regulated by TN-C at this timepoint (Figure 3.1.2).

This evidence led to the establishment of a pool of miRNAs for use in future analysis based upon the differential expression characteristics of miR-155-5p in 4h LPS treated TNC knockout BMDMs (Figure 5.3.1b and Table 5.3.1). This pool used the p-value (0.61813) and relative read count change (-3000) of miR-155-5p as a minimum threshold. This also served to remove miR-30a-3p

and miR-30c-2-3p from the analysis pool, as these miRNAs though differentially expressed have very low total reads and are thus likely not biologically relevant.

miRNA	Log2Fold Change	Read Count Change	P-value*	Dominant Strand
miR-30a-5p	-1.8587	-15423	2.34E-13	5p
miR-221-5p	-0.94831	-11951	0.011391	3p
miR-7a-5p	-0.75046	-52164	0.052963	5p
miR-125a-5p	-0.71933	-6277	0.096392	5p
miR-21a-5p	-0.58457	-1679937	0.095311	5p
miR-10a-5p	-0.54547	-22063	0.20277	5p
miR-30d-5p	-0.39115	-70725	0.15523	5p
miR-30e-5p	-0.37556	-6167	0.26745	5p
let-7f-5p	-0.35826	-22448	0.16427	5p
miR-99b-5p	-0.34052	-18411	0.33288	5p
let-7c-5p	-0.33346	-5643	0.26746	5p
miR-146b-5p	-0.28129	-14118	0.40549	5p
miR-26a-5p	-0.26787	-22137	0.467	5p

miR-125b-5p	-0.25421	-3421	0.38115	5p
miR-99a-5p	-0.25209	-25589	0.31028	5p
let-7a-5p	-0.25102	-4610	0.29291	5p
let-7i-5p	-0.24963	-34464	0.41748	5p
miR-146a-5p	-0.20877	-4625	0.47316	5p
let-7g-5p	-0.17779	-5078	0.50439	5p
miR-191-5p	-0.14575	-4989	0.52805	5p
miR-155-5p	-0.12884	-3153	0.61803	5p

Table 5.3.1. A miR-155-5p calibrated pool of miRNA differentially expressed between WT LPS and TNC KO LPS datasets. miRNAs are grouped based upon minimum thresholds set by miR-155-5p, known to be regulated by TNC knockout. p-value = <0.61803 and relative read count change <-3000.

Using the newly established pool of TNC KO downregulated miRNAs, KEGG and GO analyses were performed as previously, using the DIANA-mirPath v.3 webtool and DIANA-microT-CDS database in order to identify potential pathway links to TN-C (Figure 5.3.1c/d) ^{514,605}.

KEGG analysis identified multiple associations between downregulated miRNA targets and TN-C linked pathways. These include ECM-receptor interactions, MAPK signalling, Hippo signalling, regulation of the actin cytoskeleton and TGF-beta signalling (Figure 5.3.1c) ^{311,570,571,615}. Meanwhile GO analysis associated these miRNAs with TN-C linked ontologies such as morphogenesis, cytoskeletal organisation and cell-cell signalling ^{311,412,616}. These terms are also

found in the inflammatory associated miRNA-linked ontologies identified previously (Figure 5.3.1d), potentially linking the TNC regulated miRNA to changes in macrophage morphology indicative of inflammatory activation.

5.3.2 – TNC knockout increases the abundance of miRNA 3p strands and decreases that of 5p strands only in LPS induced BMDMs.

When compiling the pool of miRNAs downregulated by TNC knockout the dataset was observed to primarily consisted of mature miRNAs from the 5p strand, with these 5p miRNAs being the dominant strand listed by miRbase in all cases but miR-221 (Table 5.3.1). Notably, previous analysis into the expression of miRNAs during LPS stimulation showed both 5p and 3p strands of various miRNAs to be induced (Figure 5.2.3). This led to a more in-depth analysis of miRNA 5p and 3p strands abundance in TNC knockout BMDMs (Figure 5.3.2).

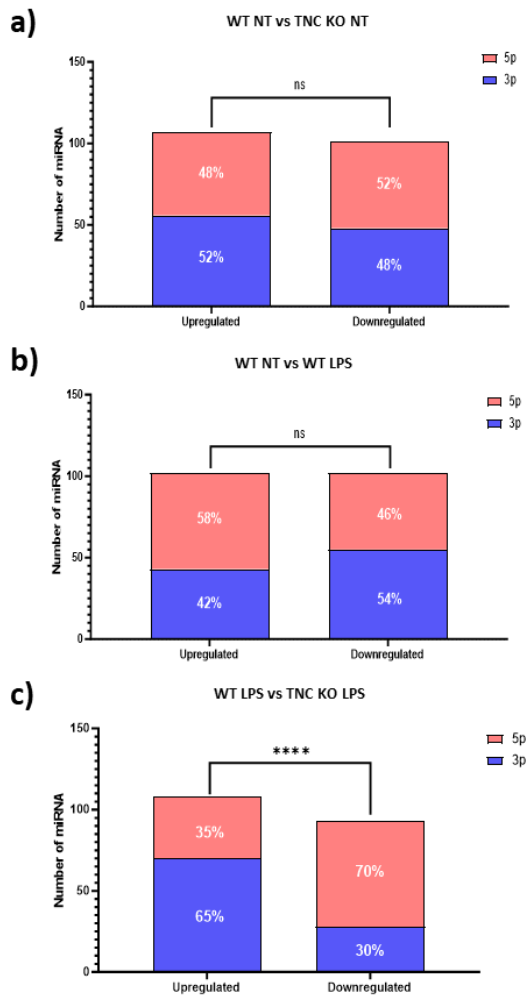


Figure 5.3.2. TNC knockout in LPS stimulated cells leads to a significant downregulation in 5p and upregulation in 3p mature miRNA strands. Total RNA was extracted from wild-type and TNC KO BMDM cells untreated or stimulated with 100ng/mL LPS for 4 hours (n=3). Small RNA-SEQ and subsequent differential expression analysis was performed by Novogene. Differentially expressed miRNA were placed into upregulated (>5% read count change, >10 read count change) and downregulated (<-5% read count change, <-10 read count change) groups. The number of 3p and 5p miRNA strands in each group was quantified and significant difference between the groups determined by a Fischer's Test. a) n=107 upregulated, 101

downregulated. Fischer's Test; $p > 0.05$, ns. b) $n = 102$ upregulated, 102 downregulated.

Fischer's Test; $p > 0.05$, ns. c) $n = 108$ upregulated, $n = 93$ downregulated. Fischer's Test; $p < 0.0001$, ***, odds ratio = 4.28 (2.41-7.80 95% CL).

Firstly, miRNAs from each complete dataset, not just those calibrated by miR-155-5p, were placed into upregulated and downregulated groups based upon Novogene's differential expression analysis. miRNAs with a read count change percentage greater than 5% and a read count change greater than 10 reads were considered upregulated while those with a read count change percentage less than -5% and a read count change less than -10 reads were considered downregulated by TNC KO. These parameters were chosen in order to maximise the number of miRNA sampled within each pool, while also keeping the pools at a size where analysis could be performed manually.

The percentage of 3p and 5p miRNAs in the upregulated and downregulated groups of the three differential expression analyses were calculated (Figure 5.3.2). TNC knockout BMDMs treated with LPS showed a significant difference in strand percentages between the upregulated and downregulated groups ($p < 0.0001$, odds ratio = 4.28 (2.41-7.80 95% CL) (Figure 5.3.2c), with 35% of upregulated miRNAs ($n = 108$) being 5p with this proportion doubling to 70% in the downregulated group ($n = 93$). However, when examining differential expression groups for TNC KO in non-treated cells (Figure 5.3.2a) and LPS treatment in wild-type cells (Figure 5.3.2b) no significant difference in strand percentages was found. This implies that it is a combination of TNC knockout and 4 hours LPS induction which is inducing the upregulation in 3p and downregulation in 5p strands.

In order to identify whether changes to miRNA strand abundance in upregulated and downregulated groups represented potential arm-switching events, 5p and 3p miRNAs within each group were further subdivided and compared (Figure 5.3.3).

5p and 3p miRNAs were classified as “arm-switching” if their alternative strand was found within the opposite groups (i.e. if the 5p strand was downregulated and the 3p strand was upregulated by TNC KO in LPS treated BMDMs). Significantly more 5p arm-switching was identified in the downregulated group (24% of miRNAs) compared to the upregulated group (1.8% of miRNAs), with the reverse being true for 3p arm-switching (Figure 5.3.3a/b). No such significant difference was identified in other experimental groups except for a significant association of arm-switching 3p and miRNAs downregulated in wild-type LPS treated BMDMs compared to non-treated BMDMs (12% of miRNAs) (Figure 5.3.3a/b).

5p and 3p miRNAs were classified as “independent” if their alternative strand was not found within either group (i.e. if the 5p strand was downregulated and the 3p strand was not up- nor downregulated by TNC KO in LPS treated BMDMs). Significantly more independent 5p was identified in the downregulated group (34% of miRNA) compared to the upregulated group (13% of miRNA), with no significant difference found between the 3p miRNA groups nor in the groups derived from WT NT vs TNC KO NT and WT NT vs WT LPS differential expression analyses (Figure 5.3.3c/d).

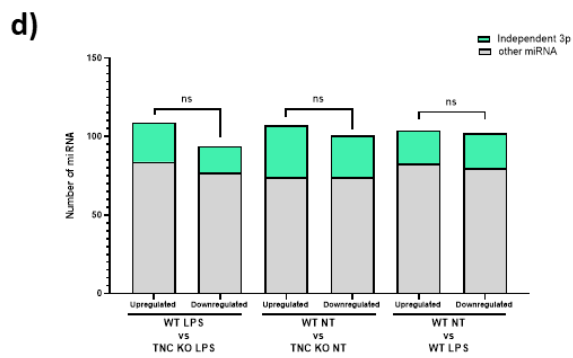
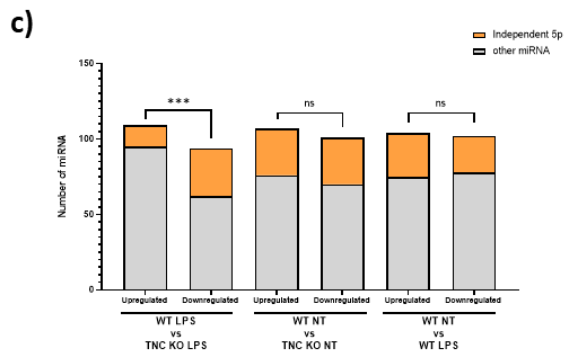
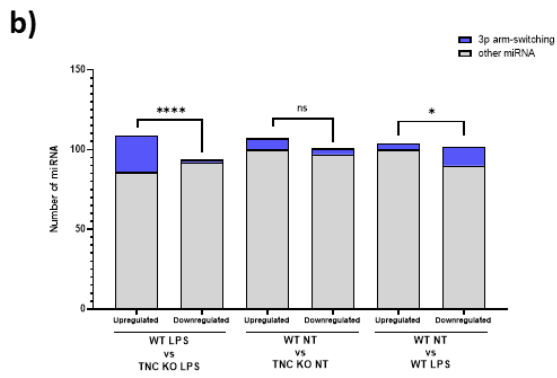
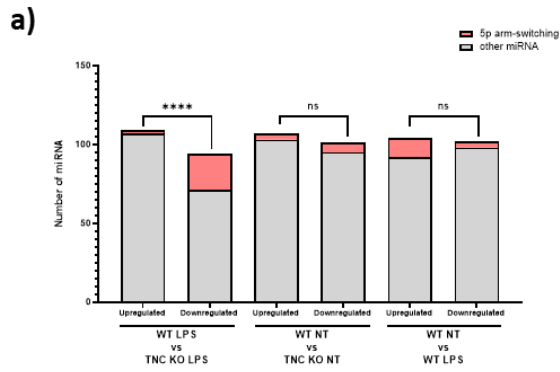


Figure 5.3.3. The downregulation in 5p miRNAs in TNC knockout LPS stimulated BMDMs is potentially the result of arm-switching. Total RNA was extracted from wild-type and TNC KO BMDM cells untreated or stimulated with 100ng/mL LPS for 4 hours (n=3). Small RNA-SEQ and subsequent differential expression analysis was performed by Novogene. Differentially expressed miRNAs were placed into upregulated (>5% read count change, >10 read count change) and downregulated (<-5% read count change, <-10 read count change) groups. The following categories of miRNAs were established and quantified in both downregulated and upregulated groups with significant difference between the groups determined by a Fischer's Test. **a)** 5p arm-switching were categorised as 5p miRNAs with their matching 3p strand within the other group. Fischer's Test; $p < 0.0005^{****}$, odds ratio: 17.33 (4.383-75.62 95% CL), ns. **b)** 3p arm-switching were categorised as 3p miRNAs with their matching 5p strand within the other group. Fischer's Test; $p < 0.0005^{****}$, odds ratio: 0.08129 (0.01860 to 0.3199 95% CL), $p < 0.05^*$, odds ratio: 3.333 (1.021 to 9.676% CL), ns. **c)** Independent 5p were categorised as 5p miRNAs with their matching 3p strand not present within the other group. Fischer's Test; $p < 0.005^{***}$, odds ratio: 3.502 (1.700 to 7.238 95% CL), ns. **d)** Independent 3p were categorised as 3p miRNAs with their matching 5p strand not present within the other group. Fischer's Test; $p > 0.05$, ns.

5.3.3 – Analysis of miRNA isomerism in TNC knockout BMDMs during LPS stimulation

One possible explanation for the upregulation in 3p miRNAs caused by TNC knockout is a change in miRNA isomerism leading to a modification to the process of strand selection. This is the process whereby one of the two miRNA strands is bound by the AGO complex while the other is lost and degraded. Multiple factors oversee which strand is retained including the thermodynamic properties and nucleotide composition of the miRNA termini

^{109,112,113,617}. As such miRNA isomerism has been shown to impact strand selection through changes to the miRNA ends ¹³⁵.

Whether TNC knockout potentially influences miRNA isomerism occurrence was next examined using the miR-155-5p calibrated pool of downregulated miRNAs (Table 5.3.1). Analysis of miRNA isomerism was performed as described previously (Figure 5.3.4). Comparison of miRNA isomerism occurrence was conducted between wild-type and TNC knockout 4-hour LPS treated BMDMs (Figure 5.3.4a). No significant change in miRNA isomerism occurrence was found in any of the downregulated miRNAs. Further analysis was performed on the change in miRNA isomerism occurrence of individual nucleotides within miR-155-5p and 3p (Figure 5.3.4b/c). miR-155-5p showed no significant change in nucleotide isomerism between wild-type and TNC knockout while miR-155-3p showed a significant overall increase in isomerism occurrence ($p < 0.01$). miR-155-3p has increased isomerism occurrence at multiple sites which show no isomerism in the wild-type, with none of these events occurring in $> 0.5\%$ of the miRNA population. As such it is unlikely that this is a biologically significant effect.

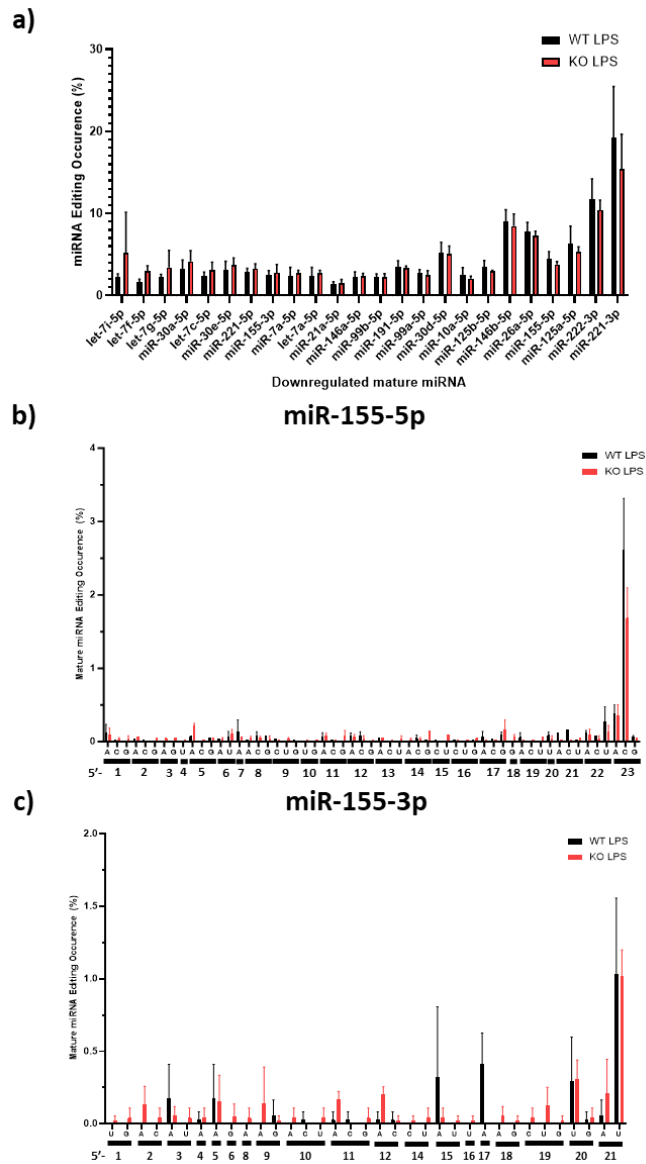


Figure 5.3.4. TNC KO in 4h LPS induced BMDMs causes a significant overall increase in miR-155-3p miRNA isomerism but in other miRNAs. Total RNA was extracted from wild-type and TNC KO BMDM cells stimulated with 100ng/mL LPS for 4 hours (n=3). Small RNA-SEQ and subsequent differential expression analysis was performed by Novogene. miRNA isomerism events were determined through alignment of unannotated sRNA reads with mature miRNA

from miRbase 22.1. Percentage occurrence of miRNA isomerism events is relative to the total miRNA reads in that sample. a) The miRNA isomerism occurrence within the miR-155-5p derived group, \pm SD, was compared between TNC KO and wild-type 4h LPS treated samples. Single / multiple Mann Whitney U test; $p > 0.05$, ns. b) Percentage occurrence of specific miRNA nucleotide isomerism events was determined relative to the total canonical nucleotide reads in that sample. The location of each isomerism event relative to the 5' end of the mature miRNAs was noted, with miRNA isomerism occurrence determined \pm SD. miRNA-155-5p, single/multiple Mann Whitney U; $p > 0.05$, ns. c) miR-155-3p, single Mann Whitney U; $p < 0.01$, **. Multiple Mann Whitney U; $p > 0.05$, ns.

The upregulation of the 3p strand by TNC knockout is interesting, especially with this solely occurring in LPS stimulated cells. How this occurs is yet unexplained, with our examination of miR-155-3p showing a significant induction of miRNA isomerism events but none of a large enough frequency to warrant a change in strand selection.

5.4.0 – Analysis of pri-miRNA cis-acting elements in TNC knockout macrophages

5.4.1 – Examining the association between regulation of miRNA by TN-C and the presence of cis-acting elements.

Previous experimental evidence gathered in collaboration with Nicole Zordan indicated that the regulation of miR-155 by TN-C potentially occurs in part due to a reduction in pri-miR-155 associating with the microprocessor. This led to our next method of analysis, conducting a comprehensive annotation of pri-miRNA features and motifs linked to regulation of microprocessor activity

before using the RNA-SEQ dataset to examine correlations between the presence of these cis-acting elements and miRNA regulation by TN-C.

In brief, multiple cis-acting pri-miRNA elements are known to modulate miRNA-microprocessor association and resultant pri-miRNA cleavage.

Amongst these are the CNNC, basal UG, basal mGHG, apical mGHG and apical UGUG motifs, as well as lower stem stability and the size of the apical loop, all being shown to have differing impacts on pri-miRNA-microprocessor association and cleavage (Figure 5.4.1)^{142,146,147,149}.

a)

Feature	Motif / Characteristic	Location	Impact on pri-miRNA processing	References
Basal UG	UG	5' -14	Facilitates DROSHA binding	²⁵⁸
Apical UGUG	UGUG (UGU/GUG)	5' +21/22/23	Facilitates DGCR8 binding	²⁵⁸
Basal mGHG	G(A/T/C)G Must be aligned No bulge Score >38	5' -7 to -5 3' -5 to -3	Improves accuracy of Drosha processing	¹⁴²
Apical mGHG	G(A/T/C)G Must be aligned No bulge Score >38	-7 from apical loop	Causes off-target Drosha binding	¹⁴⁹
CNNC	CNNC (DNNC/CNND)	3' +17	Common motif for RBP co-factors	¹⁶¹
Lower-stem stability	Fewer than 4 mismatches	5' -1 to -13	Facilitates DROSHA binding	¹⁵³

Apical loop size	N/A	Beginning of the apical loop	Aids DGCR8 incorporation	618
------------------	-----	------------------------------	--------------------------	-----

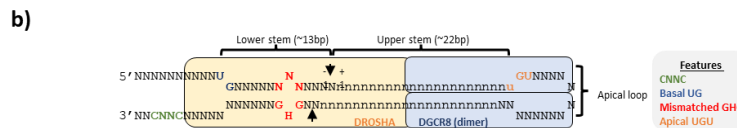


Figure 5.4.1. cis-regulatory features of pri-miRNA transcripts have a significant impact on miRNA processing. a) Key cis-regulatory pri-miRNA elements, their sequence, location and impact on pri-miRNA processing are summarised. This served as a guide for downstream identification of these features. b) A schematic representation of a pri-miRNA transcript with critical cis-regulatory features and structural elements labelled, as well as the association of Drosha and the DGCR8 dimer in the microprocessor complex.

5.4.2 – Lower stem region stability is the only cis-regulatory element of pri-miRNA associated with miRNAs downregulated by TNC knockout.

In order to identify cis-acting elements potentially linked to the regulation of pri-miRNA by TN-C within LPS stimulated macrophages the occurrence of these features in miRNA regulated by TNC KO in 4h LPS treated BMDMs was assessed.

In order to identify whether downregulated miRNA, derived from the miR-155-5p calibrated pool outlined previously (Table 5.3.1), were associated with particular cis-regulatory elements a control pool of miRNA was created. miRNA from the complete WT LPS vs TNC KO differential expression analysis dataset showing a percentage read count change between -5% and 5%, and

an absolute read count change of between -100 and 100 were utilised (Table 5.4.1).

miRNA	Log2Fold Change	Read Count Change	P-value*
miR-351-5p	0.055505	35	0.84263
miR-125b-2-3p	0.055473	79	0.87629
miR-101b-3p	0.042487	61	0.88914
miR-16-1-3p	0.038158	20	0.91466
miR-28a-3p	0.024297	8	0.92171
miR-423-3p	0.012364	71	0.96591
miR-339-5p	0.0096432	10	0.97161
miR-130b-5p	0.0027293	3	0.99256
miR-423-5p	-0.0031153	-8	0.99108
miR-142a-5p	-0.0031327	-9	0.98956
miR-103-3p	-0.0038507	-53	0.9847
miR-17-5p	-0.023061	-42	0.93781
miR-181b-5p	-0.023818	-40	0.93398
miR-27b-5p	-0.052214	-15	0.82502

Table 5.4.1. Control miRNA dataset. miRNAs derived from the WT LPS vs TNC KO LPS differential expression analysis. % read count change <5% and >-5% and an absolute read count change >-100 and <100.

Utilising these groups, the abundance of each cis-regulated element was determined using the criteria outlined previously (Figure 5.4.1) which follows previous analysis performed by Narry Kim (Table 5.4.2 and Table 5.4.3) ¹⁵³. Importantly, our dataset consisted of mouse miRNA while Narry Kim examined human miRNAs, which could lead to slight changes in motif composition or location, although all motifs have been confirmed to be conserved throughout mammals. The occurrence of a “functional” basal or apical mGHG motif was determined using Kwon *et al.*, 2019’s previous analysis of human mGHG motifs, wherein a “mGHG score” was developed through assessing the degree to which each mGHG motif impacted processing, with a score > 38 representing a functional motif ¹⁴².

miRNA	Stable Stem	Basal UG	CNNC	Apical UGUG	Basal mGHG	Apical mGHG
Pri-miR-351	✗	✗	CNNC	✗	46.01	Bulge
Pri-miR-125b-2	✓	✓	CNNC	✗	43.52	Bulge
Pri-miR-101b	✓	✓	✗	UGU	Non-aligned	27.54
Pri-miR-16-1	✗	✓	CNND	✗	Non-aligned	44.13
Pri-miR-28a	✓	✓	CNNC	✗	57.43	Bulge
Pri-miR-423	✓	✗	CNND	✗	11.74	45.06
Pri-miR-339	✓	✗	DNNC	✗	77.38	28.71
Pri-miR-130b	✗	✗	✗	UGUG	14.66	Bulge
Pri-miR-423	✓	✗	CNND	✗	11.74	45.06
Pri-miR-142a	✓	✗	CNNC	✗	10.95	45.06
Pri-miR-103	✓	✗	✗	UGU	66.43	28.71
Pri-miR-17	✓	✗	✗	✗	Non-aligned	Bulge
Pri-miR-181b	✗	✗	DNNC	✗	76.31	20.59
Pri-miR-27b	✓	✗	✗	✗	Non-aligned	41.75

Table 5.4.2. Control miRNAs cis-regulatory element. The presence of a UG motif at position -14, a UGUG/UGU/GUG motif at position +21/22/23 and a CNNC/DNNC/CNND motif at +17 downstream of the 3' end was determined. >4 nucleotide mismatches from position -1 to -13 indicated the lack of a stable stem. The presence of a basal mGHG motif at 5'-7 to -5 and 3' -5

to -3 and an apical mGHG motif -7 from the apical loop was determined for each miRNA with unaligned sequence and the presence of a bulge or pseudo-knot disqualifying the motif.

pri-miRNA	Stable Stem	Basal UG	CNNC	Apical UGUG	Basal mGHG	Apical mGHG
Pri-miR-30a	✓	✓	CNNC	✗	23.82	11.34
Pri-miR-221	✗	✗	DNNC	✗	59.05	Non-aligned
Pri-miR-7a	✓	✗	✗	UGU	64.62	10.37
Pri-miR-125a	✓	✓	CNND	✗	95.93	41.75
Pri-miR-21a	✓	✗	✗	✗	46.01	Bulge
Pri-miR-10a	✓	✗	DNNC	UGU	26.79	35.60
Pri-miR-30d	✓	✗	✗	✗	32.76	Bulge
Pri-miR-30e	✓	✗	CNNC	✗	Bulge	37.37
Pri-let-7f	✓	✗	✗	UGUG	Bulge	Bulge
Pri-miR-99b	✓ (pseudoknot)	✓	✗	✗	13.68	Bulge
Pri-let-7c	✓	✗	✗	✗	23.98	19.08
Pri-miR-146b	✓	✓	CNND	UGUG	74.74	68.30
Pri-miR-26a	✓ (pseudoknot)	✗	CNNC	UGUG	44.75	3.87
Pri-miR-125b	✓	✓	CNNC	✗	43.53	Bulge
Pri-miR-99a	✓	✓	CNND	✗	Non-aligned	20.73
Pri-let-7a	✓	✗	✗	✗	Non-aligned	Bulge
Pri-let-7i	✓	✗	✗	✗	Non-aligned	Bulge
Pri-miR-146a	✗	✓	✗	✗	Non-aligned	15.71
Pri-let-7g	✓	✗	✗	UGAG	23.98	Bulge
Pri-miR-191	✓	✗	CNNC	UGU	14.87	41.75
Pri-miR-155	✓	✗	✗	✗	Non-aligned	1.92

Table 5.4.3. Downregulated miRNAs cis-regulatory element. The presence of a UG motif at position -14, a UGUG/UGU/GUG motif at position +21/22/23 and a CNNC/DNNC/CNND motif at +17 downstream of the 3' end was determined. >4 nucleotide mismatches from position -1 to -13 indicated the lack of a stable stem. The presence of a basal mGHG motif at 5'-7 to -5

and 3' -5 to -3 and an apical mGHG motif -7 from the apical loop was determined for each miRNA with unaligned sequence and the presence of a bulge or pseudo-knot disqualifying the motif.

In order to identify cis-regulatory elements significantly associated with miRNA downregulated by TNC knockout the occurrence of each cis-regulatory element within control and downregulated miRNA groups were compared (Figure 5.4.2).

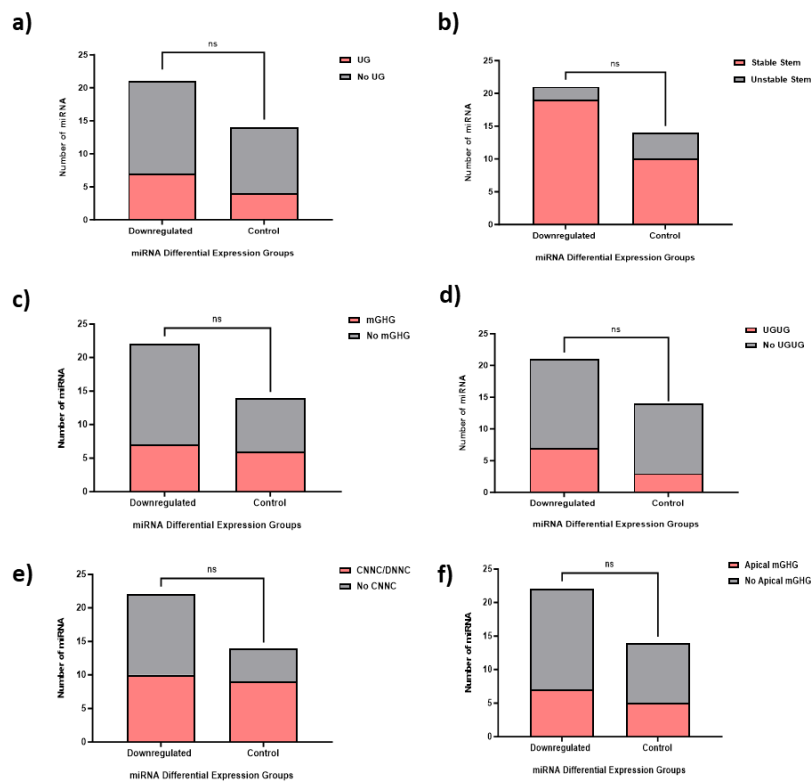


Figure 5.4.2. Lower stem region stability is the only cis-regulatory element of pri-miRNAs that significantly occurs in miRNAs downregulated in TNC knockout samples. Total RNA was extracted from wild-type and TNC KO BMDM cells stimulated with 100ng/mL LPS for 4 hours (n=3). Small RNA-SEQ and subsequent differential expression analysis was performed by

Novogene. miRNAs were grouped based upon the effect of TNC knockout on their expression in 4h LPS induced samples into downregulated (% read count change= \leq -5%, read count change= \leq -3000, n=22), upregulated (% read count change= \geq 5%, read count change= \geq 1000, n=15) and control (% read count change=-5%-5%, read count change=-100-+100, n=14) groups. a) The presence of a UG motif at position -14 was determined for miRNA in each group. b) The presence of a stable stem was determined, with >4 nucleotide mismatches from position -1 to -13 indicating instability. This was done for miRNAs in each group. c) The presence of a basal mGHG motif at 5'-7 to -5 and 3' -5 to -3 was determined for miRNAs in each group. Unaligned sequence and the presence of a bulge or pseudo-knot disqualified the motif. Only functional mGHG motifs with a score >38 , derived from the average processing impact of human mGHG motifs, were used in the analysis. d) The presence of an UGUG/UGU/GUG motif at +21/22/23 was determined for miRNAs in each group. e) The presence of a CNNC/DNNC/CNND motif at 3'+17 was determined for miRNAs in each group. f) The presence of an apical mGHG motif -7 from the apical loop was determined for miRNAs in each group. Unaligned sequence and the presence of a bulge or pseudo-knot disqualified the motif. Only functional mGHG motifs with a score >38 , derived from the average processing impact of human mGHG motifs, were used in analysis. All comparisons were performed using a Fischer's Test, $p \geq 0.05$ (ns).

This analysis showed no significant change in the occurrence of basal UG, apical UGUG, apical mGHG, basal mGHG, CNNC motifs nor stable lower stem between the two groups (Figure 5.4.2). Between the two groups all the motifs, with the exception of the CNNC, were absent in at least half of miRNA.

The low proportion of miRNAs containing each feature is not surprising as it is likely a natural outcome of our strict identification criteria coupled with the already reported low abundance of these features¹⁵³. The robust presence of

the CNNC motif in all groups reduces the likelihood that an RBP may be involved in the regulation of miRNAs by TNC at the microprocessor.

5.4.3 – The composition of the mGHG motif does not have a significant impact on miRNA regulation by TN-C.

As previously outlined the functionality of an mGHG motif in directing DROSHA cleavage of pri-miRNA is dependent on its sequence composition and resultant association with the DROSHA dsRBD domain. Previous research by Kwon et al., 2019 has created an index of mGHG motifs and their experimentally derived processing scores in human pri-miRNA ¹⁴². Following from examining the abundance of solely “functional” mGHG motifs, which surpass the score threshold of 38, I next examined whether a correlation exists between miRNA regulation by TN-C and mGHG functionality.

Using the downregulated and control miRNA groups outlined previously the composition of each basal and apical mGHG motif were analysed, with an mGHG score derived for each sequence using the Kwon et al., 2019 index (Figure 5.4.3). A total mGHG score was derived by subtracting the apical mGHG score, with these motifs known to negatively contribute to pri-miRNA cleavage, from the basal mGHG score, these motifs being associated with increase cleavage fidelity.

The basal mGHG, apical mGHG and total mGHG score of the two miRNA groups were compared, finding no significant difference in score amongst them (Figure 5.4.3a/c/e). Likewise simple linear regression analysis comparing

each mGHG score to miRNA log fold change with TNC KO found no significant association (Figure 5.4.3b/d/f).

Overall, this analysis showed the regulation of miRNA by TN-C to not be associated with the presence or functionality of the mGHG motif.

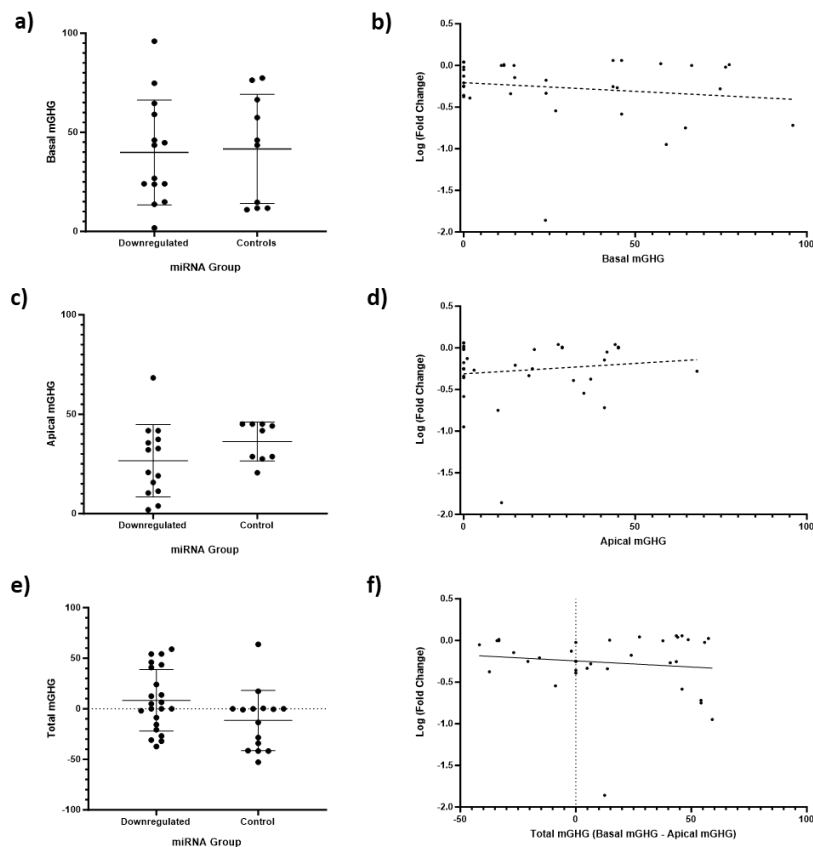


Figure 5.4.3. mGHG motif does not have a significant impact on miRNA regulation by TNC.

Total RNA was extracted from wild-type and TNC KO BMDM cells stimulated with 100ng/mL LPS for 4 hours (n=3). Small RNA-SEQ and subsequent differential expression analysis were performed by Novogene. miRNAs were grouped based upon the effect of TNC knockout on their expression in 4h LPS induced samples into downregulated (% read count change= \leq -5%, read count change= \leq -3000, n=22) and control (% read count change=-5%-5%, read count change=-100-+100, n=14) groups. a) The presence of a basal mGHG motif at 5'-7 to -5 and 3' -

5 to -3 was determined for miRNAs in each group. Unaligned sequence and the presence of a bulge or pseudo-knot disqualified the motif. mGHG motif score derived from the average processing impact of human mGHG motifs were used in analysis (Kwon et al., 2019). The score of these motifs was compared between group \pm SD. Kruskal wallis; $p > 0.05$, ns. b) The basal mGHG score was compared to the fold change of miRNAs from all the groups caused by TNC knockout. Simple linear regression; $R^2 = 0.029$, $p > 0.05$, ns. c) The score of an apical mGHG motif -7 from the apical loop was determined for miRNAs in each group with the mGHG score derived as above. The score of these motifs was compared between groups \pm SD, Kruskal wallis; $p > 0.05$, ns. The apical mGHG score was compared to the fold change of miRNAs from all the groups caused by TNC knockout. Simple linear regression; $R^2 = 0.015$, $p > 0.05$, ns. e) The combined score of the basal mGHG motif minus the apical mGHG motif was determined for miRNAs in each group. The total score of these motifs was compared between groups \pm SD, Kruskal wallis; $p > 0.05$, ns. f) The total mGHG score was compared to the fold change of miRNAs from all the groups caused by TNC knockout. Simple linear regression; $R^2 = 0.029$, $p > 0.05$, ns.

5.4.4 – Neither apical loop size nor stem binding energy correlate with miRNA regulation by TNC knockout.

Previous analysis failed to implicate lower stem stability in potentially being linked to pri-miRNA regulation by TNC KO (Figure 5.4.2b). However, the method used to analyse this stability was binary, with a threshold of 4 mismatched nucleotides classifying a stem as “unstable”, which does not take into account the thermodynamic properties imparted by different nucleotide compositions and secondary structures^{109,112,113,617}. In addition, apical loop size has also been associated with reduced miRNA enrichment within literature sources, thought to be due to a smaller loop impeding DGCR8 association¹⁴⁷. Through examination of apical loop size and more detailed

scrutiny of lower stem stability in pri-miRNAs downregulated by TNC KO, I further examined the role of structural cis-acting regulators in TN-Cs regulation of pri-miRNAs.

The secondary structure of pri-miRNAs within the miR-155-5p calibrated dataset downregulated by TNC KO was determined using mxfold and pseudo-viewer packages^{515,619}. The prior utilises deep learning technology to provide a more accurate structure than other packages, while the later specifically identifies pseudo-knot structures occurring in some pri-miRNAs. RNA co-fold was used to calculate the free energy of binding for each pri-miRNA lower stem region with both this and the number of nucleotides in each apical loop plotted against miRNA log fold change in expression (Figure 5.4.4)⁶¹⁹.

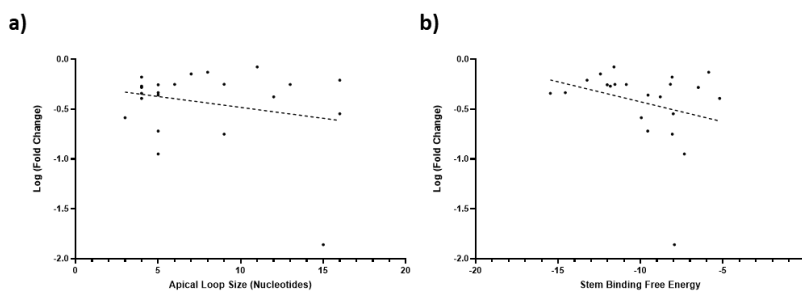


Figure 5.4.4. Neither apical loop size nor stem binding energy correlate with miRNA

regulation by TNC KO. Total RNA was extracted from wild-type and TNC KO BMDM cells stimulated with 100ng/mL LPS for 4 hours (n=3). Small RNA-SEQ and subsequent differential expression analysis was performed by Novogene. miR-155-5p derived miRNA downregulated by TNC KO were used for analysis. Pri-miRNA structure was determined using mxfold and pseudo-viewer packages. a) The number of nucleotides in the apical loop of each miRNA were counted with this plotted against the miRNAs TNC KO induced fold change. b) The free energy of binding of each pri-miRNA lower stem was determined by inputting the 5' -1 to -13

sequence and its binding partner into RNA co-fold. Significance of correlation was determined using Simple Linear Regression; $p > 0.05$.

No significant correlation was found to occur between TNC KO induced pri-miRNA downregulation and either apical loop size or stem binding free energy (Figure 5.4.4a/b). The downregulated miRNA were found to feature a range of loop sizes, ranging from 3 to 17nt, with the majority comprising of <7nts (Figure 5.4.4b). Although not significant there does appear to be a mild correlation between stem binding free energy and miRNA downregulation by TNC KO, with free binding energy reducing with reducing miRNA expression.

Although not showing significant correlations, these findings do conform to trends seen in the literature. The abundance of apical loops <7nts in our downregulated dataset corresponds to the finding of Roden *et al.*, 2017 that apical loops <7nts show reduced enrichment (Figure 5.4.4b)¹⁴⁷. Likewise reduced stem-binding free energy in our dataset aligns with reduced miRNA expression, possibly representing a decline in DROSHA association with the pri-miRNA (Figure 5.4.4a). However, neither structural element's impact on pri-miRNA processing appears to be affected by TNC knockout.

5.4.5 – Pri-miRNA processing score is significantly higher in miRNAs downregulated by TNC knockout.

When examining cis-acting pri-miRNA features it is important to note that each features impact upon pri-miRNA processing is known to be dependent on multiple contextual factors including the presence of other features. For instance, the presence of a stable stem region or a basal UG and one other

feature has been found to be sufficient to enhance effective pri-miRNA processing¹⁵³. Thus, in addition to these features presence in pri-miRNAs it is also of interest to assess the impact the combination of features may have on processing and whether there exists a link between pri-miRNA processing efficiency and regulation by TN-C.

In order to quantify the processing efficiency imparted by the various combinations of features found within the pri-miRNA dataset a “processing score” was calculated (Figure 5.4.5). This score was derived from literature sources including a large-scale *in vitro* processing experiment of all described *cis*-regulatory elements except apical mGHG and apical loop size¹⁵³. This experiment outlines that the incorporation of a stable lower strand together with a basal UG motif had the greatest impact on processing, followed by an apical UGUG and a functional mGHG motif. This led to a +2 score being given for UG or a stable lower strand in our analysis, while a +1 was given for UGUG or mGHG elements. Finally a -1 was given if an apical mGHG was present, this motif being associated with reduced productive processing¹⁴⁹.

The processing score for each pri-miRNA in the respective downregulated or control datasets were calculated. In addition, correlation analysis was performed on the downregulated group to identify whether a link exists between features associated with processing efficiency and downregulated in TNC KO (Figure 5.4.5a/b/c)). Finally, pri-miRNAs upregulated or unchanged (control) in the wild-type untreated vs wild-type 4h LPS treatment differential

expression dataset was examined to identify whether processing score is linked to miRNA induction outside of TNC KO (Figure 5.4.5d).

a)

Feature	Impact on processing	Processing Score
BasalUG	↑↑	+2
ApicalUGUG	↑	+1
Basal mGHG	↑	+1
Apical mGHG	↓	-0.5
Stable lower stem	↑↑	+2

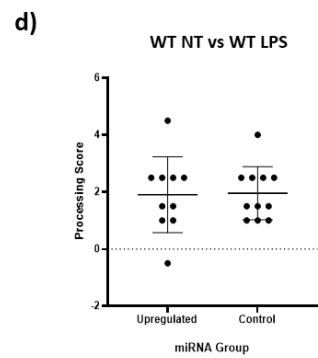
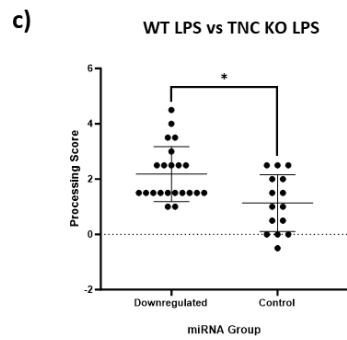
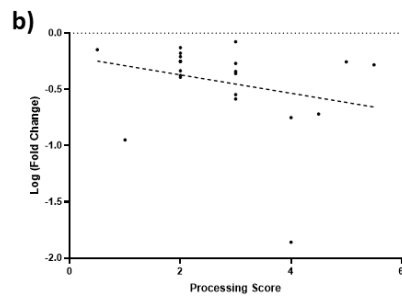


Figure 5.4.5. pri-miRNA processing score is significantly higher in miRNA downregulated by TNC knockout. Total RNA was extracted from wild-type and TNC KO BMDM cells unstimulated or stimulated with 100ng/mL LPS for 4 hours (n=3). Small RNA-SEQ and subsequent

differential expression analysis was performed by Novogene. a) Literature analysis was performed to identify the relative impact of each cis-regulatory element on pri-miRNA processing and a “processing score” was derived¹⁵³. b) The processing score of miR-155-5p derived miRNAs downregulated by TNC KO were calculated and plotted against their log fold change, Simple Linear Regression; $R^2=0.07$, $p>0.05$, ns. c) miRNAs were grouped based upon the effect of TNC knockout on their expression in 4h LPS induced samples into downregulated (% read count change= $<-5\%$, read count change= <-3000 , $n=22$) and control (% read count change= $-5\%-5\%$, read count change= $-100-+100$, $n=14$) groups. The processing score for each miRNA was determined and compared between groups, \pm SD. Kruskal-Wallis; $p<0.05$, *. d) miRNAs significantly upregulated in 4h LPS treated samples relative to wild-type samples had their processing score compared to a control miRNA group (% read count change= $-5\%-5\%$, read count change= $-100-+100$, $n=11$) \pm SD. Mann Whitney U; $p>0.05$.

No significant association was identified by simple linear regression analysis between the log fold change in pri-miRNA downregulated by TNC KO and their processing scores ($p = > 0.05$), although a degree of negative association is shown to occur (Figure 5.4.5b). Downregulated pri-miRNAs show a significantly greater mean processing score of 2.18 compared to the control groups 1.13 ($p = > 0.05$) (Figure 5.4.5c). No significant difference is found to occur in processing score between the control and pri-miRNAs upregulated by LPS induction in wild-type cells with the control having a mean processing score of 1.95 compared to the score of 1.90 for the upregulated group (Figure 5.4.5d).

Combining these results creates an intriguing picture of the relationship between cis-acting feature linked processing and regulation by TNC KO.

Downregulation by TNC KO shows an association with increased pri-miRNA

processing score (Figure 5.4.5c). This is potentially linked to our sampling criteria, which selects miRNA with a high read count change, <-3000 , thus selecting miRNAs whose pri-miRNA are highly expressed, likely due to efficient processing. However, the LPS treated wild-type sample, which does not show an association between processing score and upregulation, shows a higher average control group score than the TNC KO sample, even though both groups were selected by the same criteria (Figure 5.4.5d). This provides evidence for TNC KO preferentially regulating miRNAs with a higher processing score. Higher processing score is linked to the presence of a basal UG or stable lower stem, thus this implicates modifications to DROSHA pri-miRNA binding in TN-Cs mechanism of miRNA regulation.

5.4.0 - Discussion

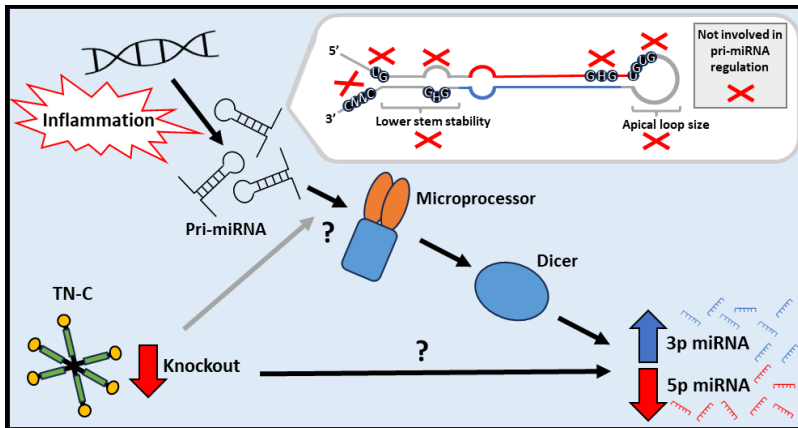


Figure 5.4.1. Chapter six conclusions and further questions. Although no relationship was identified between pri-miRNA elements and their miRNAs regulation by TN-C, evidence for a novel mechanism of TNC-dependent miRNA arm-switching has been identified. Grey arrows represent potential pathways established outside of this thesis. Question marks note pathways in which future investigation is required.

The macrophage inflammatory cascade has been extensively studied, with RNA-seq analysis providing an ideal means of mapping these dynamic networks and being utilised to great effect to examine the expression characteristics of macrophages in a range of inflammatory contexts. Thus, our examination of the expression of miRNA during the early acute-inflammatory response to LPS aimed to provide additional depth to this understanding, with no previous examination of miRNA having been conducted utilising this inflammatory induction methodology.

RNA-seq analysis of whole RNA extracts from 4h LPS treated BMDMs identified eleven significantly upregulated (miR-155-3p, miR-155-5p, miR-147-

3p, miR-147-5p, miR-146b-3p, miR-199a-5p, miR-221-5p, miR-1945, miR-455-5p, miR-21a-3p and miR-222-3p) and two downregulated (miR-339-3p and miR-30c-1-3p) mature miRNAs. The regulation of a number of these miRNAs, including the miR-155 and miR-147 strands, are in accord with a previous RNA-seq analysis wherein Lu *et al.*, 2016 examined BMDMs polarised using dual treatment with 4hs LPS and IFN- γ ⁶⁰⁹. IFN- γ acts as an endogenous signal molecule of the JAK/STAT pathway, sensitizing macrophages to further enhance their inflammatory induction upon exposure to pathogen products, such as LPS's activation of the TLR4 pathway ⁶²⁰. However, our detection of significant changes in miR-21a-3p, miR-1945, miR-222-3p, miR-339-3p and miR-30c-1-3p are not found in this previous work, potentially illustrating miRNA regulation unique to macrophages induced solely by LPS. LPS stimulation of BMDMs without IFN- γ priming has been linked to activation of a unique subset of TFs and transcriptional co-factors not found in IFN- γ primed BMDMs, which may account for our uniquely regulated miRNA ⁶²⁰. For example, DDX5, a known promoter of miR-21 expression within breast cancer cell lines, is upregulated only in solely 4h LPS induced macrophages ^{620,621}.

RNA-seq analysis of TNC knockout BMDMs stimulated with LPS for 4h was conducted, showing a significant downregulation in the expression of miR-30a-5p, miR-30a-3p and miR-30c-2-3p. miR-30a-5p has been shown to exhibit both pro- and anti-inflammatory effects within macrophage cells through inhibition of STAT1 and SOCS3 mRNA translation, respectively ^{622,623}. Multiple post-transcriptional mechanisms of miR-30a-5p regulation have been described. This includes the impairment of microprocessor association via

ADAR1 mediated A-to-I editing of pri-miR-30a in macrophage cells and miRNA sponging by the lncRNA HCG18, LINC00461, KCNQIOT1 and TSIX in osteoarthritis, osteoporosis, colorectal cancer and osteolysis respectively⁶²⁴⁻⁶²⁸. Meanwhile, miR-30a-3p, as the lower expressed strand of miR-30a, is minimally studied in the macrophage, with miR-30a-3p-expressing head-and-neck small cell carcinoma secretomes being shown to induce a pro-inflammatory phenotype in tumour-associated macrophages, presumably through their known inhibition of TGF- β signalling⁶²⁹. Finally, miR-30c-2-3p has been identified as a negative regulator of NF- κ B signalling through direct targeting of the TNFR/NF- κ B adaptor protein tumour necrosis factor receptor type 1-associated DEATH domain protein (TRADD) in breast cancer⁶³⁰.

Intriguingly, miR-30a-5p and miR-30c-2-3p also exhibit significant downregulation due to TNC knockout in non-LPS induced BMDMs, while miR-30a-3p shows significant downregulation in TNC knockout human fibroblasts (unpublished data). This implicates a potential conserved mechanism whereby TN-C promotes miRNA expression independent of inflammatory pathways. Examination of the TransmiR database identifies serum-response-factor (SRF) as one of the TFs predicted to regulate these two miRNA transcripts. Through its known regulation of the actin cytoskeleton, TN-C may in turn modulate Megakaryoblastic leukemia-1/2 (MAL1/2), the dissociation of which from G-actin leads to transactivation of SRF-dependent genes^{311,631,632}.

Although a novel finding, the regulation of miR-30 family members alone provides little insight into the potential post-transcriptional regulation of miR-

155 by TN-C. As such, direct examination of miR-155 and similarly regulated miRNAs was necessary in order to isolate shared features which contribute to their regulation by TN-C.

Piccinini and Zordan previously verified the regulation of miR-155-5p by TN-C in BMDMs using both qPCR and northern blot analysis, with previous work herein refuting this activity within RAW 246.7 cells (Section 3.3.0), this contrasting previous evidence^{289,511}. Corroborating results from RAW 246.7 cells, this RNA-seq analysis did not identify miR-155-5p as differentially expressed when comparing TNC knockout and wild-type BMDMs treated with LPS for 4h. This may illustrate the importance of LPS stimulation timing in observing maximal miR-155-5p downregulation as a result of TN-C ablation. The 4h timepoint for LPS treatment was selected in order to best observe the potential regulation of miR-155 resulting from changes to its microprocessor binding seen in our RIP analysis using 2h LPS treated RAW246.7 cells. Both Zordan and Piccinini identified a significant reduction in miR-155 expression by qPCR with 24h LPS treatment, with Piccinini also seeing a significant reduction at 8h^{289,511}. Within both experiments 4h LPS treatment did not elicit a significant reduction in miR-155-5p expression in TNC KO BMDMs. The lack of significance at 4h is potentially due to TN-Cs regulation of miR-155 relying upon an inflammatory factor which is only induced later in the inflammatory cascade. In order to fully clarify miR-155s regulation by TN-C via RNA-seq at the 4h LPS timepoint changes may be made to our methodology. For example, increasing the number of BMDM replicates would reduce the high variability of our data likely caused by the differing inflammatory dynamics of BMDMs

differentiated from mouse-isolated stem-cells which, although being of the same genotype, exhibit differing inflammatory competencies. Additionally, examination of the 8h LPS timepoint in TNC knockout BMDMs via RNA-SEQ would better aid examination of miRNAs besides miR-155-5p at a point in inflammatory induction where TN-C has an already validated impact on miRNA expression.

In order to examine the similarities between miRNAs regulated by TN-C in 4h LPS stimulated BMDMs, the expression profile of miR-155-5p was used to generate a pool of miRNAs potentially being regulated by TN-C. Amongst others this pool included miR-30a-5p, miR-125a-5p, miR-21a-5p, let-7c-5p, miR-125b-5p, let-7i-5p, miR-146a-5p, let-7g-5p and miR-155-5p, all of which were previously identified as being significantly regulated by TN-C within microarray analysis of TNC KO BMDMs stimulated with 8h LPS ²⁸⁹. Notably, follow-up qPCR analysis of miR-21a-5p and miR-146a-5p by Piccinini and Midwood 2012 found a non-significant reduction in the miRNAs expression at both 4 and 8h of LPS stimulation in wild-type and TNC knockout BMDMs ²⁸⁹. This indicates that the impact of TN-C on miRNA expression is subtle, potentially with low biological relevancy in miRNAs with a modest inflammatory induction, such as miR-146a (~1.75 fold) and miR-21a (~1 fold) with 8h LPS treatment, but a notable impact in highly induced miRNA such as miR-155-5p (~30 fold) ²⁸⁹.

In order to ascertain the method by-which TN-C potentially regulates miRNA, a novel analysis of miRNAs 5p and 3p strand abundance was conducted. This

identified for the first time that significantly more 5p miRNA are downregulated than upregulated by TNC KO LPS treated BMDMs compared to wild-type LPS treated BMDMs, with the inverse being true for 3p miRNAs. Follow-up examination sought to identify whether this regulation of the 5p and 3p strands occurred via a process of arm-switching, with the downregulation of 5p and upregulation of 3p miRNAs taking place for both strands of the same miRNA. Examining miRNAs whose strands were differently regulated found the majority of such 5p miRNAs to be downregulated and the majority of 3p miRNAs to be upregulated by TNC KO in LPS treated BMDMs. Intriguingly, this regulatory pattern is not apparent in non-LPS treated TNC knockout samples and wild-type LPS treated samples show 3p arm-switched miRNA to be significantly associated with downregulation, rather than upregulation. This evidence implicates TN-C in the LPS dependent regulation of miRNA strand selection, although multiple questions remain as to how this mechanism may occur.

Only a single-strand of each double-stranded mature miRNA molecule is incorporated into the RISC complex, giving rise to distinct targeting dependent on the incorporated miRNAs seed sequence. This process of strand selection is dependent on the incorporation of the miRNA strands 5' end into the binding pocket of the Ago protein, located at the interface between the PIWI and MID (middle) domains, with the 3' end incorporating into a hydrophobic cavity within the PAZ domain¹⁰⁵⁻¹¹¹. Two criteria are thought to determine which of the two miRNA strands are incorporated. Firstly, Ago shows an incorporation preference for the 5' end with the lowest internal stability,

likely due to the increased access this gives to the MID/PAZ binding pocket ¹¹²⁻
¹¹⁴. Secondly, within human Ago a preference exists for incorporation of 5'
terminal uridine monophosphate (UMP) and adenosine monophosphate
(AMP), with evidence showing that 5' terminal cytidine and guanosine
monophosphate sterically clash with a nucleotide specificity loop found within
the MID domain, this leading to reduced incorporation ^{106,107,114}. These
characteristics result in one miRNA strand showing consistent higher
expression, and thus activity within the cell. However, multiple mechanism of
arm-switching have been observed, whereby a regulatory event leads to a
dynamic increase in the incorporation of the typically non-dominant strand
and a decrease in incorporation of the typically dominant strand. Our
evidence suggests that a large-scale example of such an event may be
occurring with TNC KO within LPS stimulated BMDMs. Intriguingly, we also
identified a significant abundance of downregulated 5p miRNA whose 3p
strand showed no change in expression. This potentially implies a concerted
mechanism that downregulates 5p miRNA expression, irrespective of whether
an arm-switching event may arise.

RNA-remodelling factors have been shown to act upon the exposed 5' and 3'
terminal ends of pri-, pre- and mature miRNA leading to changes in terminal
nucleotide identity and thermodynamics which result in modified
incorporation into the RISC. Examples of these include adenosine deaminase
acting on RNA (ADAR) and 3' terminal uridyl transferase 4-7 (TUT4-7), which
regulate miRNA strand selection through adenosine to inosine deamination of
nucleotides within pri- and pre-miRNA and 3' uridylation of pre-miRNA,

respectively ^{130,613,624,633,634}. Such changes, as is the case for TUT4-7, can in turn influence cleavage by Dicer, allowing modifications to the exposed termini of pre-miRNA to modify the upstream cut site and new miRNA end characteristics ¹³⁵. However, examination of miRNA isomerism occurrence through alignment of unannotated sRNA reads with mature miRNA sequences from miRbase 22.1 found no significant change in the percentage of miRNA nucleotide isomerism between TNC KO and wild-type BMDMs treated with LPS. Additionally, no significant change in isomerism of our key candidate miR-155-5p was identified via detailed analysis of nucleotide identity. Although such examination of miR-155-3p found a significant upregulation in isomerism events with TNC KO, due to these new events occurring in <0.5% of strands and no specific nucleotide seen to be targeted this can be assumed to be an artifact of increased expression. Future expansion of this more detailed analysis to the entire miRNA dataset would aid implication of specific mechanisms of miRNA nucleotide isomerism due to the characteristic nucleotide changes they elicit.

The second such mechanism for altered strand selection involves modifications to microprocessor or Dicer mediated cleavage of the miRNA precursors, leading to alternate cut sites and resultant changes to miRNA terminal identity and thermodynamics. These events may be instigated via changes in the association of biogenesis co-factors, such as the Dicer associated factor TRBP and the Drosha associated co-factors DGCR8, DDX5/17 and SRF3 ^{145,153,635–639}. Analysis of pri-miRNA cis-regulatory elements was conducted to identify whether TNC KO regulated miRNA are associated with

specific regulatory features. No significant association was found between miRNA downregulated by TNC KO and the presence of the CNNC motif, responsible for SRF3 binding, the presence of the apical UGU motif and apical-loop size, which facilitate DGCR8 association, nor the presence of a basal UG, the presence or strength of the mGHG motif, or lower stem thermodynamic stability, these being responsible for directing and facilitating accurate Drosha cleavage of the pri-miRNA ^{92,142–145,147,148,258}.

Further analysis examined the potential contribution of each cis-acting pri-miRNA element to a literature based “processing score”, providing a quantitative means of comparing the various cis-acting element combinations found within each TN-C regulated miRNA. This identified a significant increase in processing score in miRNAs downregulated by TNC KO compared to unaffected control miRNAs with such a relationship not being found in miRNA upregulated by LPS treatment in wild-type cells. These results are intriguing, inferring that the regulation of miRNA by TN-C may, rather than being reliant on specific cis-acting elements, instead represent a less targeted mechanism of regulation in which we see the greatest impact on more efficiently processed, and thus more expressed miRNAs, such as miR-155.

Vitaly, our analysis did not examine every cis-acting pri-miRNA element. For example, the presence or absence of upper-stem mismatches and bulge regions has been shown to modulate pri-miRNA and pre-miRNA processing ¹⁵². Additionally, examination was focused upon elements that regulate at the microprocessor and not downstream of the miRNA biogenesis pathway such

as the Dicer or RISC incorporation. This is due to past research showing no change in pri-miR-155 expression with TNC KO, while downregulation in pre- and mature miR-155 were evident, thus implicating regulation at the microprocessor⁵¹¹.

As the downregulation of 5p miRNAs by TNC KO in LPS treated BMDMs does not coincide with an increase in miRNA isoforms, nor an association with any co-factor specific pri-miRNA elements, it is potentially the case that TNC KO influences strand selection through changes to the RISC complex itself. Heat-shock cognate of 71kDa (Hsc-70) and Heat-shock protein of 90kDa (Hsp-90) act as RISC chaperones, promoting conformational changes to Ago that facilitate loading of the miRNA duplex⁶⁴⁰⁻⁶⁴². Within drosophila, protein containing two dsRNA binding domains associated with Dcr-2 (R2D2) and Dcr-2 showed potential binding to the siRNA end with the highest stability, thus presenting the less stable end to Ago2⁶⁴³. A similar activity was also described for the argonaut co-factor TAR RNA-binding protein (TRBP) and protein activator of interferon-induced protein kinase (PACT) leading to the PAZ domain of Argonaute binding the less stable miRNA end^{637,644}. Although both of these functions are contested, knockdown analysis of both R2D2 and PAZ having no impact on miRNA loading or strand selection, there remains the potential for strand selection to be regulated through competitive binding of the stable miRNA end by accessory proteins^{114,116,645}. Although yet to be demonstrated directly, phosphorylation within the 5' nucleotide binding pocket of Argonaute is thought to impact its ability to bind several miRNA strands. Thus, there is a potential that post-transcriptional modification of

Argonaute by TN-C could influence strand selection⁶⁴⁶. However, the manner in which this could occur that would lead to a downregulation in the 5p strand of multiple miRNAs with dissimilar 5' termini compositions, remains to be determined.

Through RNA-SEQ analysis of TNC KO BMDMs we have made further steps in the identification of the mechanism by-which TN-C regulates miR-155. No significant association has been identified between miRNAs potentially regulated by TN-C and their pri-miRNA cis-regulatory features. This combines with a significant association between miRNAs downregulated by TNC KO and increased predicted processing efficiency to move focus away from events at the microprocessor, implicating increased expression as a targeting factor for TN-C regulation rather than the presence of shared structural features. We have also identified a potentially novel role for TN-C in the post-transcriptional regulation of miRNA strand selection within LPS stimulated BMDMs. Further RNA-SEQ examination utilising additional biological replicates will be necessary in order to validate highly variable early inflammatory miRNA expression. Additionally *in vitro* processing assay may be utilised to validate the role of cis-acting elements specifically in miR-155 regulation by TNC and mass spectrometry used to identify changes in microprocessor composition induced by TNC knockout.

Chapter 6

Final Summary

6.0.0 - Overall Discussion

6.1.0 - Summary

Following from previous work by Nicole Zordan and Anna Piccinini, this project aimed to identify by what post-transcriptional mechanism TN-C regulates the expression of the key pro-inflammatory miRNA miR-155 within the macrophage inflammatory response (Figure 6.0.1)⁵¹¹.

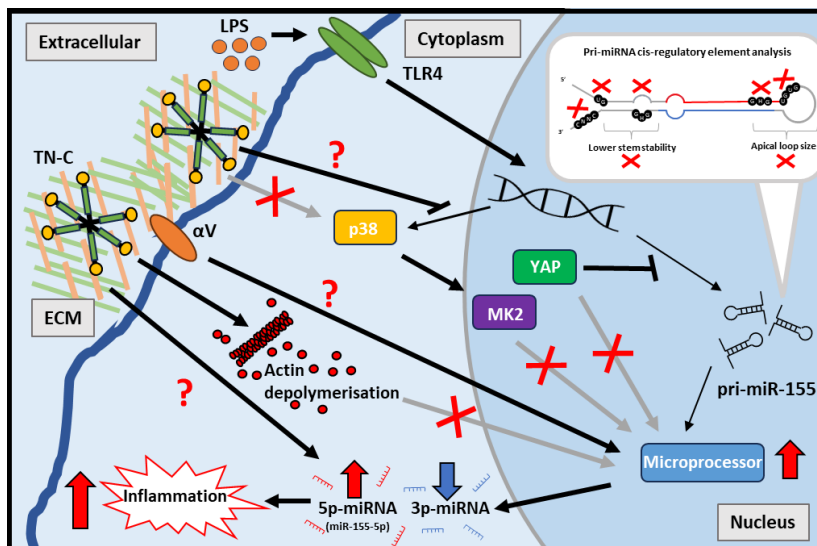


Figure 6.0.1. Graphical summary. Depicted are the multiple pathway components investigated throughout this project in RAW 246.7 macrophages and BMDMs. Grey lines featuring red crosses were experimentally invalidated pathways. Lines featuring red question marks are prospective pathways and require further validation. Blunt arrow heads represent an inhibitory pathway.

In RAW 246.7 macrophage-like cells the knockdown of TNC expression was found to associate with an increase in actin polymerization and stress fiber formation. This role of TN-C is widely reported in non-macrophage cell lines,

occurring via association of TN-C with integrins such as $\alpha 9\beta 1$ and $\alpha 5\beta 1$, and presents a means whereby TN-C has been shown to perform intracellular signaling such as via the transcriptional co-factor YAP³¹¹. Screening of potential TN-C associated integrins found knockdown of the ITGAV gene, encoding the αV integrin subunit, to elicit a downregulation in mature miR-155 expression, but not in that of pri-miR-155. This post-transcriptional mode of regulation is similar to that witnessed as a result of TN-C knockdown in BMDMs, indicating that αV integrin may form part of the TNC-miR-155 axis, potentially through a downstream signal instigated by cytoskeletal modulation.

However, the treatment of RAW 246.7 cells with actin cytoskeletal modulators, intended to mimic the cytoskeletal re-organization caused by TN-C, failed to elicit a change in miR-155 expression. This implies that although potentially integrin-associated, the modulation of miR-155 by TN-C is likely not facilitated by cytoskeletal modulation, this being further corroborated by the invalidation of the actin signal transducer YAP's role in the macrophage TNC-miR155 pathway.

The hippo pathway component YAP has recently emerged as a key regulator of macrophage pro-inflammatory induction, being implicated in the antiviral response, regulation of reactive oxygen species and TLR4 driven bacterial inflammation^{394–398}. Additionally, outside of the macrophage, YAPs activity has been shown to be inhibited by TN-Cs depolymerization of the actin cytoskeleton leading to the phosphorylation and resultant cytoplasmic

sequestration of YAP away from its nuclear targets³¹¹. One such target of YAP within the nucleus is the microprocessor associated protein p72, with YAPs association with p72 causing a downregulation in pri-miRNA processing⁹². Therefore, YAP was selected as a primary candidate, being a potential regulator of miR-155 biogenesis downstream of TN-C.

However, it can be concluded that YAP is not responsible for the downregulation of miR-155 biogenesis witnessed as a result of TN-C knockdown in RAW 246.7 cells. Ectopic expression of YAP, although eliciting a significant upregulation in miR-155 expression, also led to upregulated pri-miR-155 expression, this corresponding to a transcriptional mode of regulation rather than the post-transcriptional mechanism attributed to the regulation of miR-155 in TN-C knockout cells. This finding was further corroborated by examination of p65 localization in YAP overexpressing cells, which identified a potential decrease in nuclear localized p65 within 1-hour LPS stimulation in cells overexpressing YAP. As the NF- κ B component p65 is a key transcription factor responsible for the TLR4-dependent induction of miR-155 expression, it is likely that through reduced nuclear localization of p65 YAP may regulate miR-155 transcription²⁴¹. Finally, YAP proved to be of exceedingly low expression in RAW 246.7 cells, with immunoblotting analysis failing to detect YAP protein and qPCR only able to detect YAP mRNA close to the assay's threshold. Such low abundance of YAP is noted in published analyses of the protein in macrophages, with these primarily conducted in BMDMs which our own analysis show to have a greater degree of YAP mRNA expression than RAW 246.7 cells^{393,400,404,560,561}. Furthermore the lack of

capacity of RAW 246.7 cells to demonstrate the TNC-miR-155 mechanism may be in part determined by the low abundance of YAP within this cell line.

Multiple studies show TN-C to phosphorylate p38 α , this inflammatory kinase itself responsible for the regulation of miRNA biogenesis components such as Drosha and Ago^{491,492,494,502,503,509,510}. Additionally, through activation of the master regulator of RNA-binding proteins, MK2, the p38/MK2 pathway may directly regulate p68 and p72, two components of the microprocessor, in addition to as of yet unidentified miR-155 targeting RBPs⁵⁰⁵. Therefore, the impact of TN-C knockdown upon the phosphorylation state and localization of p38 α and MK2 was assessed.

Intriguingly, knockdown of TN-C in RAW 246.7 cells, both unstimulated or stimulated with LPS, did not elicit a visible change in p38 α phosphorylation, as was reported previously within breast cancer, macrophage inflammation and multiple models of subarachnoid hemorrhage, nor was there a consistent phosphorylation of MK2 or change in localization of either protein^{302,495,597}. Instead, total protein abundance of both p38 α and MK2 was consistently seen to increase in TNC knockdown unstimulated RAW 246.7 cells. Examination of RNA-SEQ data, derived from TNC WT and TNC KO resting BMDMs, found TNC KO to significantly increase p38 α mRNA expression compared to TNC WT. It is hypothesized that the resultant increase in p38 α protein abundance may in turn facilitate stabilization of the MK2 protein, as the p38 α -MK2 complex has been observed to protect MK2 from proteasomal degradation⁴³⁵. TN-C knockdown/knockout enhancing the expression of the pro-inflammatory

pathway component p38 α within resting macrophages is unexpected, with TN-C knockout macrophages generally showing reduced pro-inflammatory cytokine release upon LPS stimulation, while treatment with exogenous TN-C promotes inflammation through the activity of the NF- κ B, JNK and p38 α pathways^{32,302,521,598}.

It is questionable whether the increased p38 α /MK2 abundance elicited by TN-C knockdown could mediate miR-155 biogenesis without activation of either kinase being evident. The knockdown of MK2 showed no change in pri-miR-155 or mature miR-155 expression, making it unlikely that MK2 plays a role within the TNC-miR-155 axis, while further validation of the relationship between TN-C and p38 α , as outlined below, is necessary to confirm its potential for mediating miR-155 biogenesis.

Through RNA-immunoprecipitation the abundance of pri-miR-155 associated with the microprocessor component Drosha was found to be potentially reduced in TNC knockout RAW 246.7 cells. This led to an investigation into BMDM miRNAs similarly regulated by TNC knockout as miR-155 and whether any pri-miRNA cis-regulatory elements were associated with regulation by TNC, as these could facilitate regulation at the microprocessor¹⁵³.

No pri-miRNA cis-regulatory element was significantly associated with miRNAs downregulated by TN-C knockout, while analysis of two candidate pri-miRNA binding RBPs, HNRNPF and MBNL1 found the expression of neither to be significantly changed in TNC knockout RAW 246.7 cells. This analysis, coupled with the non-significance of the change in pri-miR-155 association found in

the RIP assay, likely due to an insignificant degree of TN-C knockdown, merits further investigation of the microprocessor as the location at which TNC knockdown mediates miR-155 abundance.

Intriguingly, examination of RNA-SEQ data in TNC KO BMDMs identified a significant reduction in the abundance of 5p strand miRNAs and an induction in the abundance of 3p strand miRNAs. This phenomenon was only found to occur in LPS-treated cells, and in the majority of cases represents an arm-switching event, whereby the 5p/3p preference of multiple miRNAs switches in order to favor the 3p strand. The mechanism by which this global change in miRNA arm preference could occur has yet to be identified, potentially requiring modification to the pri-/pre-miRNA cleavage by microprocessor or Dicer, leading to changes in miRNA nucleotide end architecture, or the recruitment of Ago associated factors which modulate strand-selection. For example, p38 α has been shown to regulate Ago2 and Drosha localization, the latter by a phosphorylation-dependent mechanism^{509,510}. Therefore, p38 α has the potential to bind and modify their respective functionality, giving rise to a strand bias.

It is possible that the regulation of miR-155 by TN-C is conducted via this arm-switching mechanism, with the explosively upregulated miR-155-5p strand having its expression attenuated as a result of TNC knockdown. Further *in vitro* analysis of miRNA strand abundance in TNC knockdown macrophages is necessary to validate the occurrence of this mechanism.

6.2.0 - Concluding Remarks and Future Investigations

In conclusion, although many questions still remain as to the mechanism by which TN-C may regulate miR-155 processing in macrophages, we have succeeded in identifying multiple features of this pathway which may inform future investigation; notably, the lack of actin cytoskeletal involvement, invalidation of YAP as a pathway component, and identification of p38 α and integrin α V as likely TNC signal transducers. Furthermore, a potential novel mechanism of TN-C-dependent miRNA arm-switching has been identified, presenting an intriguing means by which a regulated component of the ECM may modulate cell-wide inflammatory miRNA biogenesis. Increased expression of miR-155 and TN-C is associated with increased severity of diseases such as pneumonia, tuberculosis, and sepsis, as well being associated with cancers and autoimmune disorders^{32,208,289,647,648}. Therefore, through further clarifying the mechanism by which TN-C regulates miR-155, novel therapeutic targets for treatment of these disorders may be established.

Future investigations may include:

- Further validation of YAP's potential regulation of NF- κ B-dependent miR-155 transcription
 - Treatment of YAP overexpressing RAW246.7 cells with verteporfin, an inhibitor of YAPs nuclear import, would confirm whether YAP influences miR-155 expression from within the cytoplasm or the nucleus.

- Through performing mutagenesis on the potential protein binding domains of YAP within the YAP overexpression plasmid the involvement of direct YAP binding within this YAP-miR-155 pathway can be established. For example, the TRAF6-binding motif within the PDZ domain-binding motif.
- FLAG pulldown of the YAP-FLAG produced from the overexpression plasmid within RAW 246.7 can be used to further confirm which proteins YAP may bind to mediate p65s upregulation of miR-155 expression, such as NF-κB constituents, TAK1, or TRAF6.
- As a low YAP expression cell line, RAW 246.7 cell are not optimal to establish whether the regulation of endogenous YAP leads to changes in miR-155 expression. Therefore, the acquisition of a YAP KO BMDM model is necessary, with repetition of previous experiments within this model providing more biologically relevant insight.
- The continued investigation of TN-Cs proposed regulation of inflammatory miRNA strand-selection in BMDMs.
 - Using qPCR to validate the 5p/3p strand expression of key miRNA seen within the RNA-SEQ analysis, such as miR-155. This examination would be performed within 4h LPS induced TNC KO BMDMs, as well as TNC knockdown RAW246.7 cells, in order to clarify whether the impact of TN-C on arm-switching is BMDM specific.

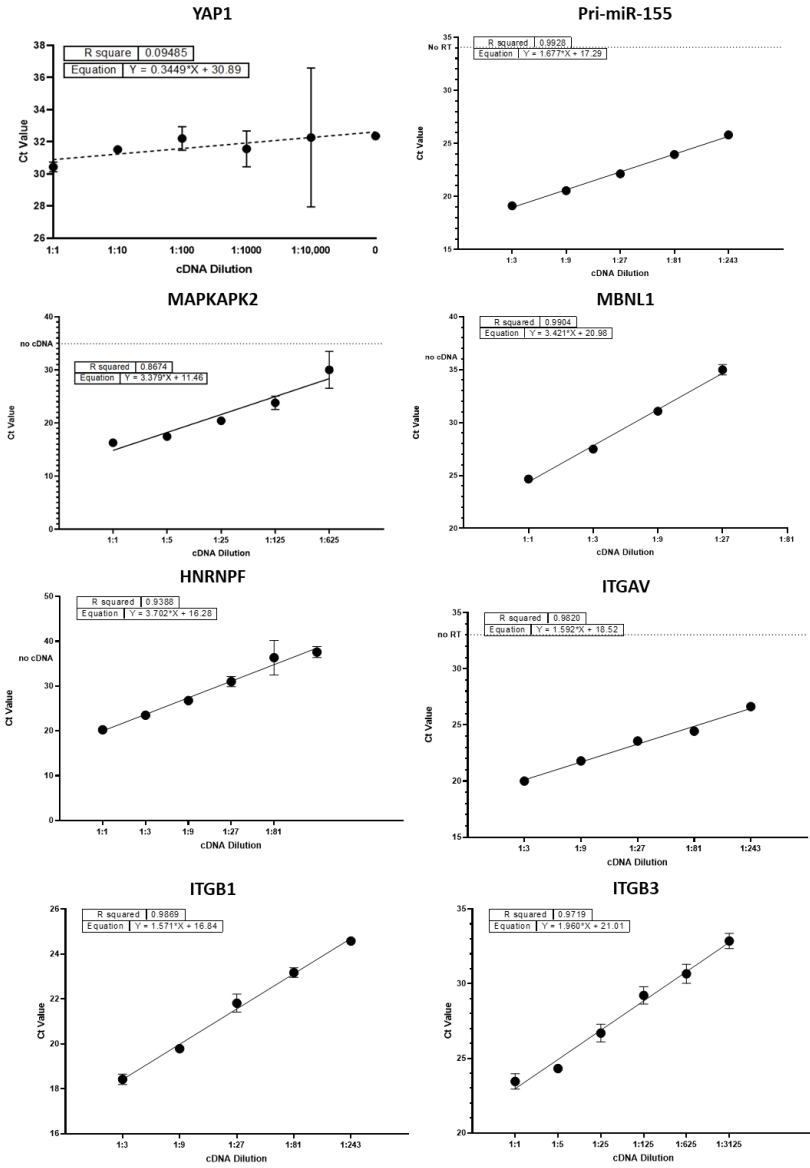
- Further validation using a gain-of-function TN-C model can be performed via the utilization of BMDMs plated on a TNC-supplemented cell-derived matrix.
- Northern blot analysis of the 3p/5p strands of the three highest expressed miRNA identified as undergoing arm-switching in order to identify the generation of isomiRs, with these being compared to a miRNA not seen to be arm-switched.
- Using pre-existing RNA-SEQ data the change in relative 3p/5p arm-abundance of each miRNA between the LPS WT and LPS TNC KO samples can be calculated. This can be combined with the known identities of mature miRNA terminal nucleotides to identify potential correlations between arm-switching occurrence and miRNA end architecture. This would aid identification of RNA modifying events which TNC may facilitate within the miRNA undergoing arm-switching.
 - In order to confirm whether specific pre-miRNA features seen in the RNA-seq analysis may give rise to arm-switching events, an *in Vitro* processing assay may be performed. This would entail the combination of a mutated pre-miRNA sequence, made to contain the identified feature, and recombinant Dicer protein, with northern blotting used to identify successful cleavage

events and whether these are modified by the features occurrence.

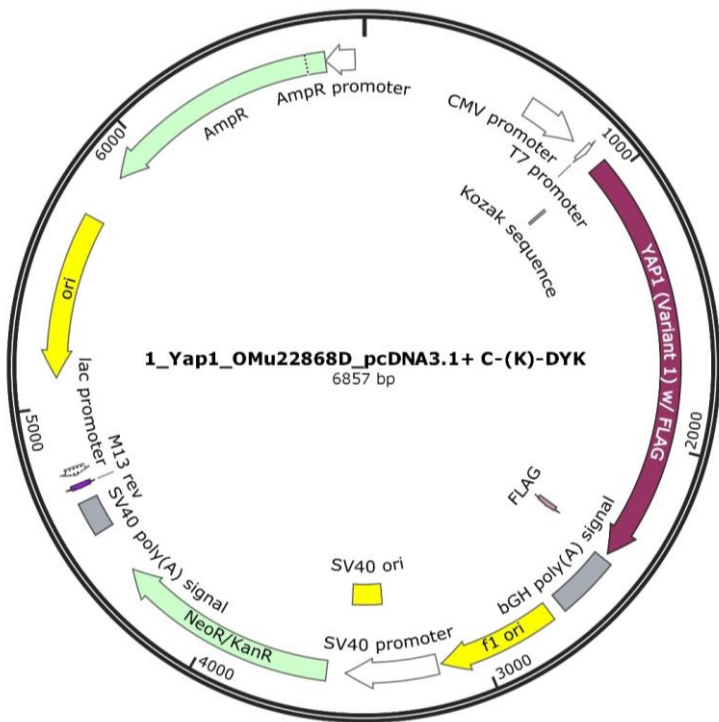
- Identification of changes in microprocessor-associated proteins elicited by TN-C knockdown and potential miR-155 regulating RBPs using an unbiased approach, such as Droscha pull-down in TN-C knockdown macrophages followed by mass spectrometry.

Chapter 7

Supplementary Figures

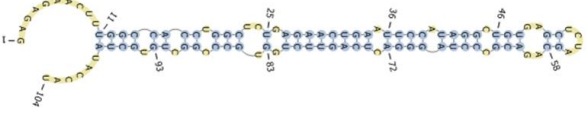
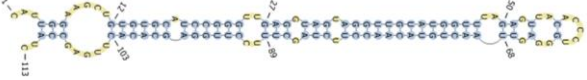
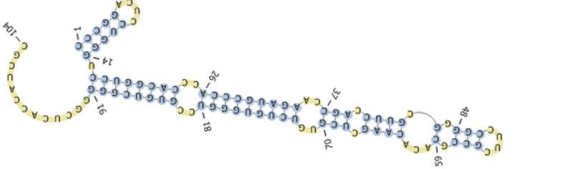
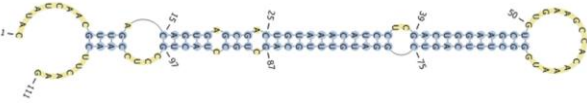


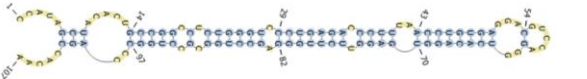

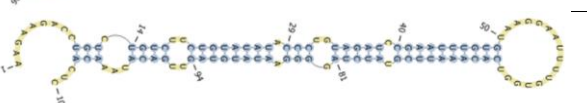
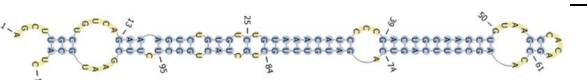




Supplementary Figure 7.1.0. Amplification efficiency of primers. Standard curves were generated for qPCR primers using serial dilutions of cDNA samples.



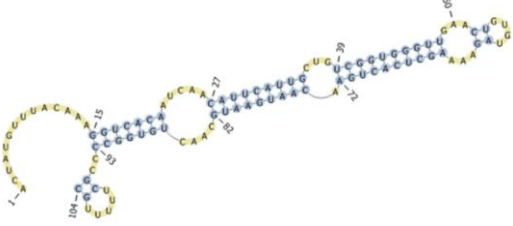
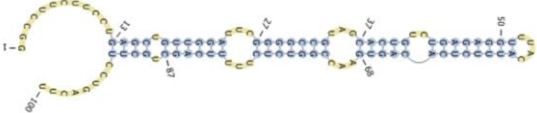
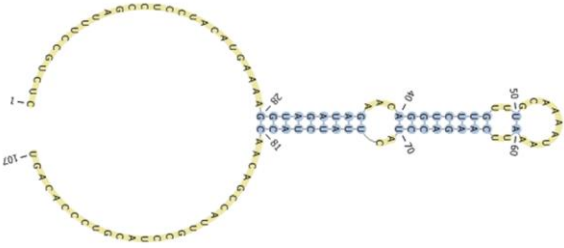
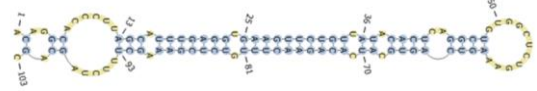
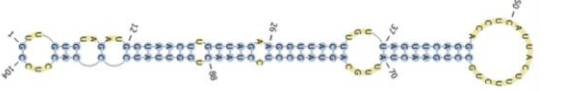

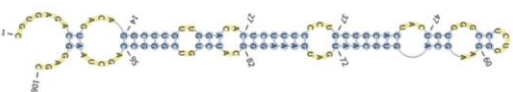
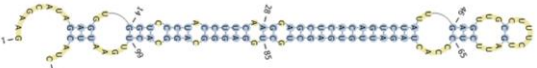
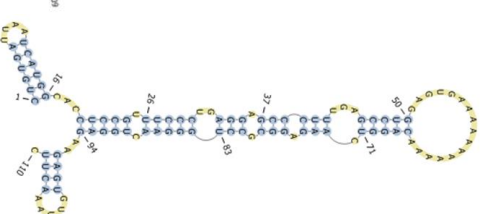
Supplementary Figure 7.2.0. pcDNA3.1(YAP1+FLAG) plasmid diagram.

Pri-miRNA	Structure
miR-155	
miR-191	
miR-222	
Let-7g	
miR-146a	
Let-7i	
Let-7a	
miR-99a	
miR-125b	
miR-26a	

miR-146b	
Let7c-1	
miR-99b	
miR-30a	
miR-221	
miR-7a	
miR-125a	
miR-21a	
miR-10a	
miR-30d	
miR-30e	
Let-7f	

Supplementary Figure 7.3.0. The predicted pri-miRNA secondary structures of miRNA downregulated by TNC knockout in LPS stimulated BMDMs. Pri-miRNA secondary structures were predicted using Mxfold and pseudoviewer 3.0 web tools as described in section 2.8.4.

Pri-miRNA	Structure
miR-107	
miR-30b	
miR-185	
miR-125b	
miR-101b	
miR-101a	
miR-423	
miR-339	
miR-142a	
miR-103	
miR-16	
miR-17	

miR-181b	
miR-128	
miR-1839	
miR-148b	
miR-872	
miR-27b	
miR-130b	
miR-28a	
miR-351	

Supplementary Figure 7.4.0. The predicted pri-miRNA secondary structures of miRNA unchanged by TNC knockout in LPS stimulated BMDMs. Pri-miRNA secondary structures were predicted using Mxfold and pseudoviewer 3.0 web tools as described in section 2.8.4.

Sample	total reads	N% > 10%	low quality	5_adapter_cont aminated	3_adapter_ null or insert null	with plovA/T/G/C	clean reads
KO_LPS_1	12616007 (100.00%)	101 (0.00%)	0 (0.00%)	13120 (0.10%)	1144895 (9.07%)	12031 (0.10%)	11445860 (90.72%)
KO_LPS_2	13556552 (100.00%)	8 (0.00%)	0 (0.00%)	5533 (0.04%)	1360523 (10.04%)	8235 (0.06%)	12182253 (89.86%)
KO_LPS_3	13446169 (100.00%)	30 (0.00%)	0 (0.00%)	6698 (0.05%)	1204120 (8.96%)	8388 (0.06%)	12226933 (90.93%)
KO_U_1	12929672 (100.00%)	30 (0.00%)	0 (0.00%)	7958 (0.06%)	1203988 (9.31%)	8909 (0.07%)	11708787 (90.56%)
KO_U_2	11196572 (100.00%)	0 (0.00%)	0 (0.00%)	5581 (0.05%)	1404531 (12.54%)	12492 (0.11%)	9773968 (87.29%)
KO_U_3	11785208 (100.00%)	51 (0.00%)	0 (0.00%)	4219 (0.04%)	884787 (7.51%)	3958 (0.03%)	10892193 (92.42%)
WT_LPS_1	12899148 (100.00%)	16 (0.00%)	0 (0.00%)	4398 (0.03%)	1182273 (9.17%)	7211 (0.06%)	11705250 (90.74%)
WT_LPS_2	12902012 (100.00%)	91 (0.00%)	0 (0.00%)	20286 (0.16%)	6573746 (50.95%)	14608 (0.11%)	6293281 (48.78%)
WT_LPS_3	12724778 (100.00%)	24 (0.00%)	0 (0.00%)	39019 (0.31%)	5926741 (46.58%)	29652 (0.23%)	6729342 (52.88%)
WT_U_2	12005884 (100.00%)	42 (0.00%)	0 (0.00%)	2138 (0.02%)	884629 (7.37%)	6724 (0.06%)	11112351 (92.56%)
WT_U_1	11584393 (100.00%)	0 (0.00%)	0 (0.00%)	18127 (0.16%)	1527155 (13.18%)	11728 (0.10%)	10027383 (86.56%)
WT_U_3	15103033 (100.00%)	502 (0.00%)	0 (0.00%)	15292 (0.10%)	1427183 (9.45%)	16561 (0.11%)	13643495 (90.34%)

Supplementary Figure 7.5.0. BMDM small RNA-SEQ sample quality-control. Clean reads = total number of clean reads after the removal of the poor-quality reads listed in the table as a percentage of total raw reads. Red is used to indicate clean reads below <60% of the total raw reads. KO = TNC knockout; WT = wild-type; U = non-stimulated; LPS = stimulated with LPS.

Sample	Total sRNA	Mapped sRNA	"+" Mapped sRNA	"-" Mapped sRNA
WT_LPS_2	5458918 (100.00%)	4506775 (82.56%)	1360446 (24.92%)	3146329 (57.64%)
WT_LPS_3	5522094 (100.00%)	4369957 (79.14%)	1552278 (28.11%)	2817679 (51.03%)
WT_LPS_1	9693215 (100.00%)	8057416 (83.12%)	2849375 (29.40%)	5208041 (53.73%)
KO_LPS_1	10278646 (100.00%)	8465739 (82.36%)	3065177 (29.82%)	5400562 (52.54%)
KO_LPS_2	10851855 (100.00%)	9141878 (84.24%)	2589850 (23.87%)	6552028 (60.38%)
KO_LPS_3	9758623 (100.00%)	7833856 (80.28%)	2568831 (26.32%)	5265025 (53.95%)
WT_U_1	9086528 (100.00%)	6953464 (76.52%)	3354742 (36.92%)	3598722 (39.61%)
WT_U_2	10502995 (100.00%)	8590821 (81.79%)	2583860 (24.60%)	6006961 (57.19%)
WT_U_3	12752355 (100.00%)	10307702 (80.83%)	3657522 (28.68%)	6650180 (52.15%)
KO_U_1	10228374 (100.00%)	8446455 (82.58%)	2950563 (28.85%)	5495892 (53.73%)
KO_U_2	9240345 (100.00%)	7546109 (81.66%)	2605101 (28.19%)	4941008 (53.47%)
KO_U_3	9164682 (100.00%)	7614908 (83.09%)	2314038 (25.25%)	5300870 (57.84%)

Supplementary Figure 7.6.0. BMDM small RNA-SEQ sample mapped reads. Mapped sRNA = the total reads mapped to the murine genome. Analysis performed by Novogene using Bowtie. KO = TNC knockout; WT = wild-type; U = non-stimulated; LPS = stimulated with LPS.

Chapter 8

Appendix

8.1.0 – Effect of low macrophage confluency on YAP expression

YAP is the primary effector of the hippo pathway, a serine/threonine kinase signalling cascade through which extracellular cues such as cell-cell contact regulate events, including cell proliferation, differentiation, and tissue homeostasis³⁶⁵. Within this pathway, YAP performs a pro-proliferative function, with extracellular cues leading to YAP inactivation and degradation, thus contextual factors such as cell confluency may have an impact on YAP expression within the macrophage.

In order to investigate this, YAP protein expression in RAW 246.7 macrophages seeded at a range of confluences was assessed (Figure 8.1.1a). Western blot analysis showed a faint band corresponding to YAP in the cell lysates obtained from the condition with the lowest cell density (0.5×10^6 seeding density) and none in the samples obtained using higher seeding densities (Figure 8.1.1b). As the low confluency sample also shows lower banding of the loading control (α -tubulin) higher YAP expression could be assumed.

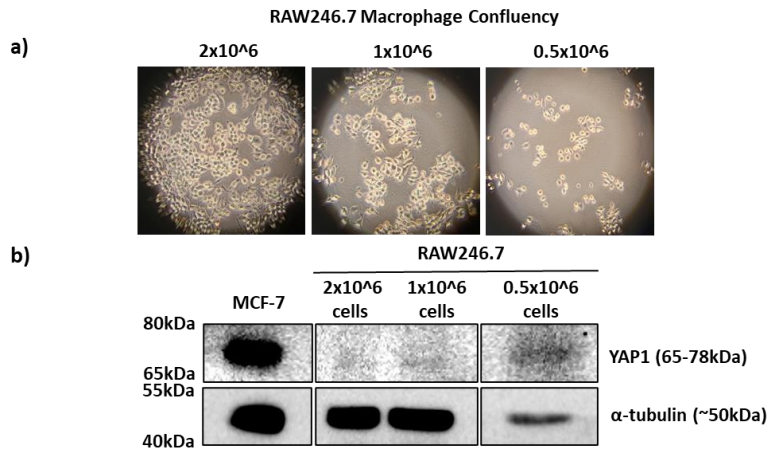


Figure 8.1.1: Low confluency potentially increases YAP expression in RAW246.7

macrophages. RAW246.7 macrophages were seeded at varying cell quantities with cell lysis performed 24h after seeding. **a)** Images of macrophages before lysis, 10x magnification. **b)** YAP1 expression was determined by Western Blot using MCF-7 as a positive control and α-tubulin as a loading control. Representative image from a single experiment.

An experimental workflow was next devised in order to ensure optimal cell confluency during siRNA treatment (~60%), low cell confluency at the end of the experiment to maximise YAP expression, and a high enough protein concentration in the cell extract. This was facilitated by initially seeding cells in a 48-well plate, to attain the correct siRNA confluency, followed by cell dissociation and re-plating into 10cm dishes 24h later (Figure 8.1.2a).

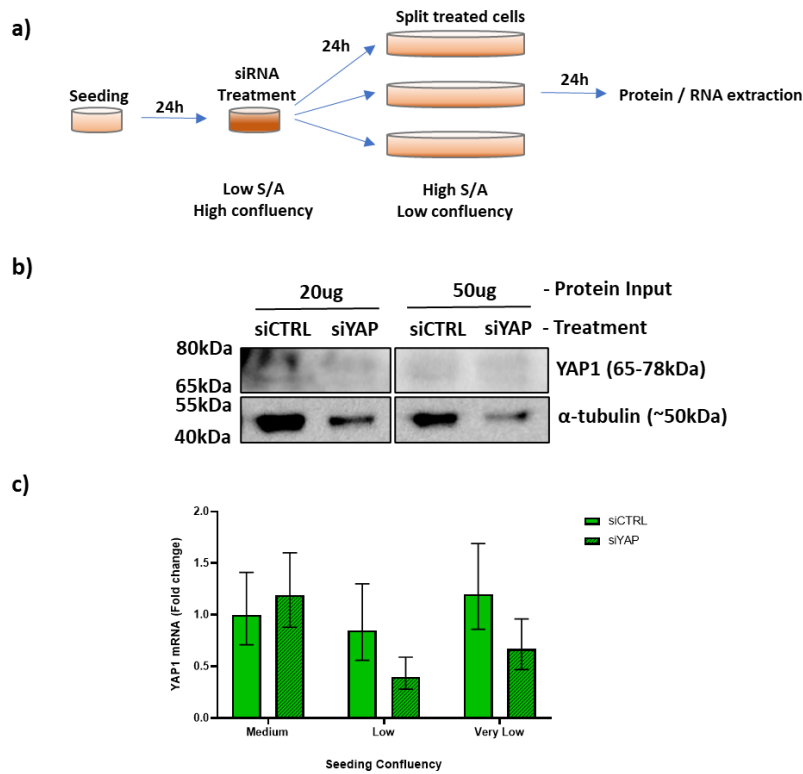


Figure 8.1.2: Validation of YAP expression in low confluency RAW246.7 macrophages using siRNA treatment. **a)** Schematic diagram of experimental workflow. RAW246.7 macrophages were seeded in a 48-well plate, 24 hours later these were transfected with 10nM of non-targeting control or YAP1 siRNA using lipofectamine RNAiMAX. 24 hours post-transfection cells were re-plated on 10cm dishes at either medium (1/2), low (1/4) or very low (1/8) dilutions before protein/RNA extraction 24 hours later. **b)** YAP1 expression was determined by Western Blot with either 20 ug or 50 ug protein input. α-tubulin was used as a loading control. Representative image from a single experiment. **c)** Expression levels of YAP1 mRNA were quantified by qPCR using HPRT1 as an endogenous housekeeping gene. Relative expression of YAP1 mRNA was determined via the $\Delta\Delta C_t$ method with siCTRL medium as the calibrator. Data derived from a single experiment, with error bars depicting upper/lower bounds.

Following this methodology YAP expression was assessed by western blot and qPCR (Figure 8.1.2b/c).

Western blot analysis of cells re-seeded at a 1 in 4 dilution (low confluency) showed no evidence of the increased YAP banding seen previously, with the faint banding present shown to be non-specific as it is unchanged by siYAP treatment (Figure 8.1.2b).

qPCR analysis showed that cells re-seeded at 1 in 4 (low confluency) or 1 in 8 (very low confluency) dilutions had their expression of YAP reduced by YAP siRNA treatment (Figure 8.1.2c). This contrasting the higher confluency of the sample with cells re-seeded at 1 in 2 dilution (medium confluency) that was not affected by siRNA treatment.

Even with YAP expression continuing to be undetectable by western blot, the apparent success of the YAP knockdown in qPCR data led to further investigation into the impact of YAP knockdown on TN-C and miR-155 within low confluency macrophages.

RAW 246.7 cells were incubated with siRNA for TNC, YAP or both using the low confluency methodology. qPCR was utilised to measure YAP, TNC and miR-155 expression as a result of this experiment (Figure 8.1.3).

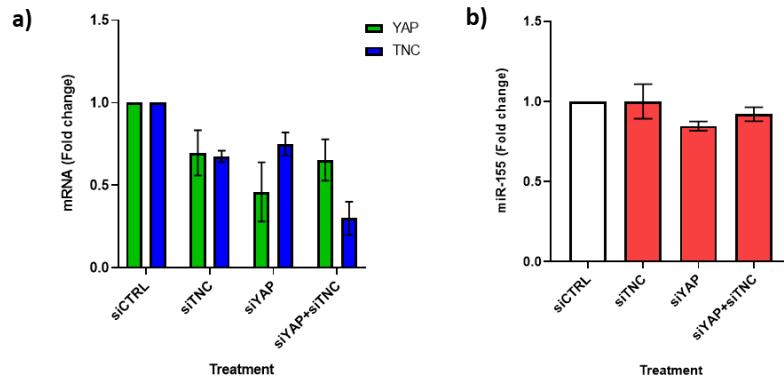


Figure 8.1.3: YAP and TN-C knockdown has no effect on miR-155 expression in LPS stimulated low confluency RAW246.7 macrophages. RAW246.7 macrophages were seeded in a 48-well plate, 24 hours later these were transfected with 10nM non-targeting control, YAP1 and/or TNC siRNA using lipofectamine RNAiMAX. 24 hours post-transfection cells were replated using a 1/4 dilution, followed by 8h LPS treatment and protein/RNA extraction. **a)** Expression levels of TN-C and YAP1 mRNA were quantified by qPCR using HPRT1 as an endogenous housekeeping gene. Relative expression of TN-C and YAP1 mRNA was determined via the $\Delta\Delta C_t$ method with siCTRL as the calibrator. \pm SEM; n=3. **b)** Mature miR-155 was quantified by qPCR using U6 snRNA as an endogenous housekeeping gene. Relative expression of miR-155 was determined via the $\Delta\Delta C_t$ method with siCTRL as the calibrator. \pm SEM; n=3; one-way anova with Tukey's multiple comparison.

siTNC treatment leads to a reduction in expression of both YAP and TNC mRNA of ~30%, with siYAP treatment having a similar impact on TNC while reducing YAP expression by ~50% (Figure 8.1.3a). Interestingly, dual treatment with siTNC and siYAP lead to the greatest reduction in TNC expression, ~75%, with only a minor decrease in YAP expression, ~30%. The low degree of TNC and YAP knockdown may be due to the cell-dissociation step of the

methodology, both genes playing vital roles in adherence and growth which may counteract the siRNA induced reduction of expression^{649–652}.

8.2.0 – Establishing an alternative cell model for examination of the potential link between TN-C, YAP and miR-155.

8.2.1 – Investigating YAP, TNC and miR-155 expression in candidate cell lines.

RAW 246.7 macrophages exhibit low YAP expression, thwarting loss-of function analysis which could identify a potential link between TN-C, YAP and miR-155 regulation. As study of the more YAP abundant primary BMDMs was not viable, due to incompatibility with siRNA transfection and animal dependency, the use of alternative immortalised non-monocytic cell lines was explored.

Alternative cell lines were selected dependent upon their known expression of YAP, TN-C, miR-155 and their availability (Table 8.2.1).

Although showing optimal characteristics, MCF-7 and MDA-MB-231 cells were not chosen due to their human origin making them incompatible with pre-established murine targeting reagents.

The expression of YAP and miR-155 in NIH-3T3 and EO771 cells were examined (Figure 8.2.3). qPCR and western blot analysis showed robust expression of YAP in both cell lines (Figure 8.2.3a/c), while qPCR also found

consistent miR-155 expression in both cell types (Figure 8.2.3b). This validation was sufficient to support future analysis using these cell lines.

Cell line	Organism	Tissue	YAP expression	miR-155 expression	TN-C expression
MCF-7	Human	Epithelial Breast Cancer	22.5nTPM (Human Protein Atlas). Detectable but low expression level ⁶⁵³ .	~3 fold greater expression than MDA-MB-231 ^{654,655} . ~45 fold lower expression than MCF-7 ²⁶⁷ .	0.1nTPM (Human Protein Atlas). Undetectable in MCF-7 lysate ⁶⁵⁶ .
MDA-MB-231	Human	Epithelial Breast Cancer	106.5nTPM (Human Protein Atlas). Highly detectable expression ⁶⁵⁷	~3 fold lower expression than MCF-7 ^{654,655} . ~45 fold higher expression than MCF-7 ²⁶⁷ .	23.1nTPM (Human Protein Atlas). Detectable in untreated cells ⁶⁵⁸ .
NIH-3T3	Mouse	Embryonic Fibroblast	Detectable but low expression level ⁶⁵⁹ .	Detectable but unknown expression level ⁶⁶⁰ .	Unknown expression level
E0771	Mouse	Epithelial-like Breast Cancer	Highly detectable expression ⁵³² .	Detectable but unknown expression level ⁶⁶¹ .	Unknown expression level

Figure 8.2.1: Table of possible alternative cell lines for examining TNC, YAP and miR-155.

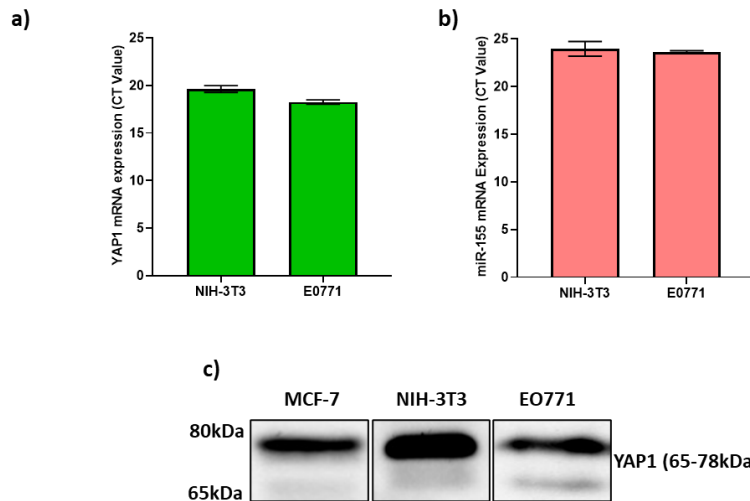


Figure 8.2.3: YAP and miR-155 are robustly expressed in NIH-3T3 and E0771 cells. Expression levels of YAP1 mRNA (a) and mature miR-155 (b) in E0771 and NIH-3T3 cells was quantified by qPCR. Data represents CT values of three technical replicates, \pm SD. c) Western blot was performed on E0771 and NIH-3T3 lysates to discern YAP1 expression. MCF-7 lysate was used as a positive control.

8.2.2 – Examining potential links between YAP, TNC and miR-155 in NIH-3T3 cells.

The abundance of YAP expression in NIH-3T3 cells allowed loss-of-function analysis to be performed using YAP and TNC siRNA. This served to both discern the potential role of YAP in miR-155 regulation as well as validate whether the effect of TNC knockdown on miR-155 expression occurs outside of macrophage cells.

YAP and TNC expression were knockdown using siRNA treatment, with relevant gene or miRNA expression examined by qPCR (Figure 8.2.4). Initial validation determined 48h of transfection to be the optimal duration for maximum YAP knockdown, this being utilised hereon (Figure 8.2.4a).

In response to single (siTNC) and dual (siTNC+siYAP) siRNA treatment, TNC mRNA expression was reduced by ~90% with the same occurring for YAP mRNA with single (siYAP) and dual (siYAP+siTNC) siRNA treatment (Figure 8.2.4b). Interestingly, siYAP treatment also halves TNC expression, a similar response to that seen previously in low confluency RAW 246.7 macrophages.

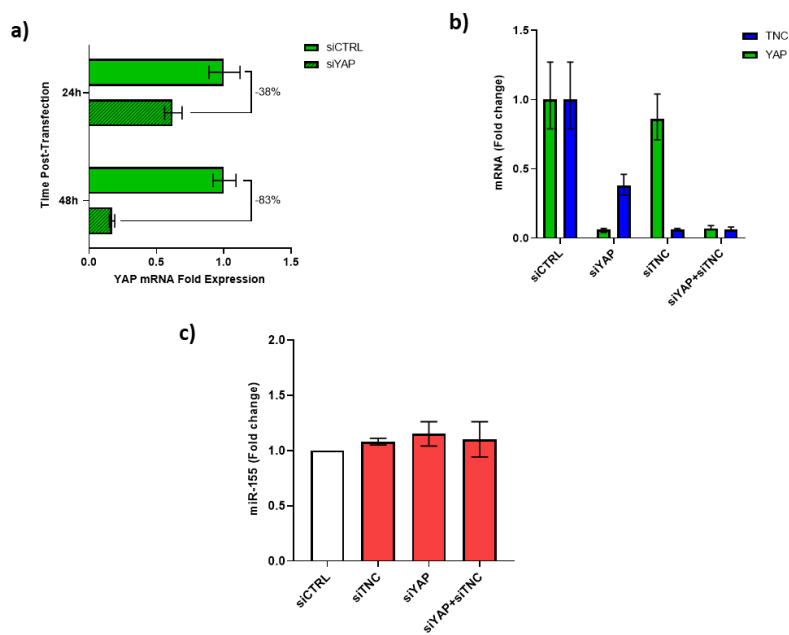


Figure 8.2.4: siTNC and siYAP treatment does not impact miR-155 expression in unstimulated NIH-3T3 cells. NIH-3T3 cells were transfected with 10nM non-targeting control, YAP1 and/or TNC siRNA using lipofectamine RNAiMAX, before RNA extraction. **a)** Expression of YAP1 mRNA in 24h or 48h transfected cells were compared by qPCR using HPRT1 as an endogenous housekeeping gene. Relative expression of YAP1 mRNA was determined via the $\Delta\Delta C_t$ method with siCTRL as the calibrator. Data derived from a single experiment, technical replicates = 3, mean fold change presented with error bars depicting \pm SD. Percentage reduction in fold change is stated. **b)** Expression of YAP1 and TNC mRNA in 48h transfected cells were quantified by qPCR using HPRT1 as an endogenous housekeeping gene. Relative

expression of mRNA was determined via the $\Delta\Delta C_t$ method with siCTRL as the calibrator. Data derived from a single experiment, technical replicates = 3, mean fold change presented with error bars depicting \pm SD. c) Mature miR-155 was quantified by qPCR using U6 snRNA as an endogenous housekeeping gene. Relative expression of miR-155 was determined via the $\Delta\Delta C_t$ method with siCTRL as the calibrator. \pm SEM; n=2.

Even with highly efficient YAP and TNC knockdown no significant change in miR-155 expression occurs with either treatment in NIH-3T3 cells (Figure 8.2.4c).

This lack of change in miR-155 expression with siYAP or siTNC treatment is hypothesised to be due to the robust expression of miR-155 in NIH-3T3 cells. This being orchestrated by a different passive induction mechanism compared to macrophage cells wherein miR-155 expression is induced from low to high levels following inflammatory induction. It is therefore the interaction of TNC with this induction which potentially elicits the downregulation in miR-155.

In order to potentially replicate the conditions in the macrophage which give rise to the regulation of miR-155 by TN-C, induction of miR-155 expression in NIH-3T3 cells was attempted (Figure 8.2.5).

Both LPS and TNF- α stimulation has been shown to induce miR-155 expression within RAW 246.7 macrophages and BMDMs, with this induction being prevented in TNC knockout or siRNA knockdown cells⁵¹¹. Fibroblasts characteristically express TLR4, responding to LPS treatment via the induction of pro-fibrotic pathways⁶⁶². Whereas, TNF treatment of NIH-3T3 cells is characterised by cytotoxicity⁶⁶³.

The pro-fibrotic signal molecule TGF- β is known to induce miR-155 expression within normal mammary and coronary artery endothelial cells, this being attributed to the downstream effector activity of Smad4^{257,664}. Moreover, TGF- β treatment also enhances mRNA TNC expression, thus showing similar functionality as LPS in both enhancing miR-155 and TNC synthesis^{499,665}.

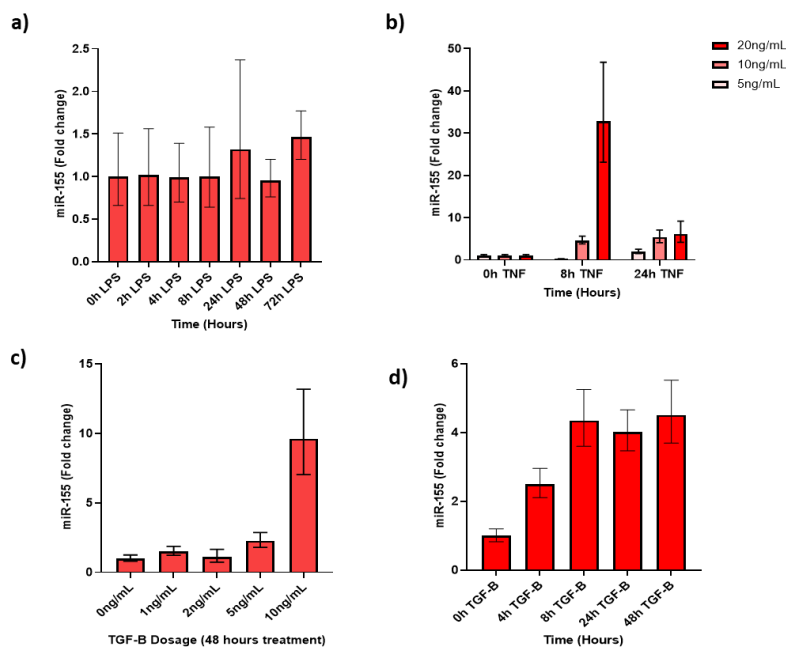


Figure 8.2.5: Optimisation of miR-155 induction in NIH-3T3 cells using TGF-B and TNF. a)

NIH-3T3 cells were treated with 100ng/mL of LPS for the durations indicated. Mature miR-155 was quantified by qPCR using U6 snRNA as an endogenous housekeeping gene. Relative expression of miR-155 was determined via the $\Delta\Delta Ct$ method with 0h LPS as the calibrator.

Data derived from a single experiment, technical replicates = 3, mean fold change presented with error bars depicting \pm SD.

b) NIH-3T3 cells were treated with varying dosages of TNF for the durations indicated. Mature miR-155 was quantified as above, with 0h TNF as the calibrator.

Data derived from a single experiment, technical replicates = 3, mean fold change presented with error bars depicting \pm SD.

c) NIH-3T3 cells were treated with varying dosages

of TGF- β for 48 hours. Mature miR-155 was quantified as above, with 0 ng/mL as the calibrator. Data derived from a single experiment, technical replicates = 3, mean fold change presented with error bars depicting \pm SD. **d)** NIH-3T3 cells were treated with 10ng/mL TGF- β for the durations indicated. Mature miR-155 was quantified as above, with 0h TGF- β as the calibrator. Data derived from a single experiment, technical replicates = 3, mean fold change presented with error bars depicting \pm SD.

NIH-3T3 cells treatment with 100ng/mL LPS for 0, 2, 4, 8, 24, 48 and 72 hours failed to elicit an induction in miR-155 expression (Figure 8.2.5a). This is notable, as the TLR4 expressing NIH-3T3 cells would be expected to respond to LPS⁶⁶⁶.

Treatment with 10 or 20ng/mL TNF for 8 or 24h both induced miR-155 expression with 20ng/mL for 8h causing the largest induction of miR-155 (Figure 8.2.5b).

Dosage examination of TGF- β for 48h shows no miR-155 induction with 1, 2 or 5ng/mL treatment, with 10ng/mL exhibiting a \sim 10-fold induction in miR-155 (Figure 8.2.5c).

Finally, TGF- β time course analysis using as dosage of 10ng/mL found miR-155 expression to be enhanced with 4h of stimulation rising higher by 8h and then sustaining the same induction for 24 and 48h (Figure 8.2.5d).

With successful induction of miR-155 in NIH-3T3 cells using TGF- β or TNF, these treatments were combined with siTNC and siYAP transfection to identify whether knockdown of these genes impacts the induction of miR-155 in NIH-3T3 cells (Figure 8.2.6).

As TGF- β is a known regulator of fibrosis, its impact on YAP and TNC expression in NIH-3T3 cells was examined alongside siRNA treatment (Figure 8.2.6a). In all non-siTNC incubated cells 10ng/mL of TGF- β applied for 24h led to an increase in TNC expression compared to non-TGF- β treated cells. This aligning with literature evidence of TGF- β as a stimulator of TNC mRNA and protein expression^{499,665}. Otherwise, YAP and TNC knockdown was consistent with siRNA treatment.

YAP and/or TNC knockdown in NIH-3T3 cells treated with 10ng/mL TGF- β for 24h does not affect expression of miR-155, as determined by qPCR (Figure 8.2.6b).

To further examine whether siTNC treatment can reduce miR-155 induction caused by TGF- β stimulation, 10ng/mL TGF- β was applied to cells for 0, 8 or 24h (Figure 8.2.6c). siTNC treatment had no effect on miR-155 expression across the timepoints analysed.

With the failure of TGF- β to induce a TN-C-regulated miR-155 induction, 20ng/mL TNF was used to stimulate NIH-3T3 cells for 0, 4, 8 or 24h (Figure 8.2.6d). Although these results produce a promising trend, with siTNC reducing miR-155 expression below that of siCTRL, the large degree of variability and single biological replicate mean more investigation using TNF treatment is necessary.

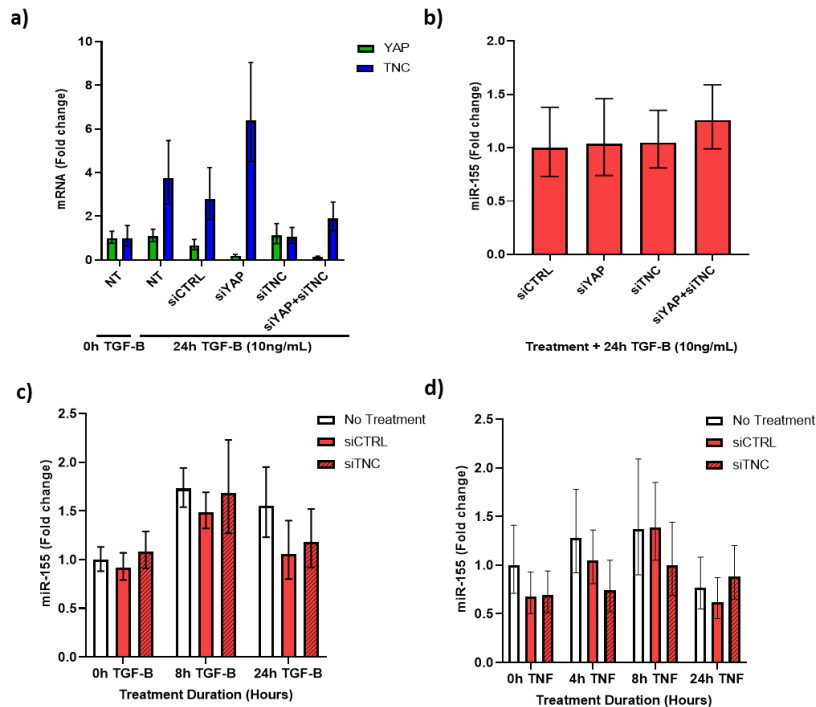


Figure 8.2.6: siTNC and siYAP treatment of stimulated NIH-3T3 cells and the impact on miR-155. **a and b)** NIH-3T3 cells were transfected with 10nM non-targeting control, YAP1 and/or TNC siRNA using lipofectamine RNAiMAX, followed by stimulation with 10ng/mL TGF-B for 24 hours and RNA extraction. **a)** Expression of YAP1 and TNC mRNA were quantified by qPCR using HPRT1 as an endogenous housekeeping gene. Relative expression of mRNA was determined via the $\Delta\Delta C_t$ method with non-treated and non-stimulated samples as the calibrator. Data derived from a single experiment, technical replicates = 3, mean fold change presented with error bars depicting \pm SD. **b)** Mature miR-155 was quantified by qPCR using U6 snRNA as an endogenous housekeeping gene. Relative expression of miR-155 was determined via the $\Delta\Delta C_t$ method with siCTRL as the calibrator. with error bars depicting \pm SD **c)** NIH-3T3 cells were transfected as outlined above with either 8h or 24h TGF-B stimulation. Mature miR-155 was quantified as above with non-treated 0h TGF-B as the calibrator. Data derived from a single experiment, technical replicates = 3, mean fold change presented with error bars depicting \pm SD. **d)** NIH-3T3 cells were transfected as outlined above with 4, 8 or 24 hours

of stimulation with 10ng/mL TNF. Mature miR-155 was quantified as above with non-treated 0h TNF as the calibrator. Data derived from a single experiment, technical replicates = 3, mean fold change presented with error bars depicting \pm SD.

These findings invalidate NIH-3T3 cells as a means of studying potential interactions between TN-C, YAP and miR-155. Although these cells express these genes in abundance, with stimulation miR-155 remains unchanged by TNC or YAP knockdown leading to the conclusion that NIH-3T3 cells do not model the same relationship between TNC and miR-155 seen in BMDMs.

8.3.1 – Investigating the Induction of miR-155 expression in EO771 cells

EO771 cells were treated with TGF- β (5 or 10ng/mL) or TNF (20 or 40ng/mL) for 24h to identify the optimal means of inducing miR-155 expression in this cell line. 10ng/mL TGF- β and both dosages of TNF induced miR-155 expression (Figure 8.3.1). As 20ng/mL showed the largest induction, 1.83-fold, this treatment was further utilised, although notably this induction is far lower than the TNC-mediated induction of miR-155 elicited by LPS treatment of macrophage cells.

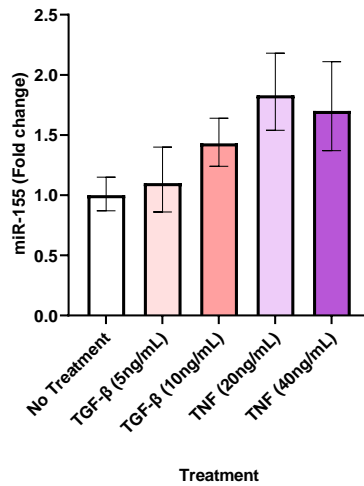


Figure 8.3.1: Optimisation of miR-155 induction using TNF and TGF-β. E0771 cells were treated with varying doses of TNF and TGF-β as depicted for 24 hours, before RNA extraction. Mature miR-155 expression was quantified by qPCR using U6 snRNA as an endogenous housekeeping gene. Relative expression of miR-155 was determined via the $\Delta\Delta C_t$ method with no treatment as the calibrator. Data derived from a single experiment, technical replicates = 3, mean fold change presented with error bars depicting \pm SD.

8.4.0 – Examination of known TN-C binding receptors with links to miR-155 expression regulation

8.4.1 – Identification of candidate receptors which may allow TN-Cs regulation of miR-155 expression.

Previous members of the Piccinini lab examined the potential miR-155 regulatory role of the experimentally validated TN-C binding receptors TLR4, EGFR and integrins $\alpha 9\beta 1$, $\alpha \nu\beta 3$ and $\alpha 5\beta 1$ ⁵¹¹. Additionally, the non-validated Mac-1 receptor and NRP1 co-receptor were also investigated. Inhibition or blockage of these candidate receptors failed to elicit the significant change in

miR-155 expression indicative of a receptor participating in the TN-C-miR-155 pathway. Receptors were blocked using function blocking antibodies, peptides and small molecule inhibitors which, in most cases, induced miR-155 expression likely due to their endotoxin content. The results were thus inconclusive.

Here, to overcome this limitation and test the potential role of integrins as receptors signalling TN-C-mediated regulation of miR-155 expression, integrin subunit knockdown experiments using siRNA technology were designed and conducted⁵¹¹.

A thorough literature search was conducted to identify additional candidate receptors with associations to TN-C and involvement in the inflammatory response (Table 8.4.1).

In order to verify the expression of candidate receptors in murine macrophages, the fragments per kilobase of transcript per million mapped reads (FPKM) for each candidate integrin subunit was gathered from RNA-Seq of 4h LPS treated BMDMs (Figure 8.4.1). ITGB1 showed the highest expression amongst candidate subunit genes, leading to selection of integrin β 1 for further validation. Of the β 1 associated subunits, α 5, α 9 and α V genes showed the highest expression, although considerably lower than that of ITGB1, and thus were examined further.

Cell surface expression of selected candidate receptors was next investigated, providing a more relevant estimation of each candidates TN-C interaction potential than mRNA expression alone. Additionally, as BMDMs are difficult-

to-transfect cells, this analysis allowed the assessment of candidate receptor expression within the siRNA-compatible RAW 246.7 cells.

Candidate receptor	TN-C association	Role in inflammation	Macrophage expression (BMDM RNA-Seq)
Integrin $\alpha 9\beta 1$	Interaction with TN-C leading to actin depolymerisation ^{311,667} .	Ligand administration increases pro-inflammatory cytokine expression in macrophages ⁵²¹ .	ITGA9 = 1.00 FPKM ITGB1 = 148.00 FPKM
	A9 β 1 neutralising antibody prevents recombinant TN-C associated cytokine expression in macrophages ⁵²⁰ .	A9 β 1 neutralising antibody prevents recombinant TN-C associated cytokine expression in macrophages ⁵²⁰ .	
Integrin $\alpha 5\beta 1$	TN-C association prevents actin polymerisation through inhibiting interaction between $\alpha 5\beta 1$ and syndecan ^{311,413,668} .	Oxidised low-density lipoproteins induce NF-kB signalling via an $\alpha 5\beta 1$ -dependent mechanism in macrophages ⁶⁶⁹ .	ITGA5 = 64.00 FPKM ITGB1 = 148.00 FPKM

Integrin $\alpha 2\beta 1$	TN-C enhances brain tumour-initiating cell proliferation through an $\alpha 2\beta 1$ -dependent pathway ⁶⁷⁰ .	Augments effector T cell expression of IFN- γ ⁶⁷¹ .	ITGA2 = 0.02 FPKM ITGB1 = 148.00 FPKM
----------------------------	---	---	--

Integrin $\alpha 8\beta 1$	Binds to the TN-C RGD domain, mediating adhesion ⁶⁷² .	N/A	ITGA8 = 0.19 FPKM ITGB1 = 148.00 FPKM
----------------------------	---	-----	--

Integrin $\alpha \nu \beta 1$	Induces epithelial to mesenchymal transition through binding to TN-C in breast cancer cells ³³¹ .	Upregulated in inflammatory lymphocyte migration ⁶⁷³ .	ITGAV = 0.25 FPKM ITGB1 = 148.00 FPKM
-------------------------------	--	---	--

Integrin $\alpha \nu \beta 3$	Blockage of this integrin prevented cell spreading on TN-C and inhibited TNC-dependent EGF-R clustering ⁶⁷⁴ .	Co-localises with TGFBR2, enhancing activation via TGF-B ⁶⁷⁵ . Regulates macrophage migration and phagocytosis ⁶⁷⁶ .	ITGAV = 0.25 FPKM ITGB3 = 0.76 FPKM
-------------------------------	--	---	--

Integrin $\alpha \nu \beta 5$	N/A	Mediates intestinal macrophage phagocytosis of apoptotic cells ⁶⁷⁷ .	ITGAV = 0.25 FPKM ITGB5 = 2.62 FPKM
-------------------------------	-----	---	--

Integrin α V β 6	Induces epithelial to mesenchymal transition through binding to TN-C in breast cancer cells ³³¹ .	Binds and activates pro-TGF- β 1 ⁶⁷⁸ . B6 knockout associated with skin inflammation and accelerated wound repair ⁶⁷⁹ .	ITGAV = 0.25 FPKM ITGB6 = 0.00 FPKM
----------------------------------	--	--	--

Integrin α V β 8	N/A	Binds and activates pro-TGF- β 1, leading to immune cell recruitment and activation ^{678,680} .	ITGAV = 0.25 FPKM ITGB8 = 0.03 FPKM
----------------------------------	-----	--	--

NRP1	Activates the TN-C dependent FAK/Akt-NF-kB pathway ⁶⁸¹ .	Expression is reduced by LPS treatment in macrophages. Loss of NRP1 elicits a proinflammatory effect ⁶⁸² .	NRP1 = 10.82 FPKM
------	---	---	-------------------

TGFB2	N/A	Activated by NRP1, facilitating herpesvirus internalisation ⁶⁸³ . Responsible for TGF-B signal transduction	TGFB2 = 23.11 FPKM
-------	-----	---	--------------------

driving
macrophages
towards a repair
phenotype⁶⁸⁴.

Table 8.4.1: Table of candidate TN-C receptors and co-receptors.

Fluorescence-activated cell sorting (FACS) assessment of RAW246.7 macrophages, non-treated or treated with LPS for 4h, was performed by Xingyu Guo. TGFBR2 and integrin β 1, α 5, α 9 and α V antibodies were used for detection, with percentage of positive cells and mean fluorescence intensity (MFI) calculated using FlowJo software (Figure 8.4.2).

Integrins β 1 and α 5 both showed low surface expression in non-treated cells which increased dramatically with LPS treatment from 0% to 99.6% and 11.1% to 89% of positive cell, respectively, with a matching trend in MFI (Figure 8.4.2 a and c). α V and α 9 surface expression was respectively increased and decreased by LPS stimulation, with these and TGFBR2 all showing very low percentage of positive cells but featuring high MFIs, indicating that a small

population of cells express these receptors in abundance (Figure 8.4.2 b, d and c).

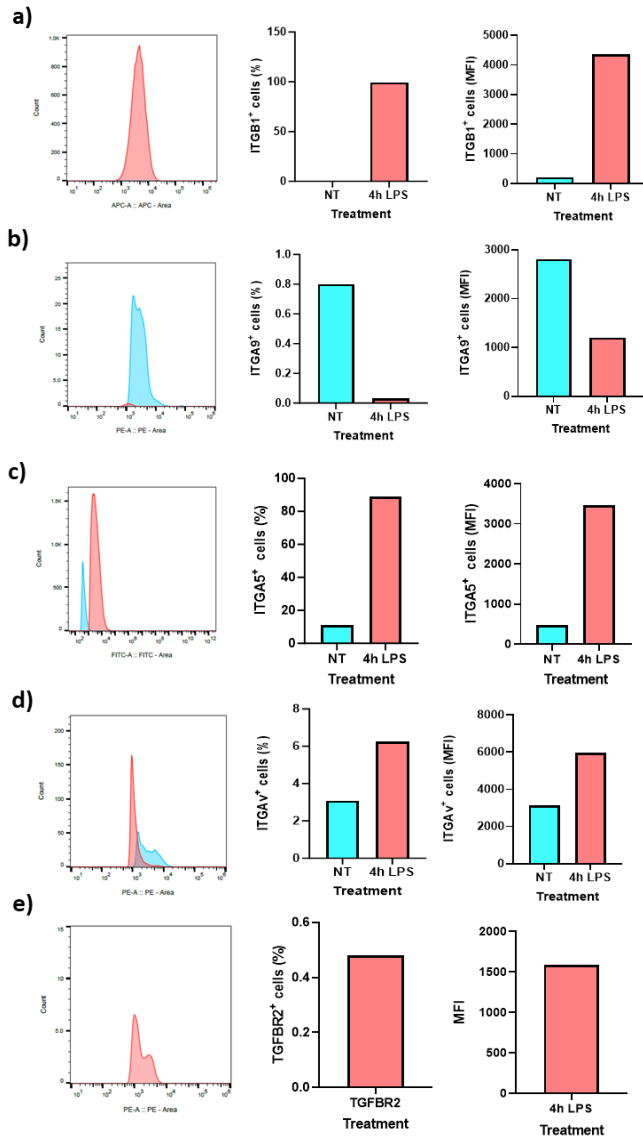


Figure 8.4.2: Examination of candidate receptor cell surface expression in unstimulated and LPS stimulated RAW 246.7 macrophages. RAW 246.7 macrophages were either non-stimulated or stimulated with 100ng/mL of LPS for 4 hours. Fluorescence-Activated Cell Sorting was performed on these samples using specific antibodies for a) Integrin β 1, b) Integrin α 9, c) Integrin α 5, d) Integrin α V and

e) TGFBR2. Samples were analysed using FlowJo software with percentage of positive cells and mean fluorescence intensity (MFI) calculated. n=1. The lab procedure was performed by Xingyu Guo.

Chapter 9

Bibliography

1. Medzhitov, R. Origin and physiological roles of inflammation. *Nature* **454**, 428–435 (2008).
2. See, H. W. & Lord, J. M. Factors underlying chronic inflammation in rheumatoid arthritis. *Archivum Immunologiae et Therapiae Experimentalis* **52**, 379–388 (2004).
3. Rubin, D. C., Shaker, A. & Levin, M. S. Chronic intestinal inflammation: inflammatory bowel disease and colitis-associated colon cancer. *Front Immunol* **3**, 107 (2012).
4. Wynn, T. A., Chawla, A. & Pollard, J. W. Origins and Hallmarks of Macrophages: Development, Homeostasis, and Disease. *Nature* **496**, 445–455 (2013).
5. Schulz, C. *et al.* A lineage of myeloid cells independent of Myb and hematopoietic stem cells. *Science* **336**, 86–90 (2012).
6. Ginhoux, F. *et al.* Fate mapping analysis reveals that adult microglia derive from primitive macrophages. *Science* **330**, 841–845 (2010).
7. Hoeffel, G. *et al.* Adult Langerhans cells derive predominantly from embryonic fetal liver monocytes with a minor contribution of yolk sac-derived macrophages. *J Exp Med* **209**, 1167–1181 (2012).
8. Park, M. D., Silvin, A., Ginhoux, F. & Merad, M. Macrophages in health and disease. *Cell* **185**, 4259–4279 (2022).
9. Italiani, P. & Boraschi, D. From Monocytes to M1/M2 Macrophages: Phenotypical vs. Functional Differentiation. *Front Immunol* **5**, 514 (2014).
10. Stout, R. D. *et al.* Macrophages Sequentially Change Their Functional Phenotype in Response to Changes in Microenvironmental Influences¹. *The Journal of Immunology* **175**, 342–349 (2005).
11. Medzhitov, R. & Horng, T. Transcriptional control of the inflammatory response. *Nat Rev Immunol* **9**, 692–703 (2009).

12. Martinez, F. O., Sica, A., Mantovani, A. & Locati, M. Macrophage activation and polarization. *FBL* **13**, 453–461 (2008).
13. Martinez, F. O. & Gordon, S. The M1 and M2 paradigm of macrophage activation: time for reassessment. *F1000Prime Rep* **6**, (2014).
14. Wolfs, I. M. J., Donners, M. M. P. C. & Winther, M. P. J. de. Differentiation factors and cytokines in the atherosclerotic plaque micro-environment as a trigger for macrophage polarisation. *Thromb Haemost* **106**, 763–771 (2011).
15. Mantovani, A. *et al.* The chemokine system in diverse forms of macrophage activation and polarization. *Trends in Immunology* **25**, 677–686 (2004).
16. Lawrence, T. & Natoli, G. Transcriptional regulation of macrophage polarization: enabling diversity with identity. *Nat Rev Immunol* **11**, 750–761 (2011).
17. Murray, P. J. & Wynn, T. A. Obstacles and opportunities for understanding macrophage polarization. *Journal of Leukocyte Biology* **89**, 557–563 (2011).
18. Loke, P. *et al.* IL-4 dependent alternatively-activated macrophages have a distinctive in vivo gene expression phenotype. *BMC Immunology* **3**, 7 (2002).
19. Van Dyken, S. J. & Locksley, R. M. Interleukin-4- and Interleukin-13-Mediated Alternatively Activated Macrophages: Roles in Homeostasis and Disease. *Annual Review of Immunology* **31**, 317–343 (2013).
20. Fairweather, D. & Cihakova, D. Alternatively activated macrophages in infection and autoimmunity. *Journal of Autoimmunity* **33**, 222–230 (2009).
21. Takeuchi, O. & Akira, S. Pattern Recognition Receptors and Inflammation. *Cell* vol. 140 805–820 Preprint at <https://doi.org/10.1016/j.cell.2010.01.022> (2010).
22. Lemaitre, B., Nicolas, E., Michaut, L., Reichhart, J. M. & Hoffmann, J. A. The dorsoventral regulatory gene cassette *spatzle/Toll/Cactus* controls the potent antifungal response in *Drosophila* adults. *Cell* **86**, 973–983 (1996).

23. Poltorak, A. *et al.* Defective LPS signaling in C3H/HeJ and C57BL/10ScCr mice: Mutations in Tlr4 gene. *Science* **282**, 2085–2088 (1998).
24. Hayashi, F. *et al.* The innate immune response to bacterial flagellin is mediated by Toll-like receptor 5. *Nature* **410**, 1099–1103 (2001).
25. Kang, J. Y. *et al.* Recognition of Lipopeptide Patterns by Toll-like Receptor 2-Toll-like Receptor 6 Heterodimer. *Immunity* **31**, 873–884 (2009).
26. Takeuchi, O. *et al.* Cutting Edge: Role of Toll-Like Receptor 1 in Mediating Immune Response to Microbial Lipoproteins. *The Journal of Immunology* **169**, 10–14 (2002).
27. Alexopoulou, L., Holt, A. C., Medzhitov, R. & Flavell, R. A. Recognition of double-stranded RNA and activation of NF- κ B by Toll-like receptor 3. *Nature* **413**, 732–738 (2001).
28. Pulendran, B., Palucka, K. & Banchereau, J. Sensing pathogens and tuning immune responses. *Science* vol. 293 253–256 Preprint at <https://doi.org/10.1126/science.1062060> (2001).
29. Hemmi, H. *et al.* A Toll-like receptor recognizes bacterial DNA. *Nature* **408**, 740–745 (2000).
30. Hidmark, A., von Saint Paul, A. & Dalpke, A. H. Cutting Edge: TLR13 Is a Receptor for Bacterial RNA. *The Journal of Immunology* **189**, 2717–2721 (2012).
31. Chávez-Sánchez, L. *et al.* Activation of TLR2 and TLR4 by minimally modified low-density lipoprotein in human macrophages and monocytes triggers the inflammatory response. *Human Immunology* **71**, 737–744 (2010).
32. Midwood, K. *et al.* Tenascin-C is an endogenous activator of Toll-like receptor 4 that is essential for maintaining inflammation in arthritic joint disease. *Nature Medicine* **15**, 774–780 (2009).

33. Hornung, V. *et al.* Quantitative Expression of Toll-Like Receptor 1–10 mRNA in Cellular Subsets of Human Peripheral Blood Mononuclear Cells and Sensitivity to CpG Oligodeoxynucleotides. *The Journal of Immunology* **168**, 4531–4537 (2002).
34. Re, F. & Strominger, J. L. Toll-like Receptor 2 (TLR2) and TLR4 Differentially Activate Human Dendritic Cells. *Journal of Biological Chemistry* **276**, 37692–37699 (2001).
35. Zarembek, K. A. & Godowski, P. J. Tissue Expression of Human Toll-Like Receptors and Differential Regulation of Toll-Like Receptor mRNAs in Leukocytes in Response to Microbes, Their Products, and Cytokines. *The Journal of Immunology* **168**, 554–561 (2002).
36. Gioannini, T. L. *et al.* Isolation of an endotoxin-MD-2 complex that produces Toll-like receptor 4-dependent cell activation at picomolar concentrations. *Proceedings of the National Academy of Sciences of the United States of America* **101**, 4186–4191 (2004).
37. Shimazu, R. *et al.* MD-2, a molecule that confers lipopolysaccharide responsiveness on toll-like receptor 4. *Journal of Experimental Medicine* **189**, 1777–1782 (1999).
38. Akashi, S. *et al.* Cutting Edge: Cell Surface Expression and Lipopolysaccharide Signaling Via the Toll-Like Receptor 4-MD-2 Complex on Mouse Peritoneal Macrophages. *The Journal of Immunology* **164**, 3471–3475 (2000).
39. Park, B. S. *et al.* The structural basis of lipopolysaccharide recognition by the TLR4-MD-2 complex. *Nature* **458**, 1191–1195 (2009).
40. Latz, E. *et al.* Ligand-induced conformational changes allosterically activate Toll-like receptor 9. *Nature Immunology* **8**, 772–779 (2007).

41. Triantafilou, K. *et al.* Fluorescence recovery after photobleaching reveals that LPS rapidly transfers from CD14 to hsp70 and hsp90 on the cell membrane. *Journal of Cell Science* **114**, 2535–2545 (2001).
42. Yamamoto, M. *et al.* TRAM is specifically involved in the Toll-like receptor 4-mediated MyD88-independent signaling pathway. *Nature Immunology* **4**, 1144–1150 (2003).
43. Latty, S. *et al.* Activation of toll-like receptors nucleates assembly of the MyDDosome signaling hub. *eLife* **7**, (2018).
44. Ferrao, R. *et al.* IRAK4 Dimerization and trans-Autophosphorylation Are Induced by Myddosome Assembly. *Molecular Cell* **55**, 891–903 (2014).
45. Lomaga, M. A. *et al.* TRAF6 deficiency results in osteopetrosis and defective interleukin-1, CD40, and LPS signaling. *Genes and Development* **13**, 1015–1024 (1999).
46. Wang, C. *et al.* TAK1 is a ubiquitin-dependent kinase of MKK and IKK. *Nature* **412**, 346–351 (2001).
47. Akira, S. & Hoshino, K. Myeloid Differentiation Factor 88–Dependent and –Independent Pathways in Toll-Like Receptor Signaling. *The Journal of Infectious Diseases* **187**, S356–S363 (2003).
48. Sharma, S. *et al.* Triggering the interferon antiviral response through an IKK-related pathway. *Science* **300**, 1148–1151 (2003).
49. Liu, T., Zhang, L., Joo, D. & Sun, S.-C. NF- κ B signaling in inflammation. *Sig Transduct Target Ther* **2**, 1–9 (2017).
50. Baeuerle, P. A. & Baltimore, D. Activation of DNA-binding activity in an apparently cytoplasmic precursor of the NF-kappa B transcription factor. *Cell* **53**, 211–217 (1988).

51. Sen, R. & Baltimore, D. Multiple nuclear factors interact with the immunoglobulin enhancer sequences. *Cell* **46**, 705–716 (1986).
52. Karin, M. & Delhase, M. The I κ B kinase (IKK) and NF- κ B: key elements of proinflammatory signalling. *Seminars in Immunology* **12**, 85–98 (2000).
53. Hayden, M. S. & Ghosh, S. Shared principles in NF-kappaB signaling. *Cell* **132**, 344–362 (2008).
54. Beinke, S. & Ley, S. C. Functions of NF-kappaB1 and NF-kappaB2 in immune cell biology. *Biochem J* **382**, 393–409 (2004).
55. Mitigation of Inflammation with Foods | Journal of Agricultural and Food Chemistry. <https://pubs.acs.org/doi/10.1021/jf3007008>.
56. Yamaguchi, K. *et al.* Identification of a member of the MAPKKK family as a potential mediator of TGF-beta signal transduction. *Science* **270**, 2008–2011 (1995).
57. Hirata, Y., Takahashi, M., Morishita, T., Noguchi, T. & Matsuzawa, A. Post-Translational Modifications of the TAK1-TAB Complex. *International Journal of Molecular Sciences* **18**, 205 (2017).
58. Symons, A., Beinke, S. & Ley, S. C. MAP kinase kinase kinases and innate immunity. *Trends in Immunology* **27**, 40–48 (2006).
59. Gazon, H., Barbeau, B., Mesnard, J.-M. & Peloponese, J.-M. Hijacking of the AP-1 Signaling Pathway during Development of ATL. *Frontiers in Microbiology* **8**, (2018).
60. Lawrence, T. The nuclear factor NF-kappaB pathway in inflammation. *Cold Spring Harbor perspectives in biology* vol. 1 Preprint at <https://doi.org/10.1101/cshperspect.a001651> (2009).

61. Schonhaler, H. B., Guinea-Viniegra, J. & Wagner, E. F. Targeting inflammation by modulating the Jun/AP-1 pathway. in *Annals of the Rheumatic Diseases* vol. 70 i109–i112 (BMJ Publishing Group Ltd, 2011).
62. Miyamoto, M. *et al.* Regulated expression of a gene encoding a nuclear factor, IRF-1, that specifically binds to IFN- β gene regulatory elements. *Cell* **54**, 903–913 (1988).
63. Platanitis, E. & Decker, T. Regulatory networks involving STATs, IRFs, and NF κ B in inflammation. *Frontiers in Immunology* vol. 9 Preprint at <https://doi.org/10.3389/fimmu.2018.02542> (2018).
64. Wang, N., Liang, H. & Zen, K. Molecular mechanisms that influence the macrophage M1-M2 polarization balance. *Frontiers in Immunology* vol. 5 Preprint at <https://doi.org/10.3389/fimmu.2014.00614> (2014).
65. Hume, D. A. The many alternative faces of macrophage activation. *Frontiers in Immunology* vol. 6 Preprint at <https://doi.org/10.3389/fimmu.2015.00370> (2015).
66. Feldmann, M., Brennan, F. M. & Maini, R. N. ROLE OF CYTOKINES IN RHEUMATOID ARTHRITIS. *Annual Review of Immunology* **14**, 397–440 (1996).
67. Neurath, M. F. Cytokines in inflammatory bowel disease. *Nature Reviews Immunology* vol. 14 329–342 Preprint at <https://doi.org/10.1038/nri3661> (2014).
68. Pai, J. K. *et al.* Inflammatory markers and the risk of coronary heart disease in men and women. *New England Journal of Medicine* **351**, 2599–2610 (2004).
69. Carpenter, S. & O'Neill, L. A. J. Recent insights into the structure of Toll-like receptors and post-translational modifications of their associated signalling proteins. *Biochemical Journal* vol. 422 1–10 Preprint at <https://doi.org/10.1042/BJ20090616> (2009).

70. Kobayashi, H. & Tomari, Y. RISC assembly: Coordination between small RNAs and Argonaute proteins. *Biochimica et Biophysica Acta - Gene Regulatory Mechanisms* vol. 1859 71–81 Preprint at <https://doi.org/10.1016/j.bbagrm.2015.08.007> (2016).
71. O'Neill, L. A., Sheedy, F. J. & McCoy, C. E. MicroRNAs: the fine-tuners of Toll-like receptor signalling. (2011) doi:10.1038/nri2957.
72. Reinhart, B. J. *et al.* The 21-nucleotide let-7 RNA regulates developmental timing in *Caenorhabditis elegans*. *Nature* **403**, 901–906 (2000).
73. Chiang, H. R. *et al.* Mammalian microRNAs: Experimental evaluation of novel and previously annotated genes. *Genes and Development* **24**, 992–1009 (2010).
74. Kozomara, A. & Griffiths-Jones, S. miRBase: Annotating high confidence microRNAs using deep sequencing data. *Nucleic Acids Research* (2014) doi:10.1093/nar/gkt1181.
75. Friedman, R. C., Farh, K. K. H., Burge, C. B. & Bartel, D. P. Most mammalian mRNAs are conserved targets of microRNAs. *Genome Research* **19**, 92–105 (2009).
76. Shenoy, A. & Belloch, R. H. Regulation of microRNA function in somatic stem cell proliferation and differentiation. *Nature Reviews Molecular Cell Biology* vol. 15 565–576 Preprint at <https://doi.org/10.1038/nrm3854> (2014).
77. Ambros, V. MicroRNAs and developmental timing. *Current Opinion in Genetics and Development* vol. 21 511–517 Preprint at <https://doi.org/10.1016/j.gde.2011.04.003> (2011).
78. Bushati, N. & Cohen, S. M. microRNA Functions. *Annual Review of Cell and Developmental Biology* **23**, 175–205 (2007).
79. Chen, X. Small RNAs and Their Roles in Plant Development. *Annual Review of Cell and Developmental Biology* **25**, 21–44 (2009).

80. Sunkar, R., Li, Y. F. & Jagadeeswaran, G. Functions of microRNAs in plant stress responses. *Trends in Plant Science* vol. 17 196–203 Preprint at <https://doi.org/10.1016/j.tplants.2012.01.010> (2012).
81. Birlik, M., Koçak, A. & Harmanci, D. Role of MicroRNAs in Rheumatoid Arthritis. in *New Developments in the Pathogenesis of Rheumatoid Arthritis* (InTech, 2017). doi:10.5772/67081.
82. Wang, M., Qin, L. & Tang, B. MicroRNAs in Alzheimer's disease. *Frontiers in Genetics* vol. 10 153 Preprint at <https://doi.org/10.3389/fgene.2019.00153> (2019).
83. Peng, Y. & Croce, C. M. The role of microRNAs in human cancer. *Signal Transduction and Targeted Therapy* vol. 1 1–9 Preprint at <https://doi.org/10.1038/sigtrans.2015.4> (2016).
84. Dawson, O. & Piccinini, A. M. miR-155-3p: processing by-product or rising star in immunity and cancer? *Open Biology* **12**, 220070 (2022).
85. Lee, Y. *et al.* MicroRNA genes are transcribed by RNA polymerase II. *EMBO Journal* **23**, 4051–4060 (2004).
86. Krol, J., Loedige, I. & Filipowicz, W. The widespread regulation of microRNA biogenesis, function and decay. *Nature Reviews Genetics* vol. 11 597–610 Preprint at <https://doi.org/10.1038/nrg2843> (2010).
87. Lee, Y., Jeon, K., Lee, J. T., Kim, S. & Kim, V. N. MicroRNA maturation: Stepwise processing and subcellular localization. *EMBO Journal* **21**, 4663–4670 (2002).
88. Lagos-Quintana, M., Rauhut, R., Lendeckel, W. & Tuschl, T. Identification of novel genes coding for small expressed RNAs. *Science* **294**, 853–858 (2001).
89. Denli, A. M., Tops, B. B. J., Plasterk, R. H. A., Ketting, R. F. & Hannon, G. J. Processing of primary microRNAs by the Microprocessor complex. *Nature* **432**, 231–235 (2004).

90. Gregory, R. I. *et al.* The Microprocessor complex mediates the genesis of microRNAs. *Nature* **432**, 235–240 (2004).
91. Han, J. *et al.* The Drosha-DGCR8 complex in primary microRNA processing. *Genes and Development* **18**, 3016–3027 (2004).
92. Mori, M. *et al.* Hippo signaling regulates microprocessor and links cell-density-dependent mirna biogenesis to cancer. *Cell* **156**, 893–906 (2014).
93. Bohnsack, M. T., Czaplinski, K. & Görlich, D. Exportin 5 is a RanGTP-dependent dsRNA-binding protein that mediates nuclear export of pre-miRNAs. *RNA* **10**, 185–191 (2004).
94. Bernstein, E., Caudy, A. A., Hammond, S. M. & Hannon, G. J. Role for a bidentate ribonuclease in the initiation step of RNA interference. *Nature* **409**, 363–366 (2001).
95. Hutvagner, G. *et al.* A cellular function for the RNA-interference enzyme dicer in the maturation of the let-7 small temporal RNA. *Science* **293**, 834–838 (2001).
96. Ketting, R. F. *et al.* Dicer functions in RNA interference and in synthesis of small RNA involved in developmental timing in *C. elegans*. *Genes and Development* **15**, 2654–2659 (2001).
97. MacRae, I. J. *et al.* Structural basis for double-stranded RNA processing by Dicer. *Science* **311**, 195–198 (2006).
98. Saito, K., Ishizuka, A., Siomi, H. & Siomi, M. C. Processing of Pre-microRNAs by the Dicer-1–Loquacious Complex in *Drosophila* Cells. *PLoS Biology* **3**, e235 (2005).
99. Tian, Y. *et al.* A Phosphate-Binding Pocket within the Platform-PAZ-Connector Helix Cassette of Human Dicer. *Molecular Cell* **53**, 606–616 (2014).

100. Zhang, H., Kolb, F. A., Jaskiewicz, L., Westhof, E. & Filipowicz, W. Single processing center models for human Dicer and bacterial RNase III. *Cell* **118**, 57–68 (2004).
101. Park, J. E. *et al.* Dicer recognizes the 5' end of RNA for efficient and accurate processing. *Nature* **475**, 201–205 (2011).
102. Chendrimada, T. P. *et al.* TRBP recruits the Dicer complex to Ago2 for microRNA processing and gene silencing. *Nature* **436**, 740–744 (2005).
103. Haase, A. D. *et al.* TRBP, a regulator of cellular PKR and HIV-1 virus expression, interacts with Dicer and functions in RNA silencing. *EMBO Reports* **6**, 961–967 (2005).
104. Lee, Y. *et al.* The role of PACT in the RNA silencing pathway. *EMBO Journal* **25**, 522–532 (2006).
105. Elkayam, E. *et al.* The structure of human argonaute-2 in complex with miR-20a. *Cell* **150**, 100–110 (2012).
106. Ma, J. B. *et al.* Structural basis for 5' -end-specific recognition of guide RNA by the *A. fulgidus* Piwi protein. *Nature* **434**, 666–670 (2005).
107. Schirle, N. T. & MacRae, I. J. Structure and Mechanism of Argonaute Proteins. in *Enzymes* vol. 32 83–100 (Academic Press, 2012).
108. Boland, A., Huntzinger, E., Schmidt, S., Izaurralde, E. & Weichenrieder, O. Crystal structure of the MID-PIWI lobe of a eukaryotic argonaute protein. *Proceedings of the National Academy of Sciences of the United States of America* **108**, 10466–10471 (2011).
109. Frank, F., Sonenberg, N. & Nagar, B. Structural basis for 5'-nucleotide base-specific recognition of guide RNA by human AGO2. *Nature* **465**, 818–822 (2010).

110. Park, M. S. *et al.* Multidomain Convergence of Argonaute during RISC Assembly Correlates with the Formation of Internal Water Clusters. *Mol Cell* **75**, 725-740.e6 (2019).
111. Wang, H.-W. *et al.* Structural insights into RNA processing by the human RISC-loading complex. *Nat Struct Mol Biol* **16**, 1148–1153 (2009).
112. Schwarz, D. S. *et al.* Asymmetry in the assembly of the RNAi enzyme complex. *Cell* **115**, 199–208 (2003).
113. Khvorova, A., Reynolds, A. & Jayasena, S. D. Functional siRNAs and miRNAs exhibit strand bias. *Cell* **115**, 209–216 (2003).
114. Suzuki, H. I. *et al.* Small-RNA asymmetry is directly driven by mammalian Argonautes. *Nature Structural and Molecular Biology* **22**, 512–521 (2015).
115. Zinovyeva, A. Y., Veksler-Lublinsky, I., Vashisht, A. A., Wohlschlegel, J. A. & Ambros, V. R. *Caenorhabditis elegans* ALG-1 antimorphic mutations uncover functions for Argonaute in microRNA guide strand selection and passenger strand disposal. *Proc Natl Acad Sci U S A* **112**, E5271-5280 (2015).
116. Medley, J. C., Panzade, G. & Zinovyeva, A. Y. microRNA strand selection: Unwinding the rules. *Wiley Interdiscip Rev RNA* **12**, e1627 (2021).
117. Fernández-Pérez, D., Brieño-Enríquez, M. A., Isoler-Alcaraz, J., Larriba, E. & Mazo, J. D. MicroRNA dynamics at the onset of primordial germ and somatic cell sex differentiation during mouse embryonic gonad development. *RNA* **24**, 287–303 (2018).
118. Fernandez-Valverde, S. L., Taft, R. J. & Mattick, J. S. Dynamic isomiR regulation in *Drosophila* development. *RNA* **16**, 1881–1888 (2010).
119. Woldemariam, N. *et al.* Expanding the miRNA Repertoire in Atlantic Salmon; Discovery of IsomiRs and miRNAs Highly Expressed in Different Tissues and Developmental Stages. *Cells* **8**, 42–42 (2019).

120. Wyman, S. K. *et al.* Post-transcriptional generation of miRNA variants by multiple nucleotidyl transferases contributes to miRNA transcriptome complexity. *Genome Research* **21**, 1450–1461 (2011).
121. Cloonan, N. *et al.* MicroRNAs and their isomiRs function cooperatively to target common biological pathways. *Genome Biology* **12**, R126 (2011).
122. Tan, G. C. *et al.* 5' isomiR variation is of functional and evolutionary importance. *Nucleic Acids Res* **42**, 9424–9435 (2014).
123. Kawahara, Y. *et al.* Redirection of silencing targets by adenosine-to-inosine editing of miRNAs. *Science* **315**, 1137–1140 (2007).
124. Bhardwaj, A. *et al.* The isomiR-140-3p-regulated mevalonic acid pathway as a potential target for prevention of triple negative breast cancer. *Breast Cancer Research* **20**, 150–150 (2018).
125. Griffiths-Jones, S., Hui, J. H. L., Marco, A. & Ronshaugen, M. MicroRNA evolution by arm switching. *EMBO reports* **12**, 172–177 (2011).
126. Yu, S. & Kim, V. N. A tale of non-canonical tails: gene regulation by post-transcriptional RNA tailing. *Nat Rev Mol Cell Biol* **21**, 542–556 (2020).
127. De Almeida, C., Scheer, H., Zuber, H. & Gagliardi, D. RNA uridylation: a key posttranscriptional modification shaping the coding and noncoding transcriptome. *Wiley Interdiscip Rev RNA* **9**, (2018).
128. Nishikura, K. A-to-I editing of coding and non-coding RNAs by ADARs. *Nat Rev Mol Cell Biol* **17**, 83–96 (2016).
129. Bazak, L. *et al.* A-to-I RNA editing occurs at over a hundred million genomic sites, located in a majority of human genes. *Genome Res* **24**, 365–376 (2014).
130. Li, L. *et al.* The landscape of miRNA editing in animals and its impact on miRNA biogenesis and targeting. *Genome Research* **28**, 132–143 (2018).

131. Han, B. W., Hung, J.-H., Weng, Z., Zamore, P. D. & Ameres, S. L. The 3'-to-5' exoribonuclease Nibbler shapes the 3' ends of microRNAs bound to Drosophila Argonaute1. *Curr Biol* **21**, 1878–1887 (2011).
132. Katoh, T. *et al.* Selective stabilization of mammalian microRNAs by 3' adenylation mediated by the cytoplasmic poly(A) polymerase GLD-2. *Genes Dev* **23**, 433–438 (2009).
133. Burroughs, A. M. *et al.* A comprehensive survey of 3' animal miRNA modification events and a possible role for 3' adenylation in modulating miRNA targeting effectiveness. *Genome Res* **20**, 1398–1410 (2010).
134. Jones, M. R. *et al.* Zcchc11-dependent uridylation of microRNA directs cytokine expression. *Nat Cell Biol* **11**, 1157–1163 (2009).
135. Kim, H. *et al.* A Mechanism for microRNA Arm Switching Regulated by Uridylation. *Molecular Cell* **78**, 1224-1236.e5 (2020).
136. Liu, N. *et al.* The exoribonuclease Nibbler controls 3' end processing of microRNAs in Drosophila. *Curr Biol* **21**, 1888–1893 (2011).
137. Katoh, T., Hojo, H. & Suzuki, T. Destabilization of microRNAs in human cells by 3' deadenylation mediated by PARN and CUGBP1. *Nucleic Acids Res* **43**, 7521–7534 (2015).
138. Yang, A. *et al.* AGO-bound mature miRNAs are oligouridylated by TUTs and subsequently degraded by DIS3L2. *Nat Commun* **11**, 2765 (2020).
139. Thornton, J. E. *et al.* Selective microRNA uridylation by Zcchc6 (TUT7) and Zcchc11 (TUT4). *Nucleic Acids Res* **42**, 11777–11791 (2014).
140. Cesarini, V. *et al.* ADAR2/miR-589-3p axis controls glioblastoma cell migration/invasion. *Nucleic Acids Res* **46**, 2045–2059 (2018).

141. Marceca, G. P. *et al.* MiREDiBase: a manually curated database of validated and putative editing events in microRNAs. 2020.09.04.283689 Preprint at <https://doi.org/10.1101/2020.09.04.283689> (2021).
142. Kwon, S. C. *et al.* Molecular Basis for the Single-Nucleotide Precision of Primary microRNA Processing. *Molecular Cell* **73**, 505-518.e5 (2019).
143. Jin, W., Wang, J., Liu, C.-P., Wang, H.-W. & Xu, R.-M. Structural Basis for pri-miRNA Recognition by Drosha. *Molecular Cell* **0**, (2020).
144. Faller, M. *et al.* DGCR8 recognizes primary transcripts of microRNAs through highly cooperative binding and formation of higher-order structures. *RNA* **16**, 1570–1570 (2010).
145. Partin, A. C. *et al.* Cryo-EM Structures of Human Drosha and DGCR8 in Complex with Primary MicroRNA. *Molecular Cell* **78**, 411-422.e4 (2020).
146. Dang, T. L. *et al.* Select amino acids in DGCR8 are essential for the UGU-pri-miRNA interaction and processing. *Communications Biology* 2020 3:1 **3**, 1–11 (2020).
147. Roden, C. *et al.* Novel determinants of mammalian primary microRNA processing revealed by systematic evaluation of hairpin-containing transcripts and human genetic variation. *Genome Research* **27**, 374–384 (2017).
148. Fang, W. & Bartel, D. P. The Menu of Features that Define Primary MicroRNAs and Enable De Novo Design of MicroRNA Genes. *Molecular Cell* **60**, 131–145 (2015).
149. Le, C. T., Nguyen, T. L., Nguyen, T. D. & Nguyen, T. A. Human disease-associated single nucleotide polymorphism changes the orientation of DROSHA on pri-mir-146a. *RNA* **26**, 1777–1786 (2020).

150. Nguyen, T. L., Nguyen, T. D., Bao, S., Li, S. & Nguyen, T. A. The internal loops in the lower stem of primary microRNA transcripts facilitate single cleavage of human Microprocessor. *Nucleic Acids Res* **48**, 2579–2593 (2020).
151. Li, S., Nguyen, T. D., Nguyen, T. L. & Nguyen, T. A. Mismatched and wobble base pairs govern primary microRNA processing by human Microprocessor. *Nat Commun* **11**, 1926 (2020).
152. Li, S., Le, T. N. Y., Nguyen, T. D., Trinh, T. A. & Nguyen, T. A. Bulges control primary miRNA processing in a position and strand-dependent manner. *RNA Biology* **18**, 1716–1716 (2021).
153. Kim, K. *et al.* A quantitative map of human primary microRNA processing sites. *Molecular Cell* **81**, 3422-3439.e11 (2021).
154. Kelaini, S., Chan, C., Cornelius, V. A. & Margariti, A. RNA-Binding Proteins Hold Key Roles in Function, Dysfunction, and Disease. *Biology (Basel)* **10**, 366 (2021).
155. Michlewski, G. & Cáceres, J. F. Antagonistic role of hnRNP A1 and KSRP in the regulation of Let-7a biogenesis. *Nat Struct Mol Biol* **17**, 1011–1018 (2010).
156. Guil, S. & Cáceres, J. F. The multifunctional RNA-binding protein hnRNP A1 is required for processing of miR-18a. *Nat Struct Mol Biol* **14**, 591–596 (2007).
157. Weiss, K., Treiber, T., Meister, G. & Schratt, G. The nuclear matrix protein Matr3 regulates processing of the synaptic microRNA-138-5p. *Neurobiology of Learning and Memory* **159**, 36–45 (2019).
158. Wu, S.-L. *et al.* Genome-wide analysis of YB-1-RNA interactions reveals a novel role of YB-1 in miRNA processing in glioblastoma multiforme. *Nucleic Acids Res* **43**, 8516–8528 (2015).
159. Liu, X. *et al.* YB1 regulates miR-205/200b-ZEB1 axis by inhibiting microRNA maturation in hepatocellular carcinoma. *Cancer Communications* **41**, 576–595 (2021).

160. Mayr, F. & Heinemann, U. Mechanisms of Lin28-Mediated miRNA and mRNA Regulation—A Structural and Functional Perspective. *Int J Mol Sci* **14**, 16532–16553 (2013).
161. Kim, K., Nguyen, T. D., Li, S. & Nguyen, T. A. SRSF3 recruits DROSHA to the basal junction of primary microRNAs. *RNA* **24**, 892–898 (2018).
162. Alarcón, C. R. *et al.* HNRNPA2B1 Is a Mediator of m(6)A-Dependent Nuclear RNA Processing Events. *Cell* **162**, 1299–1308 (2015).
163. Knuckles, P. *et al.* RNA fate determination through cotranscriptional adenosine methylation and microprocessor binding. *Nat Struct Mol Biol* **24**, 561–569 (2017).
164. Heale, B. S. E. *et al.* Editing independent effects of ADARs on the miRNA/siRNA pathways. *EMBO J* **28**, 3145–3156 (2009).
165. Trabucchi, M. *et al.* The RNA-binding protein KSRP promotes the biogenesis of a subset of microRNAs. *Nature* **459**, 1010–1014 (2009).
166. Kawahara, Y. & Mieda-Sato, A. TDP-43 promotes microRNA biogenesis as a component of the Drosha and Dicer complexes. *Proc Natl Acad Sci U S A* **109**, 3347–3352 (2012).
167. Chen, Y. *et al.* Rbfox proteins regulate microRNA biogenesis by sequence-specific binding to their precursors and target downstream Dicer. *Nucleic Acids Res* **44**, 4381–4395 (2016).
168. Ouyang, H. *et al.* The RNA binding protein EWS is broadly involved in the regulation of pri-miRNA processing in mammalian cells. *Nucleic Acids Res* **45**, 12481–12495 (2017).
169. Choudhury, N. R. *et al.* Tissue-specific control of brain-enriched miR-7 biogenesis. *Genes Dev* **27**, 24–38 (2013).

170. Rau, F. *et al.* Misregulation of miR-1 processing is associated with heart defects in myotonic dystrophy. *Nat Struct Mol Biol* **18**, 840–845 (2011).
171. Volk, N. & Shomron, N. Versatility of MicroRNA Biogenesis. *PLOS ONE* **6**, e19391 (2011).
172. Kim, K. K., Yang, Y., Zhu, J., Adelstein, R. S. & Kawamoto, S. Rbfox3 Controls the Biogenesis of a Subset of MicroRNAs. *Nat Struct Mol Biol* **21**, 901–910 (2014).
173. Morlando, M. *et al.* FUS stimulates microRNA biogenesis by facilitating co-transcriptional Drosha recruitment. *The EMBO Journal* **31**, 4502–4510 (2012).
174. Sakamoto, S. *et al.* The NF90-NF45 Complex Functions as a Negative Regulator in the MicroRNA Processing Pathway. *Mol Cell Biol* **29**, 3754–3769 (2009).
175. Zhao, L., Mao, Y., Zhao, Y. & He, Y. DDX3X promotes the biogenesis of a subset of miRNAs and the potential roles they played in cancer development. *Sci Rep* **6**, 32739 (2016).
176. Hammond, S. M., Boettcher, S., Caudy, A. A., Kobayashi, R. & Hannon, G. J. Argonaute2, a link between genetic and biochemical analyses of RNAi. *Science* **293**, 1146–1150 (2001).
177. Schirle, N. T. & MacRae, I. J. The crystal structure of human argonaute2. *Science* **336**, 1037–1040 (2012).
178. Lytle, J. R., Yario, T. A. & Steitz, J. A. Target mRNAs are repressed as efficiently by microRNA-binding sites in the 5' UTR as in the 3' UTR. *Proceedings of the National Academy of Sciences of the United States of America* **104**, 9667–9672 (2007).
179. Liu, J. *et al.* Argonaute2 is the catalytic engine of mammalian RNAi. *Science* **305**, 1437–1441 (2004).
180. Meister, G. *et al.* Human Argonaute2 mediates RNA cleavage targeted by miRNAs and siRNAs. *Molecular Cell* **15**, 185–197 (2004).

181. Iwakawa, H. & Tomari, Y. The Functions of MicroRNAs: mRNA Decay and Translational Repression. *Trends in Cell Biology* vol. 25 651–665 Preprint at <https://doi.org/10.1016/j.tcb.2015.07.011> (2015).
182. Bartel, D. P. MicroRNAs: Target Recognition and Regulatory Functions. *Cell* vol. 136 215–233 Preprint at <https://doi.org/10.1016/j.cell.2009.01.002> (2009).
183. Ameres, S. L. & Zamore, P. D. Diversifying microRNA sequence and function. *Nature Reviews Molecular Cell Biology* vol. 14 475–488 Preprint at <https://doi.org/10.1038/nrm3611> (2013).
184. Iwakawa, H. & Tomari, Y. Life of RISC: Formation, action, and degradation of RNA-induced silencing complex. *Molecular Cell* **82**, 30–43 (2022).
185. Banani, S. F., Lee, H. O., Hyman, A. A. & Rosen, M. K. Biomolecular condensates: organizers of cellular biochemistry. *Nat Rev Mol Cell Biol* **18**, 285–298 (2017).
186. Parker, R. & Sheth, U. P Bodies and the Control of mRNA Translation and Degradation. *Molecular Cell* **25**, 635–646 (2007).
187. Luo, Y., Na, Z. & Slavoff, S. A. P-Bodies: Composition, Properties, and Functions. *Biochemistry* **57**, 2424–2431 (2018).
188. Bagga, S. *et al.* Regulation by let-7 and lin-4 miRNAs results in target mRNA degradation. *Cell* **122**, 553–563 (2005).
189. Behm-Ansmant, I. *et al.* mRNA degradation by miRNAs and GW182 requires both CCR4:NOT deadenylase and DCP1:DCP2 decapping complexes. *Genes and Development* **20**, 1885–1898 (2006).
190. Fabian, M. R. *et al.* MiRNA-mediated deadenylation is orchestrated by GW182 through two conserved motifs that interact with CCR4-NOT. *Nature Structural and Molecular Biology* **18**, 1211–1217 (2011).

191. Braun, J. E., Huntzinger, E., Fauser, M. & Izaurralde, E. GW182 proteins directly recruit cytoplasmic deadenylase complexes to miRNA targets. *Molecular Cell* **44**, 120–133 (2011).
192. Jinek, M., Fabian, M. R., Coyle, S. M., Sonenberg, N. & Doudna, J. A. Structural insights into the human GW182-PABC interaction in microRNA-mediated deadenylation. *Nature Structural and Molecular Biology* **17**, 238–240 (2010).
193. Behm-Ansmant, I. *et al.* mRNA degradation by miRNAs and GW182 requires both CCR4:NOT deadenylase and DCP1:DCP2 decapping complexes. *Genes and Development* **20**, 1885–1898 (2006).
194. Rehwinkel, J., Behm-Ansmant, I., Gatfield, D. & Izaurralde, E. A crucial role for GW182 and the DCP1:DCP2 decapping complex in miRNA-mediated gene silencing. *RNA* **11**, 1640–1647 (2005).
195. Eulalio, A. *et al.* Target-specific requirements for enhancers of decapping in miRNA-mediated gene silencing. *Genes and Development* **21**, 2558–2570 (2007).
196. Braun, J. E. *et al.* A direct interaction between DCP1 and XRN1 couples mRNA decapping to 5' exonucleolytic degradation. *Nature Structural and Molecular Biology* **19**, 1324–1331 (2012).
197. Makino, S., Mishima, Y., Inoue, K. & Inada, T. Roles of mRNA fate modulators Dhh1 and Pat1 in TNRC6-dependent gene silencing recapitulated in yeast. *Journal of Biological Chemistry* **290**, 8331–8347 (2015).
198. Moretti, F., Kaiser, C., Zdanowicz-Specht, A. & Hentze, M. W. PABP and the poly(A) tail augment microRNA repression by facilitated miRISC binding. *Nature Structural and Molecular Biology* **19**, 603–608 (2012).

199. Zekri, L., Kuzuoğlu-Öztürk, D. & Izaurralde, E. GW182 proteins cause PABP dissociation from silenced miRNA targets in the absence of deadenylation. *The EMBO Journal* **32**, 1052–1065 (2013).
200. Kanwar, J. R., Mahidhara, G. & Kanwar, R. K. MicroRNA in human cancer and chronic inflammatory diseases. *Frontiers in Bioscience - Scholar* vol. 2 S 1113–1126 Preprint at <https://doi.org/10.2741/s121> (2010).
201. Taganov, K. D., Boldin, M. P., Chang, K. J. & Baltimore, D. NF- κ B-dependent induction of microRNA miR-146, an inhibitor targeted to signaling proteins of innate immune responses. *Proceedings of the National Academy of Sciences of the United States of America* **103**, 12481–12486 (2006).
202. Thai, T. H. *et al.* Regulation of the germinal center response by MicroRNA-155. *Science* **316**, 604–608 (2007).
203. Bayraktar, R., Bertilaccio, M. T. S. & Calin, G. A. The interaction between two worlds: MicroRNAs and Toll-like receptors. *Frontiers in Immunology* vol. 10 Preprint at <https://doi.org/10.3389/fimmu.2019.01053> (2019).
204. McCoy, C. E. *et al.* IL-10 inhibits miR-155 induction by toll-like receptors. *Journal of Biological Chemistry* **285**, 20492–20498 (2010).
205. Costinean, S. *et al.* Src homology 2 domain-containing inositol-5-phosphatase and CCAAT enhancer-binding protein β are targeted by miR-155 in B cells of μ -MiR-155 transgenic mice. *Blood* **114**, 1374–1382 (2009).
206. O’Connell, R. M., Chaudhuri, A. A., Rao, D. S. & Baltimore, D. Inositol phosphatase SHIP1 is a primary target of miR-155. *Proceedings of the National Academy of Sciences of the United States of America* **106**, 7113–7118 (2009).
207. Wang, D. *et al.* MiRNA-155 Regulates the Th17/Treg Ratio by Targeting SOCS1 in Severe Acute Pancreatitis. *Frontiers in Physiology* **9**, 686–686 (2018).

208. Tili, E. *et al.* Modulation of miR-155 and miR-125b Levels following Lipopolysaccharide/TNF- α Stimulation and Their Possible Roles in Regulating the Response to Endotoxin Shock. *The Journal of Immunology* **179**, 5082–5089 (2007).
209. O’Hara, S. P. *et al.* NF κ B p50-CCAAT/enhancer-binding protein β (C/EBP β)-mediated transcriptional repression of microRNA let-7i following microbial infection. *Journal of Biological Chemistry* **285**, 216–225 (2010).
210. Bazzoni, F. *et al.* Induction and regulatory function of miR-9 in human monocytes and neutrophils exposed to proinflammatory signals. *Proceedings of the National Academy of Sciences of the United States of America* **106**, 5282–5287 (2009).
211. Sheedy, F. J. *et al.* Negative regulation of TLR4 via targeting of the proinflammatory tumor suppressor PDCD4 by the microRNA miR-21. *Nature Immunology* **11**, 141–147 (2010).
212. Rossato, M. *et al.* IL-10-induced microRNA-187 negatively regulates TNF- α , IL-6, and IL-12p40 production in TLR4-stimulated monocytes. *Proceedings of the National Academy of Sciences of the United States of America* **109**, E3101–E3110 (2012).
213. Huang, R. S., Hu, G. Q., Lin, B., Lin, Z. Y. & Sun, C. C. MicroRNA-155 silencing enhances inflammatory response and lipid uptake in oxidized low-density lipoprotein-stimulated human THP-1 macrophages. *Journal of Investigative Medicine* (2010) doi:10.2310/JIM.0b013e3181ff46d7.
214. Worm, J. *et al.* Silencing of microRNA-155 in mice during acute inflammatory response leads to derepression of c/ebp Beta and down-regulation of G-CSF. *Nucleic Acids Research* (2009) doi:10.1093/nar/gkp577.

215. Landgraf, P. *et al.* A Mammalian microRNA Expression Atlas Based on Small RNA Library Sequencing. *Cell* **129**, 1401–1414 (2007).
216. Brown, B. D. *et al.* Endogenous microRNA can be broadly exploited to regulate transgene expression according to tissue, lineage and differentiation state. *Nature Biotechnology* **25**, 1457–1467 (2007).
217. Wang, P. *et al.* Inducible microRNA-155 Feedback Promotes Type I IFN Signaling in Antiviral Innate Immunity by Targeting Suppressor of Cytokine Signaling 1. *The Journal of Immunology* **185**, 6226–6233 (2010).
218. Tili, E. *et al.* Modulation of miR-155 and miR-125b Levels following Lipopolysaccharide/TNF- α Stimulation and Their Possible Roles in Regulating the Response to Endotoxin Shock. *The Journal of Immunology* **179**, 5082–5089 (2007).
219. Kohlhaas, S. *et al.* Cutting Edge: The Foxp3 Target miR-155 Contributes to the Development of Regulatory T Cells. *The Journal of Immunology* **182**, 2578–2582 (2009).
220. Tang, B. *et al.* Identification of MyD88 as a novel target of miR-155, involved in negative regulation of Helicobacter pylori-induced inflammation. *FEBS Letters* **584**, 1481–1486 (2010).
221. Ceppi, M. *et al.* MicroRNA-155 modulates the interleukin-1 signaling pathway in activated human monocyte-derived dendritic cells. *Proceedings of the National Academy of Sciences of the United States of America* **106**, 2735–2740 (2009).
222. Androulidaki, A. *et al.* The Kinase Akt1 Controls Macrophage Response to Lipopolysaccharide by Regulating MicroRNAs. *Immunity* **31**, 220–231 (2009).
223. Ruggiero, T. *et al.* LPS induces KH-type splicing regulatory protein-dependent processing of microRNA-155 precursors in macrophages. *The FASEB Journal* **23**, 2898–2908 (2009).

224. Hou, J. *et al.* MicroRNA-146a Feedback Inhibits RIG-I-Dependent Type I IFN Production in Macrophages by Targeting TRAF6, IRAK1, and IRAK2. *The Journal of Immunology* **183**, 2150–2158 (2009).
225. Nahid, M. A., Pauley, K. M., Satoh, M. & Chan, E. K. L. miR-146a is critical for endotoxin-induced tolerance: Implication in innate immunity. *Journal of Biological Chemistry* **284**, 34590–34599 (2009).
226. Lagos, D. *et al.* MiR-132 regulates antiviral innate immunity through suppression of the p300 transcriptional co-activator. *Nature Cell Biology* **12**, 513–519 (2010).
227. Shaked, I. *et al.* MicroRNA-132 Potentiates Cholinergic Anti-Inflammatory Signaling by Targeting Acetylcholinesterase. *Immunity* **31**, 965–973 (2009).
228. Lu, T. X., Munitz, A. & Rothenberg, M. E. MicroRNA-21 Is Up-Regulated in Allergic Airway Inflammation and Regulates IL-12p35 Expression. *The Journal of Immunology* **182**, 4994–5002 (2009).
229. Moschos, S. A. *et al.* Expression profiling in vivo demonstrates rapid changes in lung microRNA levels following lipopolysaccharide-induced inflammation but not in the anti-inflammatory action of glucocorticoids. *BMC Genomics* **8**, 240 (2007).
230. Li, T. *et al.* MicroRNAs modulate the noncanonical transcription factor NF- κ B pathway by regulating expression of the kinase IKK α during macrophage differentiation. *Nature Immunology* **11**, 799–805 (2010).
231. Heikham, R. & Shankar, R. Flanking region sequence information to refine microRNA target predictions. *Journal of Biosciences* **35**, 105–118 (2010).
232. Liu, G. *et al.* miR-147, a microRNA that is induced upon toll-like receptor stimulation, regulates murine macrophage inflammatory responses.

- Proceedings of the National Academy of Sciences of the United States of America* **106**, 15819–15824 (2009).
233. El Gazzar, M. & McCall, C. E. MicroRNAs distinguish translational from transcriptional silencing during endotoxin tolerance. *Journal of Biological Chemistry* **285**, 20940–20951 (2010).
234. Alsaleh, G. *et al.* Bruton's Tyrosine Kinase Is Involved in miR-346-Related Regulation of IL-18 Release by Lipopolysaccharide-Activated Rheumatoid Fibroblast-Like Synoviocytes. *The Journal of Immunology* **182**, 5088–5097 (2009).
235. Jennewein, C., Von Knethen, A., Schmid, T. & Brüne, B. MicroRNA-27b contributes to lipopolysaccharide-mediated peroxisome proliferator-activated receptor γ (PPAR γ) mRNA destabilization. *Journal of Biological Chemistry* **285**, 11846–11853 (2010).
236. Fu, Y. *et al.* Downregulated miR-98-5p promotes PDAC proliferation and metastasis by reversely regulating MAP4K4. *Journal of Experimental and Clinical Cancer Research* **37**, 130 (2018).
237. Valadi, H. *et al.* Exosome-mediated transfer of mRNAs and microRNAs is a novel mechanism of genetic exchange between cells. *Nature Cell Biology* **9**, 654–659 (2007).
238. Tam, W., Ben-Yehuda, D. & Hayward, W. S. bic, a novel gene activated by proviral insertions in avian leukosis virus-induced lymphomas, is likely to function through its noncoding RNA. *Molecular and Cellular Biology* **17**, 1490–1502 (1997).
239. Lagos-Quintana, M. *et al.* Identification of tissue-specific MicroRNAs from mouse. *Current Biology* **12**, 735–739 (2002).

240. Tam, W. Identification and characterization of human BIC, a gene on chromosome 21 that encodes a noncoding RNA. *Gene* **274**, 157–167 (2001).
241. Elton, T. S., Selemon, H., Elton, S. M. & Parinandi, N. L. Regulation of the MIR155 host gene in physiological and pathological processes. *Gene* **532**, 1–12 (2013).
242. Mashima, R. Physiological roles of miR-155. *Immunology* **145**, 323–333 (2015).
243. Alivernini, S. *et al.* MicroRNA-155-at the critical interface of innate and adaptive immunity in arthritis. *Frontiers in Immunology* vol. 8 1932 Preprint at <https://doi.org/10.3389/fimmu.2017.01932> (2018).
244. Zhang, J. *et al.* MicroRNA-155 modulates Th1 and Th17 cell differentiation and is associated with multiple sclerosis and experimental autoimmune encephalomyelitis. *Journal of Neuroimmunology* **266**, 56–63 (2014).
245. Bhela, S. *et al.* Role of miR-155 in the pathogenesis of herpetic stromal keratitis. *American Journal of Pathology* **185**, 1073–1084 (2015).
246. Higgs, G. & Slack, F. The multiple roles of microRNA-155 in oncogenesis. *Journal of Clinical Bioinformatics* vol. 3 17 Preprint at <https://doi.org/10.1186/2043-9113-3-17> (2013).
247. Martinez-Nunez, R. T., Louafi, F. & Sanchez-Elsner, T. The interleukin 13 (IL-13) pathway in human macrophages is modulated by microRNA-155 via direct targeting of interleukin 13 receptor $\alpha 1$ (IL13R $\alpha 1$). *Journal of Biological Chemistry* **286**, 1786–1794 (2011).
248. Martinez-Nunez, R. T., Louafi, F., Friedmann, P. S. & Sanchez-Eisner, T. MicroRNA-155 modulates the pathogen binding ability of dendritic cells (DCs) by down-regulation of DC-specific intercellular adhesion molecule-3 grabbing non-integrin (DC-SIGN). *Journal of Biological Chemistry* **284**, 16334–16342 (2009).

249. Mann, M. *et al.* An NF- κ B-microRNA regulatory network tunes macrophage inflammatory responses. *Nat Commun* **8**, 851 (2017).
250. Gatto, G. *et al.* Epstein-Barr virus latent membrane protein 1 trans-activates miR-155 transcription through the NF-kappaB pathway. *Nucleic Acids Res* **36**, 6608–6619 (2008).
251. Thompson, R. C., Vardinogiannis, I. & Gilmore, T. D. Identification of an NF- κ B p50/p65-responsive site in the human MIR155HG promoter. *BMC Mol Biol* **14**, 24 (2013).
252. O’Connell, R. M., Taganov, K. D., Boldin, M. P., Cheng, G. & Baltimore, D. MicroRNA-155 is induced during the macrophage inflammatory response. *Proceedings of the National Academy of Sciences* **104**, 1604–1609 (2007).
253. Yin, Q., Wang, X., McBride, J., Fewell, C. & Flemington, E. B-cell Receptor Activation Induces BIC/miR-155 Expression through a Conserved AP-1 Element. *J Biol Chem* **283**, 2654–2662 (2008).
254. Tili, E. *et al.* Resveratrol decreases the levels of miR-155 by upregulating miR-663, a microRNA targeting JunB and JunD. *Carcinogenesis* **31**, 1561–1566 (2010).
255. Chang, S. *et al.* Tumor suppressor BRCA1 epigenetically controls oncogenic microRNA-155. *Nat Med* **17**, 1275–1282 (2011).
256. Zhao, H. *et al.* Transforming Growth Factor β 1/Smad4 Signaling Affects Osteoclast Differentiation via Regulation of miR-155 Expression. *Mol Cells* **40**, 211–221 (2017).
257. Kong, W. *et al.* MicroRNA-155 Is Regulated by the Transforming Growth Factor β /Smad Pathway and Contributes to Epithelial Cell Plasticity by Targeting RhoA. *Mol Cell Biol* **28**, 6773–6784 (2008).

258. Auyeung, V. C., Ulitsky, I., McGeary, S. E. & Bartel, D. P. Beyond secondary structure: Primary-sequence determinants license Pri-miRNA hairpins for processing. *Cell* **152**, 844–858 (2013).
259. Landeros, N., Gonzalez-Hormazabal, P., Pérez-Moreno, P., Tapia, J. C. & Jara, L. A Single Variant in Pri-miRNA-155 Associated with Susceptibility to Hereditary Breast Cancer Promotes Aggressiveness in Breast Cancer Cells. *International Journal of Molecular Sciences* **23**, 15418 (2022).
260. Zhang, X., Wan, G., Berger, F. G., He, X. & Lu, X. The ATM kinase induces microRNA biogenesis in the DNA damage response. *Mol Cell* **41**, 371–383 (2011).
261. Zhou, H. *et al.* MiR-155 and its star-form partner miR-155* cooperatively regulate type I interferon production by human plasmacytoid dendritic cells. *Blood* **116**, 5885–5894 (2010).
262. Zheng, J. *et al.* Nogo-B inhibition restricts ulcerative colitis via inhibiting p68/miR-155 signaling pathway. *International Immunopharmacology* **120**, 110378 (2023).
263. Shiohama, A., Sasaki, T., Noda, S., Minoshima, S. & Shimizu, N. Nucleolar localization of DGCR8 and identification of eleven DGCR8-associated proteins. *Exp Cell Res* **313**, 4196–4207 (2007).
264. Treiber, T. *et al.* A Compendium of RNA-Binding Proteins that Regulate MicroRNA Biogenesis. *Molecular Cell* **66**, 270-284.e13 (2017).
265. Gantier, M. P. *et al.* Analysis of microRNA turnover in mammalian cells following Dicer1 ablation. *Nucleic Acids Res* **39**, 5692–5703 (2011).
266. Xie, K. *et al.* A functional variant in miR-155 regulation region contributes to lung cancer risk and survival. *Oncotarget* **6**, 42781–42792 (2015).

267. Jiang, S. *et al.* MicroRNA-155 functions as an oncomiR in breast cancer by targeting the suppressor of cytokine signaling 1 gene. *Cancer Research* **70**, 3119–3127 (2010).
268. Liu, J., Chen, Z., Xiang, J. & Gu, X. MicroRNA-155 acts as a tumor suppressor in colorectal cancer by targeting CTHRC1 in vitro. *Oncology Letters* **15**, 5561–5568 (2018).
269. Qu, Y. *et al.* MicroRNA-155 promotes gastric cancer growth and invasion by negatively regulating transforming growth factor- β receptor 2. *Cancer Science* **109**, 618–628 (2018).
270. Baradaran, B., Shahbazi, R. & Khordadmehr, M. Dysregulation of key microRNAs in pancreatic cancer development. *Biomedicine and Pharmacotherapy* vol. 109 1008–1015 Preprint at <https://doi.org/10.1016/j.biopha.2018.10.177> (2019).
271. Lin, Q. *et al.* A cluster of specified microRNAs in peripheral blood as biomarkers for metastatic non-small-cell lung cancer by stem-loop RT-PCR. *Journal of Cancer Research and Clinical Oncology* **138**, 85–93 (2012).
272. Atakan Ekiz, H. *et al.* MicroRNA-155 coordinates the immunological landscape within murine melanoma and correlates with immunity in human cancers. *JCI Insight* **4**, (2019).
273. Liu, Q. *et al.* MiR-155 regulates glioma cells invasion and chemosensitivity by p38 isforms in vitro. *Journal of Cellular Biochemistry* **116**, 1213–1221 (2015).
274. S, L., QS, L. & L, T. MiR-155 Affects Osteosarcoma Cell Proliferation and Invasion Through Regulating NF- κ B Signaling Pathway. *European review for medical and pharmacological sciences* **22**, (2018).
275. Van Roosbroeck, K. *et al.* Combining anti-miR-155 with chemotherapy for the treatment of lung cancers. *Clinical Cancer Research* **23**, 2891–2904 (2017).

276. Chen, L., Jiang, K., Jiang, H. & Wei, P. miR-155 mediates drug resistance in osteosarcoma cells via inducing autophagy. *Experimental and Therapeutic Medicine* **8**, 527–532 (2014).
277. Tili, E., Croce, C. M. & Michaille, J. J. MiR-155: On the crosstalk between inflammation and cancer. *International Reviews of Immunology* **28**, 264–284 (2009).
278. Wilkie, K. P. & Hahnfeldt, P. Modeling the Dichotomy of the Immune Response to Cancer: Cytotoxic Effects and Tumor-Promoting Inflammation. *Bulletin of Mathematical Biology* **79**, 1426–1448 (2017).
279. Chen, S. *et al.* Host miR155 promotes tumor growth through a myeloid-derived suppressor cell-dependent mechanism. *Cancer Research* **75**, 519–531 (2015).
280. McInnes, I. B. & Schett, G. The pathogenesis of rheumatoid arthritis. *The New England journal of medicine* vol. 365 2205–2219 Preprint at <https://doi.org/10.1056/NEJMra1004965> (2011).
281. Kurowska-Stolarska, M. *et al.* MicroRNA-155 as a proinflammatory regulator in clinical and experimental arthritis. *Proceedings of the National Academy of Sciences of the United States of America* **108**, 11193–11198 (2011).
282. Elmesmari, A. *et al.* MicroRNA-155 regulates monocyte chemokine and chemokine receptor expression in Rheumatoid Arthritis. *Rheumatology (United Kingdom)* (2016) doi:10.1093/rheumatology/kew272.
283. Syed, Safiya; Amin, Mohammed; Rabquer, Bradley. miR155 Expression is Increased by Inflammation and Modulates the Expression of CD11a in Monocytes. *FASEB J* **29(Suppl 1)**, (2015).
284. Radstake, T. R. D. J. *et al.* Expression of toll-like receptors 2 and 4 in rheumatoid synovial tissue and regulation by proinflammatory cytokines interleukin-12 and interleukin-18 via interferon- γ . *Arthritis and Rheumatism* **50**, 3856–3865 (2004).

285. Lee, E. K., Kang, S. M., Paik, D. J., Kim, J. M. & Youn, J. Essential roles of Toll-like receptor-4 signaling in arthritis induced by type II collagen antibody and LPS. *International Immunology* (2005) doi:10.1093/intimm/dxh212.
286. Page, T. H. *et al.* Raised circulating tenascin-C in rheumatoid arthritis. *Arthritis Research and Therapy* **14**, (2012).
287. Raza, K. *et al.* Detection of antibodies to citrullinated tenascin-C in patients with early synovitis is associated with the development of rheumatoid arthritis. *RMD Open* **2**, e000318 (2016).
288. Aungier, S. R. *et al.* Targeting early changes in the synovial microenvironment: A new class of immunomodulatory therapy? *Annals of the Rheumatic Diseases* **78**, 186–191 (2019).
289. Piccinini, A. M. & Midwood, K. S. Endogenous Control of Immunity against Infection: Tenascin-C Regulates TLR4-Mediated Inflammation via MicroRNA-155. *Cell Reports* **2**, 914–926 (2012).
290. Hynes, R. O. The extracellular matrix: Not just pretty fibrils. *Science* vol. 326 1216–1219 Preprint at <https://doi.org/10.1126/science.1176009> (2009).
291. Lu, P., Weaver, V. M. & Werb, Z. The extracellular matrix: A dynamic niche in cancer progression. *Journal of Cell Biology* vol. 196 395–406 Preprint at <https://doi.org/10.1083/jcb.201102147> (2012).
292. Erickson, H. P. & Inglesias, J. L. A six-armed oligomer isolated from cell surface fibronectin preparations. *Nature* **311**, 267–269 (1984).
293. Jones, F. S. & Jones, P. L. The tenascin family of ECM glycoproteins: Structure, function, and regulation during embryonic development and tissue remodeling. *Developmental Dynamics* **218**, 235–259 (2000).

294. Giblin, S. P. & Midwood, K. S. Tenascin-C: Form versus function. *Cell Adhesion and Migration* vol. 9 48–82 Preprint at <https://doi.org/10.4161/19336918.2014.987587> (2015).
295. Chiquet-Ehrismann, R. *et al.* Tenascin Variants: Differential Binding to Fibronectin and Distinct Distribution in Cell Cultures and Tissues. *CELL REGULATION* vol. 2 (1991).
296. A. Ghert, M., Qi, W., P. Erickson, H., A. Block, J. & P. Scully, S. Tenascin-C Splice Variant Adhesive/anti-Adhesive Effects on Chondrosarcoma Cell Attachment to Fibronectin. *Cell Structure and Function* **26**, 179–187 (2001).
297. Chiquet-Ehrismann, R., Orend, G., Chiquet, M., Tucker, R. P. & Midwood, K. S. Tenascins in stem cell niches. *Matrix Biology* vol. 37 112–123 Preprint at <https://doi.org/10.1016/j.matbio.2014.01.007> (2014).
298. Midwood, K. S. & Orend, G. The role of tenascin-C in tissue injury and tumorigenesis. *Journal of Cell Communication and Signaling* vol. 3 287–310 Preprint at <https://doi.org/10.1007/s12079-009-0075-1> (2009).
299. Chiquet-Ehrismann, R. & Chiquet, M. Tenascins: Regulation and putative functions during pathological stress. *Journal of Pathology* vol. 200 488–499 Preprint at <https://doi.org/10.1002/path.1415> (2003).
300. Udalova, I. A., Ruhmann, M., Thomson, S. J. P. & Midwood, K. S. Expression and immune function of tenascin-C. *Critical Reviews in Immunology* **31**, 115–145 (2011).
301. Schaefer, L. Complexity of danger: The diverse nature of damage-associated molecular patterns. *Journal of Biological Chemistry* vol. 289 35237–35245 Preprint at <https://doi.org/10.1074/jbc.R114.619304> (2014).

302. Piccinini, A. M., Zuliani-Alvarez, L., Lim, J. M. P. & Midwood, K. S. Distinct microenvironmental cues stimulate divergent TLR4-mediated signaling pathways in macrophages. *Science Signaling* **9**, ra86 (2016).
303. Patel, L. *et al.* Tenascin-C induces inflammatory mediators and matrix degradation in osteoarthritic cartilage. *BMC Musculoskeletal Disorders* **12**, 164 (2011).
304. Kuriyama, N., Duarte, S., Hamada, T., Busuttil, R. W. & Coito, A. J. Tenascin-C: A novel mediator of hepatic ischemia and reperfusion injury. *Hepatology* **54**, 2125–2136 (2011).
305. Machino-Ohtsuka, T. *et al.* Tenascin-C aggravates autoimmune myocarditis via dendritic cell activation and Th17 cell differentiation. *Journal of the American Heart Association* **3**, (2014).
306. Midwood, K. S., Hussenet, T., Langlois, B. & Orend, G. Advances in tenascin-C biology. *Cellular and Molecular Life Sciences* vol. 68 3175–3199 Preprint at <https://doi.org/10.1007/s00018-011-0783-6> (2011).
307. Orend, G. & Chiquet-Ehrismann, R. Tenascin-C induced signaling in cancer. *Cancer Letters* vol. 244 143–163 Preprint at <https://doi.org/10.1016/j.canlet.2006.02.017> (2006).
308. Brellier, F. & Chiquet-Ehrismann, R. How do tenascins influence the birth and life of a malignant cell? *Journal of Cellular and Molecular Medicine* **16**, 32–40 (2012).
309. Ruiz, C. *et al.* Differential gene expression analysis reveals activation of growth promoting signaling pathways by tenascin-C. *Cancer Research* **64**, 7377–7385 (2004).

310. Saupe, F. *et al.* Tenascin-C Downregulates Wnt Inhibitor Dickkopf-1, Promoting Tumorigenesis in a Neuroendocrine Tumor Model. *Cell Reports* **5**, 482–492 (2013).
311. Sun, Z. *et al.* Tenascin-C promotes tumor cell migration and metastasis through integrin $\alpha 9 \beta 1$ -Mediated YAP inhibition. *Cancer Research* **78**, 950–961 (2018).
312. Hynes, R. O. Integrins: A family of cell surface receptors. *Cell* **48**, 549–554 (1987).
313. Hynes, R. O. Integrins: Bidirectional, allosteric signaling machines. *Cell* **110**, 673–687 (2002).
314. Vögtle, T. & Nieswandt, B. Platelet Integrins: Critical Mediators of Haemostasis and Pathological Thrombus Formation. in *Integrins in Health and Disease: Key Effectors of Cell-Matrix and Cell-Cell Interactions* (eds. Gullberg, D. & Eble, J. A.) 381–425 (Springer International Publishing, Cham, 2023). doi:10.1007/978-3-031-23781-2_12.
315. Mezu-Ndubuisi, O. J. & Maheshwari, A. The role of integrins in inflammation and angiogenesis. *Pediatr Res* **89**, 1619–1626 (2021).
316. Anderson, L. R., Owens, T. W. & Naylor, M. J. Integrins in development and cancer. *Biophys Rev* **6**, 191–202 (2013).
317. Mitroulis, I. *et al.* Leukocyte integrins: Role in leukocyte recruitment and as therapeutic targets in inflammatory disease. *Pharmacol Ther* **0**, 123–135 (2015).
318. Kadry, Y. A. & Calderwood, D. A. Chapter 22: Structural and signaling functions of integrins. *Biochimica et Biophysica Acta (BBA) - Biomembranes* **1862**, 183206 (2020).
319. Steiger, K. *et al.* There is a world beyond $\alpha \nu \beta 3$ -integrin: Multimeric ligands for imaging of the integrin subtypes $\alpha \nu \beta 6$, $\alpha \nu \beta 8$, $\alpha \nu \beta 3$, and $\alpha 5 \beta 1$ by positron emission tomography. *EJNMMI Res* **11**, 106 (2021).

320. Kechagia, J. Z., Ivaska, J. & Roca-Cusachs, P. Integrins as biomechanical sensors of the microenvironment. *Nat Rev Mol Cell Biol* **20**, 457–473 (2019).
321. Bachmann, M., Kukkurainen, S., Hytönen, V. P. & Wehrle-Haller, B. Cell Adhesion by Integrins. *Physiological Reviews* **99**, 1655–1699 (2019).
322. Li, J. & Springer, T. A. Integrin extension enables ultrasensitive regulation by cytoskeletal force. *Proceedings of the National Academy of Sciences* **114**, 4685–4690 (2017).
323. Nordenfelt, P., Elliott, H. L. & Springer, T. A. Coordinated integrin activation by actin-dependent force during T-cell migration. *Nat Commun* **7**, 13119 (2016).
324. Morse, E. M., Brahme, N. N. & Calderwood, D. A. Integrin Cytoplasmic Tail Interactions. *Biochemistry* **53**, 810–820 (2014).
325. Kim, C., Ye, F. & Ginsberg, M. H. Regulation of Integrin Activation. *Annual Review of Cell and Developmental Biology* **27**, 321–345 (2011).
326. Pouwels, J., Nevo, J., Pellinen, T., Ylännä, J. & Ivaska, J. Negative regulators of integrin activity. *Journal of Cell Science* **125**, 3271–3280 (2012).
327. Chastney, M. R., Conway, J. R. W. & Ivaska, J. Integrin adhesion complexes. *Current Biology* **31**, R536–R542 (2021).
328. Bandyopadhyay, A. & Raghavan, S. Defining the role of integrin alphavbeta6 in cancer. *Curr Drug Targets* **10**, 645–652 (2009).
329. Ramos, D. M., Dang, D. & Sadler, S. The role of the integrin alpha v beta6 in regulating the epithelial to mesenchymal transition in oral cancer. *Anticancer Res* **29**, 125–130 (2009).
330. Bates, R. C. *et al.* Transcriptional activation of integrin beta6 during the epithelial-mesenchymal transition defines a novel prognostic indicator of aggressive colon carcinoma. *J Clin Invest* **115**, 339–347 (2005).

331. Katoh, D. *et al.* Binding of $\alpha\beta 1$ and $\alpha\beta 6$ integrins to tenascin-C induces epithelial–mesenchymal transition-like change of breast cancer cells. *Oncogenesis* **2**, e65–e65 (2013).
332. Gulubova, M. & Vlaykova, T. Immunohistochemical assessment of fibronectin and tenascin and their integrin receptors $\alpha 5\beta 1$ and $\alpha 9\beta 1$ in gastric and colorectal cancers with lymph node and liver metastases. *Acta Histochem* **108**, 25–35 (2006).
333. Häkkinen, L., Hildebrand, H. C., Berndt, A., Kosmehl, H. & Larjava, H. Immunolocalization of tenascin-C, $\alpha 9$ integrin subunit, and $\alpha\beta 6$ integrin during wound healing in human oral mucosa. *J Histochem Cytochem* **48**, 985–998 (2000).
334. Yokosaki, Y., Monis, H., Chen, J. & Sheppard, D. Differential effects of the integrins $\alpha 9\beta 1$, $\alpha\beta 3$, and $\alpha\beta 6$ on cell proliferative responses to tenascin. Roles of the beta subunit extracellular and cytoplasmic domains. *J Biol Chem* **271**, 24144–24150 (1996).
335. Yokoyama, K., Erickson, H. P., Ikeda, Y. & Takada, Y. Identification of amino acid sequences in fibrinogen gamma -chain and tenascin C C-terminal domains critical for binding to integrin $\alpha\beta 3$. *J Biol Chem* **275**, 16891–16898 (2000).
336. Prieto, A. L., Edelman, G. M. & Crossin, K. L. Multiple integrins mediate cell attachment to cytotactin/tenascin. *Proc Natl Acad Sci U S A* **90**, 10154–10158 (1993).
337. Ishigaki, T. *et al.* Tenascin-C enhances crosstalk signaling of integrin $\alpha\beta 3$ /PDGFR- β complex by SRC recruitment promoting PDGF-induced proliferation and migration in smooth muscle cells. *J Cell Physiol* **226**, 2617–2624 (2011).

338. Sriramarao, P., Mendler, M. & Bourdon, M. A. Endothelial cell attachment and spreading on human tenascin is mediated by alpha 2 beta 1 and alpha v beta 3 integrins. *J Cell Sci* **105 (Pt 4)**, 1001–1012 (1993).
339. Huang, W., Chiquet-Ehrismann, R., Moyano, J. V., Garcia-Pardo, A. & Orend, G. Interference of tenascin-C with syndecan-4 binding to fibronectin blocks cell adhesion and stimulates tumor cell proliferation. *Cancer Res* **61**, 8586–8594 (2001).
340. Salmivirta, M. *et al.* Syndecan from embryonic tooth mesenchyme binds tenascin. *J Biol Chem* **266**, 7733–7739 (1991).
341. Fletcher, D. A. & Mullins, R. D. Cell mechanics and the cytoskeleton. *Nature* **463**, 485–492 (2010).
342. Huxley, H. E. Electron microscope studies on the structure of natural and synthetic protein filaments from striated muscle. *Journal of Molecular Biology* **7**, 281-IN30 (1963).
343. Woodrum, D. T., Rich, S. A. & Pollard, T. D. Evidence for biased bidirectional polymerization of actin filaments using heavy meromyosin prepared by an improved method. *J Cell Biol* **67**, 231–237 (1975).
344. Cramer, L. P., Siebert, M. & Mitchison, T. J. Identification of Novel Graded Polarity Actin Filament Bundles in Locomoting Heart Fibroblasts: Implications for the Generation of Motile Force. *J Cell Biol* **136**, 1287–1305 (1997).
345. Lazarides, E. & Burridge, K. Alpha-actinin: immunofluorescent localization of a muscle structural protein in nonmuscle cells. *Cell* **6**, 289–298 (1975).
346. Weber, K. & Groeschel-Stewart, U. Antibody to Myosin: The Specific Visualization of Myosin-Containing Filaments in Nonmuscle Cells. *Proc Natl Acad Sci U S A* **71**, 4561–4564 (1974).

347. Lazarides, E. Tropomyosin antibody: the specific localization of tropomyosin in nonmuscle cells. *J Cell Biol* **65**, 549–561 (1975).
348. Pellegrin, S. & Mellor, H. Actin stress fibres. *Journal of Cell Science* **120**, 3491–3499 (2007).
349. Svitkina, T. The Actin Cytoskeleton and Actin-Based Motility. *Cold Spring Harbor Perspectives in Biology* **10**, (2018).
350. Mullins, R. D., Heuser, J. A. & Pollard, T. D. The interaction of Arp2/3 complex with actin: nucleation, high affinity pointed end capping, and formation of branching networks of filaments. *Proc Natl Acad Sci U S A* **95**, 6181–6186 (1998).
351. Dominguez, R. Structural insights into de novo actin polymerization. *Curr Opin Struct Biol* **20**, 217–225 (2010).
352. Frieden, B. R. & Gatenby, R. A. Signal transmission through elements of the cytoskeleton form an optimized information network in eukaryotic cells. *Sci Rep* **9**, 6110 (2019).
353. Van Haastert, P. J. M. & Devreotes, P. N. Chemotaxis: signalling the way forward. *Nat Rev Mol Cell Biol* **5**, 626–634 (2004).
354. May, R. C. & Machesky, L. M. Phagocytosis and the actin cytoskeleton. *Journal of Cell Science* **114**, 1061–1077 (2001).
355. Stradal, T. E. B., Pusch, R. & Kliche, S. Molecular Regulation of Cytoskeletal Rearrangements During T Cell Signalling. in *Cell Communication in Nervous and Immune System* (eds. Gundelfinger, E. D., Seidenbecher, C. I. & Schraven, B.) 219–244 (Springer, Berlin, Heidelberg, 2006). doi:10.1007/400_022.
356. Ronzier, E. *et al.* The Actin Cytoskeleton Responds to Inflammatory Cues and Alters Macrophage Activation. *Cells* **11**, 1806–1806 (2022).

357. Webb, J. L., Harvey, M. W., Holden, D. W. & Evans, T. J. Macrophage nitric oxide synthase associates with cortical actin but is not recruited to phagosomes. *Infect Immun* **69**, 6391–6400 (2001).
358. Musial, A. & Eissa, N. T. Inducible nitric-oxide synthase is regulated by the proteasome degradation pathway. *J Biol Chem* **276**, 24268–24273 (2001).
359. Wu, C. *et al.* Loss of Arp2/3 induces an NF- κ B-dependent, nonautonomous effect on chemotactic signaling. *J Cell Biol* **203**, 907–916 (2013).
360. Vassilev, A., Kaneko, K. J., Shu, H., Zhao, Y. & DePamphilis, M. L. TEAD/TEF transcription factors utilize the activation domain of YAP65, a Src/Yes-associated protein localized in the cytoplasm. *Genes and Development* **15**, 1229–1241 (2001).
361. Tsutsumi, R. *et al.* YAP and TAZ, hippo signaling targets, act as a rheostat for nuclear SHP2 function. *Developmental Cell* **26**, 658–665 (2013).
362. Pocaterra, A., Romani, P. & Dupont, S. YAP/TAZ functions and their regulation at a glance. *Journal of Cell Science* **133**, (2020).
363. Varelas, X. The hippo pathway effectors TAZ and YAP in development, homeostasis and disease. *Development (Cambridge)* vol. 141 1614–1626 Preprint at <https://doi.org/10.1242/dev.102376> (2014).
364. Justice, R. W., Zilian, O., Woods, D. F., Noll, M. & Bryant, P. J. The *Drosophila* tumor suppressor gene *warts* encodes a homolog of human myotonic dystrophy kinase and is required for the control of cell shape and proliferation. *Genes and Development* **9**, 534–546 (1995).
365. Yu, F. X., Zhao, B. & Guan, K. L. Hippo Pathway in Organ Size Control, Tissue Homeostasis, and Cancer. *Cell* vol. 163 811–828 Preprint at <https://doi.org/10.1016/j.cell.2015.10.044> (2015).

366. Hergovich, A., Schmitz, D. & Hemmings, B. A. The human tumour suppressor LATS1 is activated by human MOB1 at the membrane. *Biochemical and Biophysical Research Communications* **345**, 50–58 (2006).
367. Yin, F. *et al.* XSpatial organization of hippo signaling at the plasma membrane mediated by the tumor suppressor merlin/NF2. *Cell* **154**, 1342 (2013).
368. Chan, E. H. Y. *et al.* The Ste20-like kinase Mst2 activates the human large tumor suppressor kinase Lats1. *Oncogene* **24**, 2076–2086 (2005).
369. Yu, F.-X. *et al.* Regulation of the Hippo-YAP pathway by G-protein coupled receptor signaling. *Cell* **150**, 780–791 (2012).
370. Furth, N. & Aylon, Y. The LATS1 and LATS2 tumor suppressors: beyond the Hippo pathway. *Cell Death Differ* **24**, 1488–1501 (2017).
371. Zhao, B. *et al.* Cell detachment activates the Hippo pathway via cytoskeleton reorganization to induce anoikis. *Genes Dev* **26**, 54–68 (2012).
372. Zhao, B., Li, L., Tumaneng, K., Wang, C. Y. & Guan, K. L. A coordinated phosphorylation by Lats and CK1 regulates YAP stability through SCF β -TRCP. *Genes and Development* **24**, 72–85 (2010).
373. Visser-Grieve, S. *et al.* LATS1 tumor suppressor is a novel actin-binding protein and negative regulator of actin polymerization. *Cell Res* **21**, 1513–1516 (2011).
374. Zhang, J., Smolen, G. A. & Haber, D. A. Negative regulation of YAP by LATS1 underscores evolutionary conservation of the Drosophila Hippo pathway. *Cancer Research* **68**, 2789–2794 (2008).
375. Hao, Y., Chun, A., Cheung, K., Rashidi, B. & Yang, X. Tumor suppressor LATS1 is a negative regulator of oncogene YAP. *Journal of Biological Chemistry* **283**, 5496–5509 (2008).

376. Kanai, F. *et al.* TAZ: A novel transcriptional co-activator regulated by interactions with 14-3-3 and PDZ domain proteins. *EMBO Journal* (2000) doi:10.1093/emboj/19.24.6778.
377. Liu, C. Y. *et al.* The hippo tumor pathway promotes TAZ degradation by phosphorylating a phosphodegron and recruiting the SCF β -TrCP E3 ligase. *Journal of Biological Chemistry* **285**, 37159–37169 (2010).
378. Lee, M. J., Byun, M. R., Furutani-Seiki, M., Hong, J. H. & Jung, H. S. YAP and TAZ regulate skin wound healing. *Journal of Investigative Dermatology* **134**, 518–525 (2014).
379. Gregorieff, A., Liu, Y., Inanlou, M. R., Khomchuk, Y. & Wrana, J. L. Yap-dependent reprogramming of Lgr5+ stem cells drives intestinal regeneration and cancer. *Nature* **526**, 715–718 (2015).
380. Baia, G. S. *et al.* Yes-associated protein 1 is activated and functions as an oncogene in meningiomas. *Molecular Cancer Research* **10**, 904–913 (2012).
381. Cottini, F. *et al.* Rescue of Hippo coactivator YAP1 triggers DNA damage-induced apoptosis in hematological cancers. *Nature Medicine* **20**, 599–606 (2014).
382. Zhang, Y. H., Li, B., Shen, L., Shen, Y. & Chen, X. D. The role and clinical significance of yes-associated protein 1 in human osteosarcoma. *International Journal of Immunopathology and Pharmacology* **26**, 157–167 (2013).
383. Tsujiura, M. *et al.* Yes-Associated Protein (YAP) modulates oncogenic features and radiation sensitivity in endometrial cancer. *PLoS ONE* **9**, (2014).
384. Rybarczyk, A. *et al.* Overexpression of the YAP1 oncogene in clear cell renal cell carcinoma is associated with poor outcome. *Oncology Reports* **38**, 427–439 (2017).

385. Sheng, X. *et al.* YAP is closely correlated with castration-resistant prostate cancer, and downregulation of YAP reduces proliferation and induces apoptosis of PC-3 cells. *Molecular Medicine Reports* **12**, 4867–4876 (2015).
386. Cordenonsi, M. *et al.* The hippo transducer TAZ confers cancer stem cell-related traits on breast cancer cells. *Cell* **147**, 759–772 (2011).
387. Wang, S. *et al.* The Crosstalk Between Hippo-YAP Pathway and Innate Immunity. *Frontiers in Immunology* vol. 11 323 Preprint at <https://doi.org/10.3389/fimmu.2020.00323> (2020).
388. Kim, W. & Jho, E. The history and regulatory mechanism of the Hippo pathway. *BMB Rep* **51**, 106–118 (2018).
389. Huse, M. Mechanical forces in the immune system. *Nat Rev Immunol* **17**, 679–690 (2017).
390. Meli, V. S., Veerasubramanian, P. K., Downing, T. L., Wang, W. & Liu, W. F. Mechanosensation to inflammation: Roles for YAP/TAZ in innate immune cells. *Science Signaling* **16**, eadc9656 (2023).
391. Karlsson, M. *et al.* A single-cell type transcriptomics map of human tissues. *Science Advances* **7**, eabh2169 (2021).
392. Zhao, L. *et al.* YAP1 is essential for osteoclastogenesis through a TEADs-dependent mechanism. *Bone* **110**, 177–186 (2018).
393. Zhou, X. *et al.* YAP Aggravates Inflammatory Bowel Disease by Regulating M1/M2 Macrophage Polarization and Gut Microbial Homeostasis. *CellReports* **27**, 1176-1189.e5 (2019).
394. Dixit, D., Ghildiyal, R., Anto, N. P. & Sen, E. Chaetocin-induced ROS-mediated apoptosis involves ATM-YAP1 axis and JNK-dependent inhibition of glucose metabolism. *Cell Death and Disease* **5**, e1212–e1212 (2014).

395. Wang, S. *et al.* YAP antagonizes innate antiviral immunity and is targeted for lysosomal degradation through IKKI-mediated phosphorylation. *Nature Immunology* **18**, 733–743 (2017).
396. Lv, Y. *et al.* YAP controls endothelial activation and vascular inflammation through TRAF6. *Circulation Research* **123**, 43–56 (2018).
397. Deng, Y. *et al.* Reciprocal inhibition of YAP/TAZ and NF- κ B regulates osteoarthritic cartilage degradation. *Nature Communications* **9**, 4564–4564 (2018).
398. Zhang, Q. *et al.* Yes-associated protein (YAP) and transcriptional coactivator with PDZ-binding motif (TAZ) mediate cell density– dependent proinflammatory responses. *Journal of Biological Chemistry* **293**, 18071–18085 (2018).
399. Mia, M. M. *et al.* YAP/TAZ deficiency reprograms macrophage phenotype and improves infarct healing and cardiac function after myocardial infarction. *PLoS Biology* **18**, (2020).
400. Yang, K. *et al.* Lactate Suppresses Macrophage Pro-Inflammatory Response to LPS Stimulation by Inhibition of YAP and NF- κ B Activation via GPR81-Mediated Signaling. *Frontiers in Immunology* **11**, 2610–2610 (2020).
401. Meli, V. S. *et al.* YAP-mediated mechanotransduction tunes the macrophage inflammatory response. *Sci Adv* **6**, eabb8471 (2020).
402. Wang, D. *et al.* YAP promotes the activation of NLRP3 inflammasome via blocking K27-linked polyubiquitination of NLRP3. *Nat Commun* **12**, 2674 (2021).
403. Song, K. *et al.* Yes-Associated Protein in Kupffer Cells Enhances the Production of Proinflammatory Cytokines and Promotes the Development of Nonalcoholic Steatohepatitis. *Hepatology* **72**, 72 (2020).
404. Liu, M. *et al.* Macrophage K63-Linked Ubiquitination of YAP Promotes Its Nuclear Localization and Exacerbates Atherosclerosis. *CellReports* **32**, (2020).

405. Previtera, M. L. & Sengupta, A. Substrate Stiffness Regulates Proinflammatory Mediator Production through TLR4 Activity in Macrophages. *PLoS One* **10**, e0145813 (2015).
406. Hwang, H.-W., Wentzel, E. A. & Mendell, J. T. Cell–cell contact globally activates microRNA biogenesis. *Proc Natl Acad Sci U S A* **106**, 7016–7021 (2009).
407. Zheng, D. *et al.* RANBP1 promotes colorectal cancer progression by regulating pre-miRNA nuclear export via a positive feedback loop with YAP. *Oncogene* **41**, 930–942 (2022).
408. Chaulk, S. G., Lattanzi, V. J., Hiemer, S. E., Fahlman, R. P. & Varelas, X. The Hippo Pathway Effectors TAZ/YAP Regulate Dicer Expression and MicroRNA Biogenesis through Let-7. *Journal of Biological Chemistry* **289**, 1886–1891 (2014).
409. Lo Sardo, F. *et al.* MCM7 and its hosted miR-25, 93 and 106b cluster elicit YAP/TAZ oncogenic activity in lung cancer. *Carcinogenesis* **38**, 64–75 (2017).
410. Zhang, H.-T. *et al.* Sequential targeting of YAP1 and p21 enhances the elimination of senescent cells induced by the BET inhibitor JQ1. *Cell Death Dis* **12**, 121 (2021).
411. Rupp, T. *et al.* Tenascin-C Orchestrates Glioblastoma Angiogenesis by Modulation of Pro- and Anti-angiogenic Signaling. *Cell Reports* **17**, 2607–2619 (2016).
412. Li, Z. *et al.* Tenascin-C-mediated suppression of extracellular matrix adhesion force promotes enthesal new bone formation through activation of Hippo signalling in ankylosing spondylitis. *Annals of the Rheumatic Diseases* annrhumdis-220002 (2021) doi:10.1136/annrhumdis-2021-220002.
413. Lee, Y. C. *et al.* Prostate tumor-induced stromal reprogramming generates Tenascin C that promotes prostate cancer metastasis through YAP/TAZ inhibition. *Oncogene* **2021** 1–13 (2021) doi:10.1038/s41388-021-02131-7.

414. He, S. *et al.* EWS-FLI1-mediated tenascin-C expression promotes tumour progression by targeting MALAT1 through integrin $\alpha 5\beta 1$ -mediated YAP activation in Ewing sarcoma. *British Journal of Cancer* **121**, 922–933 (2019).
415. Geleta, B. *et al.* Targeting Wnt/tenascin C-mediated cross talk between pancreatic cancer cells and stellate cells via activation of the metastasis suppressor NDRG1. *Journal of Biological Chemistry* **298**, (2022).
416. Azzolin, L. *et al.* YAP/TAZ incorporation in the β -catenin destruction complex orchestrates the Wnt response. *Cell* **158**, 157–170 (2014).
417. Ni, J. *et al.* Cadherin 11-mediated juxtacrine interaction of gastric cancer cells and fibroblasts promotes metastasis via YAP/tenascin-C signaling. *Science Bulletin* **67**, 1026–1030 (2022).
418. Li, Y. *et al.* Role of Yes-associated protein (YAP) in regulation of mesenchymal stem cell tenogenic differentiation. *J Mol Histol* **53**, 273–283 (2022).
419. Delve, E. *et al.* YAP/TAZ regulates the expression of proteoglycan 4 and tenascin C in superficial-zone chondrocytes. *Eur Cell Mater* **39**, 48–64 (2020).
420. Caire, R. *et al.* YAP/TAZ: Key Players for Rheumatoid Arthritis Severity by Driving Fibroblast Like Synoviocytes Phenotype and Fibro-Inflammatory Response. *Frontiers in Immunology* **12**, (2021).
421. Han, J., Lee, J. D., Tobias, P. S. & Ulevitch, R. J. Endotoxin induces rapid protein tyrosine phosphorylation in 70Z/3 cells expressing CD14. *J Biol Chem* **268**, 25009–25014 (1993).
422. Jiang, Y. *et al.* Characterization of the structure and function of a new mitogen-activated protein kinase (p38beta). *J Biol Chem* **271**, 17920–17926 (1996).
423. Li, Z., Jiang, Y., Ulevitch, R. J. & Han, J. The primary structure of p38 gamma: a new member of p38 group of MAP kinases. *Biochem Biophys Res Commun* **228**, 334–340 (1996).

424. Jiang, Y. *et al.* Characterization of the structure and function of the fourth member of p38 group mitogen-activated protein kinases, p38delta. *J Biol Chem* **272**, 30122–30128 (1997).
425. Wang, X. S. *et al.* Molecular Cloning and Characterization of a Novel p38 Mitogen-activated Protein Kinase *. *Journal of Biological Chemistry* **272**, 23668–23674 (1997).
426. Lanna, A. *et al.* A sestrin-dependent Erk-Jnk-p38 MAPK activation complex inhibits immunity during aging. *Nat Immunol* **18**, 354–363 (2017).
427. Raingeaud, J. *et al.* Pro-inflammatory cytokines and environmental stress cause p38 mitogen-activated protein kinase activation by dual phosphorylation on tyrosine and threonine. *J Biol Chem* **270**, 7420–7426 (1995).
428. Dorion, S., Lambert, H. & Landry, J. Activation of the p38 Signaling Pathway by Heat Shock Involves the Dissociation of Glutathione S-Transferase Mu from Ask1*. *Journal of Biological Chemistry* **277**, 30792–30797 (2002).
429. Han, J., Lee, J. D., Bibbs, L. & Ulevitch, R. J. A MAP kinase targeted by endotoxin and hyperosmolarity in mammalian cells. *Science* **265**, 808–811 (1994).
430. Freshney, N. W. *et al.* Interleukin-1 activates a novel protein kinase cascade that results in the phosphorylation of Hsp27. *Cell* **78**, 1039–1049 (1994).
431. Lee, J. C. *et al.* A protein kinase involved in the regulation of inflammatory cytokine biosynthesis. *Nature* **372**, 739–746 (1994).
432. Gong, X., Liu, A., Ming, X., Deng, P. & Jiang, Y. UV-induced interaction between p38 MAPK and p53 serves as a molecular switch in determining cell fate. *FEBS Lett* **584**, 4711–4716 (2010).
433. Zauberman, A., Zipori, D., Krupsky, M. & Ben-Levy, R. Stress activated protein kinase p38 is involved in IL-6 induced transcriptional activation of STAT3. *Oncogene* **18**, 3886–3893 (1999).

434. Foltz, I. N., Lee, J. C., Young, P. R. & Schrader, J. W. Hemopoietic growth factors with the exception of interleukin-4 activate the p38 mitogen-activated protein kinase pathway. *J Biol Chem* **272**, 3296–3301 (1997).
435. Gutierrez-Prat, N. *et al.* MK2 degradation as a sensor of signal intensity that controls stress-induced cell fate. *Proceedings of the National Academy of Sciences* **118**, e2024562118 (2021).
436. Adams, R. H. *et al.* Essential role of p38alpha MAP kinase in placental but not embryonic cardiovascular development. *Mol Cell* **6**, 109–116 (2000).
437. Brancho, D. *et al.* Mechanism of p38 MAP kinase activation in vivo. *Genes Dev* **17**, 1969–1978 (2003).
438. Beardmore, V. A. *et al.* Generation and characterization of p38beta (MAPK11) gene-targeted mice. *Mol Cell Biol* **25**, 10454–10464 (2005).
439. Sabio, G. *et al.* p38gamma regulates the localisation of SAP97 in the cytoskeleton by modulating its interaction with GKAP. *EMBO J* **24**, 1134–1145 (2005).
440. Raingeaud, J., Whitmarsh, A. J., Barrett, T., Dérizard, B. & Davis, R. J. MKK3- and MKK6-regulated gene expression is mediated by the p38 mitogen-activated protein kinase signal transduction pathway. *Mol Cell Biol* **16**, 1247–1255 (1996).
441. Moriguchi, T. *et al.* A Novel Kinase Cascade Mediated by Mitogen-activated Protein Kinase Kinase 6 and MKK3 *. *Journal of Biological Chemistry* **271**, 13675–13679 (1996).
442. Ichijo, H. *et al.* Induction of apoptosis by ASK1, a mammalian MAPKKK that activates SAPK/JNK and p38 signaling pathways. *Science* **275**, 90–94 (1997).
443. Hirai, S. *et al.* MST/MLK2, a member of the mixed lineage kinase family, directly phosphorylates and activates SEK1, an activator of c-Jun N-terminal kinase/stress-activated protein kinase. *J Biol Chem* **272**, 15167–15173 (1997).

444. Bagrodia, S., Dérijard, B., Davis, R. J. & Cerione, R. A. Cdc42 and PAK-mediated signaling leads to Jun kinase and p38 mitogen-activated protein kinase activation. *J Biol Chem* **270**, 27995–27998 (1995).
445. Martin, G. A., Bollag, G., McCormick, F. & Abo, A. A novel serine kinase activated by rac1/CDC42Hs-dependent autophosphorylation is related to PAK65 and STE20. *EMBO J* **14**, 1970–1978 (1995).
446. Ge, B. *et al.* MAPKK-independent activation of p38alpha mediated by TAB1-dependent autophosphorylation of p38alpha. *Science* **295**, 1291–1294 (2002).
447. Salvador, J. M. *et al.* Alternative p38 activation pathway mediated by T cell receptor-proximal tyrosine kinases. *Nat Immunol* **6**, 390–395 (2005).
448. Sun, H., Charles, C. H., Lau, L. F. & Tonks, N. K. MKP-1 (3CH134), an immediate early gene product, is a dual specificity phosphatase that dephosphorylates MAP kinase in vivo. *Cell* **75**, 487–493 (1993).
449. Nunes-Xavier, C. *et al.* Dual-specificity MAP kinase phosphatases as targets of cancer treatment. *Anticancer Agents Med Chem* **11**, 109–132 (2011).
450. Manetsch, M., Che, W., Seidel, P., Chen, Y. & Ammit, A. J. MKP-1: a negative feedback effector that represses MAPK-mediated pro-inflammatory signaling pathways and cytokine secretion in human airway smooth muscle cells. *Cell Signal* **24**, 907–913 (2012).
451. Wood, C. D., Thornton, T. M., Sabio, G., Davis, R. A. & Rincon, M. Nuclear Localization of p38 MAPK in Response to DNA Damage. *Int J Biol Sci* **5**, 428–437 (2009).
452. Han, J., Wu, J. & Silke, J. An overview of mammalian p38 mitogen-activated protein kinases, central regulators of cell stress and receptor signaling. *F1000Res* **9**, F1000 Faculty Rev-653 (2020).

453. Allen, M. *et al.* Deficiency of the stress kinase p38alpha results in embryonic lethality: characterization of the kinase dependence of stress responses of enzyme-deficient embryonic stem cells. *J Exp Med* **191**, 859–870 (2000).
454. Kang, Y. J. *et al.* Macrophage deletion of p38alpha partially impairs lipopolysaccharide-induced cellular activation. *J Immunol* **180**, 5075–5082 (2008).
455. Engelman, J. A., Lisanti, M. P. & Scherer, P. E. Specific inhibitors of p38 mitogen-activated protein kinase block 3T3-L1 adipogenesis. *J Biol Chem* **273**, 32111–32120 (1998).
456. Takenaka, K., Moriguchi, T. & Nishida, E. Activation of the Protein Kinase p38 in the Spindle Assembly Checkpoint and Mitotic Arrest. *Science* **280**, 599–602 (1998).
457. Ronkina, N. & Gaestel, M. MAPK-Activated Protein Kinases: Servant or Partner? *Annual Review of Biochemistry* **91**, 505–540 (2022).
458. Zu, Y. L. *et al.* The primary structure of a human MAP kinase activated protein kinase 2. *Biochem Biophys Res Commun* **200**, 1118–1124 (1994).
459. Stokoe, D. *et al.* MAPKAP kinase-2; a novel protein kinase activated by mitogen-activated protein kinase. *The EMBO Journal* **11**, 3985–3994 (1992).
460. Trulley, P. *et al.* Alternative Translation Initiation Generates a Functionally Distinct Isoform of the Stress-Activated Protein Kinase MK2. *Cell Reports* **27**, 2859–2870.e6 (2019).
461. Garai, Á. *et al.* Specificity of Linear Motifs That Bind to a Common Mitogen-Activated Protein Kinase Docking Groove. *Science Signaling* **5**, ra74–ra74 (2012).

462. Engel, K., Kotlyarov, A. & Gaestel, M. Leptomycin B-sensitive nuclear export of MAPKAP kinase 2 is regulated by phosphorylation. *The EMBO Journal* **17**, 3363–3371 (1998).
463. Ben-Levy, R., Hooper, S., Wilson, R., Paterson, H. F. & Marshall, C. J. Nuclear export of the stress-activated protein kinase p38 mediated by its substrate MAPKAP kinase-2. *Current Biology* **8**, 1049–1057 (1998).
464. Gaestel, M. MAPK-Activated Protein Kinases (MKs): Novel Insights and Challenges. *Frontiers in Cell and Developmental Biology* **3**, (2016).
465. Ben-Levy, R. *et al.* Identification of novel phosphorylation sites required for activation of MAPKAP kinase-2. *EMBO J* **14**, 5920–5930 (1995).
466. Neiningner, A., Thielemann, H. & Gaestel, M. FRET-based detection of different conformations of MK2. *EMBO reports* **2**, 703–708 (2001).
467. Soni, S., Anand, P. & Padwad, Y. S. MAPKAPK2: the master regulator of RNA-binding proteins modulates transcript stability and tumor progression. *Journal of Experimental & Clinical Cancer Research* **38**, 121 (2019).
468. Heidenreich, O. *et al.* MAPKAP Kinase 2 Phosphorylates Serum Response Factor in Vitro and in Vivo*. *Journal of Biological Chemistry* **274**, 14434–14443 (1999).
469. Ronkina, N., Lafera, J., Kotlyarov, A. & Gaestel, M. Stress-dependent phosphorylation of myocardin-related transcription factor A (MRTF-A) by the p38MAPK/MK2 axis. *Sci Rep* **6**, 31219 (2016).
470. Winzen, R. *et al.* The p38 MAP kinase pathway signals for cytokine-induced mRNA stabilization via MAP kinase-activated protein kinase 2 and an AU-rich region-targeted mechanism. *EMBO J* **18**, 4969–4980 (1999).
471. Neiningner, A. *et al.* MK2 targets AU-rich elements and regulates biosynthesis of tumor necrosis factor and interleukin-6 independently at different post-transcriptional levels. *J Biol Chem* **277**, 3065–3068 (2002).

472. Bakheet, T., Williams, B. R. G. & Khabar, K. S. A. ARED 3.0: the large and diverse AU-rich transcriptome. *Nucleic Acids Res* **34**, D111-114 (2006).
473. Chen, C. Y. & Shyu, A. B. AU-rich elements: characterization and importance in mRNA degradation. *Trends Biochem Sci* **20**, 465–470 (1995).
474. Kotlyarov, A. *et al.* MAPKAP kinase 2 is essential for LPS-induced TNF- α biosynthesis. *Nature Cell Biology* **1**, 94–97 (1999).
475. Ehltng, C. *et al.* Distinct Functions of the Mitogen-activated Protein Kinase-activated Protein (MAPKAP) Kinases MK2 and MK3: MK2 MEDIATES LIPOPOLYSACCHARIDE-INDUCED SIGNAL TRANSDUCERS AND ACTIVATORS OF TRANSCRIPTION 3 (STAT3) ACTIVATION BY PREVENTING NEGATIVE REGULATORY EFFECTS OF MK3* *This work was supported by the Deutsche Forschungsgemeinschaft (Bonn), through Collaborative Research Centers 575 (to J. G. B. and D. H.), and 542 (to J. B.) and through Project Ga 453/11 (to M. G.). *Journal of Biological Chemistry* **286**, 24113–24124 (2011).
476. Martin, M. U. & Wesche, H. Summary and comparison of the signaling mechanisms of the Toll/interleukin-1 receptor family. *Biochimica et Biophysica Acta (BBA) - Molecular Cell Research* **1592**, 265–280 (2002).
477. Dunne, A. & O'Neill, L. A. J. The interleukin-1 receptor/Toll-like receptor superfamily: signal transduction during inflammation and host defense. *Sci STKE* **2003**, re3 (2003).
478. Johnsen, I. B., Nguyen, T. T., Bergstrøm, B., Lien, E. & Anthonen, M. W. Toll-like receptor 3-elicited MAPK activation induces stabilization of interferon- β mRNA. *Cytokine* **57**, 337–346 (2012).
479. Shi, J.-H. & Sun, S.-C. Tumor Necrosis Factor Receptor-Associated Factor Regulation of Nuclear Factor κ B and Mitogen-Activated Protein Kinase Pathways. *Front Immunol* **9**, 1849 (2018).

480. L, Y., Mc, H. & Ye, Z. TGF-beta receptor-activated p38 MAP kinase mediates Smad-independent TGF-beta responses. *The EMBO journal* **21**, (2002).
481. Whitmarsh, A. J. A central role for p38 MAPK in the early transcriptional response to stress. *BMC Biol* **8**, 47 (2010).
482. Carballo, E. *et al.* Decreased Sensitivity of Tristetraprolin-deficient Cells to p38 Inhibitors Suggests the Involvement of Tristetraprolin in the p38 Signaling Pathway*. *Journal of Biological Chemistry* **276**, 42580–42587 (2001).
483. Tudor, C. *et al.* The p38 MAPK pathway inhibits tristetraprolin-directed decay of interleukin-10 and pro-inflammatory mediator mRNAs in murine macrophages. *FEBS Letters* **583**, 1933–1938 (2009).
484. Marchese, F. P. *et al.* MAPKAP Kinase 2 Blocks Tristetraprolin-directed mRNA Decay by Inhibiting CAF1 Deadenylase Recruitment. *Journal of Biological Chemistry* **285**, 27590–27600 (2010).
485. Ronkina, N. *et al.* MAPKAP kinases MK2 and MK3 in inflammation: Complex regulation of TNF biosynthesis via expression and phosphorylation of tristetraprolin. *Biochemical Pharmacology* **80**, 1915–1920 (2010).
486. Hitti, E. *et al.* Mitogen-activated protein kinase-activated protein kinase 2 regulates tumor necrosis factor mRNA stability and translation mainly by altering tristetraprolin expression, stability, and binding to adenine/uridine-rich element. *Molecular and Cellular Biology* **26**, 2399–2407 (2006).
487. Taylor, G. A. *et al.* A Pathogenetic Role for TNF α in the Syndrome of Cachexia, Arthritis, and Autoimmunity Resulting from Tristetraprolin (TTP) Deficiency. *Immunity* **4**, 445–454 (1996).
488. Ehltng, C. *et al.* Regulation of Suppressor of Cytokine Signaling 3 (SOCS3) mRNA Stability by TNF- α Involves Activation of the MKK6/p38MAPK/MK2 Cascade1. *The Journal of Immunology* **178**, 2813–2826 (2007).

489. Niemand, C. *et al.* Activation of STAT3 by IL-6 and IL-10 in Primary Human Macrophages Is Differentially Modulated by Suppressor of Cytokine Signaling 3 1. *The Journal of Immunology* **170**, 3263–3272 (2003).
490. Schaljo, B. *et al.* Tristetraprolin Is Required for Full Anti-Inflammatory Response of Murine Macrophages to IL-10. *The Journal of Immunology* **183**, 1197–1206 (2009).
491. Fujimoto, M. *et al.* Tenascin-C induces prolonged constriction of cerebral arteries in rats. *Neurobiology of Disease* **55**, 104–109 (2013).
492. Fujimoto, M. *et al.* Epidermal growth factor-like repeats of tenascin-C-induced constriction of cerebral arteries via activation of epidermal growth factor receptors in rats. *Brain Research* **1642**, 436–444 (2016).
493. Haddad, E.-B. *et al.* Role of p38 MAP kinase in LPS-induced airway inflammation in the rat. *Br J Pharmacol* **132**, 1715–1724 (2001).
494. Rogers, N. K. *et al.* Extra-Cellular Matrix Proteins Induce Matrix Metalloproteinase-1 (MMP-1) Activity and Increase Airway Smooth Muscle Contraction in Asthma. *PLOS ONE* **9**, e90565 (2014).
495. Wang, R. *et al.* Integrin $\beta 3$ and its ligand regulate the expression of uPA through p38 MAPK in breast cancer. *APMIS* **118**, 909–917 (2010).
496. Chen, J., Baskerville, C., Han, Q., Pan, Z. K. & Huang, S. Alpha(v) integrin, p38 mitogen-activated protein kinase, and urokinase plasminogen activator are functionally linked in invasive breast cancer cells. *J Biol Chem* **276**, 47901–47905 (2001).
497. Fujimoto, M. *et al.* Deficiency of tenascin-C and attenuation of blood-brain barrier disruption following experimental subarachnoid hemorrhage in mice. *J Neurosurg* **124**, 1693–1702 (2016).

498. Morgan, J. M., Wong, A., Yellowley, C. E. & Genetos, D. C. Regulation of tenascin expression in bone. *Journal of Cellular Biochemistry* **112**, 3354–3363 (2011).
499. Chiquet, M., Sarasa-Renedo, A. & Tunç-Civelek, V. Induction of tenascin-C by cyclic tensile strain versus growth factors: distinct contributions by Rho/ROCK and MAPK signaling pathways. *Biochimica et Biophysica Acta (BBA) - Molecular Cell Research* **1693**, 193–204 (2004).
500. Kato, N. *et al.* Critical role of p38 MAPK for regeneration of the sciatic nerve following crush injury in vivo. *J Neuroinflammation* **10**, 757 (2013).
501. Jiang, L. *et al.* Synergistic effects of cyclic strain and Th1-like cytokines on tenascin-C production by rheumatic aortic valve interstitial cells. *Clin Exp Immunol* **155**, 216–223 (2009).
502. Antoon, J. W. *et al.* Inhibition of p38 mitogen-activated protein kinase alters microRNA expression and reverses epithelial-to-mesenchymal transition. *International Journal of Oncology* **42**, 1139–1150 (2013).
503. Matou-Nasri, S. *et al.* Blockade of p38 MAPK overcomes AML stem cell line KG1a resistance to 5-Fluorouridine and the impact on miRNA profiling. *PLOS ONE* **17**, e0267855 (2022).
504. Lu, E., Su, J., Zhou, Y., Zhang, C. & Wang, Y. CCL20/CCR6 promotes cell proliferation and metastasis in laryngeal cancer by activating p38 pathway. *Biomedicine & Pharmacotherapy* **85**, 486–492 (2017).
505. Hong, S. *et al.* Signaling by p38 MAPK Stimulates Nuclear Localization of the Microprocessor Component p68 for Processing of Selected Primary MicroRNAs. *Sci Signal* **6**, 10.1126/scisignal.2003706 (2013).

506. Boucas, J. *et al.* Label-Free Protein-RNA Interactome Analysis Identifies Khsrp Signaling Downstream of the p38/Mk2 Kinase Complex as a Critical Modulator of Cell Cycle Progression. *PLoS ONE* **10**, e0125745 (2015).
507. P, B. *et al.* p38-dependent phosphorylation of the mRNA decay-promoting factor KSRP controls the stability of select myogenic transcripts. *Molecular cell* **20**, (2005).
508. Horman, S. R. *et al.* Akt-Mediated Phosphorylation of Argonaute 2 Downregulates Cleavage and Upregulates Translational Repression of MicroRNA Targets. *Molecular Cell* **50**, 356–367 (2013).
509. Pantazopoulou, V. I. *et al.* AGO2 localizes to cytokinetic protrusions in a p38-dependent manner and is needed for accurate cell division. *Commun Biol* **4**, 1–18 (2021).
510. Yang, Q. *et al.* Stress Induces p38 MAPK-Mediated Phosphorylation and Inhibition of Drosha-Dependent Cell Survival. *Molecular Cell* **57**, 721–734 (2015).
511. Zordan, N. Investigating how tenascin-C regulates miR-155 expression. *Thesis (PhD), University of Nottingham* (2021).
512. Alazawi, W. *et al.* Stat2 loss leads to cytokine-independent, cell-mediated lethality in LPS-induced sepsis. *Proceedings of the National Academy of Sciences of the United States of America* **110**, 8656–8661 (2013).
513. Gagliardi, M. & Matarazzo, M. R. RIP: RNA Immunoprecipitation. *Methods Mol Biol* **1480**, 73–86 (2016).
514. Vlachos, I. S. *et al.* DIANA-miRPath v3.0: deciphering microRNA function with experimental support. *Nucleic Acids Research* **43**, W460–W460 (2015).

515. Sato, K., Akiyama, M. & Sakakibara, Y. RNA secondary structure prediction using deep learning with thermodynamic integration. *Nature Communications* **2021** *12:1* **12**, 1–9 (2021).
516. Byun, Y. & Han, K. PseudoViewer3: generating planar drawings of large-scale RNA structures with pseudoknots. *Bioinformatics* **25**, 1435–1437 (2009).
517. Lee, C.-H. & Choi, E. Y. Macrophages and Inflammation. *Journal of Rheumatic Diseases* **25**, 11–18 (2018).
518. Ye, J. *et al.* miR-155 Regulated Inflammation Response by the SOCS1-STAT3-PDCD4 Axis in Atherogenesis. *Mediators Inflamm* **2016**, 8060182 (2016).
519. Nazari-Jahantigh, M. *et al.* MicroRNA-155 promotes atherosclerosis by repressing Bcl6 in macrophages. *J Clin Invest* **122**, 4190–4202 (2012).
520. Kanayama, M. *et al.* $\alpha 9\beta 1$ integrin-mediated signaling serves as an intrinsic regulator of pathogenic Th17 cell generation. *J Immunol* **187**, 5851–5864 (2011).
521. Kanayama, M. *et al.* Alpha9 integrin and its ligands constitute critical joint microenvironments for development of autoimmune arthritis. *J Immunol* **182**, 8015–8025 (2009).
522. Ning, L. *et al.* Tenascin-C Is Increased in Inflammatory Bowel Disease and Is Associated with response to Infliximab Therapy. *Biomed Res Int* **2019**, 1475705 (2019).
523. Zhang, X., Edwards, J. P. & Mosser, D. M. The Expression of Exogenous Genes in Macrophages: Obstacles and Opportunities. *Methods Mol Biol* **531**, 123 (2009).
524. Wakatsuki, T., Schwab, B., Thompson, N. C. & Elson, E. L. Effects of cytochalasin D and latrunculin B on mechanical properties of cells. *Journal of cell science* **114**, 1025–1036 (2001).

525. Holzinger, A. Jasplakinolide: an actin-specific reagent that promotes actin polymerization. *Methods in molecular biology (Clifton, N.J.)* **586**, 71–87 (2009).
526. Mir, S. S., Bhat, H. F. & Bhat, Z. F. Dynamic actin remodeling in response to lysophosphatidic acid. *Journal of biomolecular structure & dynamics* **38**, 5253–5265 (2020).
527. Yung, Y. C., Stoddard, N. C. & Chun, J. LPA receptor signaling: pharmacology, physiology, and pathophysiology. *Journal of Lipid Research* **55**, 1192–1214 (2014).
528. Fan, H. *et al.* Lysophosphatidic acid inhibits bacterial endotoxin-induced pro-inflammatory response: potential anti-inflammatory signaling pathways. *Molecular medicine (Cambridge, Mass.)* **14**, 422–428 (2008).
529. Kustermans, G., El Benna, J., Piette, J. & Legrand-Poels, S. Perturbation of actin dynamics induces NF-kappaB activation in myelomonocytic cells through an NADPH oxidase-dependent pathway. *The Biochemical journal* **387**, 531–540 (2005).
530. Marques, J. T. & Williams, B. R. G. Activation of the mammalian immune system by siRNAs. *Nat Biotechnol* **23**, 1399–1405 (2005).
531. Meng, Z. & Lu, M. RNA Interference-Induced Innate Immunity, Off-Target Effect, or Immune Adjuvant? *Frontiers in Immunology* **8**, (2017).
532. Wang, T. *et al.* YAP promotes breast cancer metastasis by repressing growth differentiation factor-15. *Biochimica et Biophysica Acta (BBA) - Molecular Basis of Disease* **1864**, 1744–1753 (2018).
533. Mattiske, S., Suetani, R. J., Neilsen, P. M. & Callen, D. F. The oncogenic role of miR-155 in breast cancer. *Cancer Epidemiol Biomarkers Prev* **21**, 1236–1243 (2012).

534. Ou, C. *et al.* Dual roles of yes-associated protein (YAP) in colorectal cancer. *Oncotarget* **8**, 75727–75741 (2017).
535. Zhao, T. *et al.* HTLV-1 activates YAP via NF- κ B/p65 to promote oncogenesis. *Proceedings of the National Academy of Sciences* **119**, e2115316119 (2022).
536. Berghaus, L. J. *et al.* Innate immune responses of primary murine macrophage-lineage cells and RAW 264.7 cells to ligands of Toll-like receptors 2, 3, and 4. *Comp Immunol Microbiol Infect Dis* **33**, 443–454 (2010).
537. Chamberlain, L. M., Godek, M. L., Gonzalez-Juarrero, M. & Grainger, D. W. Phenotypic non-equivalence of murine (monocyte-) macrophage cells in biomaterial and inflammatory models. *J Biomed Mater Res A* **88**, 858–871 (2009).
538. Godek, M. L., Duchsherer, N. L., McElwee, Q. & Grainger, D. W. Morphology and growth of murine cell lines on model biomaterials. *Biomed Sci Instrum* **40**, 7–12 (2004).
539. Godek, M. L., Sampson, J. A., Duchsherer, N. L., McElwee, Q. & Grainger, D. W. Rho GTPase protein expression and activation in murine monocytes/macrophages is not modulated by model biomaterial surfaces in serum-containing in vitro cultures. *J Biomater Sci Polym Ed* **17**, 1141–1158 (2006).
540. Zanoni, I. *et al.* CD14 controls the LPS-induced endocytosis of Toll-like Receptor 4. *Cell* **147**, 868–880 (2011).
541. Moore, K. J. *et al.* Divergent response to LPS and bacteria in CD14-deficient murine macrophages. *J Immunol* **165**, 4272–4280 (2000).
542. Wright, S. D., Ramos, R. A., Tobias, P. S., Ulevitch, R. J. & Mathison, J. C. CD14, a receptor for complexes of lipopolysaccharide (LPS) and LPS binding protein. *Science* **249**, 1431–1433 (1990).

543. Brooks, S. A. & Blackshear, P. J. Tristetraprolin (TTP): interactions with mRNA and proteins, and current thoughts on mechanisms of action. *Biochim Biophys Acta* **1829**, 666–679 (2013).
544. Bhattacharyya, S., Kumar, P., Tsuchiya, M., Bhattacharyya, A. & Biswas, R. Regulation of miR-155 biogenesis in cystic fibrosis lung epithelial cells: Antagonistic role of two mRNA-destabilizing proteins, KSRP and TTP. *Biochemical and Biophysical Research Communications* **433**, 484–488 (2013).
545. Remenyi, J., Bajan, S., Fuller-Pace, F. V., Arthur, J. S. C. & Hutvagner, G. The loop structure and the RNA helicase p72/DDX17 influence the processing efficiency of the mice miR-132. *Sci Rep* **6**, 22848 (2016).
546. Wada, T., Kikuchi, J. & Furukawa, Y. Histone deacetylase 1 enhances microRNA processing via deacetylation of DGCR8. *EMBO Reports* **13**, 142–149 (2012).
547. Andrews, S. L. *et al.* SVEP1 influences monocyte to macrophage differentiation via integrin $\alpha 4\beta 1/\alpha 9\beta 1$ and Rho/Rac signalling. *Biochimica et Biophysica Acta (BBA) - Molecular Cell Research* **1870**, 119479 (2023).
548. Abshire, M. Y., Thomas, K. S., Owen, K. A. & Bouton, A. H. Macrophage motility requires distinct $\alpha 5\beta 1$ /FAK and $\alpha 4\beta 1$ /paxillin signaling events. *J Leukoc Biol* **89**, 251–257 (2011).
549. Delve, E. *et al.* CDC42 regulates the expression of superficial zone molecules in part through the actin cytoskeleton and myocardin-related transcription factor-A. *Journal of Orthopaedic Research* **36**, 2421–2430 (2018).
550. Mouilleron, S., Guettler, S., Langer, C. A., Treisman, R. & McDonald, N. Q. Molecular basis for G-actin binding to RPEL motifs from the serum response factor coactivator MAL. *EMBO J* **27**, 3198–3208 (2008).
551. Olson, E. N. & Nordheim, A. Linking actin dynamics and gene transcription to drive cellular motile functions. *Nat Rev Mol Cell Biol* **11**, 353–365 (2010).

552. Posern, G., Miralles, F., Guettler, S. & Treisman, R. Mutant actins that stabilise F-actin use distinct mechanisms to activate the SRF coactivator MAL. *The EMBO Journal* **23**, 3973–3983 (2004).
553. Parreno, J. *et al.* Expression of type I collagen and tenascin C is regulated by actin polymerization through MRTF in dedifferentiated chondrocytes. *FEBS Lett* **588**, 3677–3684 (2014).
554. Jain, N. & Vogel, V. Spatial confinement downsizes the inflammatory response of macrophages. *Nat Mater* **17**, 1134–1144 (2018).
555. Huang, Y., Haas, C. & Ghadiali, S. N. Influence of Transmural Pressure and Cytoskeletal Structure on NF- κ B Activation in Respiratory Epithelial Cells. *Cellular and molecular bioengineering* **3**, 415–415 (2010).
556. Németh, Z. H. *et al.* Disruption of the actin cytoskeleton results in nuclear factor- κ B activation and inflammatory mediator production in cultured human intestinal epithelial cells. *Journal of cellular physiology* **200**, 71–81 (2004).
557. Wang, P. *et al.* Micro-RNA-155 is induced by K-Ras oncogenic signal and promotes ROS stress in pancreatic cancer. *Oncotarget* **6**, 21148–21158 (2015).
558. Ungvari, Z. *et al.* Aging-induced dysregulation of dicer1-dependent microRNA expression impairs angiogenic capacity of rat cerebrovascular endothelial cells. *The journals of gerontology. Series A, Biological sciences and medical sciences* **68**, 877–891 (2013).
559. Liu, B., Chen, Y. & St. Clair, D. K. ROS and p53: a versatile partnership. *Free radical biology & medicine* **44**, 1529–1535 (2008).
560. Zhang, Q. *et al.* Hippo signalling governs cytosolic nucleic acid sensing through YAP/TAZ-mediated TBK1 blockade. *Nature Cell Biology* **19**, 362–374 (2017).

561. Thaventhiran, J. E. D. *et al.* Activation of the Hippo pathway by CTLA-4 regulates the expression of Blimp-1 in the CD8 + T cell. *Proceedings of the National Academy of Sciences of the United States of America* **109**, E2223–E2223 (2012).
562. Zhou, X. *et al.* Microenvironmental sensing by fibroblasts controls macrophage population size. *Proc Natl Acad Sci U S A* **119**, e2205360119 (2022).
563. Artlett, C. M., Sassi-Gaha, S., Hope, J. L., Feghali-Bostwick, C. A. & Katsikis, P. D. Mir-155 is overexpressed in systemic sclerosis fibroblasts and is required for NLRP3 inflammasome-mediated collagen synthesis during fibrosis. *Arthritis Research & Therapy* **19**, 144 (2017).
564. Warga, E., Anderson, J., Tucker, M., Harris, E. & Elmer, J. Transcriptomic analysis of the innate immune response to in vitro transfection of plasmid DNA. *Molecular Therapy - Nucleic Acids* **31**, 43–56 (2023).
565. Kim, T. *et al.* Aspartate-glutamate-alanine-histidine box motif (DEAH)/RNA helicase A helicases sense microbial DNA in human plasmacytoid dendritic cells. *Proc Natl Acad Sci U S A* **107**, 15181–15186 (2010).
566. Liu, S. *et al.* DHX9 contributes to the malignant phenotypes of colorectal cancer via activating NF- κ B signaling pathway. *Cell. Mol. Life Sci.* **78**, 8261–8281 (2021).
567. Jing, H. *et al.* DExD/H-Box Helicase 36 Signaling via Myeloid Differentiation Primary Response Gene 88 Contributes to NF- κ B Activation to Type 2 Porcine Reproductive and Respiratory Syndrome Virus Infection. *Front Immunol* **8**, 1365 (2017).
568. Karreth, F. A., Tay, Y. & Pandolfi, P. P. Target competition: transcription factors enter the limelight. *Genome Biology* **15**, 114 (2014).
569. Qin, J. Y. *et al.* Systematic Comparison of Constitutive Promoters and the Doxycycline-Inducible Promoter. *PLoS One* **5**, e10611 (2010).

570. Scott Swindle, C. *et al.* Epidermal growth factor (EGF)-like repeats of human tenascin-C as ligands for EGF receptor. *The Journal of cell biology* **154**, 459–468 (2001).
571. Tucker, R. P. & Chiquet-Ehrismann, R. Tenascin-C: Its functions as an integrin ligand. *The international journal of biochemistry & cell biology* **65**, 165–168 (2015).
572. Yoshida, T., Akatsuka, T. & Imanaka-Yoshida, K. Tenascin-C and integrins in cancer. *Cell Adh Migr* **9**, 96–104 (2015).
573. Midwood, K. S., Chiquet, M., Tucker, R. P. & Orend, G. Tenascin-C at a glance. *Journal of Cell Science* **129**, 4321–4327 (2016).
574. Tiedje, C. *et al.* The p38/MK2-Driven Exchange between Tristetraprolin and HuR Regulates AU-Rich Element-Dependent Translation. *PLoS Genet* **8**, e1002977 (2012).
575. Legnini, I., Morlando, M., Mangiacavalli, A., Fatica, A. & Bozzoni, I. A Feedforward Regulatory Loop between HuR and the Long Noncoding RNA linc-MD1 Controls Early Phases of Myogenesis. *Mol Cell* **53**, 506–514 (2014).
576. Keniry, A. *et al.* The H19 lincRNA is a developmental reservoir of miR-675 that suppresses growth and Igf1r. *Nat Cell Biol* **14**, 659–665 (2012).
577. Gais, P. *et al.* TRIF Signaling Stimulates Translation of TNF- α mRNA via Prolonged Activation of MK2. *The Journal of Immunology* **184**, 5842–5848 (2010).
578. Tiedje, C. *et al.* The RNA-binding protein TTP is a global post-transcriptional regulator of feedback control in inflammation. *Nucleic Acids Res* **44**, 7418–7440 (2016).

579. Ludwig, B. S., Kessler, H., Kossatz, S. & Reuning, U. RGD-Binding Integrins Revisited: How Recently Discovered Functions and Novel Synthetic Ligands (Re-)Shape an Ever-Evolving Field. *Cancers (Basel)* **13**, 1711 (2021).
580. Jiang, P. & Collier, H. Functional Interactions Between microRNAs and RNA Binding Proteins. *Microna* **1**, 70–79 (2012).
581. Connerty, P., Ahadi, A. & Hutvagner, G. RNA Binding Proteins in the miRNA Pathway. *Int J Mol Sci* **17**, 31 (2015).
582. Benoit Bouvrette, L. P., Bovaird, S., Blanchette, M. & Lécuyer, E. oRNAment: a database of putative RNA binding protein target sites in the transcriptomes of model species. *Nucleic Acids Research* **48**, D166–D173 (2020).
583. Tang, R. *et al.* The polymorphic terminal-loop of pre-miR-1307 binding with MBNL1 contributes to colorectal carcinogenesis via interference with Dicer1 recruitment. *Carcinogenesis* **36**, 867–875 (2015).
584. Michlewski, G., Guil, S., Semple, C. A. & Cáceres, J. F. Posttranscriptional Regulation of miRNAs Harboring Conserved Terminal Loops. *Mol Cell* **32**, 383–393 (2008).
585. Wang, Z. *et al.* The structure of mitogen-activated protein kinase p38 at 2.1-Å resolution. *Proc Natl Acad Sci U S A* **94**, 2327–2332 (1997).
586. Love, M. I., Huber, W. & Anders, S. Moderated estimation of fold change and dispersion for RNA-seq data with DESeq2. *Genome Biology* **15**, 550 (2014).
587. Martin, F. J. *et al.* Ensembl 2023. *Nucleic Acids Research* **51**, D933–D941 (2023).
588. Maik-Rachline, G., Lifshits, L. & Seger, R. Nuclear P38: Roles in Physiological and Pathological Processes and Regulation of Nuclear Translocation. *Int J Mol Sci* **21**, 6102 (2020).

589. ANTONOV, A. S. *et al.* α V β 3 Integrin Regulates Macrophage Inflammatory Responses via PI3 Kinase/Akt-Dependent NF- κ B Activation. *J Cell Physiol* **226**, 469–476 (2011).
590. Aziz, Md. M. *et al.* MFG-E8 Attenuates Intestinal Inflammation in Murine Experimental Colitis by Modulating Osteopontin-Dependent α V β 3 Integrin Signaling1. *The Journal of Immunology* **182**, 7222–7232 (2009).
591. Wang, H. *et al.* A Photoresponsive Hyaluronan Hydrogel Nanocomposite for Dynamic Macrophage Immunomodulation. *Advanced Healthcare Materials* **8**, 1801234 (2019).
592. Taciak, B. *et al.* Evaluation of phenotypic and functional stability of RAW 264.7 cell line through serial passages. *PLoS ONE* **13**, (2018).
593. Qin, W., Cho, K. F., Cavanagh, P. E. & Ting, A. Y. Deciphering molecular interactions by proximity labeling. *Nat Methods* **18**, 133–143 (2021).
594. Jd, M. *et al.* Engineered ascorbate peroxidase as a genetically encoded reporter for electron microscopy. *Nature biotechnology* **30**, (2012).
595. Di, K. *et al.* Probing nuclear pore complex architecture with proximity-dependent biotinylation. *Proceedings of the National Academy of Sciences of the United States of America* **111**, (2014).
596. Chiquet-Ehrismann, R., Kalla, P., Pearson, C. A., Beck, K. & Chiquet, M. Tenascin interferes with fibronectin action. *Cell* **53**, 383–390 (1988).
597. Okada, T. & Suzuki, H. The Role of Tenascin-C in Tissue Injury and Repair After Stroke. *Frontiers in Immunology* **11**, (2021).
598. Shimojo, N. *et al.* Tenascin-C May Accelerate Cardiac Fibrosis by Activating Macrophages via the Integrin α V β 3/Nuclear Factor- κ B/Interleukin-6 Axis. *Hypertension* **66**, 757–766 (2015).
599. Bartel, D. P. Metazoan MicroRNAs. *Cell* **173**, 20–20 (2018).

600. Nguyen, H. M., Nguyen, T. D., Nguyen, T. L. & Nguyen, T. A. Orientation of Human Microprocessor on Primary MicroRNAs. *Biochemistry* **58**, 189–198 (2019).
601. Ha, M. & Kim, V. N. Regulation of microRNA biogenesis. *Nature Reviews Molecular Cell Biology* **15**, 509–524 (2014).
602. Kim, H. *et al.* Bias-minimized quantification of microRNA reveals widespread alternative processing and 3' end modification. *Nucleic Acids Res* **47**, 2630–2640 (2019).
603. Langmead, B., Trapnell, C., Pop, M. & Salzberg, S. L. Ultrafast and memory-efficient alignment of short DNA sequences to the human genome. *Genome Biol* **10**, R25 (2009).
604. Friedländer, M. R., Mackowiak, S. D., Li, N., Chen, W. & Rajewsky, N. miRDeep2 accurately identifies known and hundreds of novel microRNA genes in seven animal clades. *Nucleic Acids Research* **40**, 37–52 (2012).
605. Paraskevopoulou, M. D. *et al.* DIANA-microT web server v5.0: service integration into miRNA functional analysis workflows. *Nucleic acids research* **41**, (2013).
606. Garcia, D. M. *et al.* Weak Seed-Pairing Stability and High Target-Site Abundance Decrease the Proficiency of Isy-6 and Other miRNAs. *Nature structural & molecular biology* **18**, 1139–1139 (2011).
607. Narayan, N., Bracken, C. P. & Ekert, P. G. MicroRNA-155 expression and function in AML: An evolving paradigm. *Experimental Hematology* **62**, 1–6 (2018).
608. Drexler, S. K., Kong, P. L., Wales, J. & Foxwell, B. M. Cell signalling in macrophages, the principal innate immune effector cells of rheumatoid arthritis. *Arthritis Research & Therapy* **10**, 216–216 (2008).

609. Lu, L. *et al.* Time Series miRNA-mRNA integrated analysis reveals critical miRNAs and targets in macrophage polarization. *Scientific Reports* **6**, 1–14 (2016).
610. Liu, G. *et al.* miR-147, a microRNA that is induced upon toll-like receptor stimulation, regulates murine macrophage inflammatory responses. *Proceedings of the National Academy of Sciences of the United States of America* **106**, 15819–15824 (2009).
611. Zhou, Y. *et al.* The regulatory effect of microRNA-21a-3p on the promotion of telocyte angiogenesis mediated by PI3K (p110 α)/AKT/mTOR in LPS induced mice ARDS. *Journal of Translational Medicine* **17**, 427 (2019).
612. Tong, Z., Cui, Q., Wang, J. & Zhou, Y. TransmiR v2.0: an updated transcription factor-microRNA regulation database. *Nucleic acids research* **47**, D253–D258 (2019).
613. Kim, H. & Kim, J. MicroRNA arm switching regulated by uridylation. *bioRxiv Molecular Biology* 2020.04.06.027813-2020.04.06.027813 (2020) doi:10.1101/2020.04.06.027813.
614. Kozomara, A., Birgaoanu, M. & Griffiths-Jones, S. miRBase: from microRNA sequences to function. *Nucleic Acids Research* **47**, D155–D155 (2019).
615. Aubert, A. *et al.* Latent TGF- β Activation Is a Hallmark of the Tenascin Family. *Frontiers in Immunology* **12**, 1557–1557 (2021).
616. Cheng, X., Li, F. & Tao, Z. Tenascin-C promotes epithelial-to-mesenchymal transition and the mTOR signaling pathway in nasopharyngeal carcinoma. *Oncology Letters* **22**, (2021).
617. Krol, J. *et al.* Structural features of microRNA (miRNA) precursors and their relevance to miRNA biogenesis and small interfering RNA/short hairpin RNA design. *The Journal of biological chemistry* **279**, 42230–42239 (2004).

618. Zhang, X. & Zeng, Y. The terminal loop region controls microRNA processing by Drosha and Dicer. *Nucleic Acids Research* **38**, 7689–7697 (2010).
619. Proctor, J. R. & Meyer, I. M. CoFold: an RNA secondary structure prediction method that takes co-transcriptional folding into account. *Nucleic Acids Research* **41**, e102–e102 (2013).
620. Das, A. *et al.* High-Resolution Mapping and Dynamics of the Transcriptome, Transcription Factors, and Transcription Co-Factor Networks in Classically and Alternatively Activated Macrophages. *Front Immunol* **9**, 22 (2018).
621. Wang, D., Huang, J. & Hu, Z. RNA Helicase DDX5 Regulates MicroRNA Expression and Contributes to Cytoskeletal Reorganization in Basal Breast Cancer Cells. *Mol Cell Proteomics* **11**, M111.011932 (2012).
622. Wang, Y. *et al.* STAT1 Regulates MD-2 Expression in Monocytes of Sepsis via miR-30a. *Inflammation* **37**, 1903–1911 (2014).
623. Zhang, Y. *et al.* MicroRNA-30a-5p silencing polarizes macrophages toward M2 phenotype to alleviate cardiac injury following viral myocarditis by targeting SOCS1. *American Journal of Physiology-Heart and Circulatory Physiology* **320**, H1348–H1360 (2021).
624. Shangxun, Z. *et al.* ADAR1 Alleviates Inflammation in a Murine Sepsis Model via the ADAR1-miR-30a-SOCS3 Axis. *Mediators of Inflammation* **2020**, e9607535 (2020).
625. Zhang, Y. *et al.* Long noncoding RNA LINC00461 induced osteoarthritis progression by inhibiting miR-30a-5p. *Aging* **12**, 4111–4123 (2020).
626. Che, M., Gong, W., Zhao, Y. & Liu, M. Long noncoding RNA HCG18 inhibits the differentiation of human bone marrow-derived mesenchymal stem cells in osteoporosis by targeting miR-30a-5p/NOTCH1 axis. *Mol Med* **26**, 106 (2020).

627. Xian, D., Niu, L., Zeng, J. & Wang, L. LncRNA KCNQ1OT1 Secreted by Tumor Cell-Derived Exosomes Mediates Immune Escape in Colorectal Cancer by Regulating PD-L1 Ubiquitination via MiR-30a-5p/USP22. *Front Cell Dev Biol* **9**, 653808 (2021).
628. Bu, Y., Zheng, D., Wang, L. & Liu, J. LncRNA TSIX promotes osteoblast apoptosis in particle-induced osteolysis by down-regulating miR-30a-5p. *Connective Tissue Research* **59**, 534–541 (2018).
629. Conrad, O. *et al.* Tumor-Suppressive and Immunomodulating Activity of miR-30a-3p and miR-30e-3p in HNSCC Cells and Tumoroids. *International Journal of Molecular Sciences* **24**, 11178 (2023).
630. Shukla, K. Regulation of NF- κ B signaling and cell cycle progression by microRNA-30c-2-3p in breast cancer. <https://archiv.ub.uni-heidelberg.de/volltextserver/17696/> (2014) doi:10.11588/heidok.00017696.
631. Settleman, J. A nuclear MAL-function links Rho to SRF. *Mol Cell* **11**, 1121–1123 (2003).
632. Midwood, K. S. & Schwarzbauer, J. E. Tenascin-C Modulates Matrix Contraction via Focal Adhesion Kinase- and Rho-mediated Signaling Pathways. *MBoC* **13**, 3601–3613 (2002).
633. Iizasa, H. *et al.* Editing of Epstein-Barr virus-encoded BART6 microRNAs controls their dicer targeting and consequently affects viral latency. *Journal of Biological Chemistry* **285**, 33358–33370 (2010).
634. Yang, W. *et al.* Modulation of microRNA processing and expression through RNA editing by ADAR deaminases. *Nature Structural and Molecular Biology* **13**, 13–21 (2006).
635. Kim, Y. *et al.* Deletion of human tarbp2 reveals cellular microRNA targets and cell-cycle function of TRBP. *Cell Reports* **9**, 1061–1074 (2014).

636. Lee, H. Y. & Doudna, J. A. TRBP alters human precursor microRNA processing in vitro. *RNA* **18**, 2012–2019 (2012).
637. Wilson, R. C. *et al.* Dicer-TRBP complex formation ensures accurate mammalian MicroRNA biogenesis. *Molecular Cell* **57**, 397–407 (2015).
638. Lambert, M. P. *et al.* The RNA helicase DDX17 controls the transcriptional activity of REST and the expression of proneural microRNAs in neuronal differentiation. *Nucleic Acids Research* **46**, 7686–7700 (2018).
639. Ngo, T. D., Partin, A. C. & Nam, Y. RNA Specificity and Autoregulation of DDX17, a Modulator of MicroRNA Biogenesis. *Cell Reports* **29**, 4024–4035.e5 (2019).
640. Nakanishi, K. Anatomy of RISC: how do small RNAs and chaperones activate Argonaute proteins? *Wiley Interdisciplinary Reviews. RNA* **7**, 637 (2016).
641. Pare, J. M. *et al.* Hsp90 Regulates the Function of Argonaute 2 and Its Recruitment to Stress Granules and P-Bodies. *Mol Biol Cell* **20**, 3273–3284 (2009).
642. Tahbaz, N. *et al.* Characterization of the interactions between mammalian PAZ PIWI domain proteins and Dicer. *EMBO Reports* **5**, 189 (2004).
643. Tomari, Y., Matranga, C., Haley, B., Martinez, N. & Zamore, P. D. A protein sensor for siRNA asymmetry. *Science* **306**, 1377–1380 (2004).
644. Noland, C. L., Ma, E. & Doudna, J. A. siRNA Repositioning for Guide Strand Selection by Human Dicer Complexes. *Mol Cell* **43**, 110–121 (2011).
645. Okamura, K., Robine, N., Liu, Y., Liu, Q. & Lai, E. C. R2D2 Organizes Small Regulatory RNA Pathways in *Drosophila*. *Mol Cell Biol* **31**, 884–896 (2011).
646. Rüdell, S. *et al.* Phosphorylation of human Argonaute proteins affects small RNA binding. *Nucleic Acids Res* **39**, 2330–2343 (2011).

647. Huang, J. *et al.* MiR-155 is upregulated in patients with active tuberculosis and inhibits apoptosis of monocytes by targeting FOXO3. *Mol Med Rep* **12**, 7102–7108 (2015).
648. Leng, R.-X., Pan, H.-F., Qin, W.-Z., Chen, G.-M. & Ye, D.-Q. Role of microRNA-155 in autoimmunity. *Cytokine Growth Factor Rev* **22**, 141–147 (2011).
649. Bornstein, P. Matricellular proteins: An overview. *Journal of Cell Communication and Signaling* **3**, 163–165 (2009).
650. Mason, D. E. *et al.* YAP and TAZ limit cytoskeletal and focal adhesion maturation to enable persistent cell motility. *J Cell Biol* **218**, 1369–1389 (2019).
651. Nardone, G. *et al.* YAP regulates cell mechanics by controlling focal adhesion assembly. *Nat Commun* **8**, 15321 (2017).
652. Imanaka-Yoshida, K. *et al.* Tenascin-C Modulates Adhesion of Cardiomyocytes to Extracellular Matrix during Tissue Remodeling after Myocardial Infarction. *Lab Invest* **81**, 1015–1024 (2001).
653. Wei, C. & Li, X. Verteporfin inhibits cell proliferation and induces apoptosis in different subtypes of breast cancer cell lines without light activation. *BMC Cancer* **20**, 1042 (2020).
654. Jiang, Y. *et al.* Application and Evaluation of [99mTc]-Labeled Peptide Nucleic Acid Targeting MicroRNA-155 in Breast Cancer Imaging. *Mol Imaging* **19**, 1536012120916124 (2020).
655. Zhang, C.-M., Zhao, J. & Deng, H.-Y. MiR-155 promotes proliferation of human breast cancer MCF-7 cells through targeting tumor protein 53-induced nuclear protein 1. *Journal of Biomedical Science* **20**, 79 (2013).
656. Nagaharu, K. *et al.* Tenascin C Induces Epithelial-Mesenchymal Transition–Like Change Accompanied by SRC Activation and Focal Adhesion Kinase

- Phosphorylation in Human Breast Cancer Cells. *Am J Pathol* **178**, 754–763 (2011).
657. Sorrentino, G. *et al.* Glucocorticoid receptor signalling activates YAP in breast cancer. *Nat Commun* **8**, 14073 (2017).
658. Wawrzyniak, D. *et al.* Down-regulation of tenascin-C inhibits breast cancer cells development by cell growth, migration, and adhesion impairment. *PLoS One* **15**, e0237889 (2020).
659. Nishimoto, M. *et al.* Transformation of normal cells by aberrant activation of YAP via cMyc with TEAD. *Sci Rep* **9**, 10933 (2019).
660. Zhou, X. *et al.* Melanoma cell-secreted exosomal miR-155-5p induce proangiogenic switch of cancer-associated fibroblasts via SOCS1/JAK2/STAT3 signaling pathway. *J Exp Clin Cancer Res* **37**, 242 (2018).
661. Wang, J. *et al.* Breast cancer cell-derived microRNA-155 suppresses tumor progression via enhancing immune cell recruitment and antitumor function. *J Clin Invest* **132**, e157248.
662. Bhattacharyya, S., Midwood, K. S., Yin, H. & Varga, J. Toll-Like Receptor-4 Signaling Drives Persistent Fibroblast Activation and Prevents Fibrosis Resolution in Scleroderma. *Adv Wound Care (New Rochelle)* **6**, 356–369 (2017).
663. Tartaglia, L. A. *et al.* The two different receptors for tumor necrosis factor mediate distinct cellular responses. *Proc Natl Acad Sci U S A* **88**, 9292–9296 (1991).
664. Wang, J. *et al.* The mechanism of TGF- β /miR-155/c-Ski regulates endothelial-mesenchymal transition in human coronary artery endothelial cells. *Bioscience Reports* **37**, BSR20160603 (2017).

665. Pearson, C. A., Pearson, D., Shibahara, S., Hofsteenge, J. & Chiquet-Ehrismann, R. Tenascin: cDNA cloning and induction by TGF-beta. *EMBO J* **7**, 2977–2982 (1988).
666. Su, A. I. *et al.* A gene atlas of the mouse and human protein-encoding transcriptomes. *Proc Natl Acad Sci U S A* **101**, 6062–6067 (2004).
667. San Martin, R. *et al.* Tenascin-C and Integrin $\alpha 9$ Mediate Interactions of Prostate Cancer with the Bone Microenvironment. *Cancer Res* **77**, 5977–5988 (2017).
668. Jachetti, E. *et al.* Tenascin-C Protects Cancer Stem-like Cells from Immune Surveillance by Arresting T-cell Activation. *Cancer Res* **75**, 2095–2108 (2015).
669. Yurdagul, A. *et al.* $\alpha 5\beta 1$ Integrin Signaling Mediates Oxidized Low-Density Lipoprotein-Induced Inflammation and Early Atherosclerosis. *Arteriosclerosis, Thrombosis, and Vascular Biology* **34**, 1362–1373 (2014).
670. Sarkar, S. *et al.* Activation of NOTCH Signaling by Tenascin-C Promotes Growth of Human Brain Tumor-Initiating Cells. *Cancer Research* **77**, 3231–3243 (2017).
671. Boisvert, M., Gendron, S., Chetoui, N. & Aoudjit, F. Alpha2beta1 integrin signaling augments T cell receptor-dependent production of interferon-gamma in human T cells. *Molecular Immunology* **44**, 3732–3740 (2007).
672. Schnapp, L. M. *et al.* The Human Integrin $\alpha 8\beta 1$ Functions as a Receptor for Tenascin, Fibronectin, and Vitronectin (*). *Journal of Biological Chemistry* **270**, 23196–23202 (1995).
673. Fernandes, N. R. J. *et al.* CD4+ T Cell Interstitial Migration Controlled by Fibronectin in the Inflamed Skin. *Front Immunol* **11**, 1501 (2020).
674. Jones, P. L., Crack, J. & Rabinovitch, M. Regulation of Tenascin-C, a Vascular Smooth Muscle Cell Survival Factor that Interacts with the $\alpha v\beta 3$ Integrin to

- Promote Epidermal Growth Factor Receptor Phosphorylation and Growth.
Journal of Cell Biology **139**, 279–293 (1997).
675. Scaffidi, A. K. *et al.* $\alpha\beta 3$ Integrin Interacts with the Transforming Growth Factor β (TGF β) Type II Receptor to Potentiate the Proliferative Effects of TGF $\beta 1$ in Living Human Lung Fibroblasts *. *Journal of Biological Chemistry* **279**, 37726–37733 (2004).
676. Bishop, G. G. *et al.* Selective $\alpha\beta 3$ -Receptor Blockade Reduces Macrophage Infiltration and Restenosis After Balloon Angioplasty in the Atherosclerotic Rabbit. *Circulation* **103**, 1906–1911 (2001).
677. Kumawat, A. K. *et al.* Expression and characterization of $\alpha\beta 5$ integrin on intestinal macrophages. *European Journal of Immunology* **48**, 1181–1187 (2018).
678. Dong, X., Hudson, N. E., Lu, C. & Springer, T. A. Structural determinants of integrin β -subunit specificity for latent TGF- β . *Nat Struct Mol Biol* **21**, 1091–1096 (2014).
679. Xie, Y., Gao, K., Häkkinen, L. & Larjava, H. S. Mice lacking $\beta 6$ integrin in skin show accelerated wound repair in dexamethasone impaired wound healing model. *Wound Repair and Regeneration* **17**, 326–339 (2009).
680. McCarty, J. H. $\alpha\beta 8$ integrin adhesion and signaling pathways in development, physiology and disease. *Journal of Cell Science* **133**, jcs239434 (2020).
681. Naik, A. *et al.* Neuropilin-1 promotes the oncogenic Tenascin-C/integrin $\beta 3$ pathway and modulates chemoresistance in breast cancer cells. *BMC Cancer* **18**, 533–533 (2018).
682. Dai, X. *et al.* A novel role for myeloid cell-specific neuropilin 1 in mitigating sepsis. *FASEB J* **31**, 2881–2892 (2017).

683. Lu, Z.-Z. *et al.* Neuropilin 1 is an entry receptor for KSHV infection of mesenchymal stem cell through TGFBR1/2-mediated macropinocytosis. *Sci Adv* **9**, eadg1778.
684. Gong, D. *et al.* TGF β signaling plays a critical role in promoting alternative macrophage activation. *BMC Immunol* **13**, 31 (2012).

Chapter 9

Additional content

9.1.0 – Covid-19 Impact Statement

The worldwide COVID-19 pandemic began in early 2020, during the first year of my PhD, with both the illness and the necessary preventative measures taken by the UK government and University of Nottingham significantly impacting my academic progress.

The initial lockdown measures of 2020 led to my first months in the lab of Dr Anna Piccinini taking place from home. As a result, initial training in vital lab based skills could not be undertaken, with my time instead focused on planning and the development of a review paper (Section 10.0.0). This was in addition to previous lab members, whose work I would be developing, not

being able to demonstrate first hand their techniques and best practices before their PhD funding ended during the lockdown.

Once the initial lockdown ended, I was able to return to the lab during the summer of 2020. However, as the number of lab members present at one time was limited to avoid potential disease spread, vital one-to-one demonstration was difficult, leading to my slow progress even with frequent lab attendance. Additionally, as contact with COVID-19 was unavoidable, experiments would be frequently interrupted by periods of self-isolation, often with cell cultures needing to be restarted in their entirety.

All of this was in addition to the considerable stress of the situation, worrying for the wellbeing of friends and family, as well as for the future.

9.2.0 – Professional Internship Programme

For three months, from May-July 2022, I conducted an internship with the medical writing company, Porterhouse Medical as part of the BBSRC DTP professional internship programme (PIP).

During my time with Porterhouse, I worked on a variety of projects, editing, amending, referencing, and writing from scratch multiple forms of copy intended for use by health care professionals.

For example, a focus of my work was to develop slide decks to be presented at a global conference on ophthalmology. This helped develop my attention to detail, as strict medical compliance laws govern what can and cannot be

included in such presentations, with accurate citations and obedience of copyright being just two areas of heavy scrutiny.

Furthermore, this placement honed my ability to work as part of a team, being encouraged to outsource jobs such as the development of graphics and editorial scrutiny to specialised creative and editing departments. This requiring a skill of its own to succinctly and accurately brief non scientists on how to best present the content while being open to their own expertise.

Finally, the large variety of work led me to experience new areas of science on a week by week basis, with ophthalmology, epilepsy, narcolepsy and haematology all being areas I developed my knowledge base in, while as a whole I gained many insights into the ins and outs of the pharmaceuticals industry.

Chapter 10

Publications